

**NIST NCSTAR 1-3E**

**Federal Building and Fire Safety Investigation of the  
World Trade Center Disaster**

# **Physical Properties of Structural Steels**

Stephen W. Banovic  
Christopher N. McCowan  
William E. Luecke



**NIST NCSTAR 1-3E**

**Federal Building and Fire Safety Investigation of the  
World Trade Center Disaster**

**Physical Properties of Structural  
Steels**

Stephen W. Banovic

Christopher N. McCowan

William E. Luecke

*Materials Science and Engineering Laboratory  
National Institute of Standards and Technology*

September 2005



U.S. Department of Commerce  
*Carlos M. Gutierrez, Secretary*

Technology Administration  
*Michelle O'Neill, Acting Under Secretary for Technology*

National Institute of Standards and Technology  
*William Jeffrey, Director*

#### Disclaimer No. 1

Certain commercial entities, equipment, products, or materials are identified in this document in order to describe a procedure or concept adequately or to trace the history of the procedures and practices used. Such identification is not intended to imply recommendation, endorsement, or implication that the entities, products, materials, or equipment are necessarily the best available for the purpose. Nor does such identification imply a finding of fault or negligence by the National Institute of Standards and Technology.

#### Disclaimer No. 2

The policy of NIST is to use the International System of Units (metric units) in all publications. In this document, however, units are presented in metric units or the inch-pound system, whichever is prevalent in the discipline.

#### Disclaimer No. 3

Pursuant to section 7 of the National Construction Safety Team Act, the NIST Director has determined that certain evidence received by NIST in the course of this Investigation is "voluntarily provided safety-related information" that is "not directly related to the building failure being investigated" and that "disclosure of that information would inhibit the voluntary provision of that type of information" (15 USC 7306c).

In addition, a substantial portion of the evidence collected by NIST in the course of the Investigation has been provided to NIST under nondisclosure agreements.

#### Disclaimer No. 4

NIST takes no position as to whether the design or construction of a WTC building was compliant with any code since, due to the destruction of the WTC buildings, NIST could not verify the actual (or as-built) construction, the properties and condition of the materials used, or changes to the original construction made over the life of the buildings. In addition, NIST could not verify the interpretations of codes used by applicable authorities in determining compliance when implementing building codes. Where an Investigation report states whether a system was designed or installed as required by a code *provision*, NIST has documentary or anecdotal evidence indicating whether the requirement was met, or NIST has independently conducted tests or analyses indicating whether the requirement was met.

#### Use in Legal Proceedings

No part of any report resulting from a NIST investigation into a structural failure or from an investigation under the National Construction Safety Team Act may be used in any suit or action for damages arising out of any matter mentioned in such report (15 USC 281a; as amended by P.L. 107-231).

**National Institute of Standards and Technology National Construction Safety Team Act Report 1-3E  
Natl. Inst. Stand. Technol. Natl. Constr. Sfty. Tm. Act Rpt. 1-3E, 162 pages (September 2005)  
CODEN: NSPUE2**

U.S. GOVERNMENT PRINTING OFFICE  
WASHINGTON: 2005

---

For sale by the Superintendent of Documents, U.S. Government Printing Office  
Internet: [bookstore.gpo.gov](http://bookstore.gpo.gov) — Phone: (202) 512-1800 — Fax: (202) 512-2250  
Mail: Stop SSOP, Washington, DC 20402-0001

## ABSTRACT

---

This report describes the physical properties of the structural steel recovered from the World Trade Center (WTC) towers. Analytical techniques were used to determine and evaluate the chemistry, microstructure, and thermal properties of the steels. While not a physical property, hardness of the steels was also measured and discussed in relation to strengthening mechanisms of the material. The primary focus was on structural components with known as-built locations from WTC 1 and WTC 2. Evaluation of samples without known as-built locations was conducted in order to fully characterize all of the structural elements. The physical property information was found useful in helping to identify specific grades and producers of steel used for the various components. In addition, the thermal properties were developed for the use in the models of the building response to fire. Although no recovered structural elements were from WTC 7, physical property data of steels from this building were estimated based upon values found in the literature. In addition to the structural steel, chemistry information was measured for a piece of the aluminum façade used on the WTC towers and the sprayed fire-resistive material applied to the structural elements of WTC 1 and WTC 2.

Keywords: Chemistry, hardness, microstructure, physical property, steel, thermal properties, World Trade Center.

This page intentionally left blank.

# TABLE OF CONTENTS

---

Abstract .....	iii
List of Figures .....	ix
List of Tables .....	xiii
List of Acronyms and Abbreviations .....	xv
Metric Conversion Table .....	xvii
Preface .....	xxi
Acknowledgments .....	xxx
Executive Summary .....	xxxiii
<b>Chapter 1</b>	
<b>Introduction .....</b>	<b>1</b>
1.1 Scope of Report .....	1
<b>Chapter 2</b>	
<b>Background of Structural Steels .....</b>	<b>3</b>
2.1 Brief Review of Structural Steels Specified in the Construction of the WTC Towers .....	3
2.1.1 Specified and Contemporaneously Available Steels for Construction of the WTC Towers .....	4
<b>Chapter 3</b>	
<b>Experimental Procedures .....</b>	<b>5</b>
3.1 Sample Documentation and Removal .....	5
3.2 Chemical Analysis .....	5
3.3 Metallography .....	6
3.3.1 Sample Preparation .....	6
3.3.2 Ferrite Grain Size Measurements .....	6
3.3.3 Pearlite Volume Fraction Measurements .....	6
3.4 Hardness Testing .....	7
3.5 Furnace Exposure .....	7
<b>Chapter 4</b>	
<b>Chemical Analysis Results .....</b>	<b>11</b>
4.1 Exterior Panel Material .....	11
4.1.1 Perimeter Columns .....	11

4.1.2	Spandrel Plates .....	14
4.1.3	Spandrel Splice Plates .....	14
4.1.4	Floor Truss Connectors .....	15
4.2	Core Material .....	16
4.2.1	Wide Flange Core Columns .....	16
4.2.2	Built-Up Box Core Columns .....	16
4.2.3	Channel.....	16
4.2.4	Core Truss Seat .....	17
4.3	Floor Truss Material .....	17
4.3.1	Rod .....	17
4.3.2	Chord/Angle.....	17
4.4	Summary .....	17

Chapter 5

**Metallographic Analysis Results..... 31**

5.1	Exterior Panel Material .....	31
5.1.1	Perimeter Columns .....	31
5.1.2	Spandrel Plates .....	34
5.1.3	Spandrel Splice Plates .....	36
5.1.4	Floor Truss Connectors .....	36
5.2	Core Material .....	38
5.2.1	Wide Flange Core Columns .....	38
5.2.2	Built-Up Box Core Columns .....	38
5.2.3	Channel.....	38
5.2.4	Core Truss Seat .....	39
5.3	Floor Truss Material .....	39
5.3.1	Rod .....	39
5.3.2	Chord/Angle.....	39
5.4	Furnace Exposure of WTC steel .....	40
5.4.1	Hot-Rolled Flange and Spandrel Plates.....	40
5.4.2	Quenched-and-Tempered Flange Plate .....	41
5.4.3	Exterior Panel Floor Truss Seat.....	41
5.5	Summary .....	41

Chapter 6	
<b>Hardness Analysis Results</b> .....	<b>93</b>
6.1 Perimeter Panel Material.....	93
6.2 Core Column Material .....	93
6.3 Floor Truss Material .....	93
6.4 Panel Splice Connectors and Truss Connectors.....	93
6.5 Hardness Traverses Through Welds on Perimeter Columns .....	94
6.6 Hardness of Furnace Exposed Flange Plates .....	94
6.6.1 Hot-Rolled Flange and Spandrel Plates.....	94
6.6.2 Quenched-and-Tempered Flange Plate .....	95
6.6.3 Exterior Panel Floor Truss Seat.....	95
6.7 Summary .....	95
Chapter 7	
<b>Thermal Properties of WTC Structural Steel</b> .....	<b>103</b>
7.1 Introduction.....	103
7.2 Specific Heat.....	103
7.2.1 Recommended Value .....	104
7.2.2 Uncertainties.....	104
7.3 Coefficient of Thermal Expansion.....	104
7.3.1 Recommended Value .....	106
7.3.2 Uncertainties.....	106
7.4 Thermal Conductivity and Diffusivity.....	106
7.4.1 Recommended Values .....	109
7.4.2 Uncertainties.....	109
7.5 Notes on Data Sources .....	109
7.5.1 Thermal Expansion Coefficient.....	109
Chapter 8	
<b>Analysis of Aluminum Façade Used on the WTC Towers</b> .....	<b>117</b>
Chapter 9	
<b>Analysis of Sprayed Fire-Resistive Material</b> .....	<b>119</b>
Chapter 10	
<b>Findings and Conclusions</b> .....	<b>123</b>

Chapter 11	
<b>References</b> .....	<b>125</b>

## LIST OF FIGURES

---

Figure P-1. The eight projects in the federal building and fire safety investigation of the WTC disaster. ....	xxiii
Figure 3-1. a) Photograph prior to sample removal from structural element, b) photograph subsequent to sample removal from structural element, and c) photograph displaying samples to be cut for further analysis from the specimen. ....	8
Figure 3-2. Schematic indicating the viewing orientations for metallographic analysis. ....	9
Figure 4-1. Plots of mass fraction element as a function of specified minimum yield strength for the flange plates from perimeter columns. ....	18
Figure 4-2. Plots of mass fraction element as a function of specified minimum yield strength for the outer web plates from perimeter columns. ....	19
Figure 4-3. Plots of mass fraction element as a function of specified minimum yield strength for the inner web plates from perimeter columns. ....	20
Figure 4-4. Plots of mass fraction element as a function of specified minimum yield strength for the spandrel plates from the exterior panels. ....	21
Figure 5-1. Representative microstructures of hot-rolled perimeter column flange plates as a function of strength level. ....	42
Figure 5-2. a) ASTM ferrite grain size number as a function of specified minimum yield strength of the plate, and b) volume fraction of pearlite as a function of specified minimum yield strength of the plate. ....	45
Figure 5-3. Representative micrographs of ferrite morphologies observed from plates with the specified minimum yield strength less than 70 ksi. ....	46
Figure 5-4. Banding of microstructural constituents observed in a 60 ksi plate. ....	47
Figure 5-5. Distribution of microstructural constituents observed in a 60 ksi plate. ....	48
Figure 5-6. Morphologies of pearlite observed. ....	49
Figure 5-7. Possible bainite or degenerate pearlite in lower strength plates. ....	50
Figure 5-8. Non-metallic inclusions of MnS observed in the rolled plates. ....	51
Figure 5-9. Representative microstructures of quenched-and-tempered perimeter column flange plates as a function of strength level. ....	52
Figure 5-10. Microstructures from hot-rolled steels used for all inner web plates. ....	54
Figure 5-11. Polished and etched cross-section of weld between inner web and flange. ....	55
Figure 5-12. Representative micrographs from perimeter column welds of a hot-rolled steel with $F_y = 55$ ksi. ....	56

Figure 5–13. Representative microstructure of HAZ near fusion line from perimeter column weld of a quenched-and-tempered steel with  $F_y = 100$  ksi. .... 59

Figure 5–14. Microstructure from a column butt plate. .... 60

Figure 5–15. Representative microstructures of hot-rolled perimeter column spandrel plates as a function of strength level. .... 61

Figure 5–16. Representative microstructures of quenched-and-tempered perimeter column spandrel plates as a function of strength level. .... 65

Figure 5–17. Representative microstructure of spandrel splice plate. .... 67

Figure 5–18. Partially decarburized zone found near the surface of a perimeter floor truss seat. .... 68

Figure 5–19. Microstructure from an ASTM A 325 construction bolt. .... 69

Figure 5–20. Microstructures observed for standoff plates connecting floor truss seats to spandrel plates. .... 70

Figure 5–21. Etched cross-section of weld between spandrel plate. .... 71

Figure 5–22. Etched cross-section of intact weld between a standoff plate and truss seat. .... 72

Figure 5–23. Microstructure of a hot-rolled gusset plate welded to the top chord of the floor trusses. .... 73

Figure 5–24. Microstructure of a hot-rolled damper plate. .... 74

Figure 5–25. Microstructure of a hot-rolled gusset plate used to attach the damper units and the diagonal bracing straps to the perimeter columns. .... 75

Figure 5–26. Microstructure of a hot-rolled diagonal bracing strap. .... 76

Figure 5–27. Microstructure of a hot-rolled 36 ksi rolled wide flange. .... 77

Figure 5–28. Microstructure of a hot-rolled 42 ksi rolled wide flange. .... 78

Figure 5–29. Microstructure of a hot-rolled 36 ksi plate from a built-up box core column. .... 79

Figure 5–30. Microstructure of a hot-rolled 42 ksi plate from a built-up box core column. .... 80

Figure 5–31. Microstructures from channel material located in the core. .... 81

Figure 5–32. Microstructure of a hot-rolled core floor truss seat. .... 82

Figure 5–33. Microstructure from floor truss rods. .... 83

Figure 5–34. Microstructures from floor truss angles. .... 85

Figure 5–35. Change in microstructure of a 60 ksi flange plate that was heat treated in a laboratory furnace at 625 °C for various times. .... 86

Figure 5–36. Change in microstructure of a 42 ksi spandrel plate that was heat treated in a laboratory furnace at 625 °C for various times. .... 87

Figure 5–37. Change in microstructure of a 100 ksi flange plate that was heat treated in a laboratory furnace at 625 °C for various times. .... 88

Figure 5–38. Change in microstructure of a truss seat that was heat treated in a laboratory furnace at 625 °C for various times. .... 89

---

Figure 6–1. Knoop hardness traverses through welded joints.....	96
Figure 6–2. Knoop hardness traverses through welded joints.....	97
Figure 6–3. Hardness as a function of time and temperature for furnace exposure of 60 ksi flange plate. ....	98
Figure 6–4. Hardness as a function of time and temperature for furnace exposure of 42 ksi spandrel plate. ....	98
Figure 7–1. Heat capacity as a function of temperature for several low-alloy steels and pure iron. ....	110
Figure 7–2. Thermal expansion of pure iron showing the discontinuity in thermal expansion coefficient at the phase boundary. ....	111
Figure 7–3. Instantaneous thermal expansion coefficient for several low-alloy steels.....	112
Figure 7–4. Thermal conductivity as a function of temperature for 12 low-alloy steels. ....	113
Figure 7–5. Fractional error in estimating steel thermal conductivity from chemistry using Eq. 7–15.....	114
Figure 7–6. Thermal conductivity as a function of temperature, calculated from Eq. 7–15 for four grades of steel. ....	114
Figure 8–1. Differential thermal analysis scan for aluminum façade used on the WTC towers.....	117
Figure 9–1. Location of sprayed fire-resistive material that was scraped from a perimeter column of panel S-1.....	120

This page left intentionally blank.

## LIST OF TABLES

---

Table P-1.	Federal building and fire safety investigation of the WTC disaster .....	xxii
Table P-2.	Public meetings and briefings of the WTC Investigation.....	xxv
Table 4-1.	Comparison of chemistry results from two outside contractors and NIST. ....	22
Table 4-2.	Chemistry results of flange plates from perimeter columns.....	23
Table 4-3.	Chemistry results of outer web plate from perimeter columns.....	24
Table 4-4.	Chemistry results of inner web plate from perimeter columns.....	24
Table 4-5.	Chemistry results from samples that had significantly outlying values from average values of specified plate. ....	25
Table 4-6.	Chemistry results of panel splice connectors and floor truss connectors. ....	26
Table 4-7.	Chemistry results of spandrel material from perimeter columns (in mass fraction × 100). Shown are the averages with standard deviations given directly below. ....	27
Table 4-8.	Chemistry results of core column material (in mass fraction × 100). ....	28
Table 4-9.	Chemistry results of floor truss material (in mass fraction × 100). ....	29
Table 5-1.	ASTM grain size number and volume fraction pearlite for plates from the exterior panels.....	90
Table 5-2.	ASTM grain size number, volume fraction pearlite, and hardness results for panel splice connectors and floor truss connectors. ....	91
Table 5-3.	ASTM grain size number and volume fraction pearlite for core column material.....	92
Table 5-4.	ASTM grain size number, volume fraction pearlite, and hardness results for floor truss material. ....	92
Table 6-1.	Rockwell hardness data for exterior panel material. ....	99
Table 6-2.	Vickers hardness data for exterior panel material. ....	100
Table 6-3.	Rockwell and Vickers hardness data for core columns. ....	101
Table 6-4.	Hardness values for various furnace exposed WTC steel. ....	102
Table 7-1.	Mean thermal expansion coefficient. ....	115
Table 8-1.	Chemistry results for the aluminum façade used on the WTC towers. ....	118
Table 9-1.	Chemistry analysis of sprayed fire-resistive material.....	121

This page intentionally left blank.

# LIST OF ACRONYMS AND ABBREVIATIONS

---

## Acronyms

AISC	American Institute of Steel Construction
ASCE	American Society of Civil Engineers
ASTM	ASTM International
CE	carbon equivalent
CTE	coefficient of thermal expansion
DTAP	dissemination and technical assistance program
EDS	energy dispersive spectroscopy
FCAW	flux cored arc welding
FEMA	Federal Emergency Management Agency
HAZ	heat-affected zone
HRB	Rockwell Hardness B-Scale
HSLA	high-strength, low alloy
NIST	National Institute of Standards and Technology
R&D	research and development
SFRM	sprayed fire-resistive material
SMAW	shielded metal arc welding
USC	United States Code
WTC	World Trade Center
WTC 1	World Trade Center 1 (North Tower)
WTC 2	World Trade Center 2 (South Tower)
WTC 7	World Trade Center 7

## Abbreviations

°C	degrees Celsius
°F	degrees Fahrenheit
μm	micrometer
μm <sup>2</sup>	square micrometer
Al	aluminum

B	boron
C	carbon
Cr	chromium
Cu	copper
ft	foot
$F_y$	yield strength (AISC usage)
g	gram
gal	gallon
h	hour
in.	inch
K	kelvin
kg	kilogram
ksi	1,000 pounds per square inch
$m^2$	square meter
min	minute
mL	milliliter
mm	millimeter
$mm^2$	square millimeter
Mn	manganese
Mo	molybdenum
N	nitrogen
Nb	niobium
Ni	nickel
P	phosphorus
s	second
S	sulfur
Si	silicon
Ti	titanium
V	vanadium
Zr	zirconium

# METRIC CONVERSION TABLE

---



---

To convert from	to	Multiply by
-----------------	----	-------------

## AREA AND SECOND MOMENT OF AREA

square foot (ft <sup>2</sup> )	square meter (m <sup>2</sup> )	9.290 304 E-02
square inch (in. <sup>2</sup> )	square meter (m <sup>2</sup> )	6.4516 E-04
square inch (in. <sup>2</sup> )	square centimeter (cm <sup>2</sup> )	6.4516 E+00
square yard (yd <sup>2</sup> )	square meter (m <sup>2</sup> )	8.361 274 E-01

## ENERGY (includes WORK)

kilowatt hour (kW · h)	joule (J)	3.6 E+06
quad (1015 BtuIT)	joule (J)	1.055 056 E+18
therm (U.S.)	joule (J)	1.054 804 E+08
ton of TNT (energy equivalent)	joule (J)	4.184 E+09
watt hour (W · h)	joule (J)	3.6 E+03
watt second (W · s)	joule (J)	1.0 E+00

## LENGTH

foot (ft)	meter (m)	3.048 E-01
inch (in)	meter (m)	2.54 E-02
inch (in.)	centimeter (cm)	2.54 E+00
micron (m)	meter (m)	1.0 E-06
yard (yd)	meter (m)	9.144 E-01

## MASS DIVIDED BY AREA

pound per square foot (lb/ft <sup>2</sup> )	kilogram per square meter (kg/m <sup>2</sup> )	4.882 428 E+00
pound per square inch (not pound force) (lb/in. <sup>2</sup> )	kilogram per square meter (kg/m <sup>2</sup> )	7.030 696 E+02

## MASS DIVIDED BY LENGTH

pound per foot (lb/ft)	kilogram per meter (kg/m)	1.488 164 E+00
pound per inch (lb/in.)	kilogram per meter (kg/m)	1.785 797 E+01
pound per yard (lb/yd)	kilogram per meter (kg/m)	4.960 546 E-01



<b>To convert from</b>	<b>to</b>	<b>Multiply by</b>
<b>VOLUME (includes CAPACITY)</b>		
cubic foot (ft <sup>3</sup> )	cubic meter (m <sup>3</sup> )	2.831 685 E-02
cubic inch (in. <sup>3</sup> )	cubic meter (m <sup>3</sup> )	1.638 706 E-05
cubic yard (yd <sup>3</sup> )	cubic meter (m <sup>3</sup> )	7.645 549 E-01
gallon (U.S.) (gal)	cubic meter (m <sup>3</sup> )	3.785 412 E-03
gallon (U.S.) (gal)	liter (L)	3.785 412 E+00
liter (L)	cubic meter (m <sup>3</sup> )	1.0 E-03
ounce (U.S. fluid) (fl oz)	cubic meter (m <sup>3</sup> )	2.957 353 E-05
ounce (U.S. fluid) (fl oz)	milliliter (mL)	2.957 353 E+01

This page left intentionally blank.

# PREFACE

---

## Genesis of This Investigation

Immediately following the terrorist attack on the World Trade Center (WTC) on September 11, 2001, the Federal Emergency Management Agency (FEMA) and the American Society of Civil Engineers began planning a building performance study of the disaster. The week of October 7, as soon as the rescue and search efforts ceased, the Building Performance Study Team went to the site and began its assessment. This was to be a brief effort, as the study team consisted of experts who largely volunteered their time away from their other professional commitments. The Building Performance Study Team issued its report in May 2002, fulfilling its goal “to determine probable failure mechanisms and to identify areas of future investigation that could lead to practical measures for improving the damage resistance of buildings against such unforeseen events.”

On August 21, 2002, with funding from the U.S. Congress through FEMA, the National Institute of Standards and Technology (NIST) announced its building and fire safety investigation of the WTC disaster. On October 1, 2002, the National Construction Safety Team Act (Public Law 107-231), was signed into law. The NIST WTC Investigation was conducted under the authority of the National Construction Safety Team Act.

The goals of the investigation of the WTC disaster were:

- To investigate the building construction, the materials used, and the technical conditions that contributed to the outcome of the WTC disaster.
- To serve as the basis for:
  - Improvements in the way buildings are designed, constructed, maintained, and used;
  - Improved tools and guidance for industry and safety officials;
  - Recommended revisions to current codes, standards, and practices; and
  - Improved public safety.

The specific objectives were:

1. Determine why and how WTC 1 and WTC 2 collapsed following the initial impacts of the aircraft and why and how WTC 7 collapsed;
2. Determine why the injuries and fatalities were so high or low depending on location, including all technical aspects of fire protection, occupant behavior, evacuation, and emergency response;
3. Determine what procedures and practices were used in the design, construction, operation, and maintenance of WTC 1, 2, and 7; and
4. Identify, as specifically as possible, areas in current building and fire codes, standards, and practices that warrant revision.

NIST is a nonregulatory agency of the U.S. Department of Commerce’s Technology Administration. The purpose of NIST investigations is to improve the safety and structural integrity of buildings in the United States, and the focus is on fact finding. NIST investigative teams are authorized to assess building performance and emergency response and evacuation procedures in the wake of any building failure that has resulted in substantial loss of life or that posed significant potential of substantial loss of life. NIST does not have the statutory authority to make findings of fault nor negligence by individuals or organizations. Further, no part of any report resulting from a NIST investigation into a building failure or from an investigation under the National Construction Safety Team Act may be used in any suit or action for damages arising out of any matter mentioned in such report (15 USC 281a, as amended by Public Law 107-231).

### Organization of the Investigation

The National Construction Safety Team for this Investigation, appointed by the then NIST Director, Dr. Arden L. Bement, Jr., was led by Dr. S. Shyam Sunder. Dr. William L. Grosshandler served as Associate Lead Investigator, Mr. Stephen A. Cauffman served as Program Manager for Administration, and Mr. Harold E. Nelson served on the team as a private sector expert. The Investigation included eight interdependent projects whose leaders comprised the remainder of the team. A detailed description of each of these eight projects is available at <http://wtc.nist.gov>. The purpose of each project is summarized in Table P–1, and the key interdependencies among the projects are illustrated in Fig. P–1.

**Table P–1. Federal building and fire safety investigation of the WTC disaster.**

Technical Area and Project Leader	Project Purpose
Analysis of Building and Fire Codes and Practices; Project Leaders: Dr. H. S. Lew and Mr. Richard W. Bukowski	Document and analyze the code provisions, procedures, and practices used in the design, construction, operation, and maintenance of the structural, passive fire protection, and emergency access and evacuation systems of WTC 1, 2, and 7.
Baseline Structural Performance and Aircraft Impact Damage Analysis; Project Leader: Dr. Fahim H. Sadek	Analyze the baseline performance of WTC 1 and WTC 2 under design, service, and abnormal loads, and aircraft impact damage on the structural, fire protection, and egress systems.
Mechanical and Metallurgical Analysis of Structural Steel; Project Leader: Dr. Frank W. Gayle	Determine and analyze the mechanical and metallurgical properties and quality of steel, weldments, and connections from steel recovered from WTC 1, 2, and 7.
Investigation of Active Fire Protection Systems; Project Leader: Dr. David D. Evans; Dr. William Grosshandler	Investigate the performance of the active fire protection systems in WTC 1, 2, and 7 and their role in fire control, emergency response, and fate of occupants and responders.
Reconstruction of Thermal and Tenability Environment; Project Leader: Dr. Richard G. Gann	Reconstruct the time-evolving temperature, thermal environment, and smoke movement in WTC 1, 2, and 7 for use in evaluating the structural performance of the buildings and behavior and fate of occupants and responders.
Structural Fire Response and Collapse Analysis; Project Leaders: Dr. John L. Gross and Dr. Therese P. McAllister	Analyze the response of the WTC towers to fires with and without aircraft damage, the response of WTC 7 in fires, the performance of composite steel-trussed floor systems, and determine the most probable structural collapse sequence for WTC 1, 2, and 7.
Occupant Behavior, Egress, and Emergency Communications; Project Leader: Mr. Jason D. Averill	Analyze the behavior and fate of occupants and responders, both those who survived and those who did not, and the performance of the evacuation system.
Emergency Response Technologies and Guidelines; Project Leader: Mr. J. Randall Lawson	Document the activities of the emergency responders from the time of the terrorist attacks on WTC 1 and WTC 2 until the collapse of WTC 7, including practices followed and technologies used.

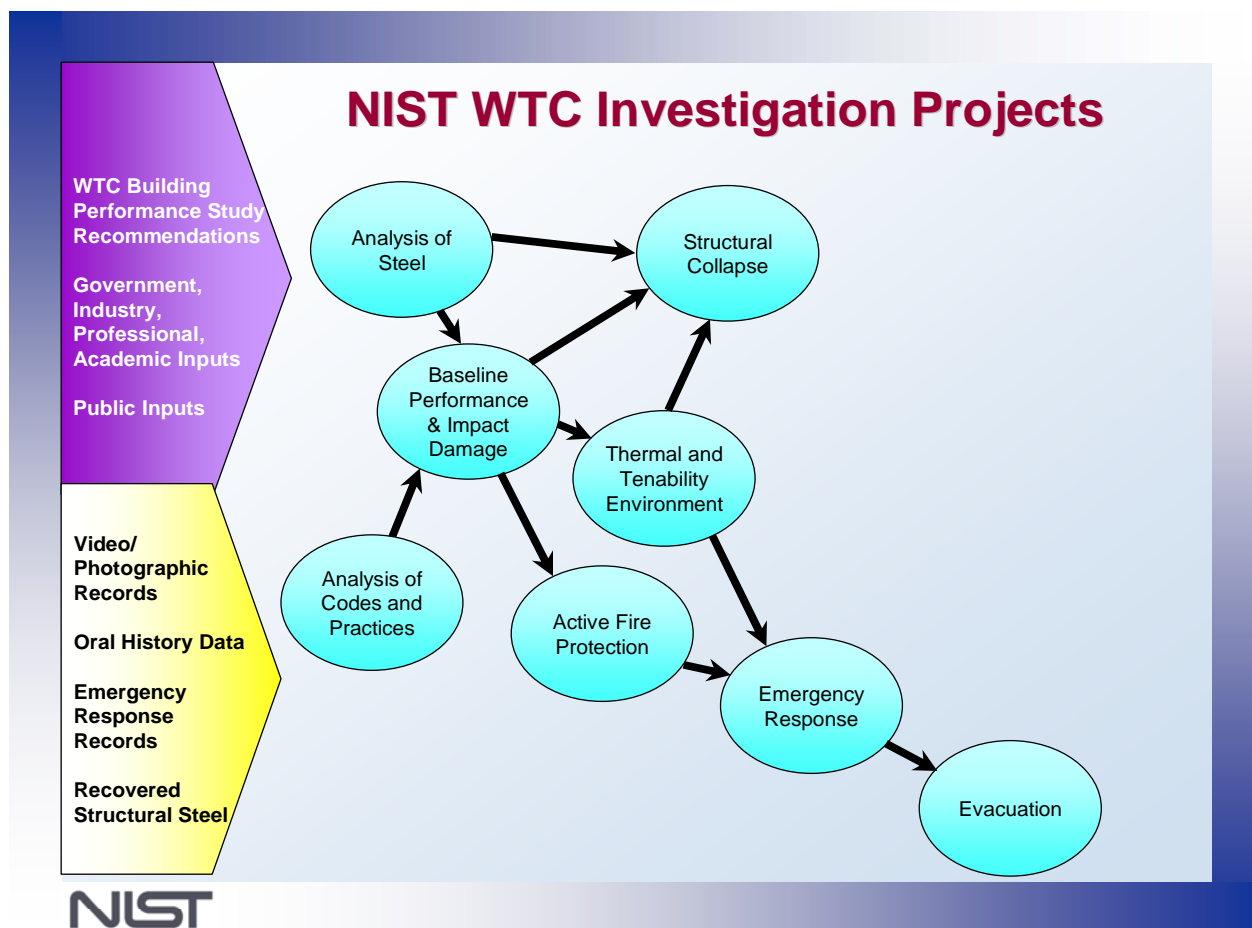


**Figure P-1. The eight projects in the federal building and fire safety investigation of the WTC disaster.**

### **National Construction Safety Team Advisory Committee**

The NIST Director also established an advisory committee as mandated under the National Construction Safety Team Act. The initial members of the committee were appointed following a public solicitation. These were:

- Paul Fitzgerald, Executive Vice President (retired) FM Global, National Construction Safety Team Advisory Committee Chair
- John Barsom, President, Barsom Consulting, Ltd.
- John Bryan, Professor Emeritus, University of Maryland
- David Collins, President, The Preview Group, Inc.
- Glenn Corbett, Professor, John Jay College of Criminal Justice
- Philip DiNunno, President, Hughes Associates, Inc.

- Robert Hanson, Professor Emeritus, University of Michigan
- Charles Thornton, Co-Chairman and Managing Principal, The Thornton-Tomasetti Group, Inc.
- Kathleen Tierney, Director, Natural Hazards Research and Applications Information Center, University of Colorado at Boulder
- Forman Williams, Director, Center for Energy Research, University of California at San Diego

This National Construction Safety Team Advisory Committee provided technical advice during the Investigation and commentary on drafts of the Investigation reports prior to their public release. NIST has benefited from the work of many people in the preparation of these reports, including the National Construction Safety Team Advisory Committee. The content of the reports and recommendations, however, are solely the responsibility of NIST.

### **Public Outreach**

During the course of this Investigation, NIST held public briefings and meetings (listed in Table P–2) to solicit input from the public, present preliminary findings, and obtain comments on the direction and progress of the Investigation from the public and the Advisory Committee.

NIST maintained a publicly accessible Web site during this Investigation at <http://wtc.nist.gov>. The site contained extensive information on the background and progress of the Investigation.

### **NIST's WTC Public-Private Response Plan**

The collapse of the WTC buildings has led to broad reexamination of how tall buildings are designed, constructed, maintained, and used, especially with regard to major events such as fires, natural disasters, and terrorist attacks. Reflecting the enhanced interest in effecting necessary change, NIST, with support from Congress and the Administration, has put in place a program, the goal of which is to develop and implement the standards, technology, and practices needed for cost-effective improvements to the safety and security of buildings and building occupants, including evacuation, emergency response procedures, and threat mitigation.

The strategy to meet this goal is a three-part NIST-led public-private response program that includes:

- A federal building and fire safety investigation to study the most probable factors that contributed to post-aircraft impact collapse of the WTC towers and the 47-story WTC 7 building, and the associated evacuation and emergency response experience.
- A research and development (R&D) program to (a) facilitate the implementation of recommendations resulting from the WTC Investigation, and (b) provide the technical basis for cost-effective improvements to national building and fire codes, standards, and practices that enhance the safety of buildings, their occupants, and emergency responders.

**Table P–2. Public meetings and briefings of the WTC Investigation.**

<b>Date</b>	<b>Location</b>	<b>Principal Agenda</b>
June 24, 2002	New York City, NY	Public meeting: Public comments on the <i>Draft Plan</i> for the pending WTC Investigation.
August 21, 2002	Gaithersburg, MD	Media briefing announcing the formal start of the Investigation.
December 9, 2002	Washington, DC	Media briefing on release of the <i>Public Update</i> and NIST request for photographs and videos.
April 8, 2003	New York City, NY	Joint public forum with Columbia University on first-person interviews.
April 29–30, 2003	Gaithersburg, MD	NCST Advisory Committee meeting on plan for and progress on WTC Investigation with a public comment session.
May 7, 2003	New York City, NY	Media briefing on release of <i>May 2003 Progress Report</i> .
August 26–27, 2003	Gaithersburg, MD	NCST Advisory Committee meeting on status of the WTC investigation with a public comment session.
September 17, 2003	New York City, NY	Media and public briefing on initiation of first-person data collection projects.
December 2–3, 2003	Gaithersburg, MD	NCST Advisory Committee meeting on status and initial results and release of the <i>Public Update</i> with a public comment session.
February 12, 2004	New York City, NY	Public meeting on progress and preliminary findings with public comments on issues to be considered in formulating final recommendations.
June 18, 2004	New York City, NY	Media/public briefing on release of <i>June 2004 Progress Report</i> .
June 22–23, 2004	Gaithersburg, MD	NCST Advisory Committee meeting on the status of and preliminary findings from the WTC Investigation with a public comment session.
August 24, 2004	Northbrook, IL	Public viewing of standard fire resistance test of WTC floor system at Underwriters Laboratories, Inc.
October 19–20, 2004	Gaithersburg, MD	NCST Advisory Committee meeting on status and near complete set of preliminary findings with a public comment session.
November 22, 2004	Gaithersburg, MD	NCST Advisory Committee discussion on draft annual report to Congress, a public comment session, and a closed session to discuss pre-draft recommendations for WTC Investigation.
April 5, 2005	New York City, NY	Media and public briefing on release of the probable collapse sequence for the WTC towers and draft reports for the projects on codes and practices, evacuation, and emergency response.
June 23, 2005	New York City, NY	Media and public briefing on release of all draft reports for the WTC towers and draft recommendations for public comment.
September 12–13, 2005	Gaithersburg, MD	NCST Advisory Committee meeting on disposition of public comments and update to draft reports for the WTC towers.
September 13–15, 2005	Gaithersburg, MD	WTC Technical Conference for stakeholders and technical community for dissemination of findings and recommendations and opportunity for public to make technical comments.

- A dissemination and technical assistance program (DTAP) to (a) engage leaders of the construction and building community in ensuring timely adoption and widespread use of proposed changes to practices, standards, and codes resulting from the WTC Investigation and the R&D program, and (b) provide practical guidance and tools to better prepare facility owners, contractors, architects, engineers, emergency responders, and regulatory authorities to respond to future disasters.

The desired outcomes are to make buildings, occupants, and first responders safer in future disaster events.

## National Construction Safety Team Reports on the WTC Investigation

A final report on the collapse of the WTC towers is being issued as NIST NCSTAR 1. A companion report on the collapse of WTC 7 is being issued as NIST NCSTAR 1A. The present report is one of a set that provides more detailed documentation of the Investigation findings and the means by which these technical results were achieved. As such, it is part of the archival record of this Investigation. The titles of the full set of Investigation publications are:

NIST (National Institute of Standards and Technology). 2005. *Federal Building and Fire Safety Investigation of the World Trade Center Disaster: Final Report on the Collapse of the World Trade Center Towers*. NIST NCSTAR 1. Gaithersburg, MD, September.

NIST (National Institute of Standards and Technology). 2008. *Federal Building and Fire Safety Investigation of the World Trade Center Disaster: Final Report on the Collapse of World Trade Center 7*. NIST NCSTAR 1A. Gaithersburg, MD, November.

Lew, H. S., R. W. Bukowski, and N. J. Carino. 2005. *Federal Building and Fire Safety Investigation of the World Trade Center Disaster: Design, Construction, and Maintenance of Structural and Life Safety Systems*. NIST NCSTAR 1-1. National Institute of Standards and Technology. Gaithersburg, MD, September.

Fanella, D. A., A. T. Derecho, and S. K. Ghosh. 2005. *Federal Building and Fire Safety Investigation of the World Trade Center Disaster: Design and Construction of Structural Systems*. NIST NCSTAR 1-1A. National Institute of Standards and Technology. Gaithersburg, MD, September.

Ghosh, S. K., and X. Liang. 2005. *Federal Building and Fire Safety Investigation of the World Trade Center Disaster: Comparison of Building Code Structural Requirements*. NIST NCSTAR 1-1B. National Institute of Standards and Technology. Gaithersburg, MD, September.

Fanella, D. A., A. T. Derecho, and S. K. Ghosh. 2005. *Federal Building and Fire Safety Investigation of the World Trade Center Disaster: Maintenance and Modifications to Structural Systems*. NIST NCSTAR 1-1C. National Institute of Standards and Technology. Gaithersburg, MD, September.

Grill, R. A., and D. A. Johnson. 2005. *Federal Building and Fire Safety Investigation of the World Trade Center Disaster: Fire Protection and Life Safety Provisions Applied to the Design and Construction of World Trade Center 1, 2, and 7 and Post-Construction Provisions Applied after Occupancy*. NIST NCSTAR 1-1D. National Institute of Standards and Technology. Gaithersburg, MD, September.

Razza, J. C., and R. A. Grill. 2005. *Federal Building and Fire Safety Investigation of the World Trade Center Disaster: Comparison of Codes, Standards, and Practices in Use at the Time of the Design and Construction of World Trade Center 1, 2, and 7*. NIST NCSTAR 1-1E. National Institute of Standards and Technology. Gaithersburg, MD, September.

Grill, R. A., D. A. Johnson, and D. A. Fanella. 2005. *Federal Building and Fire Safety Investigation of the World Trade Center Disaster: Comparison of the 1968 and Current (2003) New*

- York City Building Code Provisions*. NIST NCSTAR 1-1F. National Institute of Standards and Technology. Gaithersburg, MD, September.
- Grill, R. A., and D. A. Johnson. 2005. *Federal Building and Fire Safety Investigation of the World Trade Center Disaster: Amendments to the Fire Protection and Life Safety Provisions of the New York City Building Code by Local Laws Adopted While World Trade Center 1, 2, and 7 Were in Use*. NIST NCSTAR 1-1G. National Institute of Standards and Technology. Gaithersburg, MD, September.
- Grill, R. A., and D. A. Johnson. 2005. *Federal Building and Fire Safety Investigation of the World Trade Center Disaster: Post-Construction Modifications to Fire Protection and Life Safety Systems of World Trade Center 1 and 2*. NIST NCSTAR 1-1H. National Institute of Standards and Technology. Gaithersburg, MD, September.
- Grill, R. A., D. A. Johnson, and D. A. Fanella. 2005. *Federal Building and Fire Safety Investigation of the World Trade Center Disaster: Post-Construction Modifications to Fire Protection, Life Safety, and Structural Systems of World Trade Center 7*. NIST NCSTAR 1-1I. National Institute of Standards and Technology. Gaithersburg, MD, September.
- Grill, R. A., and D. A. Johnson. 2005. *Federal Building and Fire Safety Investigation of the World Trade Center Disaster: Design, Installation, and Operation of Fuel System for Emergency Power in World Trade Center 7*. NIST NCSTAR 1-1J. National Institute of Standards and Technology. Gaithersburg, MD, September.
- Sadek, F. 2005. *Federal Building and Fire Safety Investigation of the World Trade Center Disaster: Baseline Structural Performance and Aircraft Impact Damage Analysis of the World Trade Center Towers*. NIST NCSTAR 1-2. National Institute of Standards and Technology. Gaithersburg, MD, September.
- Faschan, W. J., and R. B. Garlock. 2005. *Federal Building and Fire Safety Investigation of the World Trade Center Disaster: Reference Structural Models and Baseline Performance Analysis of the World Trade Center Towers*. NIST NCSTAR 1-2A. National Institute of Standards and Technology. Gaithersburg, MD, September.
- Kirkpatrick, S. W., R. T. Bocchieri, F. Sadek, R. A. MacNeill, S. Holmes, B. D. Peterson, R. W. Cilke, C. Navarro. 2005. *Federal Building and Fire Safety Investigation of the World Trade Center Disaster: Analysis of Aircraft Impacts into the World Trade Center Towers*, NIST NCSTAR 1-2B. National Institute of Standards and Technology. Gaithersburg, MD, September.
- Gayle, F. W., R. J. Fields, W. E. Luecke, S. W. Banovic, T. Foecke, C. N. McCowan, T. A. Siewert, and J. D. McColskey. 2005. *Federal Building and Fire Safety Investigation of the World Trade Center Disaster: Mechanical and Metallurgical Analysis of Structural Steel*. NIST NCSTAR 1-3. National Institute of Standards and Technology. Gaithersburg, MD, September.
- Luecke, W. E., T. A. Siewert, and F. W. Gayle. 2005. *Federal Building and Fire Safety Investigation of the World Trade Center Disaster: Contemporaneous Structural Steel Specifications*. NIST Special Publication 1-3A. National Institute of Standards and Technology. Gaithersburg, MD, September.

- Banovic, S. W. 2005. *Federal Building and Fire Safety Investigation of the World Trade Center Disaster: Steel Inventory and Identification*. NIST NCSTAR 1-3B. National Institute of Standards and Technology. Gaithersburg, MD, September.
- Banovic, S. W., and T. Foecke. 2005. *Federal Building and Fire Safety Investigation of the World Trade Center Disaster: Damage and Failure Modes of Structural Steel Components*. NIST NCSTAR 1-3C. National Institute of Standards and Technology. Gaithersburg, MD, September.
- Luecke, W. E., J. D. McColskey, C. N. McCowan, S. W. Banovic, R. J. Fields, T. Foecke, T. A. Siewert, and F. W. Gayle. 2005. *Federal Building and Fire Safety Investigation of the World Trade Center Disaster: Mechanical Properties of Structural Steels*. NIST NCSTAR 1-3D. National Institute of Standards and Technology. Gaithersburg, MD, September.
- Banovic, S. W., C. N. McCowan, and W. E. Luecke. 2005. *Federal Building and Fire Safety Investigation of the World Trade Center Disaster: Physical Properties of Structural Steels*. NIST NCSTAR 1-3E. National Institute of Standards and Technology. Gaithersburg, MD, September.
- Evans, D. D., R. D. Peacock, E. D. Kuligowski, W. S. Dols, and W. L. Grosshandler. 2005. *Federal Building and Fire Safety Investigation of the World Trade Center Disaster: Active Fire Protection Systems*. NIST NCSTAR 1-4. National Institute of Standards and Technology. Gaithersburg, MD, September.
- Kuligowski, E. D., D. D. Evans, and R. D. Peacock. 2005. *Federal Building and Fire Safety Investigation of the World Trade Center Disaster: Post-Construction Fires Prior to September 11, 2001*. NIST NCSTAR 1-4A. National Institute of Standards and Technology. Gaithersburg, MD, September.
- Hopkins, M., J. Schoenrock, and E. Budnick. 2005. *Federal Building and Fire Safety Investigation of the World Trade Center Disaster: Fire Suppression Systems*. NIST NCSTAR 1-4B. National Institute of Standards and Technology. Gaithersburg, MD, September.
- Keough, R. J., and R. A. Grill. 2005. *Federal Building and Fire Safety Investigation of the World Trade Center Disaster: Fire Alarm Systems*. NIST NCSTAR 1-4C. National Institute of Standards and Technology. Gaithersburg, MD, September.
- Ferreira, M. J., and S. M. Strege. 2005. *Federal Building and Fire Safety Investigation of the World Trade Center Disaster: Smoke Management Systems*. NIST NCSTAR 1-4D. National Institute of Standards and Technology. Gaithersburg, MD, September.
- Gann, R. G., A. Hamins, K. B. McGrattan, G. W. Mulholland, H. E. Nelson, T. J. Ohlemiller, W. M. Pitts, and K. R. Prasad. 2005. *Federal Building and Fire Safety Investigation of the World Trade Center Disaster: Reconstruction of the Fires in the World Trade Center Towers*. NIST NCSTAR 1-5. National Institute of Standards and Technology. Gaithersburg, MD, September.
- Pitts, W. M., K. M. Butler, and V. Junker. 2005. *Federal Building and Fire Safety Investigation of the World Trade Center Disaster: Visual Evidence, Damage Estimates, and Timeline Analysis*. NIST NCSTAR 1-5A. National Institute of Standards and Technology. Gaithersburg, MD, September.

Hamins, A., A. Maranghides, K. B. McGrattan, E. Johnsson, T. J. Ohlemiller, M. Donnelly, J. Yang, G. Mulholland, K. R. Prasad, S. Kukuck, R. Anleitner and T. McAllister. 2005. *Federal Building and Fire Safety Investigation of the World Trade Center Disaster: Experiments and Modeling of Structural Steel Elements Exposed to Fire*. NIST NCSTAR 1-5B. National Institute of Standards and Technology. Gaithersburg, MD, September.

Ohlemiller, T. J., G. W. Mulholland, A. Maranghides, J. J. Filliben, and R. G. Gann. 2005. *Federal Building and Fire Safety Investigation of the World Trade Center Disaster: Fire Tests of Single Office Workstations*. NIST NCSTAR 1-5C. National Institute of Standards and Technology. Gaithersburg, MD, September.

Gann, R. G., M. A. Riley, J. M. Repp, A. S. Whittaker, A. M. Reinhorn, and P. A. Hough. 2005. *Federal Building and Fire Safety Investigation of the World Trade Center Disaster: Reaction of Ceiling Tile Systems to Shocks*. NIST NCSTAR 1-5D. National Institute of Standards and Technology. Gaithersburg, MD, September.

Hamins, A., A. Maranghides, K. B. McGrattan, T. J. Ohlemiller, and R. Anleitner. 2005. *Federal Building and Fire Safety Investigation of the World Trade Center Disaster: Experiments and Modeling of Multiple Workstations Burning in a Compartment*. NIST NCSTAR 1-5E. National Institute of Standards and Technology. Gaithersburg, MD, September.

McGrattan, K. B., C. Bouldin, and G. Forney. 2005. *Federal Building and Fire Safety Investigation of the World Trade Center Disaster: Computer Simulation of the Fires in the World Trade Center Towers*. NIST NCSTAR 1-5F. National Institute of Standards and Technology. Gaithersburg, MD, September.

Prasad, K. R., and H. R. Baum. 2005. *Federal Building and Fire Safety Investigation of the World Trade Center Disaster: Fire Structure Interface and Thermal Response of the World Trade Center Towers*. NIST NCSTAR 1-5G. National Institute of Standards and Technology. Gaithersburg, MD, September.

Gross, J. L., and T. McAllister. 2005. *Federal Building and Fire Safety Investigation of the World Trade Center Disaster: Structural Fire Response and Probable Collapse Sequence of the World Trade Center Towers*. NIST NCSTAR 1-6. National Institute of Standards and Technology. Gaithersburg, MD, September.

Carino, N. J., M. A. Starnes, J. L. Gross, J. C. Yang, S. Kukuck, K. R. Prasad, and R. W. Bukowski. 2005. *Federal Building and Fire Safety Investigation of the World Trade Center Disaster: Passive Fire Protection*. NIST NCSTAR 1-6A. National Institute of Standards and Technology. Gaithersburg, MD, September.

Gross, J., F. Hervey, M. Izydorek, J. Mammoser, and J. Treadway. 2005. *Federal Building and Fire Safety Investigation of the World Trade Center Disaster: Fire Resistance Tests of Floor Truss Systems*. NIST NCSTAR 1-6B. National Institute of Standards and Technology. Gaithersburg, MD, September.

Zarghamee, M. S., S. Bolourchi, D. W. Eggers, Ö. O. Erbay, F. W. Kan, Y. Kitane, A. A. Liepins, M. Mudlock, W. I. Naguib, R. P. Ojdrovic, A. T. Sarawit, P. R. Barrett, J. L. Gross, and

T. P. McAllister. 2005. *Federal Building and Fire Safety Investigation of the World Trade Center Disaster: Component, Connection, and Subsystem Structural Analysis*. NIST NCSTAR 1-6C. National Institute of Standards and Technology. Gaithersburg, MD, September.

Zarghamee, M. S., Y. Kitane, Ö. O. Erbay, T. P. McAllister, and J. L. Gross. 2005. *Federal Building and Fire Safety Investigation of the World Trade Center Disaster: Global Structural Analysis of the Response of the World Trade Center Towers to Impact Damage and Fire*. NIST NCSTAR 1-6D. National Institute of Standards and Technology. Gaithersburg, MD, September.

Averill, J. D., D. S. Mileti, R. D. Peacock, E. D. Kuligowski, N. Groner, G. Proulx, P. A. Reneke, and H. E. Nelson. 2005. *Federal Building and Fire Safety Investigation of the World Trade Center Disaster: Occupant Behavior, Egress, and Emergency Communication*. NIST NCSTAR 1-7. National Institute of Standards and Technology. Gaithersburg, MD, September.

Fahy, R., and G. Proulx. 2005. *Federal Building and Fire Safety Investigation of the World Trade Center Disaster: Analysis of Published Accounts of the World Trade Center Evacuation*. NIST NCSTAR 1-7A. National Institute of Standards and Technology. Gaithersburg, MD, September.

Zmud, J. 2005. *Federal Building and Fire Safety Investigation of the World Trade Center Disaster: Technical Documentation for Survey Administration*. NIST NCSTAR 1-7B. National Institute of Standards and Technology. Gaithersburg, MD, September.

Lawson, J. R., and R. L. Vettori. 2005. *Federal Building and Fire Safety Investigation of the World Trade Center Disaster: The Emergency Response Operations*. NIST NCSTAR 1-8. National Institute of Standards and Technology. Gaithersburg, MD, September.

McAllister, T., R. G. Gann, J. D. Averill, J. L. Gross, W. L. Grosshandler, J. R. Lawson, K. B. McGrattan, H. E. Nelson, W. M. Pitts, K. R. Prasad, F. H. Sadek. 2008. *Federal Building and Fire Safety Investigation of the World Trade Center Disaster: Structural Fire Response and Probable Collapse Sequence of World Trade Center Building 7*. NIST NCSTAR 1-9. National Institute of Standards and Technology. Gaithersburg, MD, November.

MacNeill, R., S. Kirkpatrick, B. Peterson, and R. Bocchieri. 2008. *Federal Building and Fire Safety Investigation of the World Trade Center Disaster: Global Structural Analysis of the Response of World Trade Center Building 7 to Fires and Debris Impact Damage*. NIST NCSTAR 1-9A. National Institute of Standards and Technology. Gaithersburg, MD, November.

## ACKNOWLEDGMENTS

---

The National Institute of Standards and Technology (NIST) thanks the volunteers of the Structural Engineers Association of New York for their efforts in the recovery of the steel components. Countless hours were unselfishly spent in the recovery yards searching for these invaluable pieces that are an integral component of this investigation. Without their efforts, this report would not have been possible.

The Federal Emergency Management Agency/American Society of Civil Engineers Building Performance Study Team; Professor A. Astaneh-Asl of the University of California, Berkeley, California; and the National Science Foundation are also acknowledged for their help in the recovery effort.

Mr. David R. Kelley of NIST is recognized for all of his efforts in sample removal, metallographic preparation, and hardness evaluation of the World Trade Center (WTC) steels.

Dr. Kil-Won Moon of NIST is recognized for the differential thermal analysis of the aluminum façade used on the WTC towers.

Ms. Maureen E. Williams of NIST is recognized for characterizing the sprayed fire-resistive material removed from a perimeter column from the WTC towers.

Mr. Rodney D. Jiggetts of NIST is recognized for filming sample removal during the initial stages of the investigation.

Ms. Sandra Claggett of NIST is recognized for conducting the initial volume fraction pearlite and grain size measurements.

Dr. Donald E. Kramer and Dr. Michael F. Savage, both formerly of NIST, are recognized for their help in sample removal in the early stages of the investigation.

Dr. Gregory C. Turk, Dr. John R. Sieber, and Dr. Michael R. Winchester of NIST are recognized for their contributions to the chemical analysis of the structural steels.

Mr. Arlan O. Benschoter and Dr. Arnold R. Marder of the Department of Materials Science and Engineering, Lehigh University, are thanked for the numerous conversations concerning the metallography of carbon steels and review of this report.

This page intentionally left blank.

## EXECUTIVE SUMMARY

---

This report describes the physical properties of the structural steel recovered from the World Trade Center (WTC) towers, including the chemical composition, microstructure, and thermal properties of the steels. While not a physical property, hardness of the steels also was measured and discussed in relation to strengthening mechanisms of the material. The primary focus was on structural components with known as-built locations from WTC 1 and WTC 2. In order to fully characterize all of the structural elements, some samples were evaluated that did not have known as-built locations. The physical property information was found useful in helping to identify specific grades and producers of steel used for the various components located within the towers. In addition, the thermal properties were developed for use in the models of the building response to fire. Although no recovered structural elements were from WTC 7, physical property data of steels from this building were estimated based upon values found in the literature.

In addition to the structural steel, chemistry information was obtained for a piece of the aluminum façade used on the WTC towers and the sprayed fire-resistive material (SFRM) found on the structural elements from WTC 1 and WTC 2.

The major findings of this report are:

- Two different microstructural types were observed for the recovered WTC steels: hot-rolled for low strength components and quenched-and-tempered for high strength components.
- In general, the steel used for the construction of the WTC towers was found to be of good quality. There did not appear to be atypical defects in the microstructure as a result of processing of the individual plates. Further, the weldments used to build-up the box columns and attach the floor truss connectors to the columns were sound with no visible flaws.
- For a given yield strength ( $F_y$ ), the flange, outer web, and spandrel steel in the perimeter panels were found to be nearly identical, with indistinguishable chemistries and similar microstructures and hardness values. The inner web was found to be distinguishable from the other plates, for  $F_y$  less than 80 ksi, in terms of the physical properties evaluated. Inner webs with  $F_y$  equal to 80 ksi and 100 ksi were the same steel as used for the flanges. These results support the contemporaneous documents stating that the flange, outer web, and spandrel plates were produced by a single company (Yawata Iron and Steel Co.) and that the inner web plates were primarily supplied domestically.
- The recovered core columns were found to vary in composition for a given  $F_y$  and shape (built-up box, rolled wide-flange). This result is consistent with the contemporaneous documents stating that numerous suppliers produced the steel to be used for these structural components.
- Butt plates of the perimeter panel met chemistry specifications for several Yawata steels.

- Construction bolts were either A 325 or A 490 bolts. This was primarily determined by the stampings on the head. One bolt designated as A 325 was analyzed and met the chemistry specifications for A 325 Type 1.
- Chords and rods that composed the floor trusses, supplied by Laclede Steel Co., were either ASTM International (ASTM) A 36 or ASTM A 242.
- Other structural elements (floor truss connectors, core channels, spandrel splice plates, etc.) met specifications for ASTM A 36. Compositions varied significantly, which may indicate that numerous suppliers completed the steel orders for these components.
- Discernible changes to the microstructure of furnace exposed WTC steel were observed when exposed to a temperature of 625 °C for as little as 0.25 h. At or below 500 °C, no indication of microstructural change was apparent using light optical microscopy. The hardness of these samples varied for a given temperature and material type, but correlated well with microstructural observations:
  - Hot-rolled steels below 500 °C experienced a slight increase in hardness, which may be due to strain-age hardening effects;
  - Hot-rolled steels at 500 °C and 625 °C experienced a decrease in hardness. Depending upon the prior thermomechanical history, an increase in hardness was observed if the extent of spheroidization was such that large carbide particles formed; and
  - Quenched-and-tempered steels at 625 °C had a continual decrease in hardness up to the maximum exposure time of 2 h.

These results were used in the report “Damage and Failure Modes of Structural Steel Components” (NIST NCSTAR 1-3C)<sup>1</sup> to assess the steel for fire-related damage.

- Microhardness traces across weld cross-sections from perimeter panel columns displayed an increase in hardness near the fusion line in the heat affected zone of the base plate. This was related to the alteration of microstructure due to the heat input from the welding process.
- Thermal property values as a function of temperature were provided for modeling the structural steel response to fire. These properties include specific heat ( $C_p$ ), coefficient of thermal expansion ( $\alpha$ ), and thermal conductivity ( $k$ ).
- A piece of the aluminum façade used on the WTC towers was analyzed and found to be consistent with the non-heat treatable aluminum-manganese alloy AA 3003.
- A sample of SFRM scraped from a recovered perimeter column of WTC 1 was chemically analyzed. While the chemical composition of the material was proprietary, the results were consistent, on a qualitative basis, with the information presently found on the manufacturer’s web site.

---

<sup>1</sup> This reference is to one of the companion documents from this Investigation. A list of these documents appears in the Preface to this report.

# Chapter 1

## INTRODUCTION

---

The purpose of the mechanical and metallurgical analysis of structural steel was to analyze structural steel available from World Trade Center (WTC) 1, 2, and 7 for determining the metallurgical and mechanical properties and quality of the metal, weldments, and connections, and providing these data to other investigation projects. The properties determined were used in two ways: (1) properties were correlated with the design requirements of the buildings to determine whether the specified steel met the design requirements, and (2) properties were supplied as input for models of building performance.

This report is an output of a specific task of the WTC Investigation defined as:

Determine the metallurgical and mechanical properties of the steel, weldments, and connections, including temperature dependence of properties. The grades of steel will be identified in the columns, welds, spandrels, trusses, truss seats, and fasteners. The identification will include composition, microstructure, mechanical, and impact properties. This project will provide steel property data, including models of elevated temperature behavior for relevant steels, to estimate damage to the structural steel members from aircraft impact, evaluate structural fire response, and study the initiation and propagation of structural collapse in the project on Structural Fire Response and Collapse Analysis.

### 1.1 SCOPE OF REPORT

This report describes in detail the physical properties of the structural steel used in the construction of the WTC towers, including the chemical composition, microstructure, and thermal properties of the steels. While not a physical property, hardness of the steels was also measured and discussed in relation to strengthening mechanisms of the material. Physical property information was useful in helping to identify specific grades and producers of steel used for the various components located within the towers. These analyses were made only for steel from WTC 1 and WTC 2 as no steel was recovered from WTC 7. Physical property data of steels from this building were estimated based upon values found in the literature. In addition, thermal properties were developed for use in models of the building response to fire.

In addition to the structural steel, chemistry information was obtained for the aluminum façade used on the WTC towers and the sprayed fire-resistive material applied to the structural elements of WTC 1 and WTC 2.

This page intentionally left blank.

## Chapter 2

# BACKGROUND OF STRUCTURAL STEELS

---

### 2.1 BRIEF REVIEW OF STRUCTURAL STEELS SPECIFIED IN THE CONSTRUCTION OF THE WTC TOWERS

The report “Contemporaneous Structural Steel Specifications” (NIST NCSTAR 1-3A)<sup>1</sup> presents a detailed discussion of the types of structural steel specified in the design drawings for the World Trade Center (WTC) towers, and thus, these steels will be only briefly reviewed here. The major structural steel components used in the WTC towers were primarily low carbon alloy steels with carbon contents less than 0.2 percent. (The reader is referred to other sources for an in-depth review of the microstructures of the Fe-C steels [Irvine 1967; Krauss 1980; Leslie 1981; Samuels 1980; Gladman 1996; Bramfitt and Benscoter 2002].) Both low-alloy hot-rolled and quench-and-tempered high-strength, low alloy grades were used in the WTC towers; the latter for applications where a higher strength to weight ratio was beneficial, such as for the exterior columns on upper floors of the building. Unfortunately no direct references discussing specific production conditions for WTC steels were noted in the open literature.

It was found that Skilling, Helle, Christiansen, & Robertson, structural engineers for the WTC towers, specified the type of steel to be used for each structural piece by the minimum specified yield strength. For example, a “50 ksi steel” is a steel with a minimum yield strength of 50,000 pounds per square inch. Thus, this report will continue with this designation for the steel. The structural plans called for the following:

- Perimeter columns were fabricated from 12 grades of steel with  $F_y = (36, 42, 45, 46, 50, 55, 60, 65, 70, 75, 80, \text{ and } 100)$  ksi. (Two additional grades, 85 ksi and 90 ksi, were specified, but later replaced with 100 ksi steel).
- Spandrels were to be fabricated from 12 grades of steel with  $F_y = (36, 42, 45, 46, 50, 55, 60, 65, 70, 75, 80, \text{ and } 85)$  ksi.
- Built-up core box columns were to be fabricated from two grades of steel with 36 ksi and 42 ksi minimum yield strengths.
- Rolled wide-flange shapes were to be fabricated from steels with  $F_y = (36, 42, 45, \text{ and } 50)$  ksi, but there were very few 45 ksi or 50 ksi core columns.
- For the floor trusses, the top chord angles, as well as most round bars, were to be fabricated to meet ASTM International (ASTM) A 242 ( $F_y = 50$  ksi); some of the round bars and the bottom chord angles were specified as ASTM A 36.
- Floor truss seats were specified to be fabricated from steel with  $F_y = 36$  ksi minimum.

---

<sup>1</sup> This reference is to one of the companion documents from this Investigation. A list of these documents appears in the Preface to this report.

For the floor truss components, specific ASTM materials were specified for fabrication. However, while specifications (ASTM, American Iron and Steel Institute, etc.) typically place limits on chemical composition or mechanical properties or, most commonly, both, it is important to remember that an ASTM standard can permit a wide variety of steel compositions and strengths. Therefore, a specific steel might be capable of meeting several distinct ASTM steel standards. For instance, ASTM A 36 only specifies a minimum 36 ksi yield strength, an upper and lower tensile strength and carbon, manganese, silicon, phosphorus, and sulfur contents. Many high-strength low-alloy steels designed to meet other ASTM structural steel standards (e.g., A 572, A 242) will also meet A 36. Simply identifying a specific steel as meeting a given ASTM standard will not uniquely identify its composition or mechanical properties. Thus, many of the steels used in the construction of the WTC towers may not be unambiguously identified as to their exact specifications.

### **2.1.1 Specified and Contemporaneously Available Steels for Construction of the WTC Towers**

There were many domestic and Japanese steels allowed in the contracts between the Port Authority of New York and New Jersey and all the fabricators. A collection of relevant ASTM structural steel standards from 1970, as well as data relating to the physical and mechanical properties of the Japanese steels, can be found in NIST NCSTAR 1-3A.

## Chapter 3

# EXPERIMENTAL PROCEDURES

---

This chapter describes the practices and procedures used to analyze and evaluate the physical properties of the recovered World Trade Center (WTC) steel.

### 3.1 SAMPLE DOCUMENTATION AND REMOVAL

All samples for analysis underwent similar documentation and removal procedures from the recovered structural members. Once a specific sample was identified to be removed, the sample was given an alphanumeric identification code, marked on the component with rolling direction of the plate specified, and a photograph taken of the sample to indicate location and orientation with respect to the entire element (Fig. 3–1a). The sample was then removed through one of two methods depending upon physical access to the sample, the size, and/or thickness of the plate being sectioned. The removal methods used were either mechanical sawing (reciprocating saw, circular saw with carbide tipped blade) or flame cutting with an oxyacetylene torch. Samples were typically cut larger than necessary in order to preserve a central portion of the sample that was unaffected (in terms of the original structure and properties) by the removal method. Once the sample was free of the structural element, a second photograph was taken with the sample positioned near its original location (Fig. 3–1b). Additional documentation was made in the laboratory after the sample had been marked for further sectioning for the analyses to be conducted (Fig. 3–1c). This section was done either by an abrasive cutoff saw or high speed saw with diamond or alumina blade. For all samples, two metallographic samples (“//” was a sample where the rolling plane was viewed and “⊥” was a longitudinal section perpendicular to the rolled surface), a sample for chemical analysis (“C”), and a sample for Rockwell Hardness testing (“H”) were sectioned from the main piece.

### 3.2 CHEMICAL ANALYSIS

Portions of all samples were sent to an outside contractor (Chicago Spectro Service Laboratory, Inc., Chicago, Illinois) for optical emissions spectroscopy. The following elements were analyzed: C, Mn, P, S, Si, Ni, Cr, Mo, Cu, V, Nb, Ti, Zr, Al, B, and N. Iron was assumed to be the balance. Tests were conducted in accordance to ASTM International (ASTM) E 415 for all elements except C; ASTM E 1019 was used for this element. The company has an annually renewed accreditation with the American Association of Analytical Laboratories.

During the initial stages of the investigation, a second contractor (Laboratory Testing, Inc., Hatfield, Pennsylvania) was also used to check for accuracy of results. Nineteen samples were analyzed with measurements made according to ASTM standards E 227, E 404, E 415, E 607, and E 1086 using optical emission spectroscopy for all elements except carbon, nitrogen, and sulfur. The concentrations of carbon, nitrogen, and sulfur were determined using LECO gas analysis according to ASTM E 1019.

Two samples were tested internally at the National Institute of Standards and Technology (NIST). The two methods used were X-ray fluorescence and Glow Discharge Optical Emission Spectroscopy. Both

measurements were made using instrumentation calibrated with NIST Steel Standard Reference Materials.

### **3.3 METALLOGRAPHY**

#### **3.3.1 Sample Preparation**

Standard metallographic procedures were used to prepare the metallographic samples. Typical metallography of a sample consisted of evaluation on both the rolling and longitudinal planes, as defined in Fig. 3–2. Once sectioned from the main piece, burrs were ground off by hand using 120 grit SiO<sub>2</sub> papers with water as a lubricant. The samples were then flushed with water followed by flushing with ethyl alcohol and drying using forced air. Sample labels were affixed to the samples and then encased in cold setting epoxy. Most samples were prepared using an automated grinding/polishing machine. Grinding steps were conducted with SiO<sub>2</sub> papers to 800 grit followed by polishing with diamond pastes of 6 micron and 0.25 micron. The final polishing step was conducted by hand using a colloidal mixture of SiO<sub>2</sub> and Al<sub>2</sub>O<sub>3</sub> with sizes of approximately 0.05 μm. Some samples that were too large to fit into the grinder/polisher sample holder (e.g., weld cross-sections) were completely prepared by hand using similar procedures listed above.

The underlying steel microstructural constituents were revealed using various etchants. Both hot-rolled and quenched-and-tempered steel microstructures were revealed using a combination of 4 percent picral (4 g picric acid, 96 mL ethyl alcohol) followed by 2 percent nital (2 mL concentration nitric acid, 98 mL ethyl alcohol). Further, prior austenite grain boundaries were attempted to be revealed using Marshall's reagent and Vilella's reagent (Bramfitt and Benschoter 2002). Following completion of etching, samples were ultrasonically cleaned in ethyl alcohol and then forced air dried.

#### **3.3.2 Ferrite Grain Size Measurements**

The ferrite grain size of the hot-rolled steels was determined according to ASTM E 1382-97, a standard test method for determining the average grain size using semiautomatic and automatic image analysis. The samples were etched prior to evaluation. The grain size was calculated using the Jeffries planimetric method. The pearlite regions were removed from the analysis, so that only the area of the ferrite grains was used in the determination of the grain size. Grain size measurements were made on cross longitudinal planes. The number of fields measured for a specific sample depended on the thickness of the steel. The first and last field of the grain boundary counts were taken from positions adjacent to the top and bottom surfaces of the plates. Then measurements at 10 or more positions between these two boundary fields were measured. Results were given in terms of an ASTM grain size number with a measure of relative accuracy also provided (defined in the standard).

#### **3.3.3 Pearlite Volume Fraction Measurements**

The volume fraction of pearlite in the hot-rolled steels was determined via an area detected measurement using automatic image analysis techniques. The samples were etched prior to evaluation. These samples were evaluated on longitudinal planes. The qualitative terms used to characterize the pearlite morphologies are taken from the ASTM E 1268 Standard Practice for Assessing the Degree of Banding or Orientation of Microstructure.

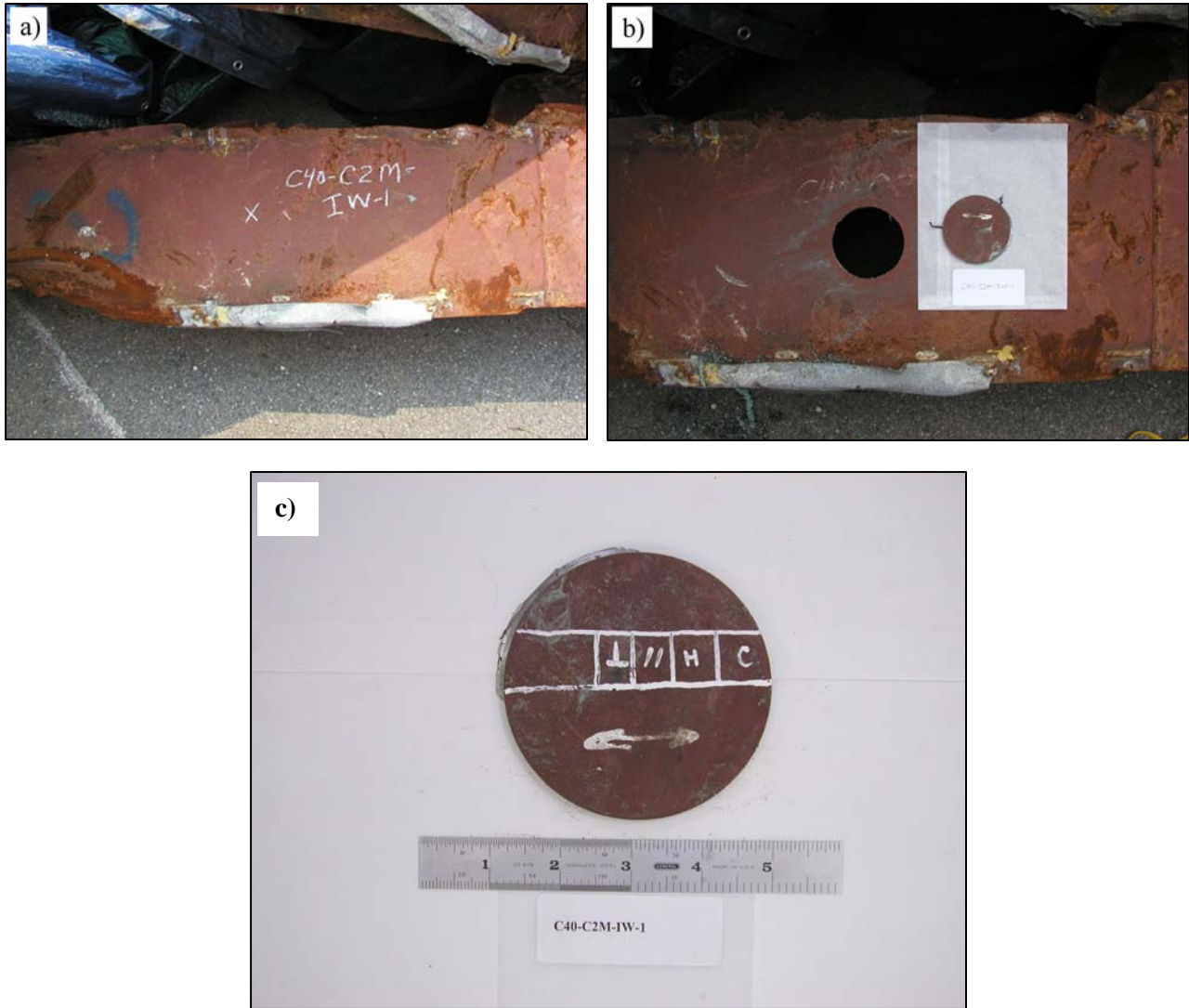
### **3.4 HARDNESS TESTING**

Three types of hardness tests were conducted on the WTC steels. Rockwell Hardness testing was conducted on un-mounted samples using the B-scale or C-scale in accordance with ASTM E 18. Two sides that were parallel to the rolling plane of the plate were ground parallel to 120 grit. Three measurements were made on each sample after an initial indent was dropped to “seat” the sample. Most hot-rolled samples were tested using the B-scale while the quenched-and-tempered samples were primarily tested on the C-scale.

Vickers microhardness testing was conducted on polished metallographic samples (parallel to the rolling plane) in accordance with ASTM E 384. Five indents were made on each sample with a load of 1 kg. Measurements were conducted using 200 times magnification. Additionally, microhardness profiles were made through weld cross-sections using a Knoop indenter with 1 kg load and measured at 200 times magnification in accordance with ASTM E 384.

### **3.5 FURNACE EXPOSURE**

Various plate materials were exposed to elevated temperatures through use of a laboratory furnace. All samples from a give material were taken from within 1 ft of each other on the same plate. The samples were ultrasonically cleaned in ethyl alcohol and air dried. A standard laboratory furnace was set at a given temperature and allowed to stabilize for a minimum of 1 h; a thermocouple was placed in the furnace at roughly the same location as the samples to monitor the temperature. Samples were exposed for 15 min and 30 min at temperatures of 200 °C, 300 °C, 400 °C, and 500 °C. Additionally, exposure at 625 °C was conducted for times of 15 min, 30 min, 60 min, and 120 min. Samples were removed from the furnace and allowed to cool in a medium of standard silica sand. The two surfaces of the plate (parallel to the rolling plane) were ground parallel to 600 grit and tested using the Rockwell B scale in accordance with ASTM E 18.



Source: NIST.

**Figure 3–1. a) Photograph prior to sample removal from structural element, b) photograph subsequent to sample removal from structural element, and c) photograph displaying samples to be cut for further analysis from the specimen. Note that the rolling direction of the plate is indicated by the white arrow. Sample shown is from a 60 ksi inner web plate from column 136 in the vicinity of the 99th floor of WTC 1 (panel C-40).**

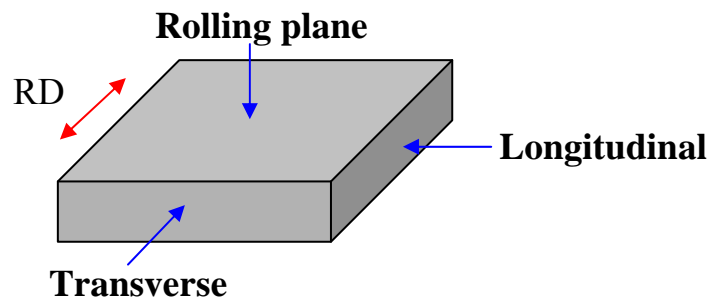


**Figure 3–2. Schematic indicating the viewing orientations for metallographic analysis. Microstructural evaluation was conducted by viewing the rolling and longitudinal planes.**

This page intentionally left blank.

## Chapter 4

# CHEMICAL ANALYSIS RESULTS

---

Chemical analysis of the recovered World Trade Center (WTC) structural steel was conducted to help identify the steels used in the towers' construction. A portion of nearly every sample removed from the structural elements was chemically analyzed (385 chemical analyses). As discussed in Sec. 3.2, in the initial stages of the investigation, two independent laboratories were sent samples from the same plate at a distance of no further than 1 ft apart. This was done for an independent check on accuracy. Comparison of two of the nineteen samples that were duplicated can be seen in Table 4-1. While not exact, the results were similar. (The choice of one laboratory over the other to continue on with the bulk of the work is not meant to imply that one laboratory outperformed the other.) Further, these two samples were also tested at the National Institute of Standards and Technology (NIST). Two different methods were used to obtain the results: X-ray fluorescence and Glow Discharge Optical Emission Spectroscopy. Both measurements were made using instrumentation calibrated with NIST standard reference materials for steel. Again similar results were observed.

The following sections discuss the chemical analysis results in relation to available structural steel at the time of the WTC towers' construction. When referring to individual chemistry specifications for contemporaneous materials, see NIST NCSTAR 1-3A. "Again, it should be noted that only 12 grades of steel were used in the construction of the towers as 85 ksi and 90 ksi steels were replaced with 100 ksi steel."

### 4.1 EXTERIOR PANEL MATERIAL

#### 4.1.1 Perimeter Columns

##### Flange Plates

Table 4-2 displays the chemical analysis results for the flange plates of the perimeter columns. The samples were separated first by specified minimum yield strength ( $F_y$ ) and then by thickness of the plate. The number of individual plates analyzed that contributed to these results for the given  $F_y$  and thickness was also shown. Each element is separately listed with the average compositional value, in percent, and standard deviation shown. Further, Fig. 4-1 shows the average value for various elements plotted as a function of  $F_y$  for plates with a thickness of 0.25 in.

The steels used for the flange plates of the perimeter panels were low carbon steels with carbon contents typically between 0.1 percent and 0.2 percent. These would be classified as high-strength, low alloy (HSLA) steels.

The carbon equivalent (CE) for these materials was also calculated and shown in Table 4-2 for the 0.25 in. plates. The CE is used to account for those elements that may affect weldability of the steel. The formula

$$CE = \%C + \frac{\%Mn}{6} + \frac{\%Cr + \%Mo + \%V}{5} + \frac{\%Si + \%Ni + \%Cu}{15} \quad (4-1)$$

reduces the significant composition variables into a single number (ASM 1983). As a rule of thumb, low carbon steels with CE equal to or less than 0.40 typically do not require preheat or post-weld heat treating. For CE more than 0.40 but less than 0.60, some preheating should be provided before welding. For CE more than 0.60, both preheat and post-weld heat treatments should be applied. For the flange materials, it appears that preheating of the plates may have been necessary.

Based upon the chemical analysis of the flange plates, the following can be concluded regarding the possible identification of the tested plates (see NIST NCSTAR 1-3A for descriptions):

$F_y = 45$  ksi: Met the Yawata “A441-modified” chemistry specification.

$F_y = 50$  ksi: Both plate sizes met the Yawata “A441-modified” chemistry specification, the 0.5625 in. plate also met “WEL-TEN 60”, “WEL-TEN 60R”, “WEL-TEN 62,” and “WEL-TEN 70” chemistry specifications.

$F_y = 55$  ksi: The 0.5625 in. plate met the Yawata “A441-modified”, all other plates met this specification in addition to “WEL-TEN 60”, “WEL-TEN 60R”, “WEL-TEN 62,” and “WEL-TEN 70” chemistry specifications.

$F_y = 60$  ksi: Both plate sizes met the Yawata “A441-modified” chemistry specification, only the 0.3125 in. plate met the “WEL-TEN 60”, “WEL-TEN 60R”, “WEL-TEN 62,” and “WEL-TEN 70” chemistry specifications.

$F_y = 65$  ksi: Met the Yawata “A441-modified”, “WEL-TEN 60”, “WEL-TEN 60R”, “WEL-TEN 62,” and “WEL-TEN 70” chemistry specifications.

$F_y = 70$  ksi: All plates met the Yawata “A441-modified”, “WEL-TEN 60”, “WEL-TEN 60R”, “WEL-TEN 62,” and “WEL-TEN 70” chemistry specifications.

$F_y = 75$  ksi: Met the Yawata “A441-modified”, “WEL-TEN 60”, “WEL-TEN 60R”, “WEL-TEN 62,” and “WEL-TEN 70” chemistry specifications.

$F_y = 80$  ksi: The 0.25 in. plate met the “WEL-TEN 60” and “WEL-TEN 70,” the 0.625 in. plate met the “WEL-TEN 60”, “WEL-TEN 60R”, “WEL-TEN 62,” and “WEL-TEN 70” chemistry specifications.

$F_y = 100$  ksi: Both gauges met the “WEL-TEN 70” and “WEL-TEN 80C” chemistry specifications.

### Outer Web Plates

Table 4-3 displays the chemical analysis results for the outer web plates of the perimeter columns. The samples were separated by specified minimum yield strength ( $F_y$ ). The number of individual plates analyzed was also shown. Each element is separately listed with the average compositional value, in

percent, and standard deviation shown. Further, Fig. 4–2 shows the average value for various elements plotted as a function of  $F_y$  for plates with a thickness of 0.25 in.

In comparing Fig. 4–2 to Fig. 4–1, it can be seen that nearly identical results were observed for the outer web plates as found for the flange material. This lends credence to the assumption that the same supplier (Yawata Iron and Steel Co.) was used for both the flange and outer web plates (NIST NCSTAR 1-3A). For example, the 60 ksi flange material with different thicknesses had chemistries that were similar but not exact, particularly for the C and V or Nb additions. However, the 0.25 in. 60 ksi plate for the flange and 0.25 in. outer web have nearly identical compositions. One further note was the similarity between 50 ksi and 55 ksi web plates. The 50 ksi web contained Nb additions similar to that of the 55 ksi plate, but these two materials were distinct in that there was a statistically significant difference in the Si contents.

Due to the similarity between these plates and the flanges, no further analysis of the outer web plates was conducted. For more information regarding possible identification of material, please refer to the discussion for the flange plates.

### Inner Web Plates

Table 4–4 displays the chemical analysis results for the inner web plates of the perimeter columns. The samples were separated by specified minimum yield strength ( $F_y$ ) with only the  $F_y$  50 ksi material having more than one gauge. Figure 4–3 shows the average value for various elements from Table 4–4 plotted as a function of  $F_y$  for plates with a thickness of 0.25 in. In addition to the number of individual plates analyzed, an “a” was placed next to the number signifying that additional plates of this thickness and  $F_y$  were not included in the average values as significant outlying chemistry values were observed. Samples with significantly outlying chemistry values, compared to those that were statistically similar, were individually shown in Table 4–5 and did not contribute to the average values found in Table 4–4.

In comparing the inner web chemistry results with those obtained for the flanges or the outer webs, there was a clear disparity for minimum yield strengths between 55 ksi and 75 ksi. The 80 ksi and 100 ksi inner web plates had very similar chemistries to the flanges and outer web and were consistent with the Yawata grades; the 50 ksi inner web plate was somewhat similar, but not exact. Contemporaneous construction documents (NIST NCSTAR 1-3A) indicate that the flanges, outer webs and spandrels of the perimeter panels were generally fabricated from Japanese steel (primarily Yawata) and the inner web from domestic steel. Other contemporaneous construction documents contain evidence that Bethlehem steel supplied most of the domestically produced steel for the perimeter panel contract. The actual fraction was unknown, and the same construction documents also show that the company that fabricated the perimeter panels purchased, or requested approval to purchase, plate from nearly every domestic steel company. Because of the lack of information in the construction record, it was impossible to unambiguously identify the source of the steel used for the inner web.

### Butt Plate

The butt plates for the individual perimeter columns were specified as having  $F_y = 50$  ksi. No other specifications were given. The chemistry results for these plates can be found in Table 4–6. Due to the high silicon content, the steel did not meet the chemistry specifications for relevant ASTM structural

steels from that era. However, it did meet the chemistry specifications for the following: Yawata “A441-modified,” “WEL-TEN 50,” “WEL-TEN 55,” all “WEL-TEN 60” designations, and “WEL-TEN 62.”

### 4.1.2 Spandrel Plates

Table 4–7 displays the chemical analysis results for the spandrel plates of the exterior panels. The samples were separated by specified minimum yield strength ( $F_y$ ) with only the  $F_y$  50 ksi and 65 ksi materials having more than one thickness. Each element is separately listed with the average compositional value, in percent, and standard deviation shown. Further, Fig. 4–4 shows the average value for various elements plotted as a function of  $F_y$  for plates with a thickness of 0.375 in. In addition to the number of individual plates analyzed, an “a” was placed next to the number signifying that additional plates of this thickness and  $F_y$  were not included in the average values as significant outlying chemistry values were observed. Samples with significantly outlying chemistry values, compared to those that were statistically similar, were individually shown in Table 4–5 and did not contribute to the average values found in Table 4–7.

In comparing the results between the spandrel plates (Fig. 4–4) and those from the flange (Fig. 4–1), it can be seen that very similar results were observed for material between 50 ksi and 75 ksi. There were minor differences associated with the Mn content for plates with  $F_y$  between 60 ksi and 75 ksi where the spandrel plates had slightly elevated levels. Additionally, the 60 ksi plate for the spandrel was strengthened with Nb as opposed to V seen in the flanges. However, if comparing similar thickness plate, it can be seen that the Nb levels for 0.3125 in. flange plate are nearly identical to the 0.375 in. spandrel plate. This lends credence to the assumption that the same supplier (Yawata) produced the flange, outer web, and spandrel plates (NIST NCSTAR 1-3A).

As similar results were observed between the spandrel and flange plates, only those materials not previously discussed in Sec. 4.1.1 will be commented on for possible identification of the plates with regard to the chemistry data:

$F_y = 36$  ksi: Met the “A-36” chemistry specification.

$F_y = 42$  ksi: Met the Yawata “A441-modified,” “WEL-TEN 60,” “WEL-TEN 60R,” “WEL-TEN 62,” and “WEL-TEN 70” chemistry specifications.

$F_y = 46$  ksi: Met the Yawata “A441-modified,” “WEL-TEN 60,” “WEL-TEN 60R,” “WEL-TEN 62,” and “WEL-TEN 70” chemistry specifications.

### 4.1.3 Spandrel Splice Plates

The splice plates for the individual exterior panels were specified as having  $F_y = 36$  ksi. No other specifications were given. The chemistry results for these plates can be found in Table 4–6 and indicates that chemistry specifications were met for ASTM A 36 and ASTM A 242.

#### 4.1.4 Floor Truss Connectors

##### Truss Seat

The structural engineering plans specified all truss seats were to have a minimum yield strength  $F_y = 36$  ksi, however, the plans do not require that the steel conform to a specific ASTM standard. Table 4–6 shows the chemistry results and indicates that chemistry specifications were met for ASTM A 36 and ASTM A 242.

##### Construction Bolts

Two types of bolts were specified for construction of the towers, either A 325 or A 490 bolts. Stampings on the bolt heads clearly indicated the bolt type. Only one A 325 bolt was tested for chemistry. The results shown in Table 4–6 indicated that it met the A 325 Type 1 chemistry specifications.

##### Standoff Plate

The structural engineering plans specified that all standoff plates were to have a minimum yield strength  $F_y = 42$  ksi. No other specifications were found. The chemistry results for these plates can be found in Table 4–6. Many of the specifications for contemporaneous ASTM structural steels were met, but none could be specifically identified. However, the additions of V would suggest that care was taken to meet the strength levels necessary.

##### Gusset Plate Welded to Top Chord of Floor Truss

No information was found specifying the grade of steel to be used for the gusset plates that were welded to the top chord of the floor trusses. However, structural engineering plans stated that “*All steel shall be ASTM A36 for locations where a specific strength requirement is not stated in the drawings.*” Given these facts, these gusset plates were assumed to be ASTM A 36. Table 4–6 shows the chemistry results and indicates that chemistry specifications were met for ASTM A 36 (bars).

##### Damper Plates

No information was found specifying the grade of steel to be used for the damper plates. However, structural engineering plans stated that “*All steel shall be ASTM A36 for locations where a specific strength requirement is not stated in the drawings.*” Given these facts, the damper plates were assumed to be ASTM A 36. Table 4–6 shows the chemistry results and indicates that chemistry specifications were met for ASTM A 36 (bars).

##### Gusset Plate for Damper Unit and Diagonal Bracing Strap Attachment

No information was found specifying the grade of steel to be used for the gusset plates that attached the damper units and diagonal bracing straps to the perimeter columns. However, structural engineering plans stated that “*All steel shall be ASTM A36 for locations where a specific strength requirement is not stated in the drawings.*” Given these facts, the gusset plates were assumed to be ASTM A 36. Table 4–6 shows the chemistry results and indicates that chemistry specifications were met for ASTM A 36.

## Diagonal Bracing Strap

No information was found specifying the grade of steel to be used for the diagonal bracing straps. However, structural engineering plans stated that “*All steel shall be ASTM A36 for locations where a specific strength requirement is not stated in the drawings.*” Given these facts, the diagonal bracing straps were assumed to be ASTM A 36. Table 4–6 shows the chemistry results and indicates that chemistry specifications were met for ASTM A 36.

## 4.2 CORE MATERIAL

Table 4–8 displays the individual chemical analysis results for each of the samples where the as-built location was known. The columns were separated by type (built-up box column or wide flange section) and then by specified minimum  $F_y$ . The plate thickness was also indicated.

### 4.2.1 Wide Flange Core Columns

The chemistry of the six wide flange sections can be found in Table 4–8. Five of the samples were specified as having a minimum yield strength of 36 ksi. While all of these core columns met ASTM A 36 chemistry specifications, sample C-30 (1008B: 104-106) was unique in that it had V additions. The other wide flange section was specified as having a minimum yield strength of 42 ksi. Sample HH (605A: 98-101) met chemistry specifications for ASTM A 440, ASTM A 441, and ASTM A 572 (both type 2 and type 4). As contemporaneous documents state that numerous suppliers were used to fill the steel orders (NIST NCSTAR 1-3A), attempts were not made to distinguish between the suppliers.

### 4.2.2 Built-Up Box Core Columns

Five built-up box columns were identified as to their as-built location. Three of these were specified as having a minimum yield strength of 36 ksi. Table 4–8 shows these chemistries with the results indicating that they met chemistry specifications for ASTM A 36. The fourth and fifth columns were specified as 42 ksi material. (The core columns are labeled as C-88a (801B: 80-83) and C-88b (801B: 77-80). The piece labeled “C-88c” was part of a flange that broke away from C-88a during transport to NIST.) While chemically similar, the materials are not identical, Table 4–8. The plates do not conform to any of the chemistry specifications mentioned in the Port of New York Authority steel contracts. However, there are several steels listed in the contracts, most notably proprietary Lukens grades (NIST NCSTAR 1-3A). NIST was not able to locate typical or specified compositions, so possibly the steel could have been shipped to one of those specifications.

### 4.2.3 Channel

No information was found specifying the grade of steel to be used for the channels. However, structural engineering plans stated that “*All steel shall be ASTM A36 for locations where a specific strength requirement is not stated in the drawings.*” Given these facts, the channels were assumed to be ASTM A 36. Table 4–6 shows the chemistry results from two individual channels and indicates that chemistry specifications were met for ASTM A 36.

#### 4.2.4 Core Truss Seat

No information was found specifying the grade of steel to be used for the core truss seats. However, structural engineering plans stated that “*All steel shall be ASTM A36 for locations where a specific strength requirement is not stated in the drawings*”. Given these facts, the core truss seats were assumed to be ASTM A 36. Table 4–6 shows the chemistry results from two individual seats and indicates that chemistry specifications were met for ASTM A 36. The two core chemistries were also compared to the average values for the perimeter panel truss seats. One was found to be similar, but not identical, while the other was found to be dissimilar, suggesting that multiple steel suppliers may have been used to fill the contracts.

### 4.3 FLOOR TRUSS MATERIAL

#### 4.3.1 Rod

Table 4–9 displays the individual chemistry results for the truss rounds that were analyzed. The diameter of the rod was also given. Chemically, all of the truss rods met chemistry specifications for ASTM A 36 and ASTM A 242 specifications. Contemporaneous construction documents indicated that Laclede Steel Co. supplied steel in the floor trusses to meet this specification as well as those for ASTM A 36 (NIST NCSTAR 1-3A).

#### 4.3.2 Chord/Angle

Table 4–9 displays the individual chemistry results for the truss angles that were analyzed. Chemically, all of the truss angles met chemistry specifications for ASTM A 242. One bottom angle (C53-BA-1) and one top angle (C53-TA-1), with their lower Mn content, also met chemistry specifications for ASTM A 36. Contemporaneous construction documents indicated that Laclede Steel Co. supplied steel in the floor trusses to meet these two specifications (NIST NCSTAR 1-3A).

### 4.4 SUMMARY

Chemical analysis of the recovered WTC steels showed a division in the types of steels used. For the lower strength components, Mn and Si were added for strength. Higher strength components contained Cr and Mo additions. Nb and V additions were used through out both types of steel. These alloying practices were typical for steels of this era. For the exterior panel material, the flange, outer web, and spandrels plates were all chemically similar, indicating fabrication by the same supplier (Yawata Iron and Steel Co.). Inner web plates with  $F_y$  equal to 80 ksi and 100 ksi were also found to conform to these chemistries. The chemistries of the inner web plates below 80 ksi were dissimilar to the flange plates for similar  $F_y$ , indicating that a different supplier(s) was most likely used to fabricate the components. These results were consistent with contemporaneous documents. For the core columns, all chemistry specifications were met for a given  $F_y$ ; however, due to the number of possible suppliers of steel, definitive identification of the steel was not possible. The other structural components (floor truss connectors, core channels, spandrel splice plates) analyzed met specifications for either ASTM A 36 or ASTM A 242 grade steels.

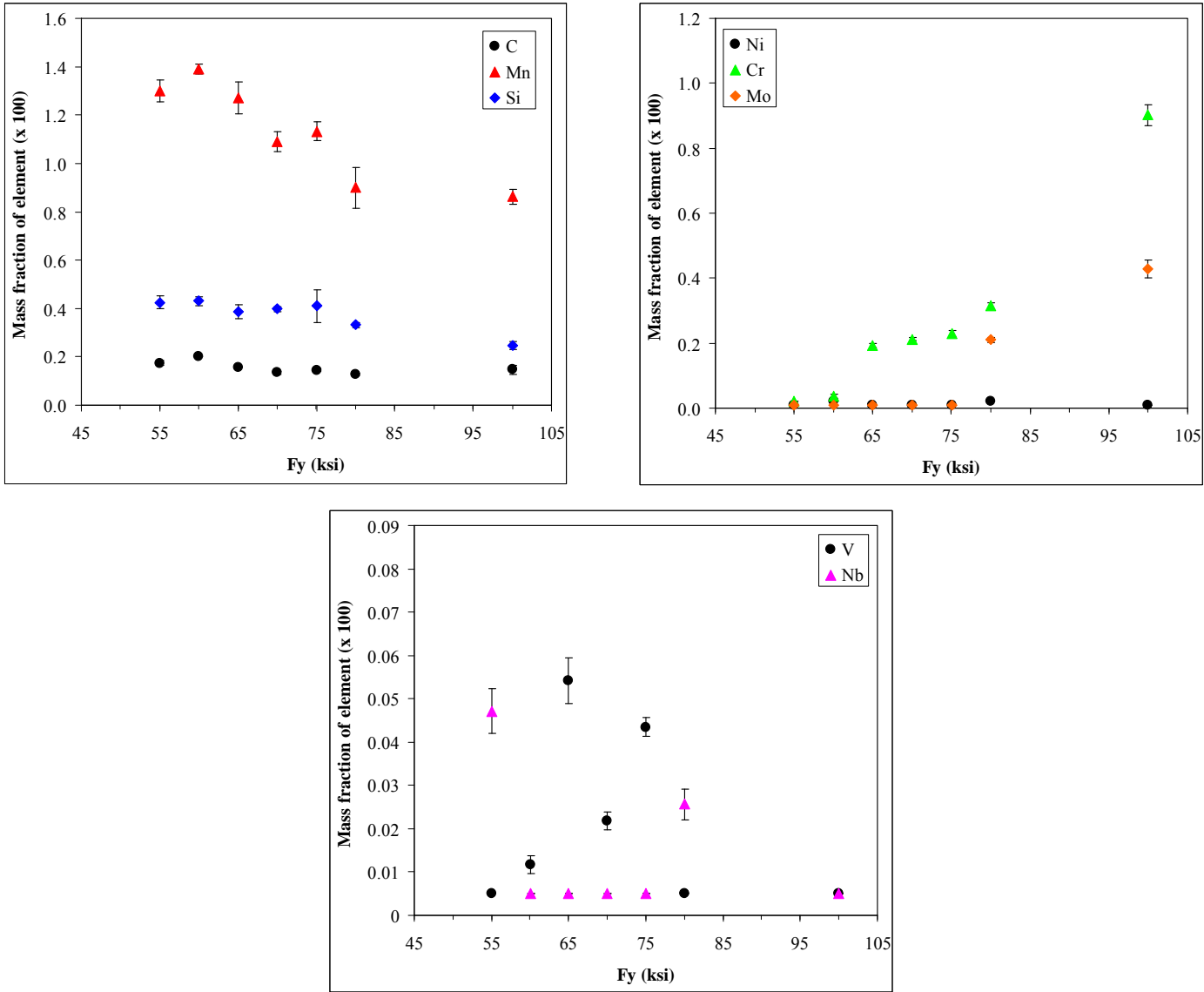


Figure 4–1. Plots of mass fraction element as a function of specified minimum yield strength for the flange plates from perimeter columns. Results for the 0.25 in. plates are shown.

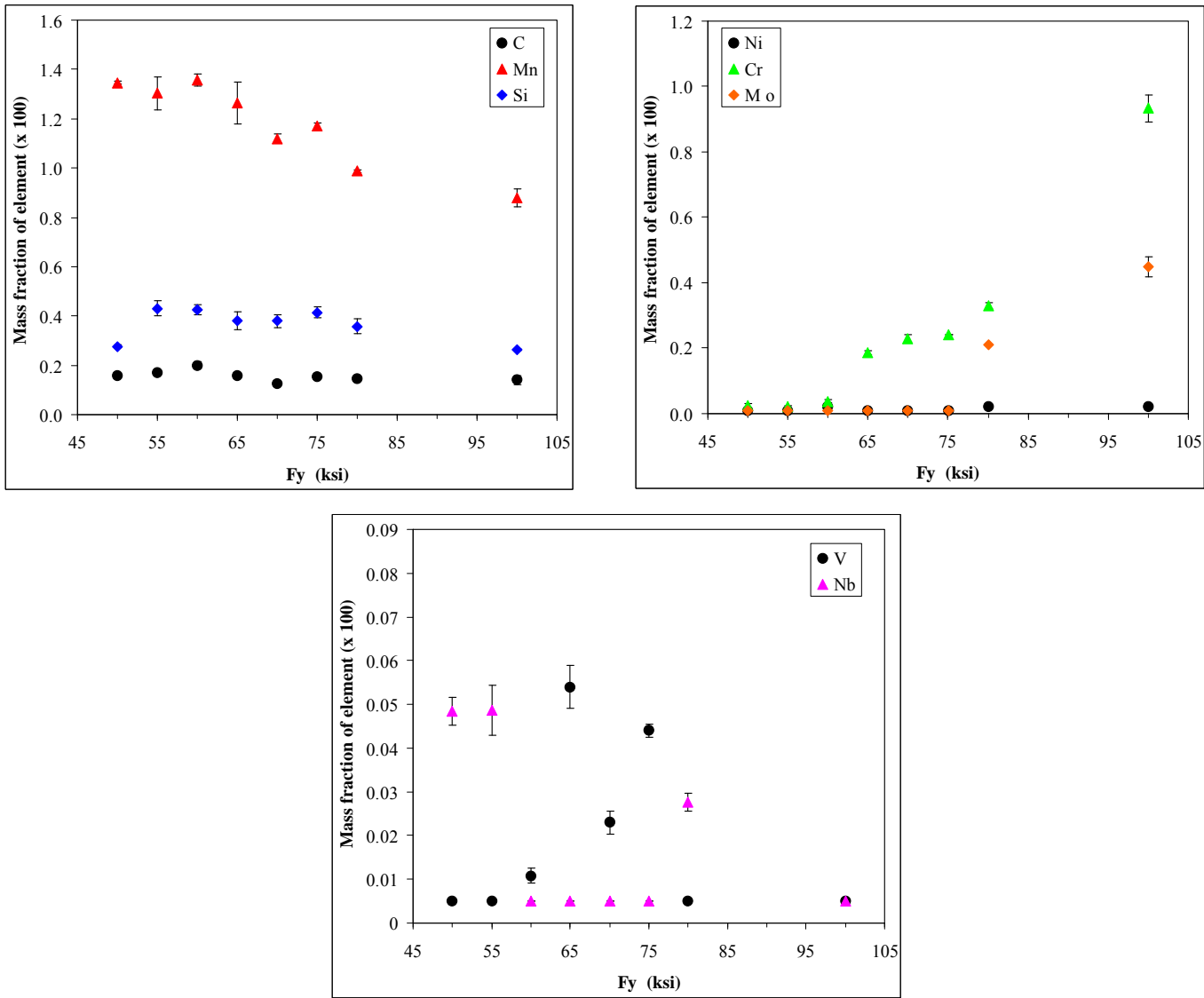


Figure 4–2. Plots of mass fraction element as a function of specified minimum yield strength for the outer web plates from perimeter columns. Results for the 0.25 in. plates are shown.

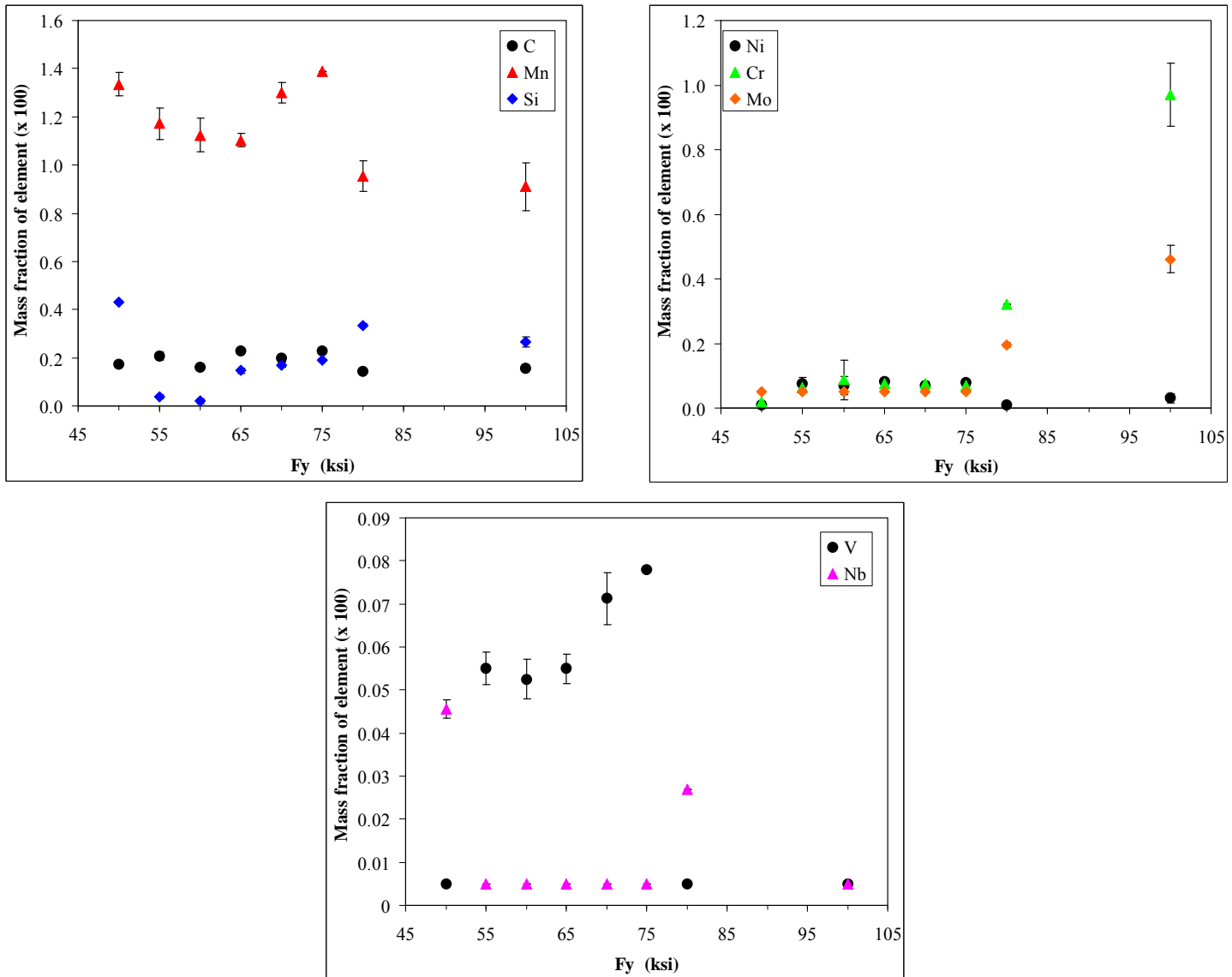


Figure 4-3. Plots of mass fraction element as a function of specified minimum yield strength for the inner web plates from perimeter columns. Results for the 0.25 in. plates are shown.

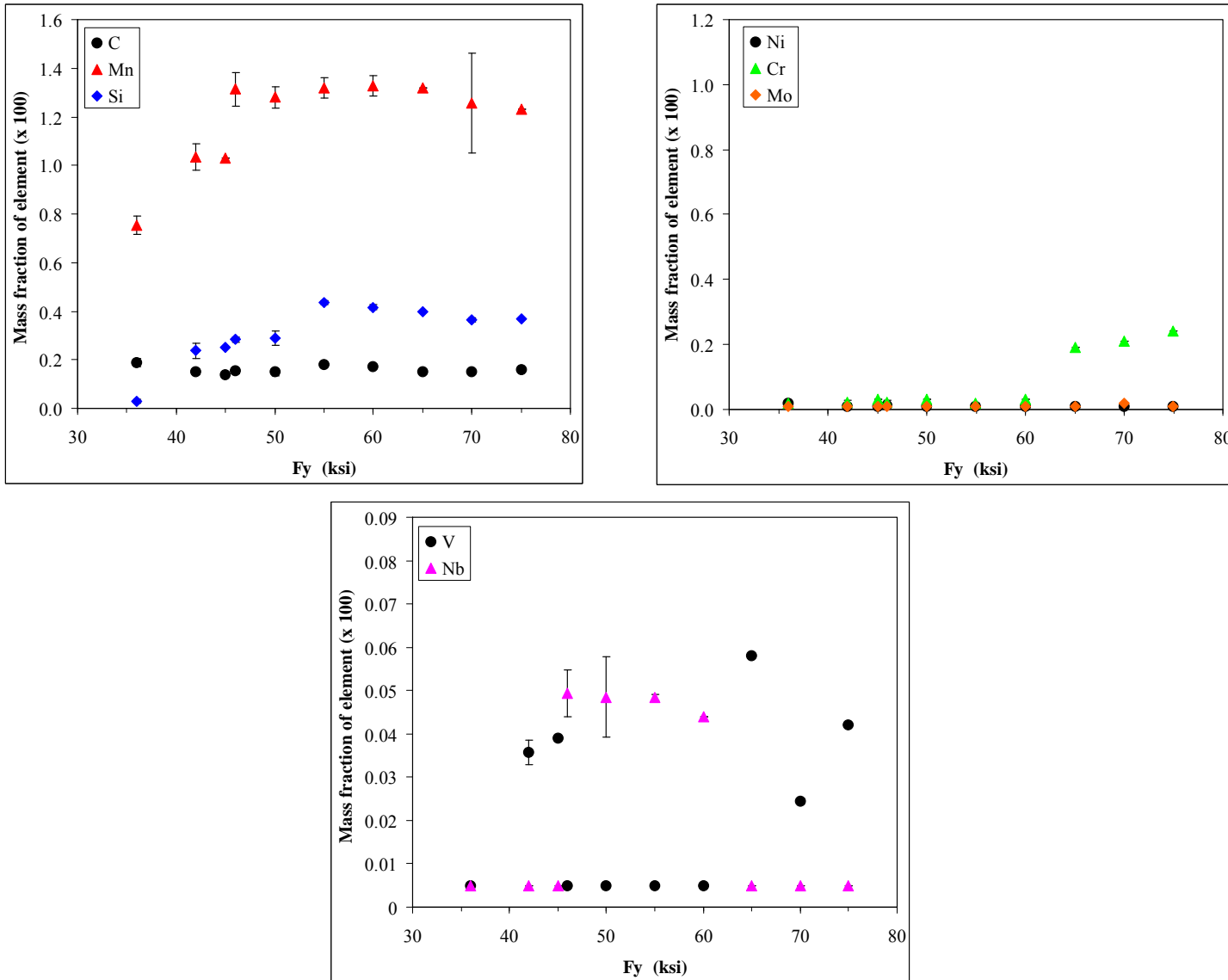


Figure 4–4. Plots of mass fraction element as a function of specified minimum yield strength for the spandrel plates from the exterior panels. Results for the 0.25 in. plates are shown.

**Table 4–1. Comparison of chemistry results from two outside contractors and NIST.**

Element	Sample 1: 60 ksi flange material from column 141, floor 100 (panel N-8)				Sample 2: 55 ksi flange plate from column 155, floor 101 (panel N-9)			
	Lab #1	Lab #2	NIST methods		Lab #1	Lab #2	NIST methods	
			XRF	GDOES			XRF	GDOES
C	0.15	0.16	NA	0.166	0.18	0.18	NA	0.171
Mn	1.35	1.42	1.45	1.44	1.37	1.42	1.44	1.42
P	0.013	0.019	0.021	0.0218	0.017	0.018	0.019	0.0188
S	0.011	0.014	0.026	0.0143	0.015	0.013	0.016	0.0128
Si	0.38	0.49	0.493	0.495	0.47	0.51	0.49	0.522
Ni	0.01	0.011	0.016	0.0167	0.01	0.011	0.015	0.0159
Cr	0.02	0.02	0.017	0.0173	0.02	0.019	0.016	0.0158
Mo	<0.01	0.072	0.0036	0.0034	<0.01	0.072	0.0036	0.0033
Cu	0.05	0.048	0.047	0.05	0.05	0.046	0.048	0.0459
V	<0.005	0.005	0.0038	0.0037	<0.005	0.004	0.0023	0.002
Nb	0.042	0.052	0.057	0.056	0.056	0.058	0.063	0.0597
Ti	<0.005	0.004	0.0035	0.0042	<0.005	0.003	0.0019	0.0029
Zr	<0.005	0.001	0.0004	NA	<0.005	0.001	NA	NA
Al	0.031	0.034	0.039	0.0336	0.033	0.032	0.036	0.0318
B	<0.0005	0.0003	NA	0.0001	<0.0005	0.0003	NA	NA
N	0.004	0.004	NA	0.0025	0.009	0.0047	NA	NA
As	NA	NA	0.015	0.0143	NA	NA	0.017	0.0176
Co	NA	NA	0.005	NA	NA	NA	0.0056	NA
Sb	NA	NA	0.0029	NA	NA	NA	0.0033	NA
Sn	NA	NA	0.006	NA	NA	NA	0.0062	NA
Ta	NA	NA	0.0052	NA	NA	NA	0.0059	NA
W	NA	NA	0.0013	NA	NA	NA	NA	NA

**Table 4–2. Chemistry results of flange plates from perimeter columns (in mass fraction × 100). Shown are the averages with standard deviations given directly below. Also calculated was the CE.**

Fy (ksi)	Thickness (in)	# of plates analyzed	C	Mn	P	S	Si	Ni	Cr	Mo	Cu	V	Nb	Ti	Zr	Al	B	N	CE
45 ksi	0.4375	2	0.20	1.23	0.01	0.02	0.26	0.01	0.03	< 0.01	0.05	<0.005	0.043	<0.005	<0.005	<0.005	<0.0005	0.009	0.43
			0.01	0.03	0.01	0.00	0.01	0.00	0.00	n/a	0.01	n/a	0.004	n/a	n/a	n/a	n/a	n/a	0.003
50 ksi	0.5	2	0.20	1.14	0.01	0.03	0.05	0.10	0.07	0.03	0.30	0.055	<0.005	<0.005	<0.005	<0.005	<0.0005	0.007	0.43
	0.01	0.04	0.00	0.01	0.01	0.01	0.00	0	0.01	0	n/a	n/a	n/a	n/a	n/a	n/a	0.004		
50 ksi	0.5625	4	0.16	1.35	0.02	0.02	0.28	0.01	0.02	< 0.01	0.04	<0.005	0.045	<0.005	<0.005	0.017	<0.0005	0.008	0.41
	0.00	0.02	0.00	0.00	0.01	0.01	0.00	n/a	0.00	n/a	0.00	n/a	0.002	n/a	n/a	0.002	n/a	0.007	
55 ksi	0.25	18	0.17	1.30	0.02	0.02	0.42	0.01	0.02	< 0.01	0.05	<0.005	0.047	<0.005	<0.005	0.028	<0.0005	0.007	0.43
	0.01	0.04	0.00	0.00	0.03	0.00	0.00	n/a	0.01	n/a	0.01	n/a	0.005	n/a	n/a	0.005	n/a	0.004	
	0.3125	10	0.17	1.30	0.02	0.02	0.42	0.01	0.03	< 0.01	0.04	<0.005	0.046	<0.005	<0.005	0.028	<0.0005	0.005	0.42
	0.01	0.06	0.00	0.01	0.03	0.00	0.01	n/a	0.01	n/a	0.01	n/a	0.006	n/a	n/a	0.010	n/a	0.004	
	0.375	9	0.17	1.28	0.01	0.01	0.43	0.01	0.02	< 0.01	0.04	<0.005	0.046	<0.005	<0.005	0.031	<0.0005	0.005	0.42
0.01	0.03	0.00	0.00	0.02	0.00	0.00	n/a	0.01	n/a	0.01	n/a	0.004	n/a	n/a	0.004	n/a	0.002		
55 ksi	0.4375	2	0.17	1.28	0.02	0.02	0.41	0.01	0.02	< 0.01	0.04	<0.005	0.046	<0.005	<0.005	0.027	<0.0005	0.011	0.42
	0.00	0.08	0.00	0.00	0.04	0.00	0.00	n/a	0.00	n/a	0.00	n/a	0.008	n/a	n/a	0.006	n/a	0.010	
55 ksi	0.5625	6	0.19	1.38	0.02	0.02	0.45	0.01	0.03	< 0.01	0.04	<0.005	0.053	<0.005	<0.005	0.043	<0.0005	0.004	0.46
	0.01	0.04	0.00	0.00	0.02	0.00	0.00	n/a	0.00	n/a	0.00	n/a	0.003	n/a	n/a	0.005	n/a	0.002	
60 ksi	0.25	3	0.20	1.39	0.02	0.02	0.43	0.02	0.04	< 0.01	0.05	0.012	<0.005	<0.005	<0.005	0.031	<0.0005	0.002	0.47
	0.00	0.02	0.00	0.01	0.02	0.00	0.01	n/a	0.00	n/a	0.00	0.002	n/a	n/a	n/a	0.003	n/a	0.001	
60 ksi	0.3125	8	0.16	1.36	0.02	0.01	0.41	0.01	0.02	< 0.01	0.05	<0.005	0.047	<0.005	<0.005	0.033	<0.0005	0.005	0.42
	0.01	0.06	0.00	0.00	0.02	0.00	0.00	n/a	0.00	n/a	0.00	n/a	0.007	n/a	n/a	0.005	n/a	0.002	
65 ksi	0.25	6	0.16	1.27	0.02	0.02	0.39	0.01	0.19	< 0.01	0.05	0.054	<0.005	<0.005	<0.005	0.033	<0.0005	0.012	0.44
			0.00	0.07	0.00	0.00	0.03	0.00	0.01	n/a	0.00	0.005	n/a	n/a	n/a	0.006	n/a	0.001	
70 ksi	0.25	4	0.14	1.09	0.01	0.01	0.40	0.01	0.21	< 0.01	0.05	0.022	<0.005	<0.005	<0.005	0.113	<0.0005	0.004	0.39
	0.01	0.04	0.00	0.00	0.01	0.00	0.01	0.01	n/a	0.00	0.002	n/a	n/a	n/a	0.005	n/a	0.002		
	0.4375	2	0.14	1.09	0.01	0.02	0.41	0.01	0.22	< 0.01	0.04	0.020	<0.005	<0.005	<0.005	0.105	<0.0005	0.006	0.39
			0.01	0.01	0.00	0.00	0.00	0.01	n/a	0.00	0.001	n/a	n/a	n/a	0.007	n/a	0.001		
70 ksi	0.75	1	0.12	1.10	0.01	0.02	0.40	0.04	0.21	< 0.01	0.05	0.024	< 0.005	< 0.005	< 0.005	0.097	< 0.0005	0.007	0.38
	n/a	n/a	n/a	n/a	n/a	n/a	n/a	n/a	n/a	n/a	n/a	n/a	n/a	n/a	n/a	n/a	n/a	n/a	
75 ksi	0.25	4	0.15	1.13	0.02	0.01	0.41	0.01	0.23	< 0.01	0.05	0.044	<0.005	<0.005	<0.005	0.113	<0.0005	0.004	0.42
			0.01	0.04	0.00	0.00	0.07	0.00	0.01	n/a	0.01	0.002	n/a	n/a	n/a	0.013	n/a	0.002	
80 ksi	0.25	5	0.13	0.90	0.02	0.02	0.33	0.02	0.32	0.21	0.20	<0.005	0.026	<0.005	<0.005	0.104	0.001	0.004	0.42
	0.00	0.08	0.00	0.00	0.01	0.01	0.01	0.01	0.01	0.11	n/a	0.004	n/a	n/a	0.005	0.000	0.002		
80 ksi	0.625	2	0.13	1.08	0.01	0.01	0.37	0.43	0.27	0.21	0.20	0.028	<0.005	<0.005	<0.005	0.041	0.002	0.009	0.43
	0.01	0.00	0.00	0.00	0.00	0.00	0.00	0.00	0.00	0.00	0.00	0.000	n/a	n/a	n/a	0.001	0.001	0.006	
100 ksi	0.25	11	0.15	0.86	0.01	0.02	0.25	0.01	0.90	0.43	0.26	<0.005	<0.005	<0.005	<0.005	0.083	0.001	0.005	0.59
	0.02	0.03	0.00	0.00	0.02	0.01	0.03	0.03	0.03	0.03	0.03	n/a	n/a	n/a	n/a	0.009	0.001	0.002	
100 ksi	1.125	1	0.15	0.80	0.01	0.01	0.23	0.01	0.88	0.33	0.31	<0.005	<0.005	<0.005	<0.005	0.053	<0.0005	0.008	0.50
	n/a	n/a	n/a	n/a	n/a	n/a	n/a	n/a	n/a	n/a	n/a	n/a	n/a	n/a	n/a	n/a	n/a	n/a	

**Table 4–3. Chemistry results of outer web plate from perimeter columns (in mass fraction × 100). Shown are the averages with standard deviations given directly below.**

Fy (ksi)	Thickness (in)	# of plates analyzed	C	Mn	P	S	Si	Ni	Cr	Mo	Cu	V	Nb	Ti	Zr	Al	B	N
50	0.25	3	0.16	1.35	0.02	0.02	0.28	0.01	0.02	<0.01	0.05	<0.005	0.048	<0.005	<0.005	0.029	<0.0005	0.009
			0.00	0.01	0.01	0.00	0.01	0.00	0.01	0.01	n/a	0.01	n/a	0.003	n/a	n/a	0.005	n/a
	0.5625	1	0.14	1.42	0.01	0.02	0.42	0.04	0.01	<0.01	0.04	<0.005	0.054	<0.005	<0.005	0.026	<0.0005	0.007
			n/a	n/a	n/a	n/a	n/a	n/a	n/a	n/a	n/a							
55	0.25	14	0.17	1.30	0.02	0.02	0.43	0.01	0.02	<0.01	0.05	<0.005	0.049	<0.005	<0.005	0.029	<0.0005	0.005
			0.01	0.07	0.00	0.00	0.03	0.00	0.00	n/a	0.01	n/a	n/a	0.006	n/a	n/a	0.006	n/a
60	0.25	4	0.20	1.36	0.02	0.01	0.43	0.02	0.04	<0.01	0.05	0.011	<0.005	<0.005	<0.005	0.031	<0.0005	0.007
			0.01	0.03	0.01	0.00	0.02	0.00	0.00	n/a	0.01	0.002	n/a	n/a	n/a	0.002	n/a	0.002
65	0.25	3	0.16	1.26	0.02	0.02	0.38	0.01	0.19	<0.01	0.05	0.054	<0.005	<0.005	<0.005	0.028	<0.0005	0.012
			0.01	0.09	0.00	0.01	0.04	0.00	0.01	n/a	0.00	0.005	n/a	n/a	n/a	0.005	n/a	0.000
70	0.25	3	0.13	1.12	0.01	0.01	0.38	0.01	0.23	<0.01	0.05	0.023	<0.005	<0.005	<0.005	0.104	<0.0005	0.004
			0.01	0.02	0.00	0.00	0.03	0.00	0.01	n/a	0.01	0.003	n/a	n/a	n/a	0.015	n/a	0.001
75	0.25	2	0.16	1.17	0.02	0.01	0.42	0.01	0.24	<0.01	0.05	0.044	<0.005	<0.005	<0.005	0.115	<0.0005	0.006
			0.01	0.01	0.00	0.01	0.02	0.00	0.00	n/a	0.01	0.001	n/a	n/a	n/a	0.007	n/a	0.002
80	0.25	3	0.15	0.99	0.02	0.02	0.36	0.02	0.33	0.21	0.26	<0.005	0.028	<0.005	<0.005	0.116	<0.0005	0.006
			0.01	0.01	0.00	0.00	0.03	0.01	0.01	0.00	0.03	n/a	0.002	n/a	n/a	0.022	n/a	0.002
100	0.25	3	0.14	0.88	0.02	0.01	0.26	0.02	0.93	0.45	0.29	<0.005	<0.005	<0.005	<0.005	0.094	<0.0005	0.007
			0.02	0.04	0.01	0.00	0.01	0.01	0.04	0.03	0.03	n/a	n/a	n/a	n/a	0.009	n/a	0.003

**Table 4–4. Chemistry results of inner web plate from perimeter columns (in mass fraction × 100). Shown are the averages with standard deviations given directly below.**

Fy (ksi)	Thickness (in)	# of plates analyzed	C	Mn	P	S	Si	Ni	Cr	Mo	Cu	V	Nb	Ti	Zr	Al	B	N
50 ksi	0.25	2 <sup>a</sup>	0.18	1.34	0.02	0.02	0.43	0.01	0.02	<0.01	0.04	<0.005	0.046	<0.005	<0.005	0.031	<0.0005	0.002
			0.01	0.05	0.00	0.00	0.00	0.00	0.00	0.00	n/a	0.00	n/a	0.002	n/a	n/a	0.001	n/a
	0.375	1	0.18	0.96	0.01	0.02	0.04	0.06	0.07	<0.01	0.25	0.054	<0.005	<0.005	0.008	<0.005	<0.0005	0.007
			n/a	n/a	n/a	n/a	n/a	n/a	n/a	n/a	n/a							
55	0.25	12 <sup>a</sup>	0.21	1.17	0.01	0.02	0.04	0.07	0.06	<0.01	0.21	0.055	<0.005	<0.005	<0.005	<0.005	<0.0005	0.008
			0.02	0.07	0.00	0.00	0.01	0.02	0.00	n/a	0.01	0.004	n/a	n/a	n/a	n/a	n/a	n/a
60	0.25	6	0.16	1.13	0.01	0.02	0.02	0.07	0.09	<0.01	0.20	0.053	<0.005	<0.005	<0.005	0.024	<0.0005	0.006
			0.01	0.07	0.01	0.01	0.01	0.03	0.06	n/a	0.07	0.005	n/a	n/a	n/a	0.008	n/a	0.003
65	0.25	3	0.23	1.10	0.01	0.03	0.15	0.08	0.08	<0.01	0.21	0.055	<0.005	<0.005	<0.005	<0.005	<0.0005	0.004
			0.00	0.03	0.00	0.00	0.01	0.01	0.01	n/a	0.02	0.003	n/a	n/a	n/a	n/a	n/a	n/a
70	0.25	3	0.20	1.30	0.01	0.02	0.17	0.07	0.08	<0.01	0.22	0.071	<0.005	<0.005	<0.005	0.014	<0.0005	0.005
			0.02	0.04	0.00	0.00	0.01	0.00	0.01	0.00	0.01	0.006	n/a	n/a	n/a	0.000	n/a	0.000
75	0.25	1	0.23	1.39	0.01	0.02	0.19	0.08	0.07	<0.01	0.24	0.078	<0.005	<0.005	<0.005	0.008	<0.0005	0.009
			n/a	n/a	n/a	n/a	n/a	n/a	n/a	n/a	n/a							
80	0.25	2	0.15	0.96	0.01	0.01	0.34	0.01	0.32	0.20	0.26	<0.005	0.027	<0.005	<0.005	0.120	0.001	0.004
			0.01	0.06	0.00	0.00	0.01	0.00	0.00	0.01	0.00	n/a	0.000	n/a	n/a	0.000	0.000	0.001
100	0.25	4 <sup>a</sup>	0.16	0.91	0.01	0.02	0.27	0.03	0.97	0.46	0.28	<0.005	<0.005	<0.005	<0.005	0.091	<0.0005	0.009
			0.01	0.10	0.01	0.01	0.02	0.01	0.10	0.04	0.04	n/a	n/a	n/a	n/a	0.013	n/a	0.005

a. Signifies that additional plates, not included in these averages because of significant outlying values, are reported in Table 4–5.

**Table 4–5. Chemistry results from samples that had significantly outlying values from average values of specified plate. All samples are from perimeter panels. Chemistry results are in mass fraction (× 100).**

Component	Fy (ksi)	Thickness (in)	Location			C	Mn	P	S	Si	Ni	Cr	Mo	Cu	V	Nb	Ti	Zr	Al	B	N
			Panel	Column	Floor																
Inner web	50	0.25	A130: 93-96	131	93	0.14	1.14	0.01	0.02	0.04	0.08	0.07	0.04	0.26	0.048	<0.005	<0.005	<0.01	<0.005	<0.0005	0.010
Inner web	55	0.25	A115: 89-92	114	89	0.19	1.27	0.02	0.02	0.40	0.01	0.02	<0.01	0.04	<0.005	0.039	<0.005	<0.005	0.029	<0.0005	0.005
Inner web	55	0.25	A136: 98-101	135	100	0.19	0.77	0.01	0.02	0.04	0.02	0.01	<0.01	0.04	<0.005	<0.005	<0.005	<0.005	<0.005	<0.0005	0.002
Inner web	55	0.25	A133: 97-100	133	100	0.20	0.69	<0.005	0.02	0.02	0.02	0.02	<0.01	0.06	<0.005	<0.005	<0.005	<0.005	<0.005	<0.0005	0.003
Inner web	55	0.25	A133: 100-103	133	103	0.21	1.17	<0.005	0.02	0.03	0.08	0.06	<0.01	0.21	<0.005	<0.005	<0.005	<0.005	<0.005	<0.0005	0.008
Inner web	100	0.25	B209: 82-85	209	83	0.15	0.86	0.02	0.02	0.24	0.02	0.98	0.45	0.27	0.006	0.051	<0.005	<0.005	0.076	0.001	0.003
Inner web	100	0.25	A451: 85-88	452	88	0.17	0.95	0.03	0.01	0.26	0.01	0.96	0.44	0.28	0.012	0.006	0.008	<0.01	0.120	0.002	0.018
Spandrel	36	0.375	A133: 97-100	n/a	100	0.10	1.41	0.01	0.02	0.55	0.02	0.04	<0.01	0.08	0.018	<0.005	0.026	<0.005	<0.005	<0.0005	0.003
Spandrel	36	0.375	A130: 93-96	n/a	94	0.11	1.47	0.01	0.01	0.49	0.04	0.05	0.03	0.13	0.029	0.008	0.027	<0.01	<0.005	<0.0005	0.018
Spandrel	42	0.375	A148: 99-102	n/a	101	0.16	1.11	0.01	0.01	0.17	0.01	0.02	<0.01	0.04	<0.005	0.027	<0.005	<0.005	0.019	<0.0005	0.003
Spandrel	42	0.375	A236: 92-95	n/a	94	0.16	1.24	0.02	0.02	0.21	0.01	0.03	<0.01	0.04	<0.005	0.041	<0.005	0.005	0.031	<0.0005	0.003
Spandrel	46	0.375	B218: 91-94	n/a	92	0.16	1.18	<0.005	0.02	0.36	0.06	0.05	<0.01	0.14	0.024	<0.005	0.018	<0.005	<0.005	<0.0005	0.006
Spandrel	60	0.375	A451: 85-88	n/a	88	0.10	1.73	0.02	0.02	0.70	0.02	0.20	0.09	0.13	0.020	0.010	0.030	<0.01	<0.005	0.001	0.020

**Table 4–6. Chemistry results of panel splice connectors and floor truss connectors (in mass fraction × 100). Shown are the averages with standard deviations given directly below. For the channels and truss seats, two samples from each were analyzed and shown separately.**

Element	Component	# of pieces analyzed	C	Mn	P	S	Si	Ni	Cr	Mo	Cu	V	Nb	Ti	Zr	Al	B	N
Perimeter panel splice	Butt plate	1	0.13	1.14	0.02	0.01	0.42	0.01	0.25	<0.01	0.06	0.04	<0.005	0.005	<0.005	0.120	<0.0005	0.005
			n/a	n/a	n/a	n/a	n/a	n/a	n/a	n/a	n/a	n/a	n/a	n/a	n/a	n/a	n/a	n/a
	Splice plate	5	0.19	0.44	<0.005	0.02	0.06	0.06	0.07	<0.01	0.22	<0.005	<0.005	<0.005	<0.005	<0.005	<0.0005	0.005
			0.01	0.04	n/a	0.00	0.02	0.03	0.01	n/a	0.04	n/a	n/a	n/a	n/a	n/a	n/a	n/a
Perimeter panel truss connector	Truss seat	7	0.19	0.44	0.01	0.02	0.06	0.09	0.07	<0.01	0.24	<0.005	<0.005	<0.005	<0.005	<0.005	<0.0005	0.007
			0.02	0.02	0.00	0.01	0.00	0.04	0.02	n/a	0.05	n/a	n/a	n/a	n/a	n/a	n/a	n/a
	Bolt	1	0.35	0.57	0.01	0.02	0.16	<0.01	0.03	<0.01	0.02	<0.005	<0.005	<0.005	<0.005	0.051	<0.0005	0.017
			n/a	n/a	n/a	n/a	n/a	n/a	n/a	n/a	n/a	n/a	n/a	n/a	n/a	n/a	n/a	n/a
	Standoff plates	2	0.12	1.07	0.01	0.02	0.03	0.06	0.07	<0.01	0.18	0.032	<0.005	0.033	<0.005	<0.005	<0.0005	0.006
			0.01	0.02	0.00	0.00	0.00	0.00	0.01	n/a	0.01	0.002	n/a	0	n/a	n/a	n/a	0.000
	Gusset plate welded to top chord of floor truss	3	0.23	0.77	0.02	0.03	0.11	0.04	0.07	0.02	0.09	<0.005	<0.005	<0.005	<0.005	<0.005	<0.0005	0.008
			0.03	0.20	0.00	0.00	0.09	0.03	0.02	0.01	0.08	n/a	n/a	n/a	n/a	n/a	n/a	n/a
	Damper plate	1	0.22	1.10	0.02	0.02	0.15	0.07	0.07	0.01	0.25	0.045	<0.005	<0.005	<0.005	0.025	<0.0005	0.006
			n/a	n/a	n/a	n/a	n/a	n/a	n/a	n/a	n/a	n/a	n/a	n/a	n/a	n/a	n/a	n/a
Gusset plate for damper unit and DBS attachment	3	0.15	0.39	0.02	0.04	0.06	0.09	0.06	0.04	0.28	<0.005	<0.005	<0.005	<0.005	<0.005	<0.0005	0.006	
		0.01	0.03	0.00	0.00	0.01	0.01	0.03	0.01	0.04	n/a	n/a	n/a	n/a	n/a	n/a	n/a	0.002
Diagonal bracing straps	2	0.20	0.50	0.02	0.03	0.04	0.09	0.09	0.01	0.29	<0.005	<0.005	<0.005	<0.005	<0.005	<0.0005	0.009	
		0.02	0.14	0.00	0.01	0.03	0.01	0.01	0.00	0.06	n/a	n/a	n/a	n/a	n/a	n/a	n/a	0.001
Core column truss connector	Channel	1	0.15	0.47	0.03	0.04	0.05	0.11	0.16	0.05	0.25	<0.005	<0.005	<0.005	<0.005	<0.0005	0.001	
		1	0.20	1.08	0.03	0.03	0.08	0.01	0.02	0.03	0.02	<0.005	<0.005	<0.005	<0.005	<0.0005	0.012	
	Truss seat	1	0.18	1.08	<0.005	0.02	0.04	0.01	0.02	<0.01	0.07	<0.005	<0.005	<0.005	<0.005	0.012	<0.0005	0.006
		1	0.28	0.6	<0.005	0.03	0.06	0.05	0.07	<0.01	0.05	<0.005	<0.005	<0.005	<0.005	0.005	<0.0005	0.007
ASTM A 36 chemistry specifications, plate < 3/4"			0.29 max		0.05 max	0.063 max												
ASTM A 242 chemistry specifications			0.22 max	1.25 max	0.05max						0.2 min							

**Table 4–7. Chemistry results of spandrel material from perimeter columns (in mass fraction × 100). Shown are the averages with standard deviations given directly below.**

Fy (ksi)	Thickness (in)	# of plates analyzed	C	Mn	P	S	Si	Ni	Cr	Mo	Cu	V	Nb	Ti	Zr	Al	B	N
36	0.375	12 <sup>a</sup>	0.19	0.75	0.01	0.02	0.03	0.02	0.02	<0.01	0.05	<0.005	<0.005	<0.005	<0.005	<0.005	<0.0005	0.004
			0.02	0.04	0.00	0.00	0.01	0.00	0.00	n/a	0.01	n/a	n/a	n/a	n/a	n/a	n/a	n/a
42	0.375	15 <sup>a</sup>	0.15	1.03	0.01	0.01	0.24	0.01	0.02	<0.01	0.05	0.036	<0.005	<0.005	<0.005	0.022	<0.0005	0.004
			0.01	0.05	0.00	0.00	0.03	0.00	0.00	n/a	0.01	0.003	n/a	n/a	n/a	0.005	n/a	n/a
45	0.375	1	0.14	1.03	0.02	0.02	0.25	0.01	0.03	<0.01	0.06	0.039	<0.005	<0.005	<0.005	0.028	<0.0005	0.009
			n/a	n/a	n/a	n/a	n/a	n/a	n/a	n/a	n/a							
46	0.375	3 <sup>a</sup>	0.15	1.31	0.01	0.02	0.28	0.01	0.02	<0.01	0.05	<0.005	0.049	<0.005	<0.005	<0.005	<0.0005	0.004
			0.01	0.07	0.00	0.00	0.01	0.01	0.01	n/a	0.01	n/a	0.006	n/a	n/a	n/a	n/a	n/a
50	0.375	2	0.15	1.28	0.02	0.02	0.29	0.01	0.03	<0.01	0.05	<0.005	0.049	<0.005	<0.005	0.028	<0.0005	0.008
			0.01	0.04	0.00	0.00	0.03	0.00	0.00	n/a	0.01	n/a	0.009	n/a	n/a	0.013	n/a	0.005
	0.4375	2	0.17	1.25	0.01	0.02	0.27	0.01	0.02	<0.01	0.03	<0.005	0.040	<0.005	<0.005	0.016	<0.0005	0.004
			0.01	0.06	0.01	0.00	0.00	0.00	0.01	n/a	0.01	n/a	0.002	n/a	n/a	0.001	n/a	0.001
55	0.375	2	0.18	1.32	0.02	0.01	0.44	0.01	0.02	<0.01	0.05	<0.005	0.049	<0.005	<0.005	0.030	<0.0005	0.005
			0.00	0.04	0.00	0.00	0.01	0.00	0.00	n/a	0.00	n/a	0.001	n/a	n/a	0.011	n/a	0.002
60	0.375	3 <sup>a</sup>	0.17	1.33	0.02	0.02	0.42	0.01	0.03	<0.01	0.05	<0.005	0.044	<0.005	<0.005	0.029	<0.0005	0.001
			0.01	0.04	0.00	0.00	0.01	0.00	0.00	n/a	0.01	n/a	0.000	n/a	n/a	0.003	n/a	0.001
65	0.375	1	0.15	1.32	0.02	0.02	0.40	0.01	0.19	<0.01	0.04	0.058	<0.005	<0.005	<0.005	0.032	<0.0005	0.014
			n/a	n/a	n/a	n/a	n/a	n/a	n/a	n/a	n/a							
	0.5625	1	0.13	1.23	0.01	0.01	0.39	0.03	0.22	<0.01	0.05	0.029	<0.005	<0.005	<0.005	0.098	<0.0005	0.004
			n/a	n/a	n/a	n/a	n/a	n/a	n/a	n/a	n/a							
	0.625	2	0.14	1.20	0.01	0.02	0.39	0.03	0.22	<0.01	0.05	0.027	<0.005	<0.005	<0.005	0.087	<0.0005	0.002
			0.00	0.06	0.00	0.00	0.01	0.00	0.00	n/a	0.00	0.003	n/a	n/a	n/a	0.008	n/a	0.001
70	0.375	2	0.15	1.26	0.02	0.02	0.37	0.01	0.21	0.02	0.04	0.025	<0.005	<0.005	<0.005	0.089	<0.0005	0.005
			0.00	0.21	0.00	0.00	0.01	0.00	0.00	0	0.00	0.001	n/a	n/a	n/a	0.008	n/a	0.001
75	0.375	1	0.16	1.23	0.02	0.01	0.37	0.01	0.24	<0.01	0.07	0.042	<0.005	<0.005	<0.005	0.106	0.001	0.002
			n/a	n/a	n/a	n/a	n/a	n/a	n/a	n/a	n/a							
80	0.5625	1	0.15	0.97	0.03	0.01	0.41	0.01	0.32	0.23	0.20	0.006	0.037	<0.005	<0.005	0.130	0.002	0.007
			n/a	n/a	n/a	n/a	n/a	n/a	n/a	n/a	n/a							

a. Signifies that additional plates, not included in these averages because of significant outlying values, are reported in Table 4–5.

**Table 4–8. Chemistry results of core column material (in mass fraction  $\times 100$ ). Shown are the averages with standard deviations given directly below.**

NIST ID	Column ID	Element	Component description	Fy (ksi)	Plate thickness (in)	C	Mn	P	S	Si	Ni	Cr	Mo	Cu	V	Nb	Ti	Zr	Al	B	N
B-6152-1	803A: 15-18	Type 380 box column	Flange	36	2	0.16	0.98	0.02	0.01	0.24	0.01	0.02	< 0.01	0.05	<0.005	<0.005	<0.005	<0.005	0.031	<0.0005	0.007
B-6152-2	504A: 33-36	Type 354 box column	Flange	36	2	0.17	0.81	<0.005	0.01	0.20	0.02	0.03	<0.01	0.05	<0.005	<0.005	<0.005	<0.005	0.013	<0.0005	0.010
C-90	701B: 12-15	Type 381 box column	Flange	36	3.15	0.15	0.84	0.01	0.01	0.20	0.02	0.03	<0.01	0.05	<0.005	<0.005	<0.005	<0.005	0.011	<0.0005	0.006
C-88b	801B: 77-80	Type 378 box column	Flange	42	1.55	0.15	1.11	<0.005	0.01	0.09	0.02	0.01	<0.01	0.02	<0.005	0.030	<0.005	<0.005	<0.005	<0.0005	0.006
C-88b	801B: 77-80	Type 378 box column	Flange	42	1.55	0.18	0.86	<0.005	0.01	0.03	0.02	0.01	<0.01	0.02	<0.005	0.011	<0.005	<0.005	<0.005	<0.0005	0.004
C-88b	801B: 77-80	Type 378 box column	Web	42	1.55	0.18	0.87	<0.005	0.02	0.03	0.02	0.02	< 0.01	0.03	<0.005	0.013	<0.005	<0.005	<0.005	<0.0005	0.006
C-88c	801b: 80-83	Type 378 box column	Flange	42	1.55	0.18	0.98	0.03	0.02	0.04	0.02	0.02	0.06	0.05	<0.005	<0.005	<0.005	<0.005	<0.005	<0.0005	0.005
C-88a	801b: 80-83	Type 378 box column	Flange	42	1.55	0.19	1.15	0.01	0.02	0.05	0.02	0.03	0.02	0.05	<0.005	<0.005	<0.005	<0.005	<0.005	0.0024	0.004
C-80	603A: 92-95	14WF184	Flange	36	1.375	0.23	0.90	0.01	0.01	0.03	0.01	0.02	0.01	0.05	<0.005	<0.005	<0.005	<0.005	<0.005	<0.0005	0.004
C-65	904A: 83-96	12WF161	Flange	36	1.5	0.23	0.74	0.01	0.02	0.02	0.02	0.02	0.01	0.05	<0.005	<0.005	<0.005	<0.005	<0.005	<0.0005	0.004
C-155	904A: 83-86	12WF161	Flange	36	1.55	0.23	0.87	<0.005	0.02	0.03	0.02	0.03	<0.01	0.06	<0.005	<0.005	<0.005	<0.005	<0.005	<0.0005	0.005
C-71	904A: 77-80	12WF190	Flange	36	1.75	0.23	0.73	0.03	0.02	0.03	0.02	0.02	0.04	0.08	<0.005	<0.005	<0.005	<0.005	<0.005	<0.0005	0.003
C-30	1008B: 104-106	14WF287	Flange	36	1.75	0.17	1.06	<0.005	0.01	0.10	0.05	0.04	<0.01	0.24	0.036	<0.005	<0.005	<0.005	<0.005	<0.0005	0.007
HH	605A: 98-101	12WF92	Flange	42	0.875	0.17	1.08	<0.005	0.01	0.03	0.02	0.02	<0.01	0.24	0.065	<0.005	<0.005	<0.005	<0.005	<0.0005	0.010

**Table 4–9. Chemistry results of floor truss material (in mass fraction × 100). Shown are the averages with standard deviations given directly below.**

Component	Sample ID	Diameter (in)	C	Mn	P	S	Si	Ni	Cr	Mo	Cu	V	Nb	Ti	Zr	Al	B	N
Bottom angle/chord	C53-BA-3	NA	0.17	0.60	0.01	0.04	0.02	0.09	0.08	0.01	0.32	0.039	<0.005	<0.005	<0.005	<0.005	<0.0005	0.009
	T1-BA-Weld	NA	0.17	0.72	0.01	0.03	0.02	0.08	0.10	<0.01	0.28	0.034	<0.005	<0.005	<0.005	0.011	<0.0005	0.008
	T1-BA-Plate	NA	0.20	0.77	0.01	0.03	0.06	0.09	0.12	<0.01	0.26	0.036	<0.005	<0.005	<0.005	0.045	<0.0005	0.008
Top angle/chord	T1-TA-Weld	NA	0.20	0.75	0.01	0.02	0.06	0.09	0.12	<0.01	0.27	0.034	<0.005	<0.005	<0.005	0.044	<0.0005	0.007
	C132-TA-3	NA	0.19	0.82	0.01	0.03	0.07	0.08	0.10	<0.01	0.32	0.038	<0.005	<0.005	<0.005	0.032	<0.0005	0.008
	C137a-TA-3	NA	0.19	0.90	0.02	0.03	0.06	0.08	0.08	0.05	0.30	0.043	<0.005	<0.005	<0.005	0.029	<0.0005	0.016
	T-1-TA-Plate	NA	0.18	0.86	0.02	0.03	0.04	0.08	0.12	0.02	0.29	0.044	0.009	<0.005	<0.005	0.015	<0.0005	0.007
	C53-TA-2	NA	0.18	0.84	0.02	0.02	0.04	0.08	0.10	<0.01	0.28	<0.005	0.018	<0.005	0.011	0.028	<0.0005	0.001
	C137f-TA-5	NA	0.18	0.84	0.02	0.02	0.07	0.06	0.05	0.01	0.22	<0.005	<0.005	<0.005	<0.005	0.038	<0.0005	0.010
	C53-TA-1	NA	0.22	0.46	<0.005	0.03	0.15	0.10	0.09	<0.01	0.48	<0.005	<0.005	<0.005	<0.005	<0.005	<0.0005	0.008
Truss rod	C106-SR-1	0.68	0.21	0.64	0.01	0.02	0.05	0.06	0.09	0.01	0.26	0.031	<0.005	<0.005	<0.005	0.017	<0.0005	0.011
	T1-SR-1	0.76	0.20	0.84	0.01	0.03	0.07	0.05	0.07	<0.01	0.12	0.035	<0.005	<0.005	<0.005	0.044	<0.0005	0.008
	C137a-SR-3	0.92	0.24	0.99	0.01	0.03	0.08	0.08	0.11	<0.01	0.27	0.038	<0.005	<0.005	<0.005	0.033	<0.0005	0.011
	C53-MR-1	0.93	0.22	0.92	0.02	0.03	0.08	0.07	0.05	0.03	0.22	0.041	<0.005	<0.005	<0.005	0.032	<0.0005	0.010
	T1-LR-1	1.00	0.21	0.79	0.01	0.02	0.05	0.04	0.04	<0.01	0.08	0.038	<0.005	<0.005	<0.005	0.033	<0.0005	0.008
	C53-LR-1	1.10	0.18	0.79	0.02	0.03	0.06	0.03	0.10	0.01	0.27	<0.005	<0.005	<0.005	<0.005	<0.005	<0.0005	0.011
	M32-LR-1	1.13	0.20	0.86	0.02	0.03	0.07	0.08	0.06	0.03	0.04	<0.005	<0.005	<0.005	<0.005	0.033	<0.0005	0.010

This page left intentionally blank.

## Chapter 5

# METALLOGRAPHIC ANALYSIS RESULTS

---

In addition to the chemical analysis, metallography of the recovered World Trade Center (WTC) structural steels was conducted to help identify the steels used in the towers' construction. The microstructure of every sample removed from the structural elements was evaluated (862 metallographic samples). This number included base plate material (viewed in two different orientations) and welded connections. Standard metallographic procedures for grinding, polishing, and etching were used to prepare the samples for examination with light optical microscopy.

### 5.1 EXTERIOR PANEL MATERIAL

#### 5.1.1 Perimeter Columns

##### Flange and Outer Web Plates

Contemporaneous documents indicate that the flange and outer web plates of the perimeter panels were produced by a Japanese steel mill (Yawata) and then shipped to the West Coast for assembly (NIST NCSTAR 1-3A). The chemistry analysis further confirmed that these plates were similar. It is likely that similar processing paths were used in fabricating the two types of plates, and thus, the microstructures of the flange and outer web are discussed together below.

Two types of steels were observed for the WTC steels from the towers. Hot-rolled steels, with ferrite-pearlite microstructures, were used for the lower strength materials. The higher strength plates had bainitic, martensitic, or a combination of the two structures as a result of quenching and tempering of the plates ("quenched-and-tempered" steels). As the structures of the steels are different, they will be discussed separately.

##### *Hot-Rolled Steels: Ferrite-Pearlite*

Plates with specified minimum yield strengths less than 70 ksi were observed to be hot-rolled steels (Fig. 5-1). Documents from Yawata state that this was the practice at the time (NIST NCSTAR 1-3A). Plates with yield strength ( $F_y$ ) less than 70 ksi were typically hot-rolled unless the following sizes were exceeded for a given  $F_y$ : 0.5 in. for 65 ksi, 1.25 in. for 60 ksi, and 1.5 in. for 55 ksi. Above these plate thicknesses for the given  $F_y$ , the steel was produced as quenched-and-tempered. The main microstructural constituents observed were ferrite and pearlite. The average ASTM International (ASTM) grain size number for the ferrite and the volume fraction pearlite, as a function of specified minimum yield strength, for these microstructures are shown in Fig. 5-2. The following observations were made concerning the microstructural features:

- Ferrite morphology. Relatively large polygonal and irregular ferrite morphologies were observed for plates with  $F_y$  equal to or less than 55 ksi (Fig. 5-3a). Similar ferrite morphologies were observed for plates with  $F_y$  of 60 ksi and 65 ksi, except the ferrite grain size was, on average, slightly smaller (Fig. 5-2a and Table 5-1). (A smaller grain size is

designated by a larger ASTM grain size number.) Additionally, the 0.25 in. plates with minimum yield strength of 60 ksi contained a faint Widmanstätten structure (Fig. 5–3b). Some of the plates, regardless of  $F_y$ , also had ferrite grains that were slightly elongated in the direction of rolling, particularly near the centerline of the plate, while ferrite grains near the surfaces were more equiaxed. The finer ferrite grain sizes observed in the higher strength plates would most likely be attributed to the particular controlled rolling practice used. A relatively faster cooling rate was suggested for the plates that developed the Widmanstätten structure; this factor, as well as higher austenitizing temperatures, promotes a needle-like morphology in 2-D (in 3-D, the shape is plate or disk-like). Further, the rolled plates were continuously cooled as the Widmanstätten ferrite will not form as a result of isothermal transformations.

- Pearlite distribution. Both banded (Fig. 5–4) and non-banded (Fig. 5–5) structures were observed. The single 45 ksi plate example had moderate banding, while banding was nearly absent for all plates with  $F_y$  equal to 50 ksi or 55 ksi. Minimum yield strengths equal to or greater than 60 ksi exhibited both types of constituent distribution. For those plates with aligned microstructural constituents, the bands of ferrite and pearlite were elongated in the rolling plane, resulting in a laminated-like structure in cross-section. The ferrite grains appear coarser in the bands containing no pearlite than in the ones with pearlite. Further, some samples possessed a gradient of banding through the thickness of the plate (Fig. 5–5) with the banding more prevalent near the centerline of the plate than near the surfaces, regardless of plate thickness. The occurrence of constituent banding in low carbon steels is common in hot-rolled steel plate.
- Pearlite morphology. Two types of pearlite morphology were found. For plates that had low banding features, dense, but distinguishable, lamellar plates (Fig. 5–6a) were observed in the pearlite colonies. The smaller colonies of the heavily banded structures (typically higher  $F_y$ ) had a “mottled” appearance (Fig. 5–6b) in addition to possible degenerate pearlite. The lamellar spacing could not be resolved light optically, and the morphology of the pearlite appeared almost granular at times. Bainite may also be present in these structures in places where the ferrite was associated with small cementite particles or as large grains in the lower strength plates (Fig. 5–7). Difference in pearlite appearance may be related to the chemistry and deoxidation practices (Samuels 1980).
- Volume fraction pearlite. The volume fraction pearlite of the flange and outer web plates was not observed to deviate significantly with strength of the plates (Fig. 5–2b and Table 5–1).
- Non-metallic inclusion morphology. The non-metallic inclusions observed in all plates were typical for hot-rolled steel. The MnS inclusions had a stringer appearance when viewed in longitudinal cross-section (Fig. 5–8). Typically, for plates with  $F_y$  equal to or less than 55 ksi, the stringers were heavier and had a higher volume fraction (qualitatively). Plates with  $F_y$  equal to 60 ksi and 65 ksi were also observed to have these morphologies, though not to the extent that the lower strength plates were observed to have them.

### ***“Quenched-and-Tempered” Steels: Bainitic/Martensitic***

According to contemporaneous Yawata documents, steel plates with minimum yield strengths equal to or greater than 70 ksi were produced using quenching and tempering steps (NIST NCSTAR 1-3A). Further,

plates exceeding the following sizes for a given  $F_y$  were also specified to be “quenched-and-tempered”: 0.5 in. for 65 ksi, 1.25 in. for 60 ksi, and 1.5 in. for 55 ksi. The different processing variables (cooling rates, tempering temperature, and tempering time) used to fabricate the plates can yield microstructures (bainite, tempered bainite, martensite, tempered martensite, or a combination of these) that appear similar using light optical microscopy techniques. In depth transmission electron microscopy (TEM) would be needed to determine the true structure of these steels. Additionally, it is unknown if these plates were truly “quenched” and then given a post-quench “temper” treatment or if the structures developed as a result of a single cooling path (accelerated cooling) without any post production steps as the actual processing parameters used to produce these plates were proprietary. As a result of the lack of processing history information, this section does not attempt to definitively identify the “quenched-and-tempered” microstructures, but suggests which phases may be present (bainite, tempered bainite, martensite, tempered martensite, or a combination of these).

Figure 5–9 displays representative structures of the quenched-and-tempered steels with varying minimum specified yield strengths. The images were taken near the centerline of the plate. The following microstructural features were observed:

- For the 70 ksi plate (Fig. 5–9a), broad needles and leaf-like ferrite grains were surrounded by coarse cementite precipitates. Prior austenite grain boundaries were not observed. Due to the morphology of the ferrite constituent, as well as the distribution of the cementite phase, it was not believed that this was a tempered martensitic structure, but more likely a coarse Widmanstätten or bainitic structure developed during cooling of the plate.
- The structure for plates with  $F_y$  equal to 75 ksi, 80 ksi, and 100 ksi had similar looking microstructures. Prior austenite grain boundaries were clearly visible. As the strength of the plate increases, the remnants of ferrite lath boundaries become more distinct. Cementite carbides were found within the prior austenite grain boundaries and what appears to be the lath boundaries. As the strength of the plate decreases, the carbides become more discernible and less widespread. Based upon these microstructural features, it was believed that these structures were tempered martensite with the amount of tempering increasing with decreasing plate strength.

### Inner Web Plates

Documentation from the construction era indicates that the inner plates of the perimeter columns were produced domestically (NIST NCSTAR 1-3A). Consistent with these documents was the chemical analyses indicating significant differences when comparing the inner web plates to the flange and outer web plates for  $F_y$  less than 80 ksi. Further, differences in the microstructures of plates with similar  $F_y$  were noted:

- Inner web plates were hot-rolled up to and including plates with  $F_y = 75$  ksi. Flange and outer web plates were hot-rolled for  $F_y$  less than or equal to 65 ksi. As any plate over 70 ksi from Yawata, regardless of thickness, was specified to be quenched-and-tempered, these results were consistent with the contemporaneous documents that stated different suppliers may have produced these plates (NIST NCSTAR 1-3A).

- Plates contained primarily polygonal or irregular ferrite. A low percentage of Widmanstätten ferrite was observed in all plates with the exception of the 50 ksi and 65 ksi plates; these two plates were heavily banded compared to the other hot-rolled inner web plates.
- While ferrite grain sizes were statistically equivalent (Fig. 5–2a) for a given  $F_y$ , the volume fraction of pearlite was higher in the inner web for  $F_y$  greater than 60 ksi (Fig. 5–2b).
- All plates had a combination of lamellar and mottled pearlite. Many times these two different morphologies were within close proximity to each other (Fig. 5–10a).
- The non-metallic inclusions were heavier and more prevalent throughout the inner web structure of all strength levels than in the flange plates (Fig. 5–10b).

Only plates with  $F_y$  of 80 ksi and 100 ksi were observed to have quenched-and-tempered microstructures; these structures were similar to those observed for flange plates of similar strength and were believed to be Yawata steel.

### **Welds Associated with Column Material**

Welds between flange and web plates were cross-sectioned and metallographically examined. An example of a weld between hot-rolled plates (55 ksi flange and inner web) is shown in Fig. 5–11. The weld appears to have been made in one pass, and from the depth of the heat affected zone (HAZ) in both plates, the heat input of the weld was high. The weld was sound with no visible flaws. A portion of the overall microstructure can be seen in Fig. 5–12a. The weld material was primarily acicular ferrite with coarse carbides dispersed throughout (Fig. 5–12b). The microstructure of the HAZ near the fusion line was found to have both blocky and acicular proeutectoid ferrite on the grain boundaries, with a Widmanstätten structure within the prior austenite grain boundaries (Fig. 5–12c). Bainite may also be present in the structure. Compared to the original plate microstructure of Fig. 5–1c, significant grain growth has occurred. Tempering of the original pearlite was also observed (Fig. 5–12d).

A weld cross-section was also prepared between plates with  $F_y = 100$  ksi. Again, the weld was primarily acicular ferrite with dispersed carbides. However, due to the relatively fast cooling rates with respect to the composition of the plates, a “quenched” structure was observed in the HAZ near the fusion line (Fig. 5–13).

### **Butt Plate**

A butt plate was removed from the unidentified panel C-68. Microstructural evidence suggested that the plate was either completely bainite (broad ferrite needles) with coarse carbides or a combination of the bainite/carbide structure and tempered or un-tempered martensite (thinner needles with well dispersed carbides), as shown in Fig. 5–14.

#### **5.1.2 Spandrel Plates**

Spandrel plates were also produced by the same Yawata steel mill that fabricated the flange and outer web plates (NIST NCSTAR 1-3A). The chemistry analysis further suggested that the plates were similar.

While similarities would be expected in the microstructures between these plates, there may be differences noted as the thinnest plate for the spandrels was 0.375 in. while flange plates with 0.25 in. thicknesses were characterized above. Only one 0.375 in. flange plate was recovered (55 ksi), and this will be specifically discussed below in comparison to 0.375 in. 55 ksi spandrel.

### Hot-Rolled Steels

Similar to the flange and outer web plates, spandrel plates with minimum yield strengths less than 70 ksi were observed to be hot-rolled with the exception of the 65 ksi plates with thicknesses over 0.5 in. Quenched-and-tempered microstructures were observed for these materials. Again, given the plate thickness and specified minimum yield strength, these microstructures were expected (NIST NCSTAR 1-3A). Figure 5–15 shows the microstructures as a function of  $F_y$ . The following features were observed in the microstructure:

- Ferrite Morphology. Similar to the flange plates, both polygonal and irregular ferrite morphologies were observed. However, the average ASTM grain size number for the spandrel plates was typically smaller (Fig. 5–2a). A faint Widmanstätten morphology was observed in the 36 ksi plate. Comparison between the two 55 ksi plates with a thickness of 0.375 in. showed similar ferrite morphologies.
- Pearlite distribution. To some degree, banding of the constituents was observed in all plates; the 36 ksi and 65 ksi plates had the least. All microstructures were relatively uniform across the plate thickness with the exception of the 45 ksi plate which had a gradient in banding from the edge to the centerline of the plate, with the latter being more heavily banded. There was a similar degree of banding between the two 0.375 in. plates (flange and spandrel) with  $F_y = 55$  ksi.
- Pearlite morphology. For the 65 ksi material with plate thickness less than or equal to 0.5 in. and those with minimum yield strengths below 50 ksi, the lamellar spacing in the pearlite, while being fine, was discernible. It also appeared that degenerate pearlite or bainite may exist in the 65 ksi plate. A mottled appearance was observed for the 50 ksi to 60 ksi plates. This was also observed for the 55 ksi flange plate with a thickness of 0.375 in.
- Volume fraction pearlite. The volume fraction pearlite was similar between the  $F_y$  values of 50 ksi to 65 ksi (Fig. 5–2b). The level was lower for the 45 ksi plate comparison, with the 42 ksi plate also having a similar volume fraction as the 45 ksi plate.
- Non-metallic inclusion morphology. The morphology of the non-metallic inclusions was similar to that described above for the flange plates.

### Quenched-and-Tempered Steels

For the plates with  $F_y$  values between 70 ksi and 80 ksi, as well as the 65 ksi plate with plate thickness greater than 0.5 in., the steels were quenched-and-tempered. The highest specified minimum yield strength for the spandrels, according to the engineering plans, was 85 ksi. An example of this plate was not recovered. Figure 5–16 displays the microstructures. For all plates, the microstructures had very

similar features to that of the flange plates of similar  $F_y$ . The 65 ksi plate may consist of a coarse Widmanstätten ferrite structure or bainite.

### **5.1.3 Spandrel Splice Plates**

The spandrel splice plates were hot-rolled steel with a relatively uniform distribution of the constituents. Surrounding the fine pearlite was primarily polygonal ferrite (Fig. 5–17). Table 5–2 displays both the ferrite grain size number and the volume fraction pearlite for the plates.

### **5.1.4 Floor Truss Connectors**

#### **Truss Seat**

Numerous truss seats were removed from the exterior columns and analyzed. The steels were hot-rolled with a relatively uniform distribution of the constituents (no banding of the pearlite). Some seats were found to contain a partially decarburized zone near the surface with a depth ranging from 400  $\mu\text{m}$  to 500  $\mu\text{m}$  (Fig. 5–18). There was no pattern (seat detail or location within the towers) to indicate which seats may have had this microstructural feature. The ferrite was primarily polygonal, and the pearlite had a mottled appearance. Table 5–2 displays both the ASTM grain size number for ferrite and the volume fraction pearlite for the seats. Additionally, some samples had thin, non-uniform oxide islands located at the interface between the steel and the paint. It was believed that these oxide phases had formed prior to application of the paint as the paint conformed to the oxide without cracking.

#### **Construction Bolts**

The A 325 construction bolt removed from panel M-2 was found to be a quenched-and-tempered steel (Fig. 5–19) with possible bainite and tempered martensite microstructures observed.

#### **Standoff Plate**

Two standoff plates were microstructurally analyzed. Both were observed to be hot-rolled steels with relatively uniform distribution of the pearlite. However, the volume fraction and distribution within the structures was very different. Figure 5–20 shows the structures from the two samples. Table 5–2 displays both the ASTM grain size number for ferrite and the volume fraction pearlite for the plates. The sample from panel M-2 contained mostly polygonal ferrite, whereas the standoff plate from panel N-8 consisted of both polygonal and Widmanstätten morphologies. The chemistries for these samples varied as the plate from M-2 contained Mo and V additions. It may be these alloying additions, in combination with processing conditions (particularly the cooling path of the plates), that led to the different morphologies between the samples. These differences would be expected as no specifications were found for the type of material to be used for these structural components.

#### ***Welded Joint Between Spandrel and Standoff Plate***

Two standoff plates were fillet welded directly to the spandrel plate with multiple pass beads observed only on the outer side of the plates. The specific arc welding process was not found within the design drawings, but due to the short welding length, shielded metal arc welding (SMAW) or flux cored arc

welding (FCAW) was most likely used. Typically, these joints were over-welded, meaning that a 3/8 in. or 1/2 in. weld may have been deposited where only a 5/16 in. bead was specified. Figure 5–21 shows one of these welds in cross-section. The standoff plate was a 42 ksi hot-rolled steel, and the spandrel shown in the images was a 65 ksi plate. The heat affected zone in the standoff plate can be seen extending through the entire thickness, while a shallower penetration was observed in the spandrel plate. This difference would be related to welding procedures and angle of the heat source with respect to the two plates. The microstructures of the weld and HAZ were very similar to that observed for welds between the perimeter column plates.

#### ***Welded Joint Between Standoff Plate and Floor Truss Seat***

Removal of the seat from the spandrel revealed that a double fillet weld was used to join the seat and the standoff plates. This clearly indicated that the standoff plate/seat assemblies were first prefabricated and then welded to the spandrel. Again, SMAW or FCAW was assumed to be the process used. Figure 5–22 shows one of these welds in cross-section. The heat affected zone from both fillet welds spans the entire standoff plate. Again, a shallower penetration was observed in the seat angle. The microstructures of the weld and HAZ were very similar to that observed for welds between the perimeter column plates (Sec. 5.1.1).

#### **Gusset Plate Welded to Top Chord of Floor Truss**

Three gusset plates from various locations within the tower were removed from columns and microstructurally analyzed. The samples were found to be hot-rolled steel with banding of the structure (Fig. 5–23). Polygonal and irregular ferrite grains were observed with those at the centerline of the plate heavily elongated. There was no loss of structure at the surfaces of the plates. The average ASTM grain size number of the ferrite can be found in Table 5–2. The pearlite content was also very high, above 0.40 volume fraction of the structure (Table 5–2).

#### **Damper**

One damper was removed from the perimeter panels and microstructurally analyzed. The sample was a hot-rolled steel composed of a banded ferrite and pearlite structure (Fig. 5–24). There was no loss of structure at the surfaces of the plates. The average ASTM grain size number of the ferrite and volume fraction pearlite can be found in Table 5–2.

#### **Gusset Plate for Damper Unit and Diagonal Bracing Strap Attachment**

Three gusset plates used for attaching the damper units and diagonal bracing straps to the perimeter columns were removed and analyzed metallographically. The plates were found to be hot-rolled steel with a relatively uniform distribution across the sections observed. A representative micrograph is shown in Fig. 5–25. The majority of the ferrite is polygonal with some irregular grains. The average ASTM grain size number of the ferrite and the volume fraction pearlite can be seen in Table 5–2.

## Diagonal Bracing Strap

Two samples of diagonal bracing straps were removed and examined. Both were hot-rolled steels that consisted of ferrite and pearlite structures that were slightly banded (Fig. 5–26). The shapes of the ferrite grains are slightly elongated in the rolling direction, particularly in the center regions of the plates. The average ASTM grain size number of the ferrite and volume fraction pearlite can be found in Table 5–2.

## 5.2 CORE MATERIAL

### 5.2.1 Wide Flange Core Columns

Five 36 ksi wide flange core columns with known as-built locations were recovered and available for analysis. The sections were found to be hot-rolled steels with a relatively uniform distribution of the constituents (ferrite and pearlite) across the sections observed. Representative micrographs are shown in Fig. 5–27. The majority of the ferrite was polygonal or blocky with some Widmanstätten. At low magnification, very localized banding of the structure can be observed. The average ASTM grain size number of the ferrite was 10.5 (Table 5–3). The pearlite constituent, at a volume fraction of 0.36 for this sample (Table 5–3), was dense with no loss of structure near the edges of the section.

There was only one 42 ksi wide flange column identified from the recovered WTC steel. The section was also a hot-rolled steel with a relatively uniform distribution of the constituents across the sections observed. Representative micrographs are shown in Fig. 5–28. The majority of the ferrite is polygonal with an average ASTM grain size number of 9.4 (Table 5–3). The pearlite constituent was dense with no loss of structure near the edges of the section.

### 5.2.2 Built-Up Box Core Columns

Three 36 ksi built-up box columns were identified from the recovered WTC steel. The sections were found to be hot-rolled steels with some banding of the constituents across the sections observed. Representative micrographs are shown in Fig. 5–29. The majority of the ferrite was polygonal or blocky with some irregular morphologies. At low magnification, banding of the structure can be observed. The average ASTM grain size number of the ferrite was 9.6 (Table 5–3). The pearlite constituent, at a volume fraction of 0.22 for this sample (Table 5–3), was dense with no loss of structure near the edges of the plate.

Two 42 ksi built-up box columns were recovered and available for analysis. Five of the eight plates available for inspection were examined. The plates were found to be hot-rolled steels with some banding of the constituents across the sections observed. Representative micrographs are shown in Fig. 5–30. The majority of the ferrite was polygonal or blocky with some Widmanstätten morphologies observed. The average ASTM grain size number of the ferrite was 11.0 (Table 5–3). The pearlite constituent, at a volume fraction of 0.29 for this sample (Table 5–3), was dense with no loss of structure near the edges of the plate.

### 5.2.3 Channel

Two samples were removed from the channels and microstructurally analyzed. Both were found to have hot-rolled structures but with vastly different distributions of the constituents. The sample from piece

C-107 had a heavily banded structure (Fig. 5–31a), while a uniform distribution of the pearlite was found in the sample from M-24 (Fig. 5–31b). Their chemistries were quite different as well, Table 4–6, with the sample from C-107 having higher contents for both C and Mn. These differences would be expected as no specifications were found for the type of material to be used for these structural components.

#### 5.2.4 Core Truss Seat

Two core seats were removed from the channels and microstructurally analyzed. The sections were found to be hot-rolled steels with a relatively uniform distribution of the constituents across the sections observed. Representative micrographs are shown in Fig. 5–32. The majority of the ferrite was polygonal. The average ASTM grain size number of the ferrite was 10.3 (Table 5–2). The pearlite constituent, at a volume fraction of 28.8 percent for this sample (Table 5–2), was dense with no loss of structure near the edges of the section.

Compared to the average for the perimeter panel floor truss seats, the grain size was statistically similar, but the volume fraction of pearlite was significantly higher.

### 5.3 FLOOR TRUSS MATERIAL

#### 5.3.1 Rod

Six different diameter rods were recovered from the floor trusses ranging in size from 0.68 in. to 1.13 in. All rods were observed to have hot-rolled microstructures with a relatively uniform distribution of the pearlite constituent. Polygonal, irregular, and Widmanstätten morphologies were observed for the ferrite; though the volume fraction and distribution within the structures was very different. Figure 5–33 shows the structures from three rods with three different diameters. The sample labeled T1-SR-1 contained mostly polygonal and irregular ferrite, whereas T1-LR-1 consisted of all three types. These rods were removed from the same floor truss and had chemistries that were very similar (Table 4–9). The sample M32-LR-1 also contained all three morphologies; however, it had a completely different distribution. The chemistry for this sample varied from the first two in that it had small Mo additions and lacked V. It may be these alloying additions, in combination with processing conditions (particularly the cooling path of the rod), that attributed to the different morphologies between the samples. (Laclede produced all rods in house.) Table 5–4 displays both the ASTM grain size number for ferrite and the volume fraction pearlite for the individual samples.

#### 5.3.2 Chord/Angle

Ten pieces of truss angle were evaluated from the floor truss material recovered. Again, all were observed to have hot-rolled microstructures with a relatively good distribution of fine pearlite. The ASTM grain size number for the ferrite and the volume fraction pearlite for some of the individual samples can be found in Table 5–4. Unlike the truss rod microstructures, angle samples with V additions had a higher volume fraction of the Widmanstätten morphology for the ferrite constituent (Fig. 5–34). Samples lacking this element contained primarily polygonal ferrite. This information suggests that the processing conditions had a strong effect on the microstructure as the correlation between chemistry and ferrite morphology is different between the rods and the angles. (Laclede produced both of these shapes in house.)

## 5.4 FURNACE EXPOSURE OF WTC STEEL

The effect of high temperature exposure due to pre-collapse fires on the structural steels is of great concern as the strength of the steel (and structural integrity of the component) decreases significantly at elevated temperature. Evidence of this exposure may be observed through changes in the steel microstructure. Therefore, four “as-fabricated” steel structures were chosen for furnace studies in order to simulate the exposure of steel to high temperature excursions. These samples were: a 60 ksi hot-rolled flange plate, a 100 ksi quenched-and-tempered flange plate, a 42 ksi hot-rolled spandrel plate, and a hot-rolled floor truss seat. The samples were chosen based upon their specified minimum yield strength and location within the building (no pre-collapse fire exposure). Unless otherwise indicated, furnace exposures consisted of placing small coupons of material into a furnace pre-heated to temperatures in the range of 200 °C to 625 °C for times up to 2 h. The samples were then removed from the furnace and allowed to cool in a medium of standard silica sand. Metallographic preparation of the samples was similar to that used above.

### 5.4.1 Hot-Rolled Flange and Spandrel Plates

A 60 ksi flange plate was chosen from panel N-7 (WTC 1, column 126, 97th floor) and a 42 ksi spandrel plate from panel N-9 (WTC 1, 102nd floor spandrel, near column 154). According to the time-fire exposure maps of NIST NCSTAR 1-3C, pre-collapse fires were not observed near either location. Further, there was no evidence, such as loss of paint or sooting on the column, that suggested post-collapse fires may have affected the material. For temperatures below 625 °C, only times of 0.25 h and 0.5 h were investigated.

For temperatures below 625 °C, there was no apparent change in structure using light optical microscopy. However, when samples were exposed to 625 °C, alteration of the microstructure was evident after only 15 min of exposure. Figure 5–35 displays representative microstructures of the exposed 60 ksi flange plate and Fig. 5–36 of the 42 ksi spandrel plate. Both figures have an “as-fabricated” structure ( $t = 0$  h) shown for comparison. For the 60 ksi flange plate, the banding of the structure remained through the 1 h exposure with it being eliminated in the 2 h time frame. With time, the change in the cementite phase was clearly visible. Initially, the pearlite was mottled, however, after the first 15 min of exposure, the cementite lamellae within the pearlite began to spheroidize, with the precipitates becoming more discernible at the longer times. After the 1 h exposure, cementite was found to form larger carbide particles in the ferrite grain boundaries. The transformation of cementite to this morphology was nearly complete after 2 h. For the 42 ksi spandrel plate, the transformation with time was also noticeable, though not to the extent seen for the flange plate. After the 2 h exposure, remnants of the initial pearlite colonies were still visible even though spheroidization was well in progress.

The difference in the kinetics of spheroidization for these two steels was most likely a result of the prior thermomechanical history. The higher strength 60 ksi flange plate experienced a significantly different control rolled schedule than the 42 ksi spandrel plate. This was clearly evident in the starting microstructures (e.g., significant banding and smaller constituent size of the 60 ksi plate). As a result, the microstructures responded differently with exposure to elevated temperatures with the 60 ksi plate having faster spheroidization kinetics than the 42 ksi spandrel plate.

### 5.4.2 Quenched-and-Tempered Flange Plate

A 100 ksi flange plate was chosen from panel C-10 (WTC 1, column 451, 88th floor). According to the time-fire exposure maps of NIST NCSTAR 1-3C, pre-collapse fires were not observed near this location. Further, there was no evidence that suggested post-collapse fires may have affected the material. Exposure was conducted only at 625 °C for up to 2 h.

Figure 5–37 displays representative microstructures of the exposed samples, as well as an “as-fabricated” structure. It can be seen that as the exposure time increased, the lath boundaries of the martensitic structure become less distinguishable, while the cementite precipitates becoming more discernable.

### 5.4.3 Exterior Panel Floor Truss Seat

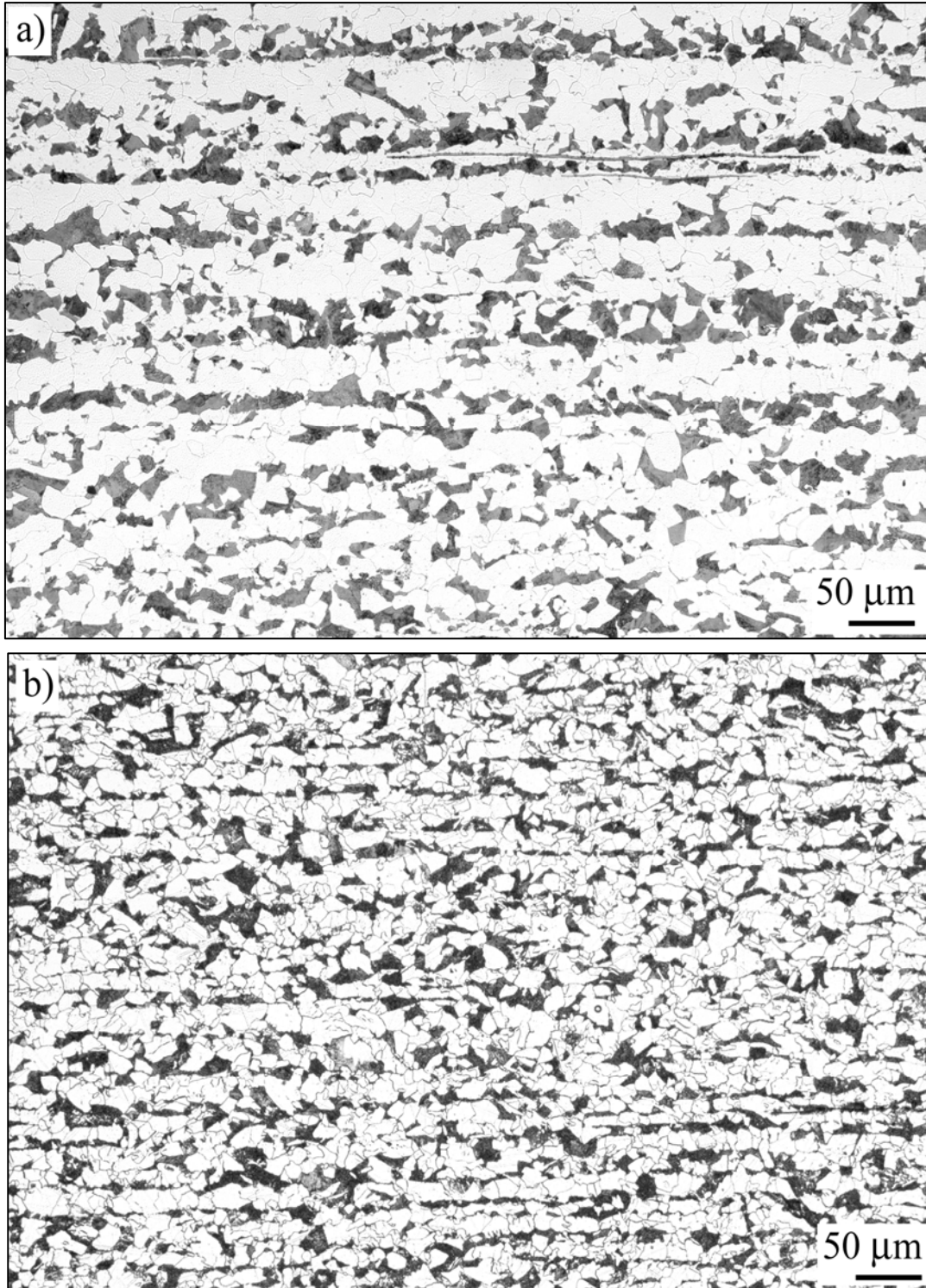
A floor truss seat was chosen from C-18 (WTC 2, column 231, 95th floor). According to the time-fire exposure maps of NIST NCSTAR 1-3C, pre-collapse fires were not observed near this location. Further, there was no evidence, such as loss of paint or sooting on the column, that suggested post-collapse fires may have affected the material.

For temperatures below 625 °C, there was no apparent change in structure using light optical microscopy. However, when samples were exposed to 625 °C, alteration of the microstructure was evident after only 15 min of exposure. Figure 5–38 displays representative microstructures of the exposed floor truss seat. The as-fabricated structure ( $t = 0$  h) was shown for comparison. At 0.25 h, some spheroidization can be observed, however, it was very clear in the 0.5 h time frame. Continued exposure resulted in the remnants of the initial pearlite colonies still being visible even though spheroidization was well in progress. Similar to that of the 42 ksi spandrel plate, the kinetics of spheroidization were much slower for this component than for the 60 ksi flange plate.

## 5.5 SUMMARY

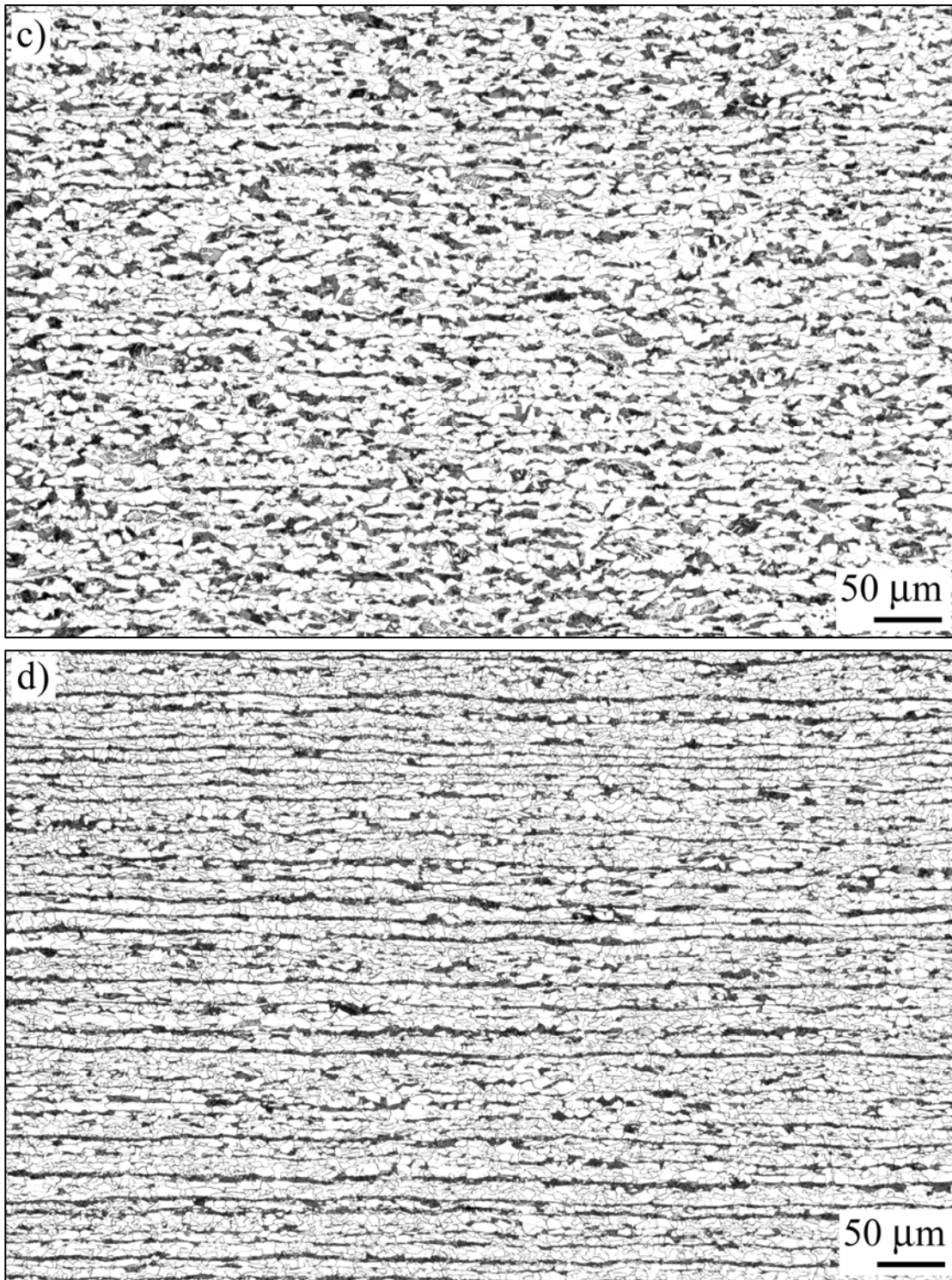
Two types of steels were observed from the recovered WTC steels: hot-rolled for the lower strength materials and quenched-and-tempered for the higher strength plates/components. The hot-rolled steels had ferrite-pearlite microstructures while the quenched-and-tempered structures exhibited possible bainitic/martensitic structures. For each of type of steel, the types of structures observed were expected for steels of that era. Further, while microstructural features may have varied from plate to plate (for a given  $F_y$ ) or across an individual plate thickness or component, there was no indication that the practices followed to produce the plates were improper or that the mechanical properties of the component may have been negatively affected.

In addition to the “as-fabricated” structures, it was shown that an elevated temperature exposure (625 °C) for a minimum of 15 min was found to produce significant changes to the microstructure for both hot-rolled and quenched-and-tempered steels. Temperatures at 500 °C and below showed no change using light optical microscopy. Further, the prior thermomechanical treatment of the component appeared to dictate the kinetic rate of spheroidization.



Source: NIST.

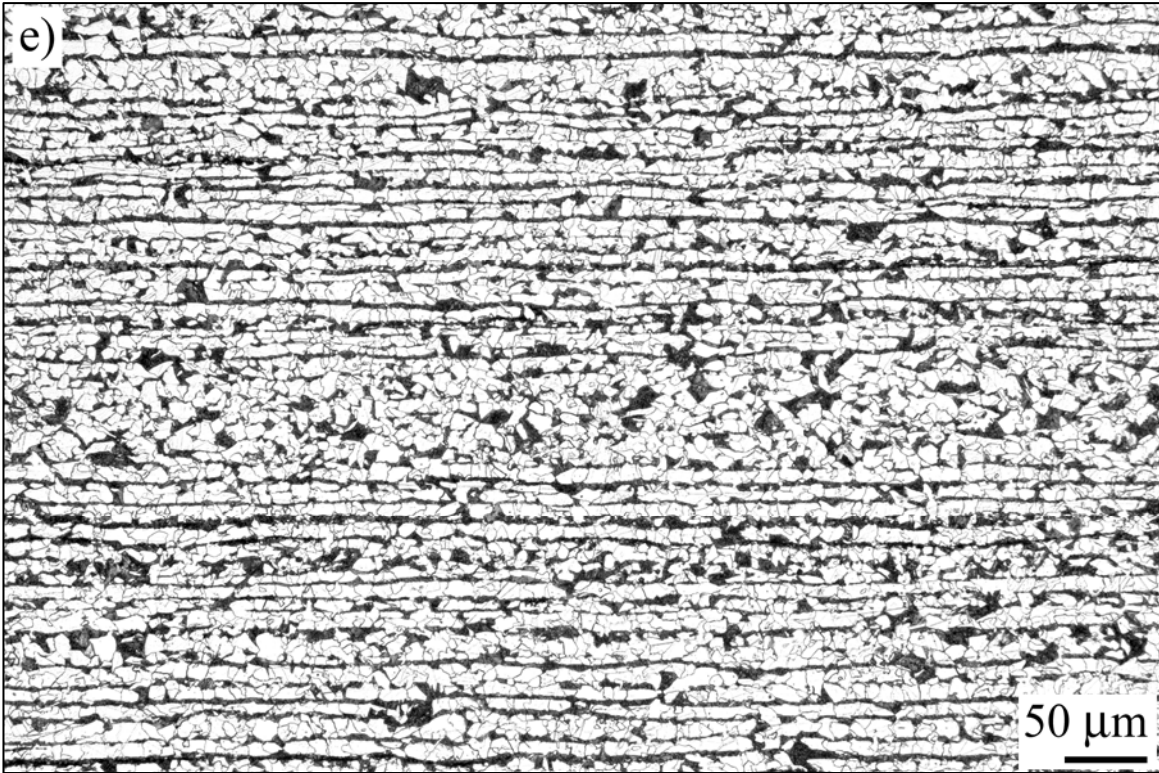
**Figure 5–1. Representative microstructures of hot-rolled perimeter column flange plates as a function of strength level. The images were taken near the centerline of the plate.**  
a)  $F_y = 45$  ksi (panel ASCE-3, unidentified perimeter column with “45” flange stamping);  
b)  $F_y = 50$  ksi (panel M-26, WTC 1, 129, 90th floor). Both with 2 percent nital and 4 percent picral etch.



Source: NIST.

**Figure 5–1. Representative microstructures of hot-rolled perimeter column flange plates as a function of strength level. The images were taken near the centerline of the plate.**

**c)  $F_y = 55$  ksi (panel M-20, WTC 1, column 121, 100th floor); d)  $F_y = 60$  ksi (panel N-7, WTC 1, column 126, 97th floor). Both with 2 percent nital and 4 percent picral etch (continued).**



Source: NIST.

**Figure 5–1. Representative microstructures of hot-rolled perimeter column flange plates as a function of strength level. The images were taken near the centerline of the plate.**  
**e)  $F_y = 65$  ksi (panel N-99, WTC 1, column 149, 99th floor). 2 percent nital and 4 percent picral etch (continued).**

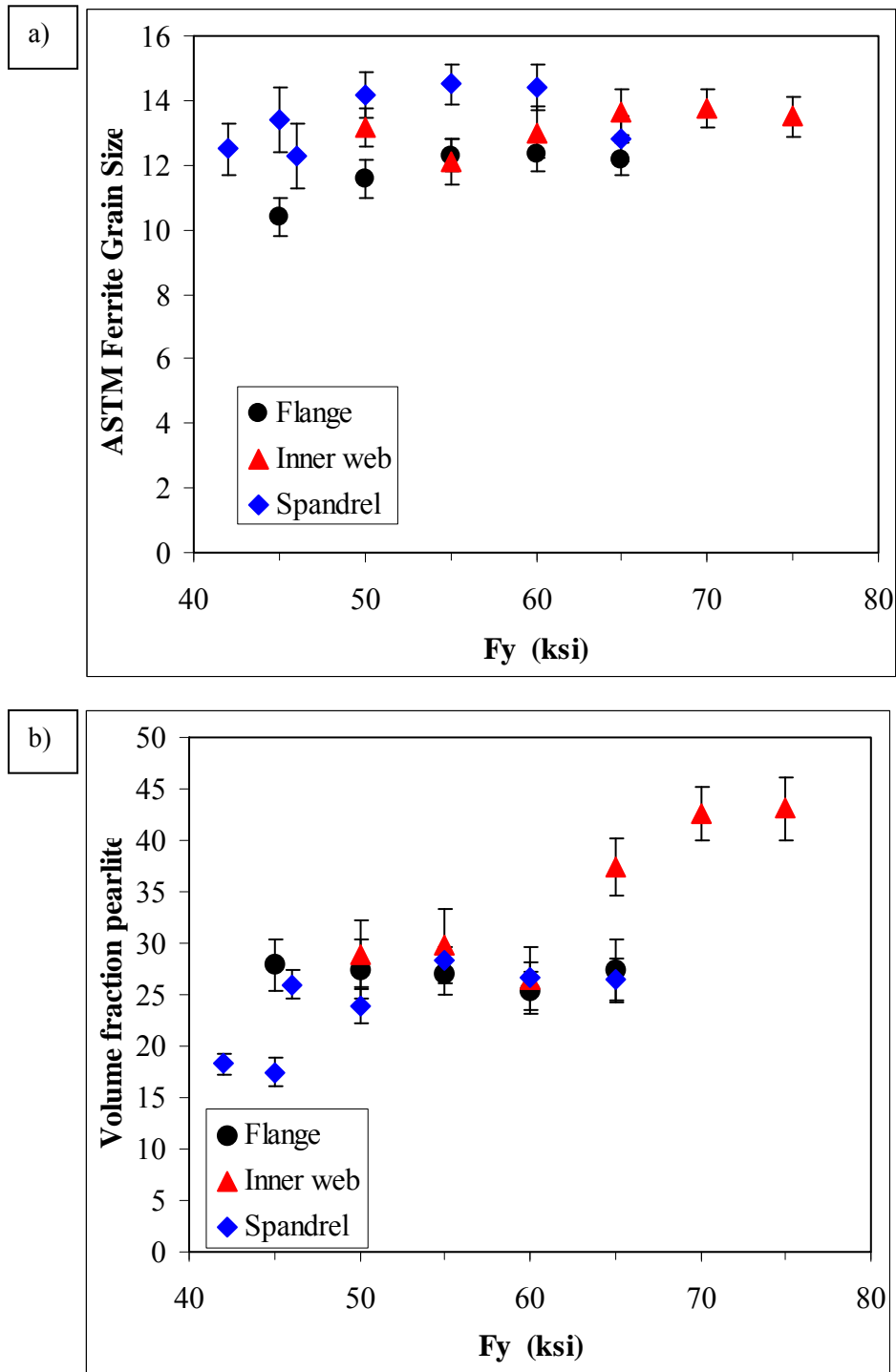
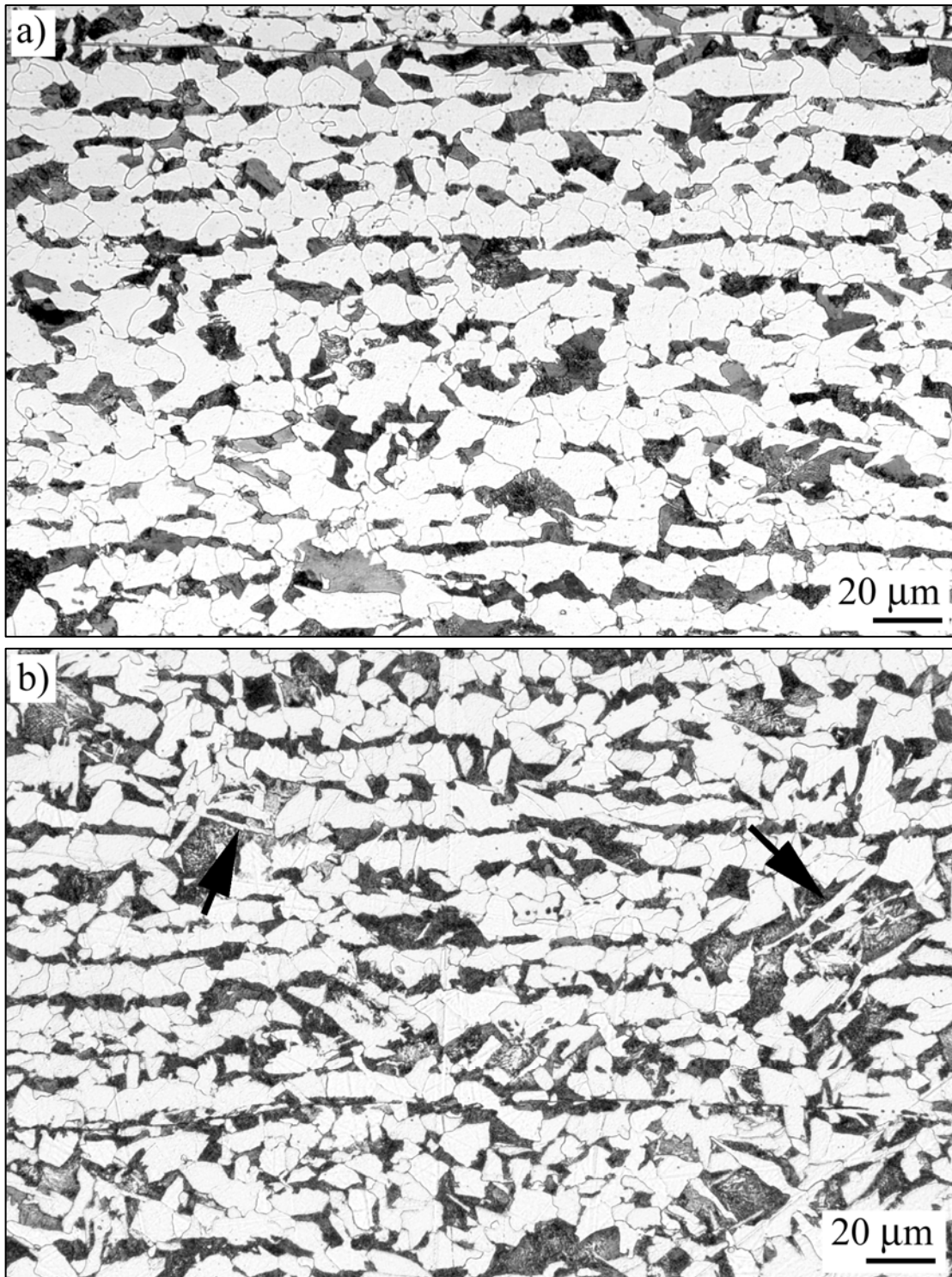
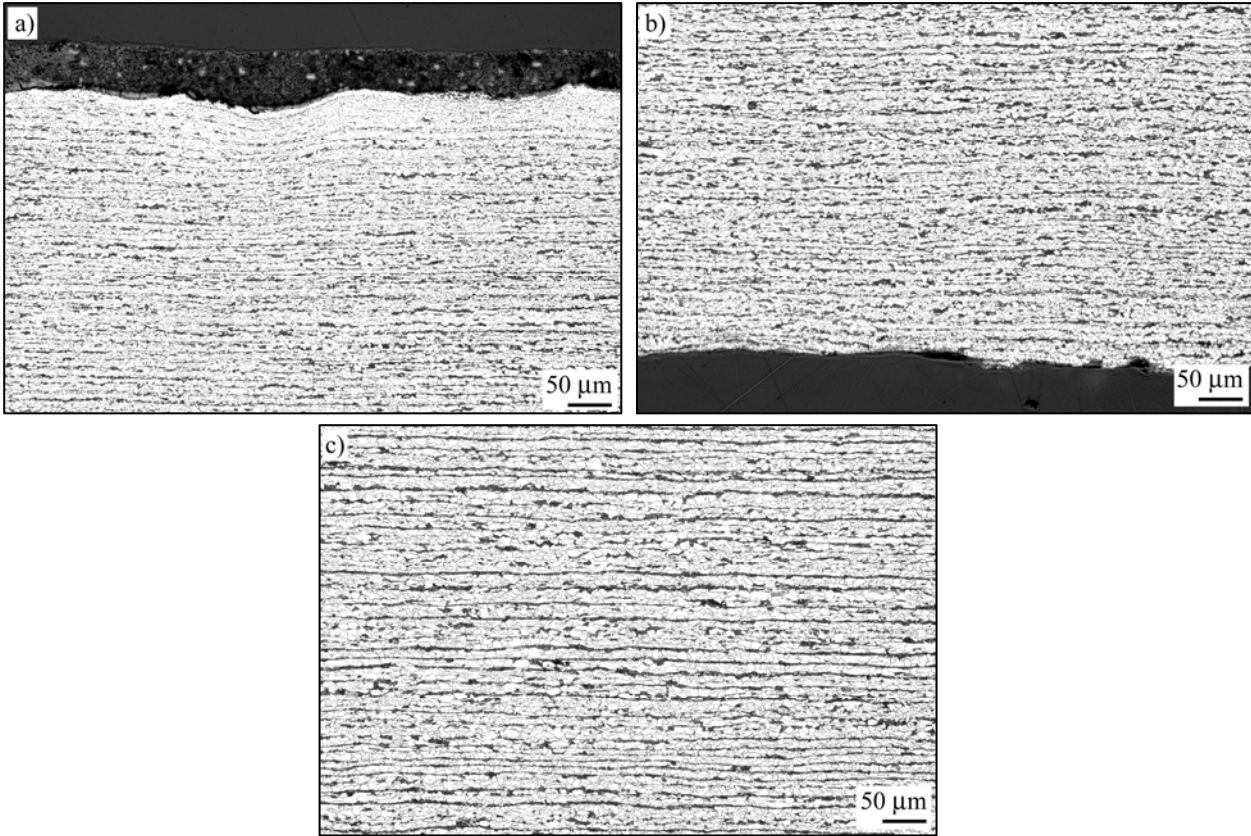


**Figure 5-2. a) ASTM ferrite grain size number as a function of specified minimum yield strength of the plate, and b) volume fraction of pearlite as a function of specified minimum yield strength of the plate. Various perimeter panel plates are shown in both graphs.**



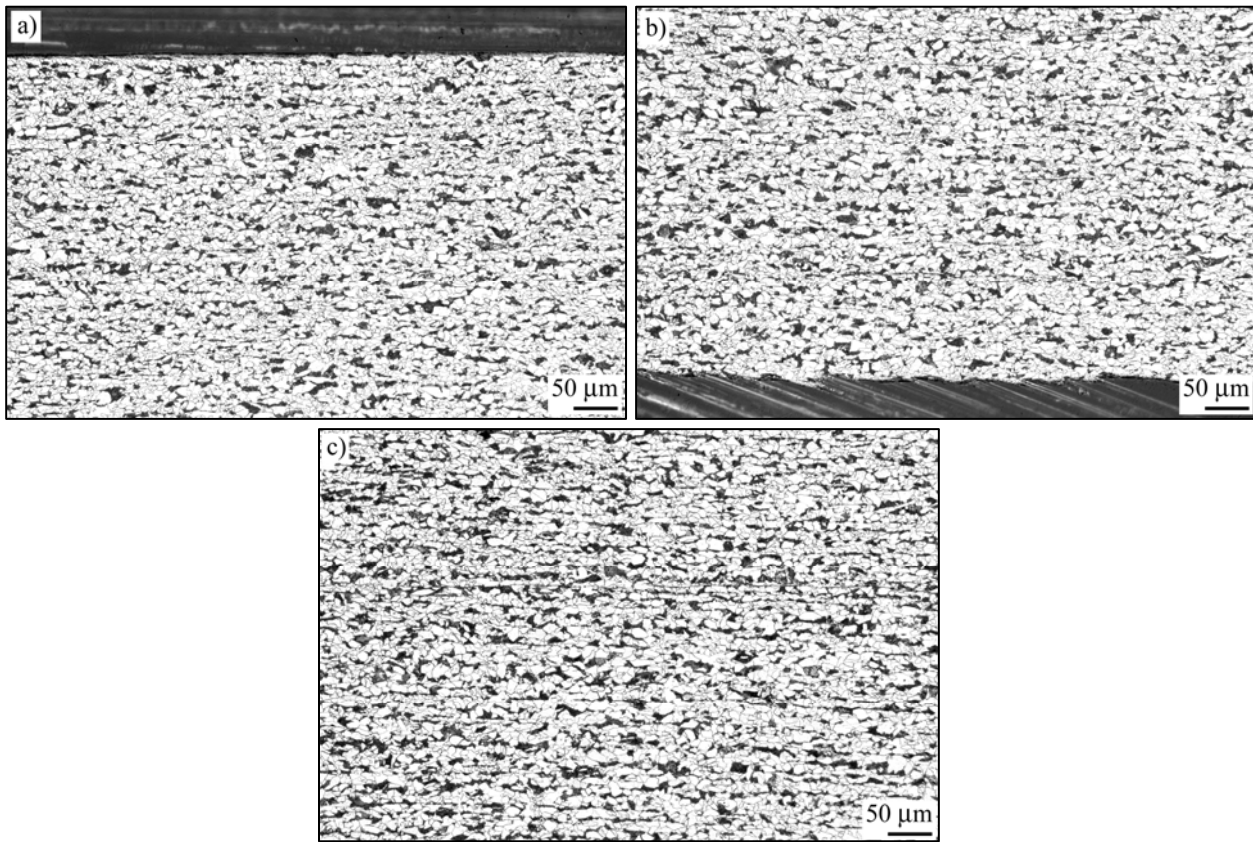
Source: NIST.

**Figure 5–3. Representative micrographs of ferrite morphologies observed from plates with the specified minimum yield strength less than 70 ksi. a) Polygonal and irregular ferrite grains (panel M-26, WTC 1, column 129, 90th floor), b) 0.25 in. thick plate with  $F_y = 60$  ksi, in addition to polygonal and irregular ferrite grains, a faint Widmanstätten structure (ferrite needles) was developed (panel K-1, WTC 1, column 210, 97th floor). Both with 2 percent nital and 4 percent picral etch.**



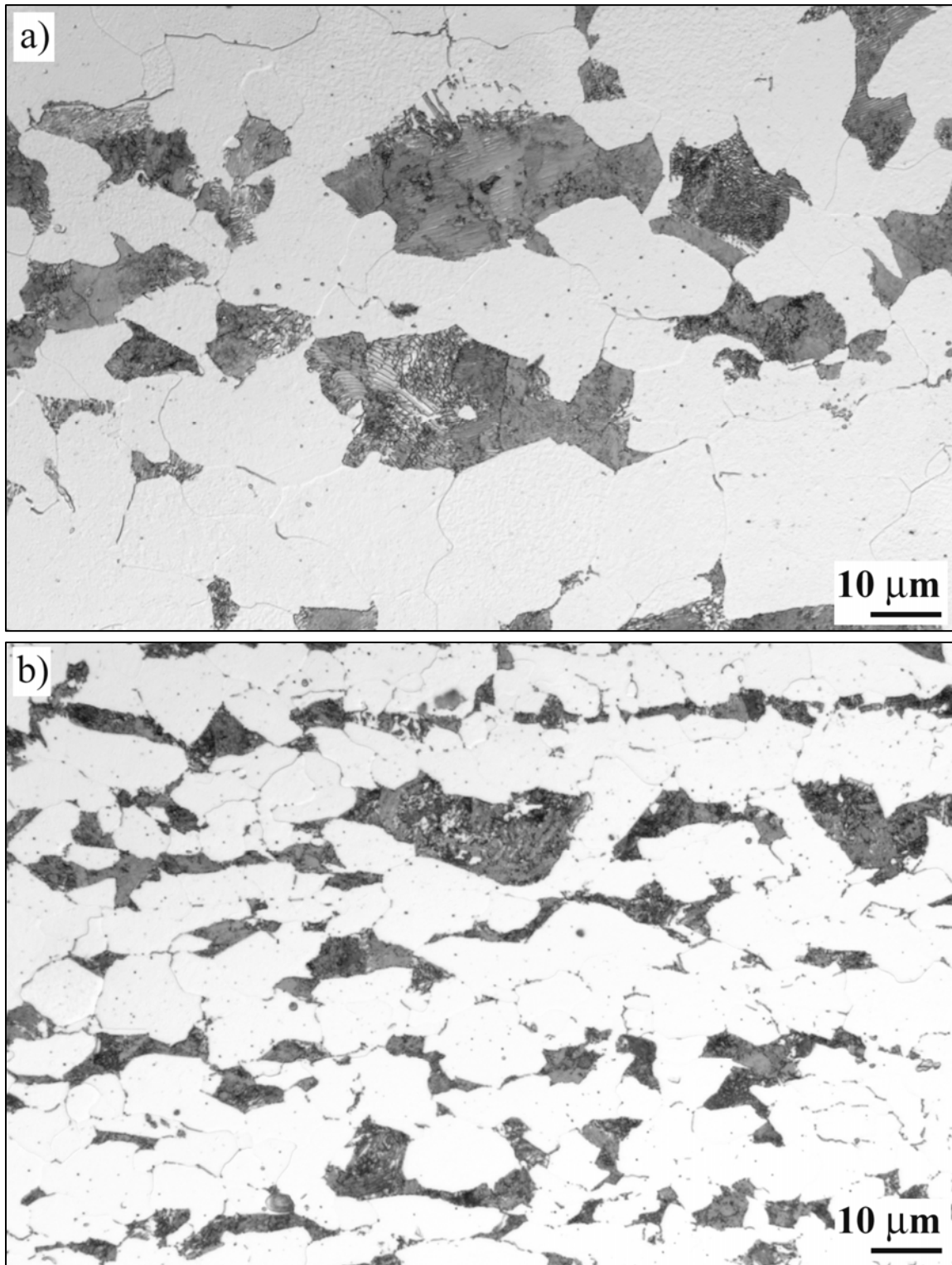
Source: NIST.

**Figure 5–4. Banding of microstructural constituents observed in a 60 ksi plate. a) and b) are opposite surfaces of the plate showing banding of the constituents; c) was taken near the centerline of the plate showing heavy banding (panel N-7, WTC 1, column 126, 97th floor). 2 percent nital and 4 percent picral etch.**



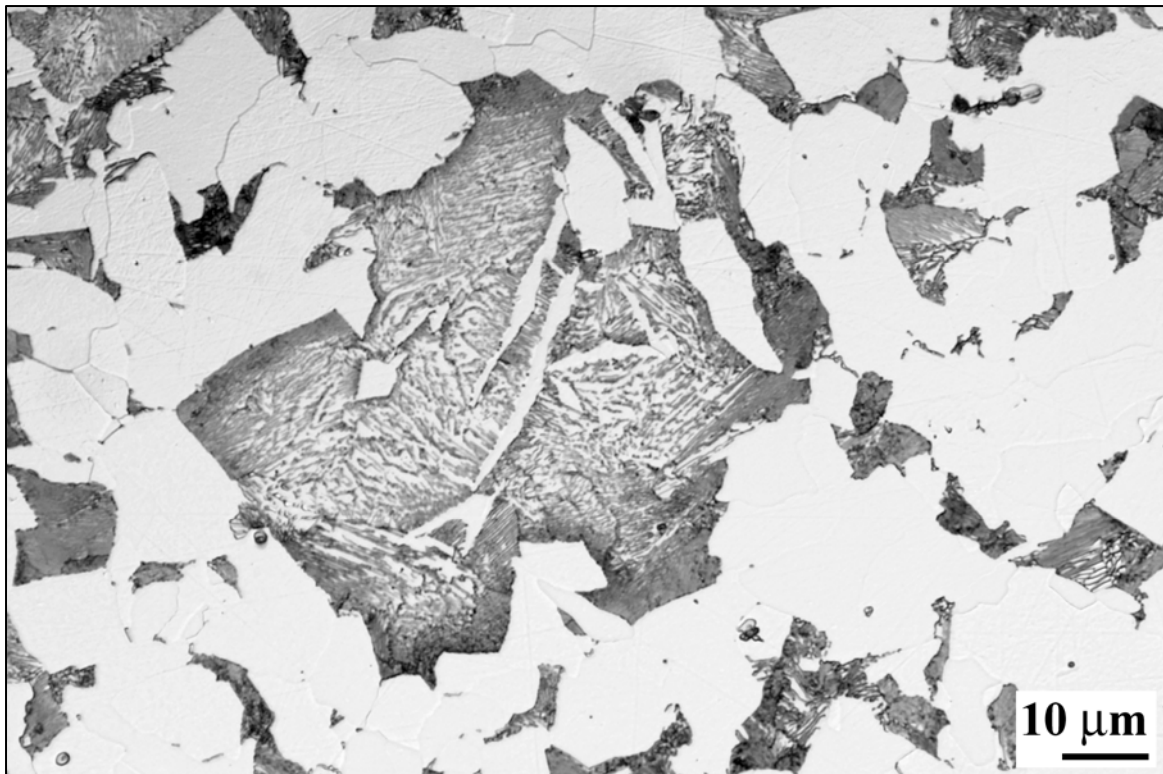
Source: NIST.

**Figure 5–5. Distribution of microstructural constituents observed in a 60 ksi plate. a) and b) are opposite surfaces of the plate showing nearly uniform distribution of constituents; c) was taken near the centerline of the plate showing some banding effects (panel N-8, WTC 1, column 142, 97th floor). 2 percent nital and 4 percent picral etch.**



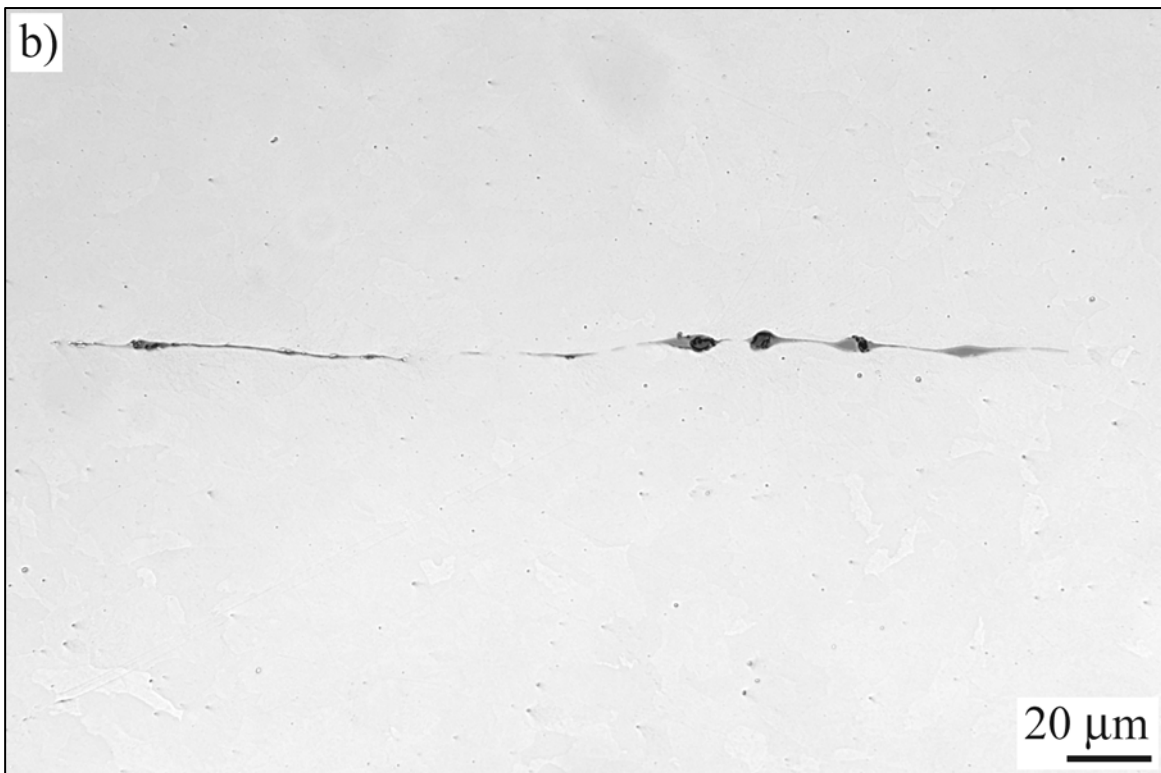
Source: NIST.

**Figure 5–6. Morphologies of pearlite observed. a) Pearlite with observable lamellar spacing (panel ASCE-3, unidentified perimeter column with “45” stamping on flange plate) and b) mottled appearance where the lamellar spacing were not visible and may have a granular morphology (panel C-40, WTC 1, column 136, 98th floor). Both with 2 percent nital and 4 percent picral etch.**



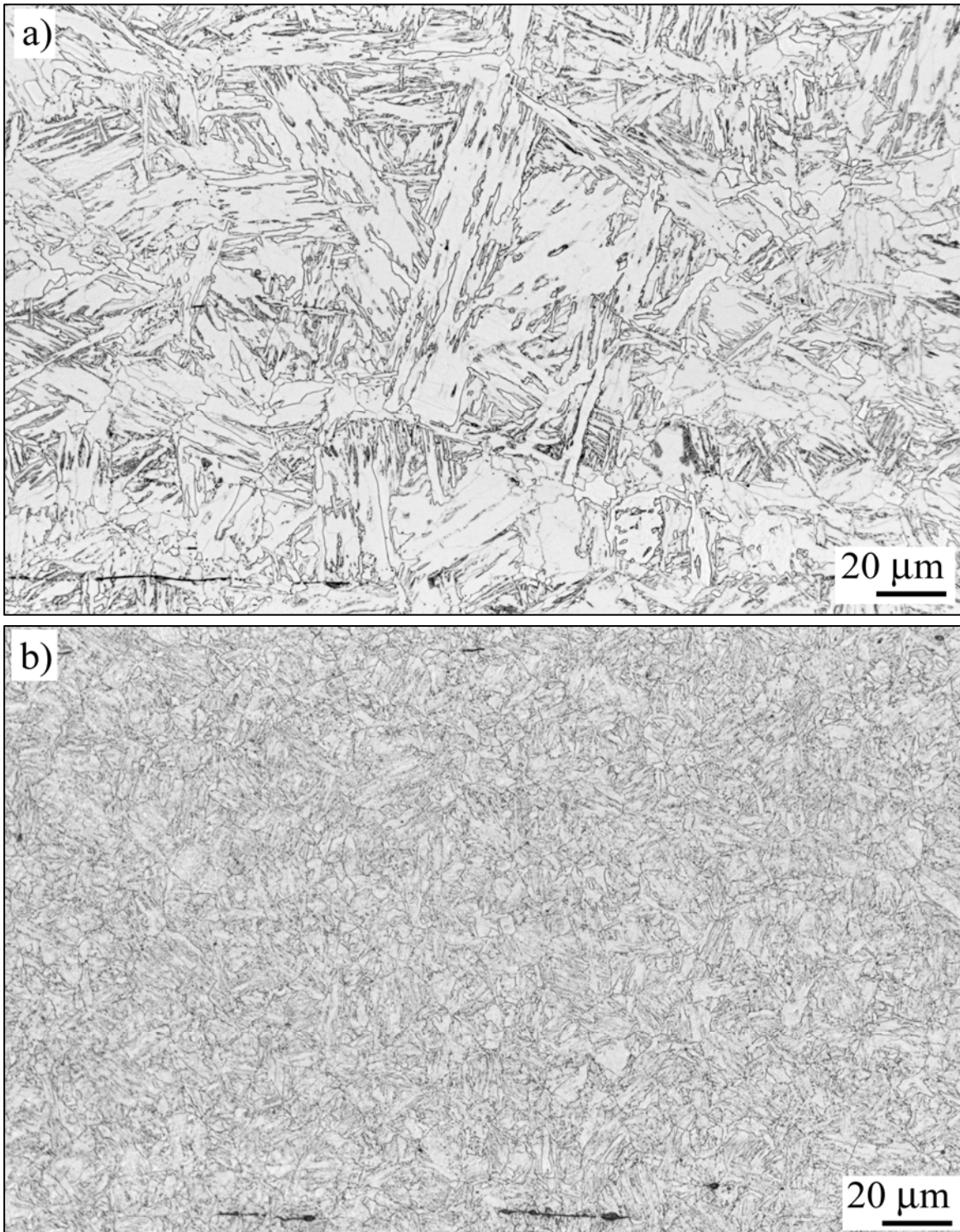
Source: NIST.

**Figure 5–7. Possible bainite or degenerate pearlite in lower strength plates. (panel M-27, WTC 1, column 131, 93rd floor). 2 percent nital and 4 percent picral etch.**



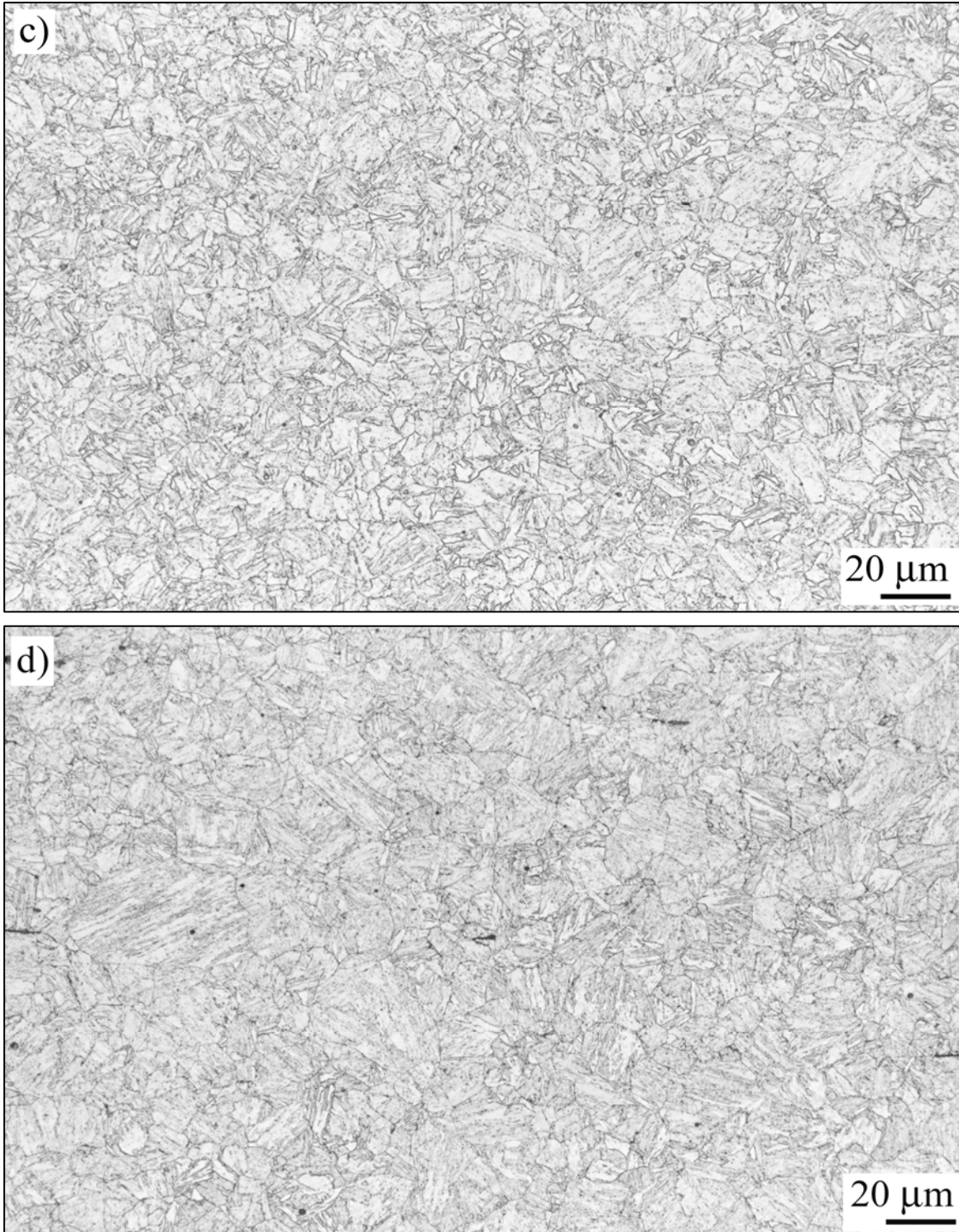
Source: NIST.

**Figure 5–8. Non-metallic inclusions of MnS observed in the rolled plates. a) Thin stringers aligned with the rolling direction of the plate (panel S-14, WTC 2, column 217, 92nd floor and b) thin stringers with other secondary phases (panel N-10, WTC 1, column 114, 91st floor). Samples in the as-polished condition.**



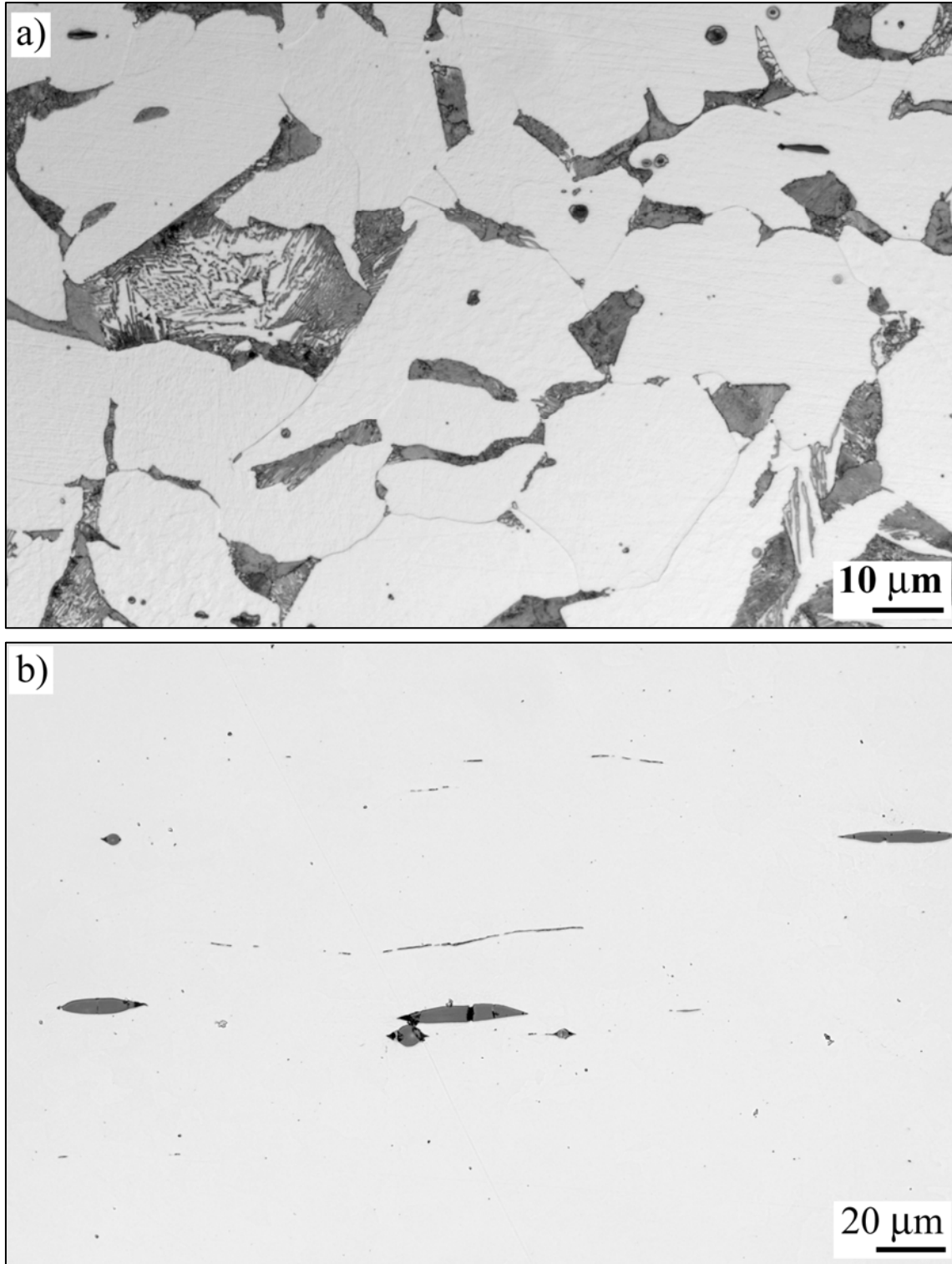
Source: NIST.

**Figure 5–9. Representative microstructures of quenched-and-tempered perimeter column flange plates as a function of strength level. The images were taken near the centerline of the plate. a)  $F_y = 70$  ksi (panel S-10, WTC 1, column 224, 94th floor); b)  $F_y = 75$  ksi (panel C-22, WTC 1, 157, 95th floor). Both with 2 percent nital and 4 percent picral etch.**



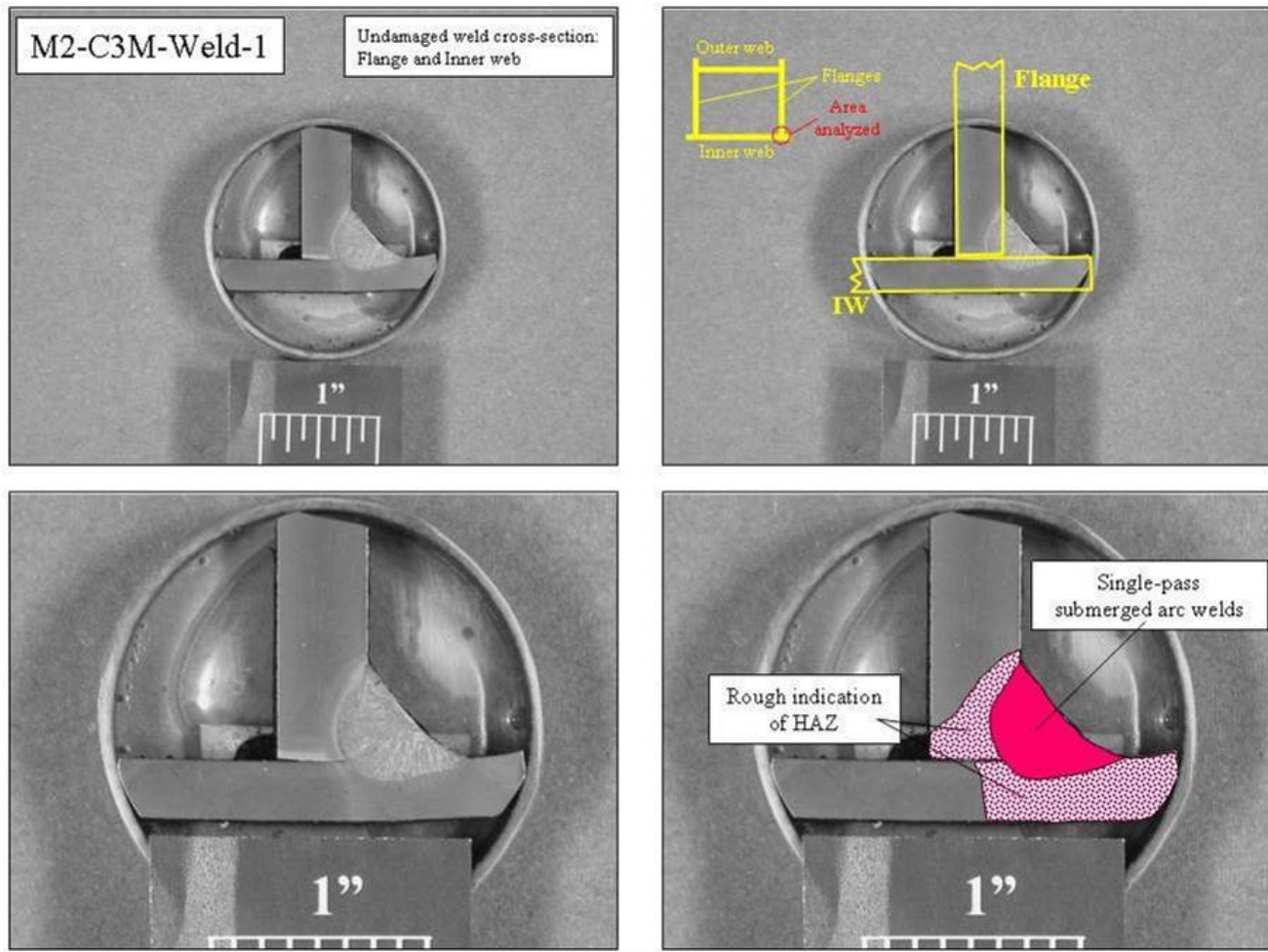
Source: NIST.

**Figure 5–9. Representative microstructures of quenched-and-tempered perimeter column flange plates as a function of strength level. The images were taken near the centerline of the plate. c)  $F_y = 80$  ksi (panel C-25, WTC 1, column 207, 89th floor), d)  $F_y = 100$  ksi (panel C-14, WTC 2, 259, 87th floor). Both with 2 percent nital and 4 percent picral etch (continued).**



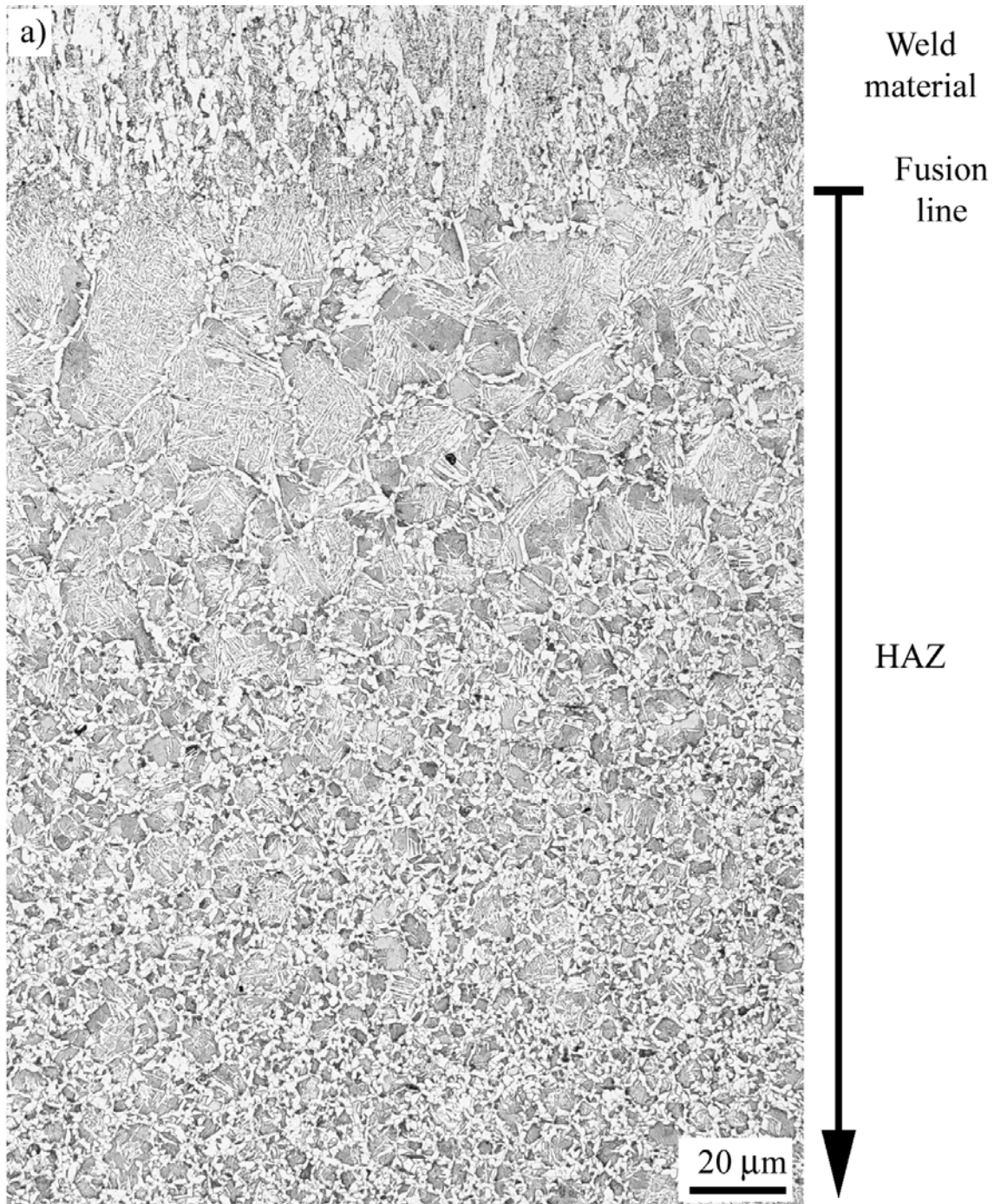
Source: NIST.

**Figure 5–10. a) Microstructures from hot-rolled steels used for all inner web plates, pearlite was observed to be mottled and lamellar; sample shown from panel C-40 (WTC 1, column 135, 100th floor). 2 percent nital and 4 percent picral etch. b) Heavy second phase observed in inner web, from panel M-20 (WTC 1, column 121, 100th floor). Sample in the as-polished condition.**



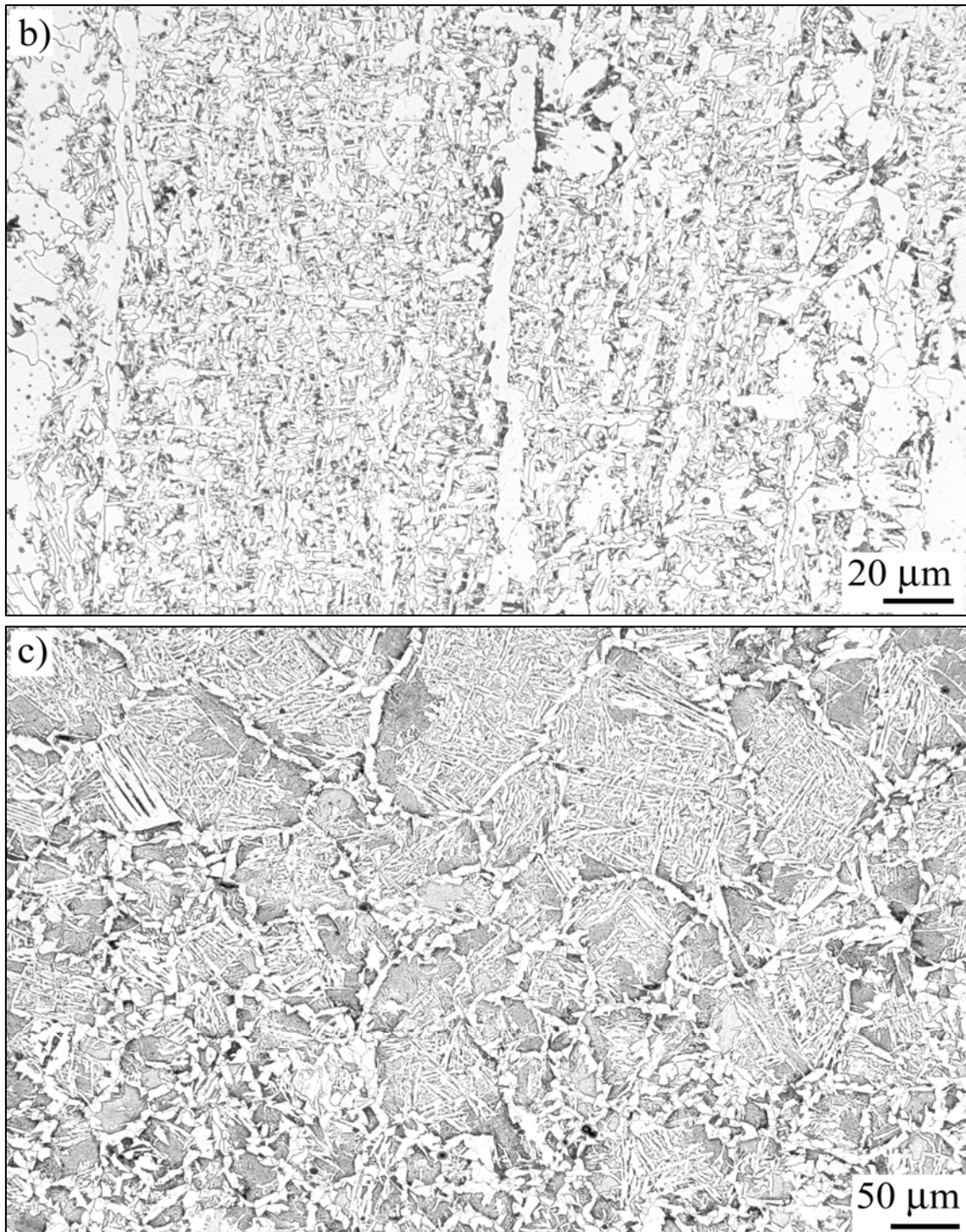
Source: NIST.

**Figure 5–11. Polished and etched cross-section of weld between inner web and flange. The sample was removed from an undamaged portion of column of panel M-2 (WTC 1, column 129, 97th floor) that was directly hit by the plane. 2 percent nital and 4 percent picral etch.**



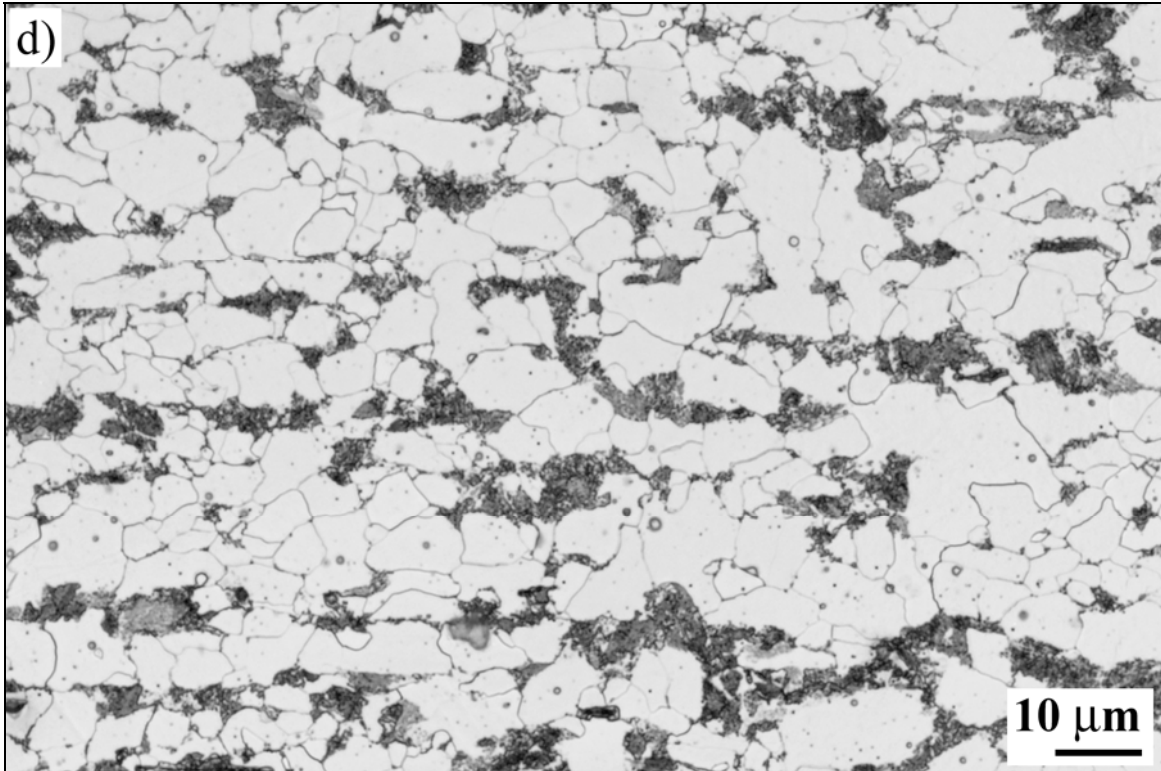
Source: NIST.

**Figure 5–12. Representative micrographs from perimeter column welds of a hot-rolled steel with  $F_y = 55$  ksi. a) Low magnification showing weld material and portion of HAZ. Sample shown was from panel M-2 (WTC 1, column 129, 97th floor). 2 percent nital and 4 percent picral etch.**



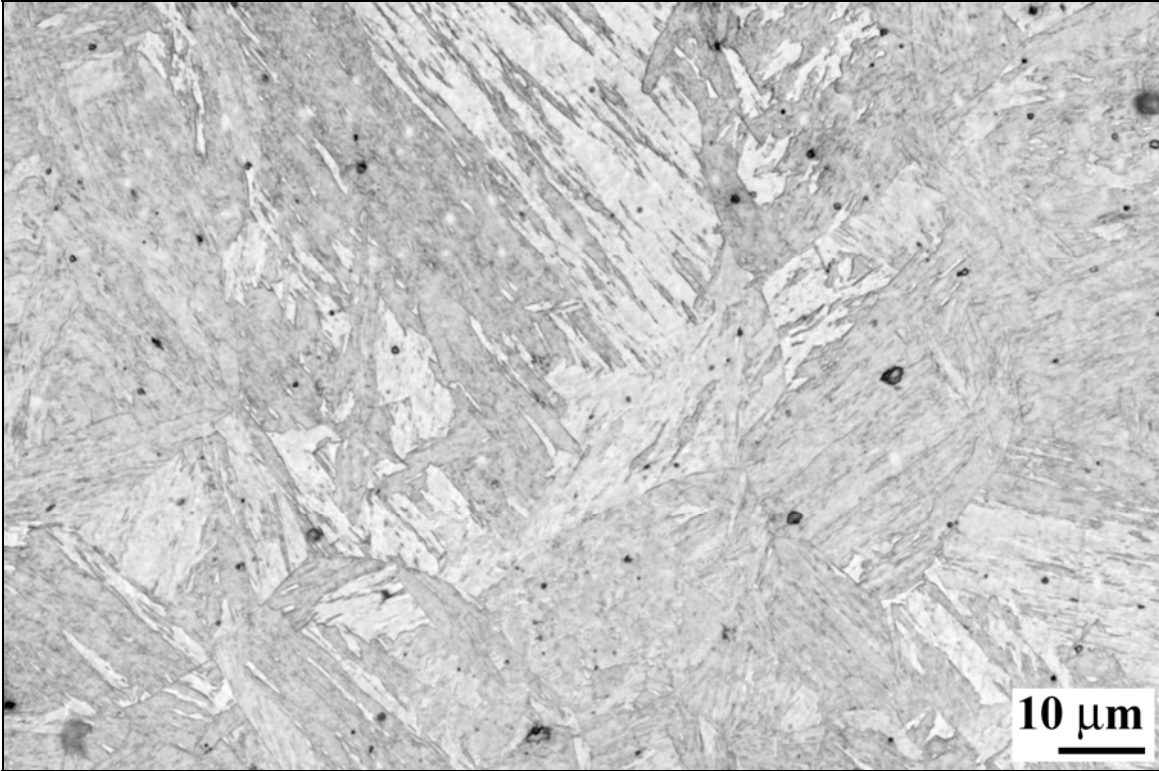
Source: NIST.

**Figure 5-12. Representative micrographs from perimeter column welds of a hot-rolled steel with  $F_y = 55$  ksi. b) Weld material that was primarily acicular ferrite with carbide dispersion and c) HAZ near the fusion line showing grain growth and formation of Widmanstätten and acicular ferrite. Bainite may also be present in areas where ferrite contains small cementite particles. Sample shown was from panel M-2 (WTC 1, column 129, 97th floor). Both with 2 percent nital and 4 percent picral etch (continued).**



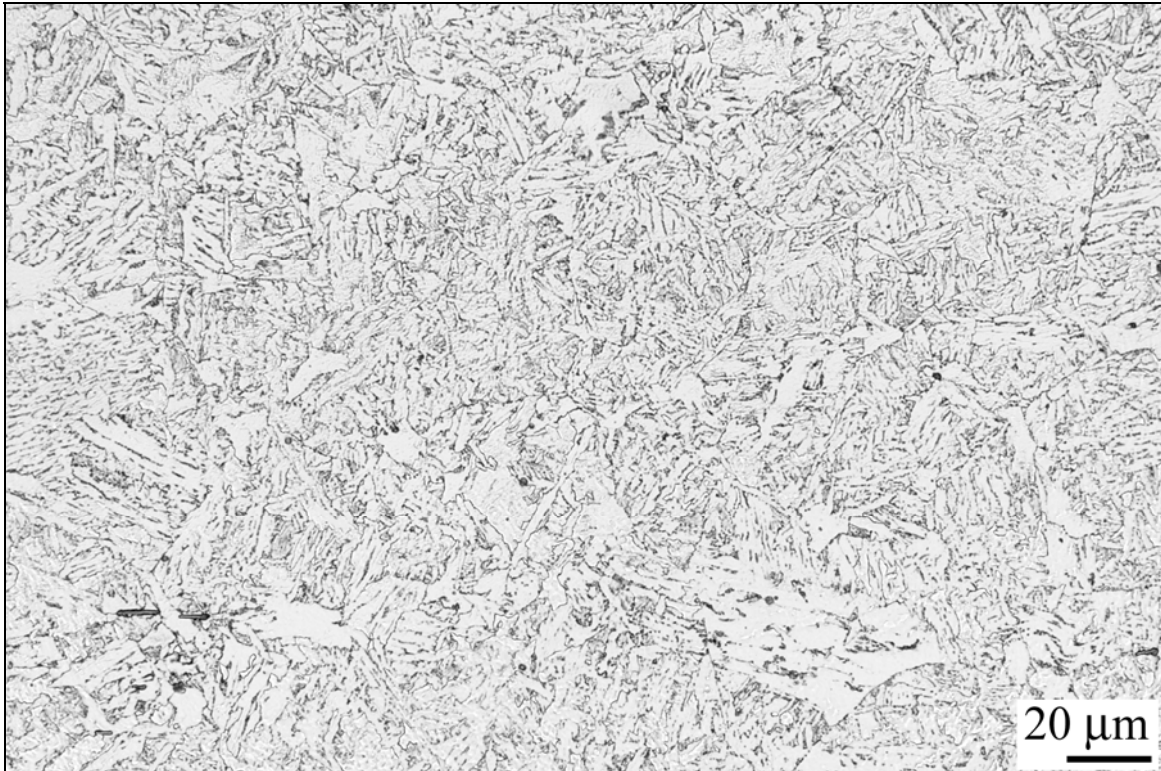
Source: NIST.

**Figure 5–12. Representative micrographs from perimeter column welds of a hot-rolled steel with  $F_y = 55$  ksi. d) Tempering of the original pearlite in the structure. Sample shown was from panel M-2 (WTC 1, column 129, 97th floor). 2 percent nital and 4 percent picral etch (continued).**



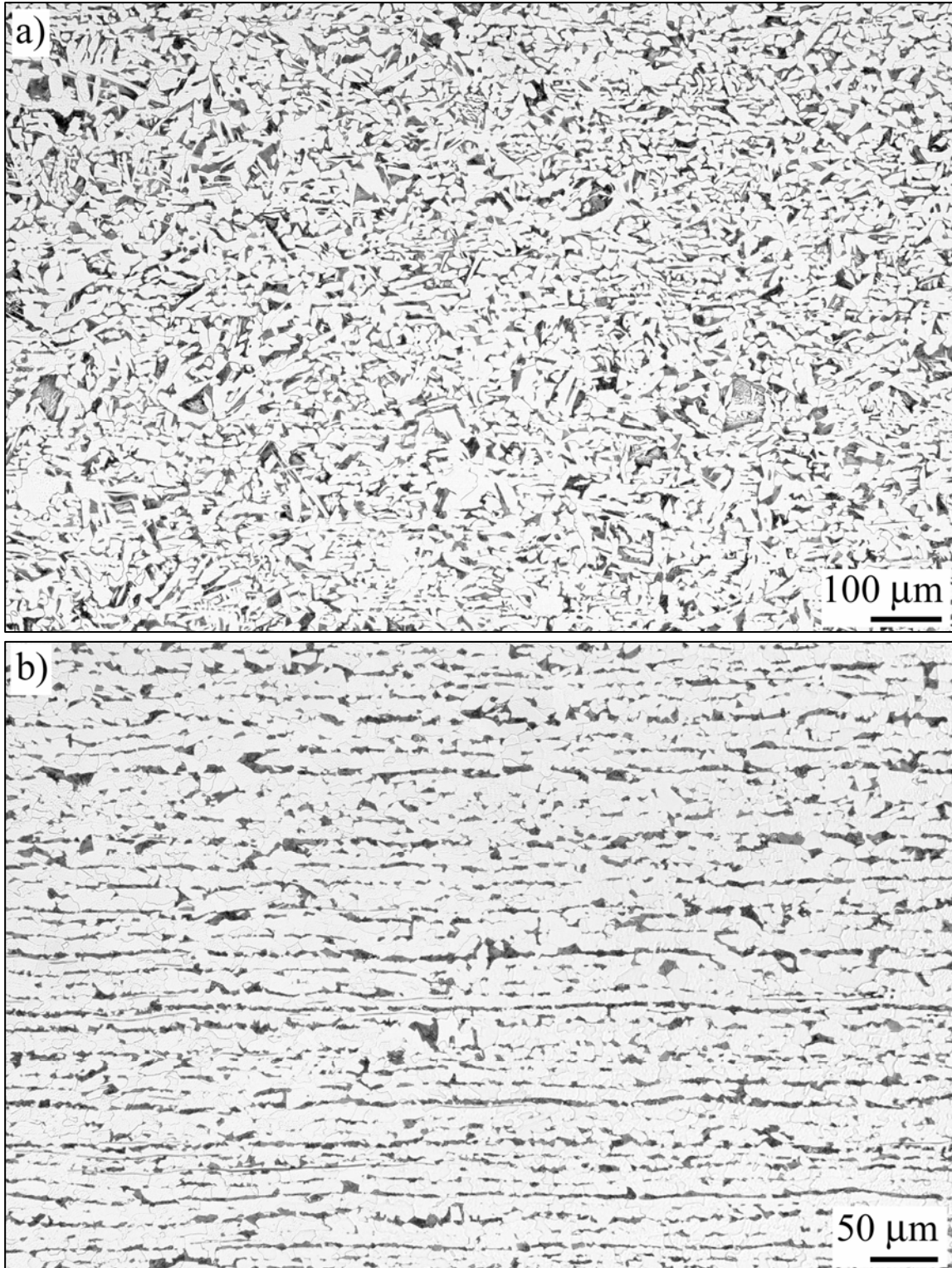
Source: NIST.

**Figure 5–13. Representative microstructure of HAZ near fusion line from perimeter column weld of a quenched-and-tempered steel with  $F_y = 100$  ksi. Sample shown was from panel C-10 (WTC 1, column 452, 86th floor). 2 percent nital and 4 percent picral etch.**



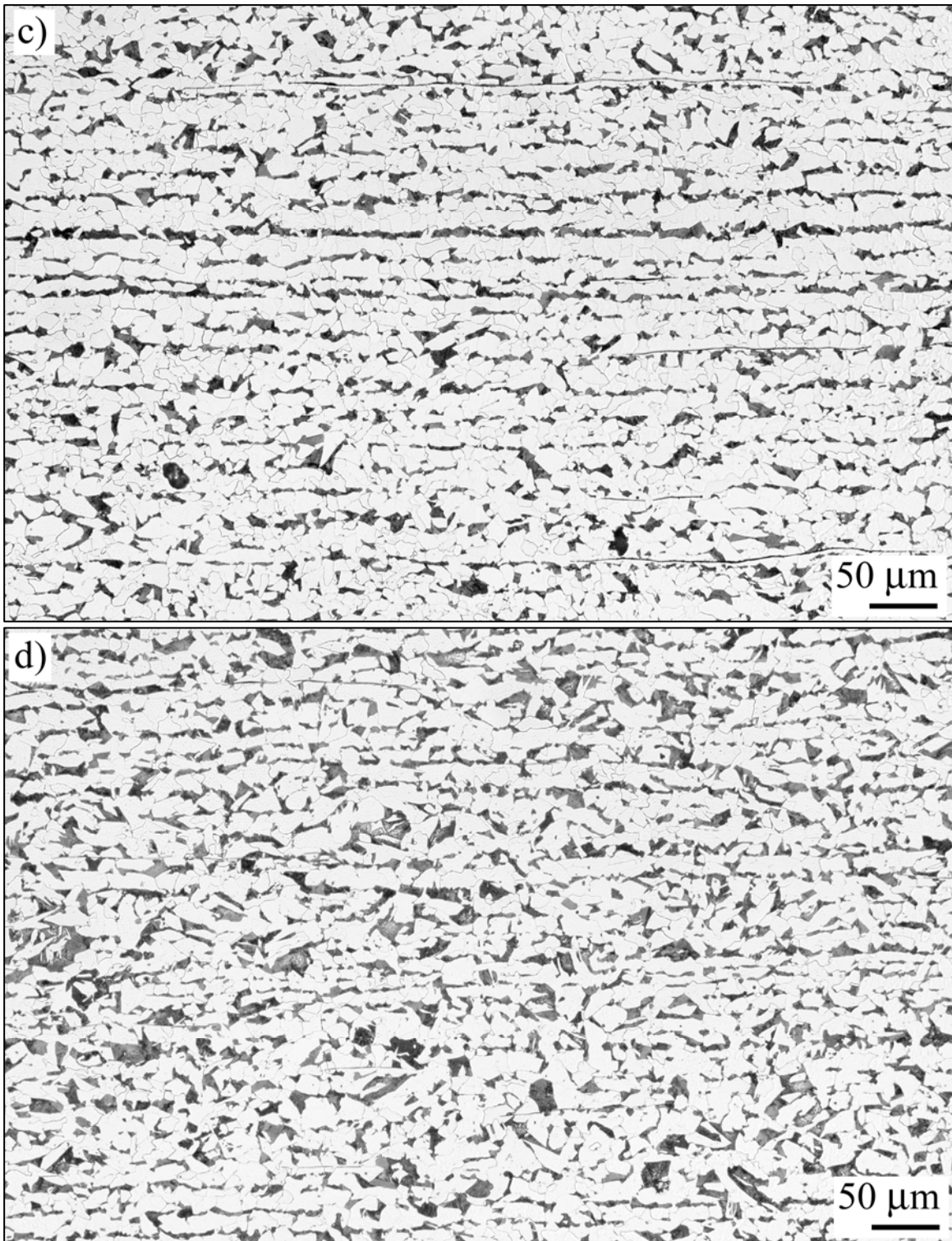
Source: NIST.

**Figure 5–14. Microstructure from a column butt plate. Sample shown was from unidentified panel C-68. 2 percent nital and 4 percent picral etch.**



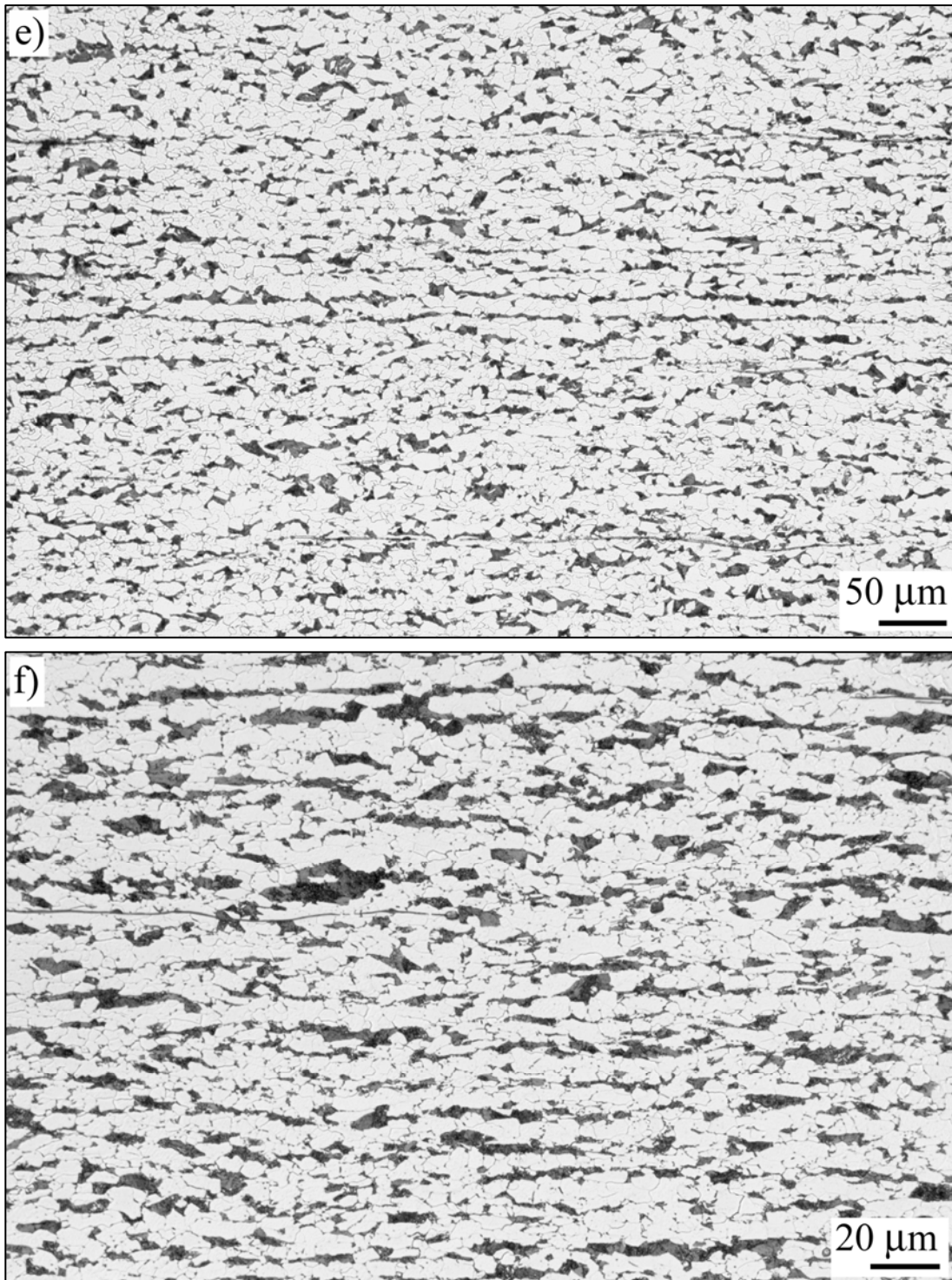
Source: NIST.

**Figure 5-15. Representative microstructures of hot-rolled perimeter column spandrel plates as a function of strength level. The images were taken near the centerline of the plate. a)  $F_y = 36$  ksi (panel N-9, WTC 1, column 153, 102nd floor); b)  $F_y = 2$  ksi (panel C-40, WTC 1, 136, 99th floor). Both with 2 percent nital and 4 percent picral etch.**



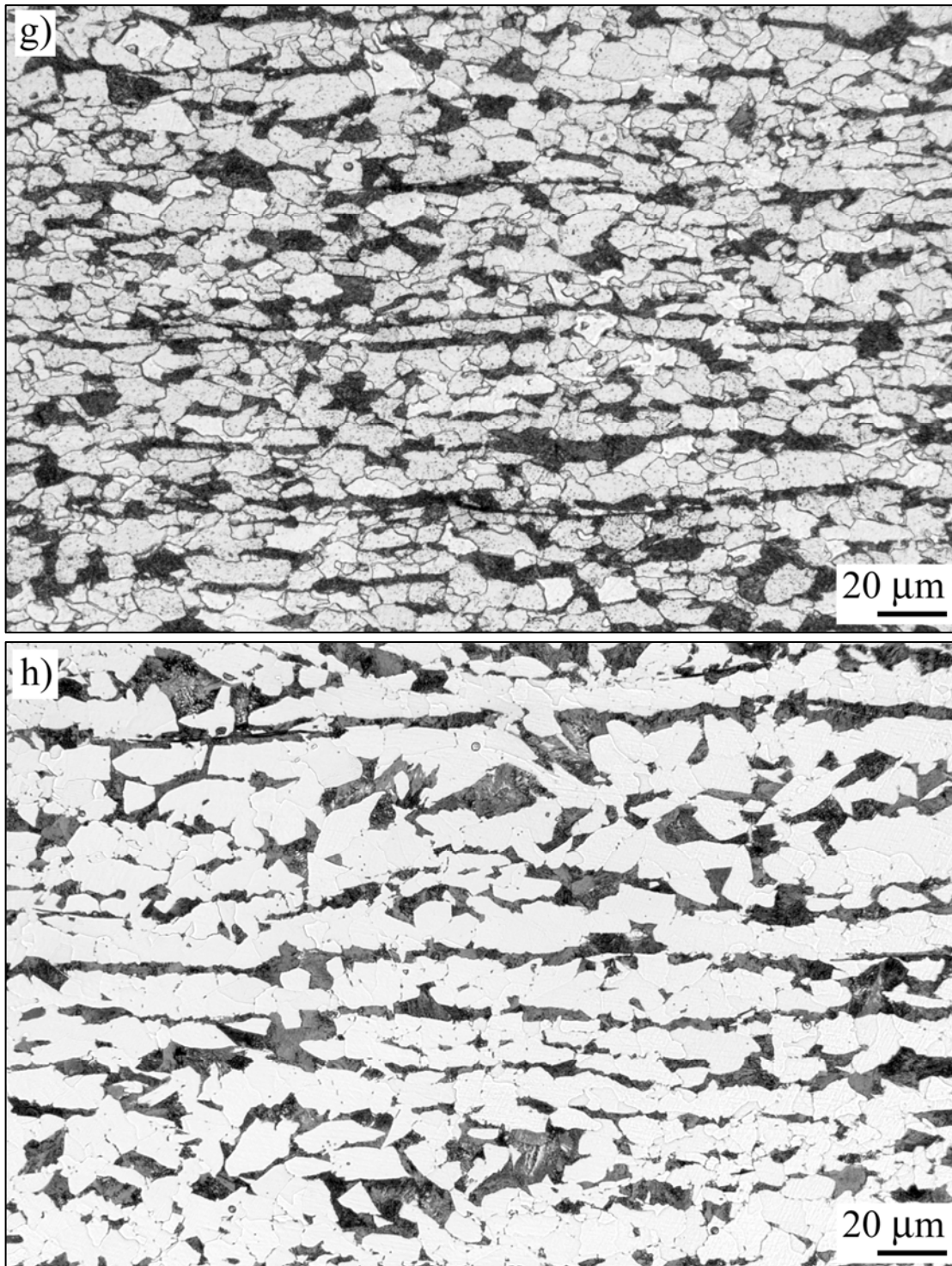
Source: NIST.

**Figure 5–15. Representative microstructures of hot-rolled perimeter column spandrel plates as a function of strength level. The images were taken near the centerline of the plate. c)  $F_y = 45$  ksi (panel N-99, WTC 1, column 147, 100th floor); d)  $F_y = 46$  ksi (panel S-14, WTC 2, 218, 92nd floor). Both with 2 percent nital and 4 percent picral etch (continued).**



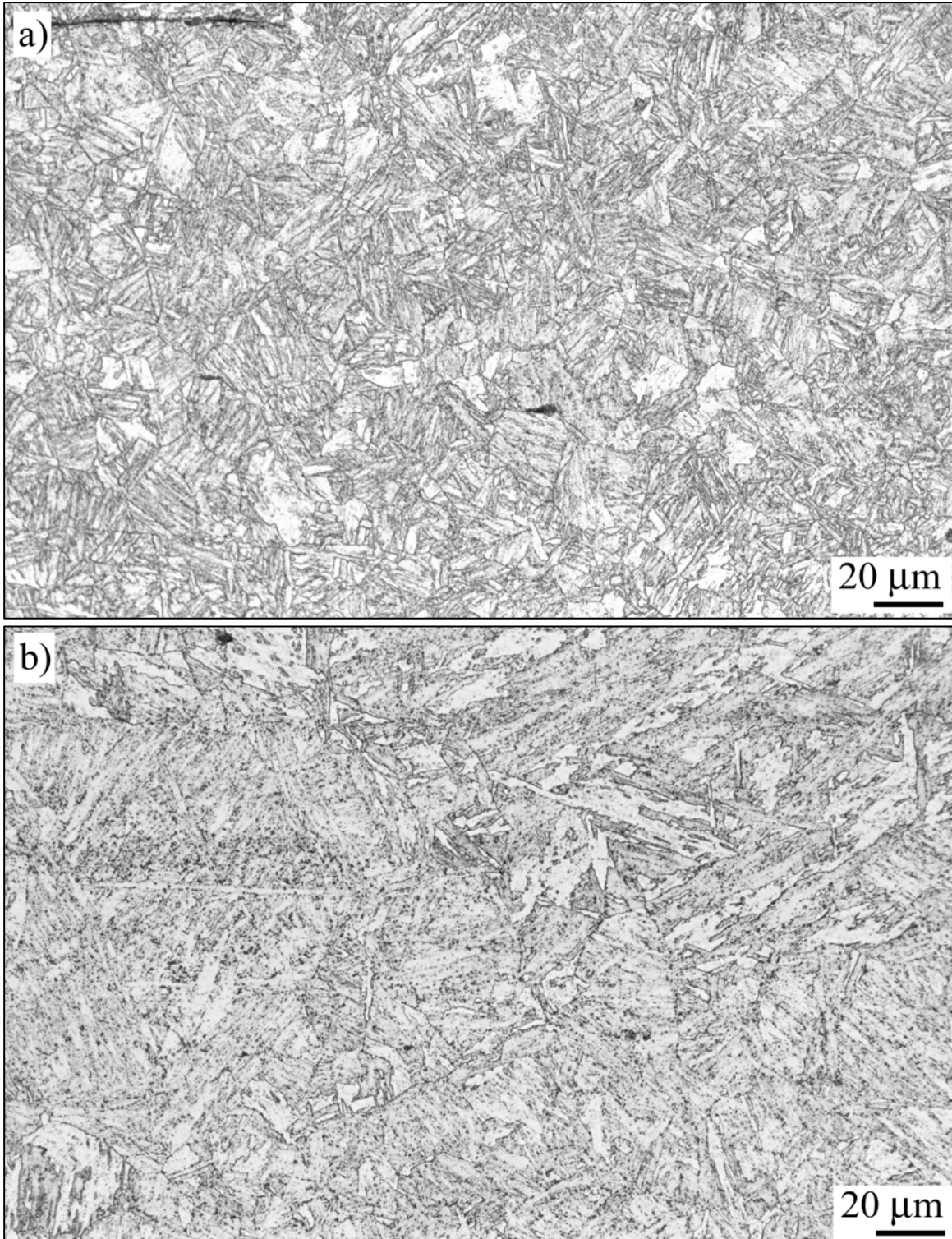
Source: NIST.

**Figure 5–15. Representative microstructures of hot-rolled perimeter column spandrel plates as a function of strength level. The images were taken near the centerline of the plate. e)  $F_y = 50$  ksi (panel N-12, WTC 1, column 206, 93rd floor); f)  $F_y = 55$  ksi (panel C-25, WTC 1, 206, 91st floor). Both with 2 percent nital and 4 percent picral etch (continued).**



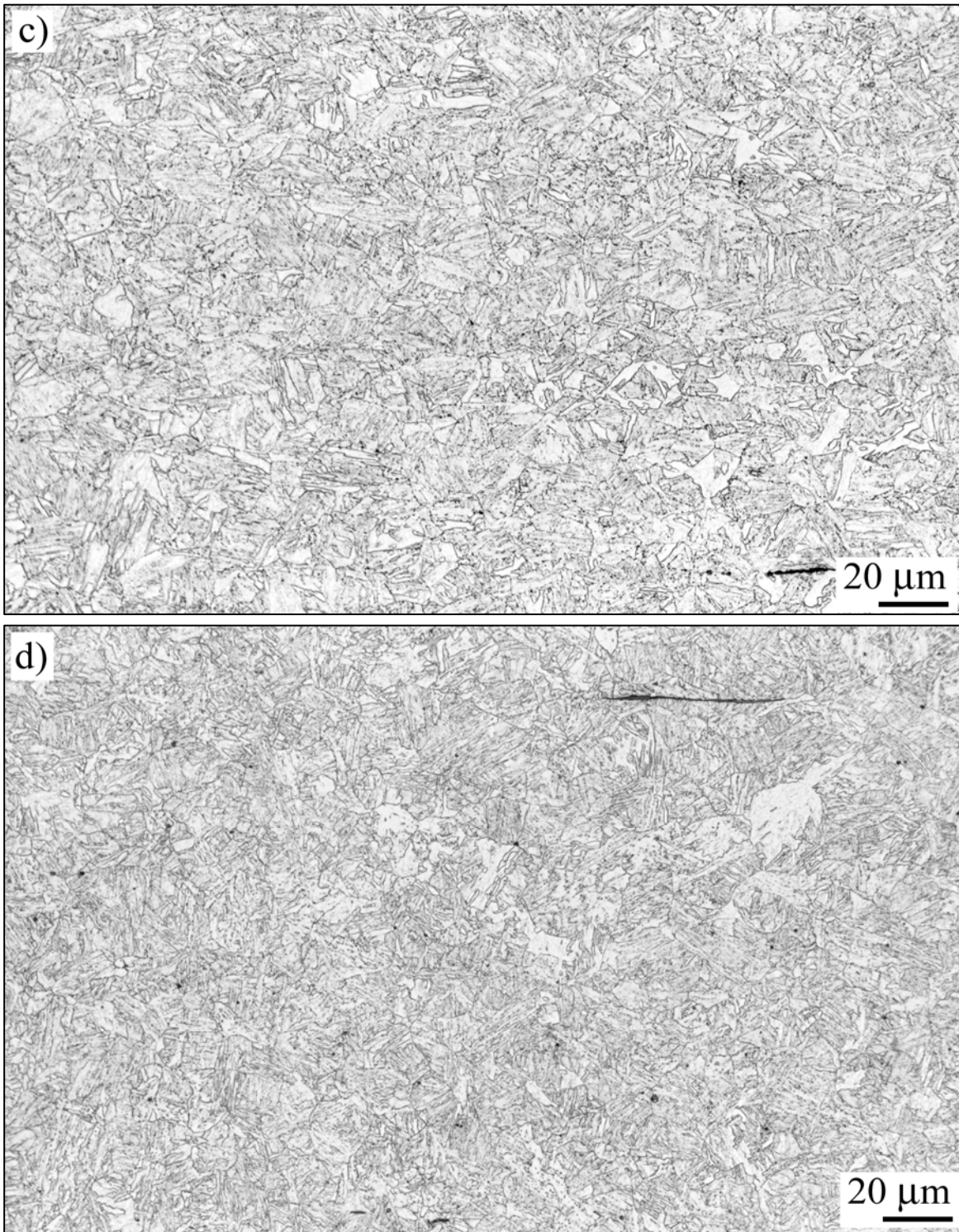
Source: NIST.

**Figure 5–15. Representative microstructures of hot-rolled perimeter column spandrel plates as a function of strength level. The images were taken near the centerline of the plate. g)  $F_y = 60$  ksi (panel C-22, WTC 1, column 156, 95th floor), h)  $F_y = 65$  ksi with plate thickness equal to or less than 0.5 in. (panel C-22, WTC 1, 157, 94th floor). Both with 2 percent nital and 4 percent picral etch (continued).**



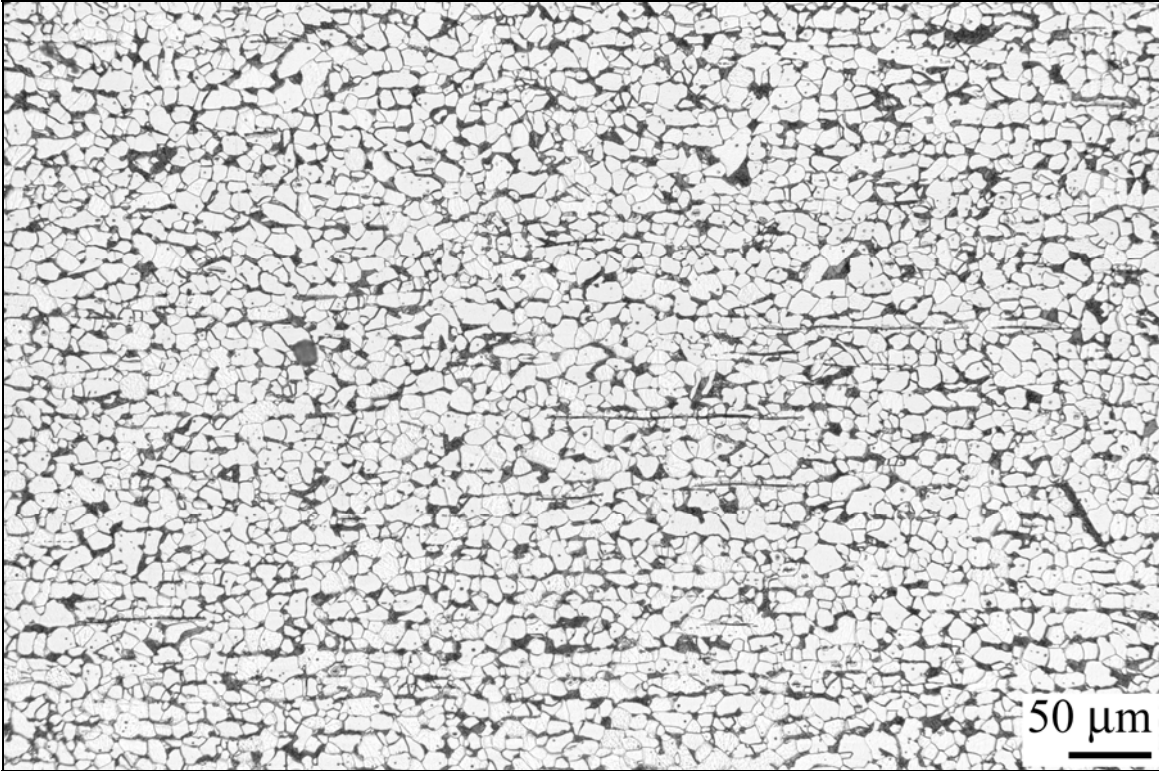
Source: NIST.

**Figure 5–16. Representative microstructures of quenched-and-tempered perimeter column spandrel plates as a function of strength level. The images were taken near the centerline of the plate. a)  $F_y = 65$  ksi with plate thickness greater than 0.5 in. (panel C-46, WTC 2, 58, 69th floor) b)  $F_y = 70$  ksi (panel C-13a, WTC 2, column 159, 92nd floor). Both with 2 percent nital and 4 percent picral etch.**



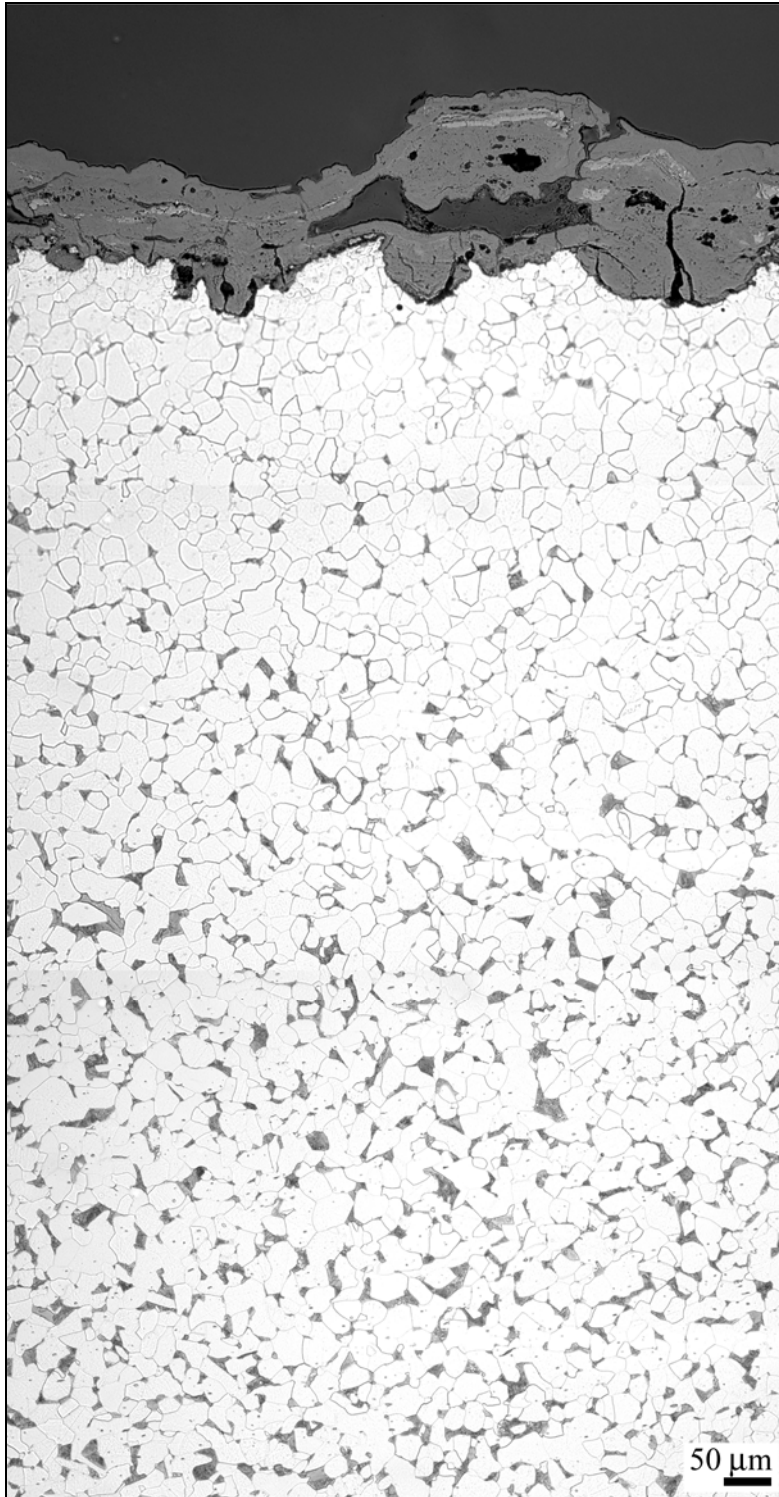
Source: NIST.

**Figure 5–16. Representative microstructures of quenched-and-tempered perimeter column spandrel plates as a function of strength level. The images were taken near the centerline of the plate. c)  $F_y = 75$  ksi (panel C-14, WTC 2, 259, 86th floor) and d)  $F_y = 80$  ksi (panel C-24, WTC 2, column 202, 77th floor). Both with 2 percent nital and 4 percent picral etch (continued).**



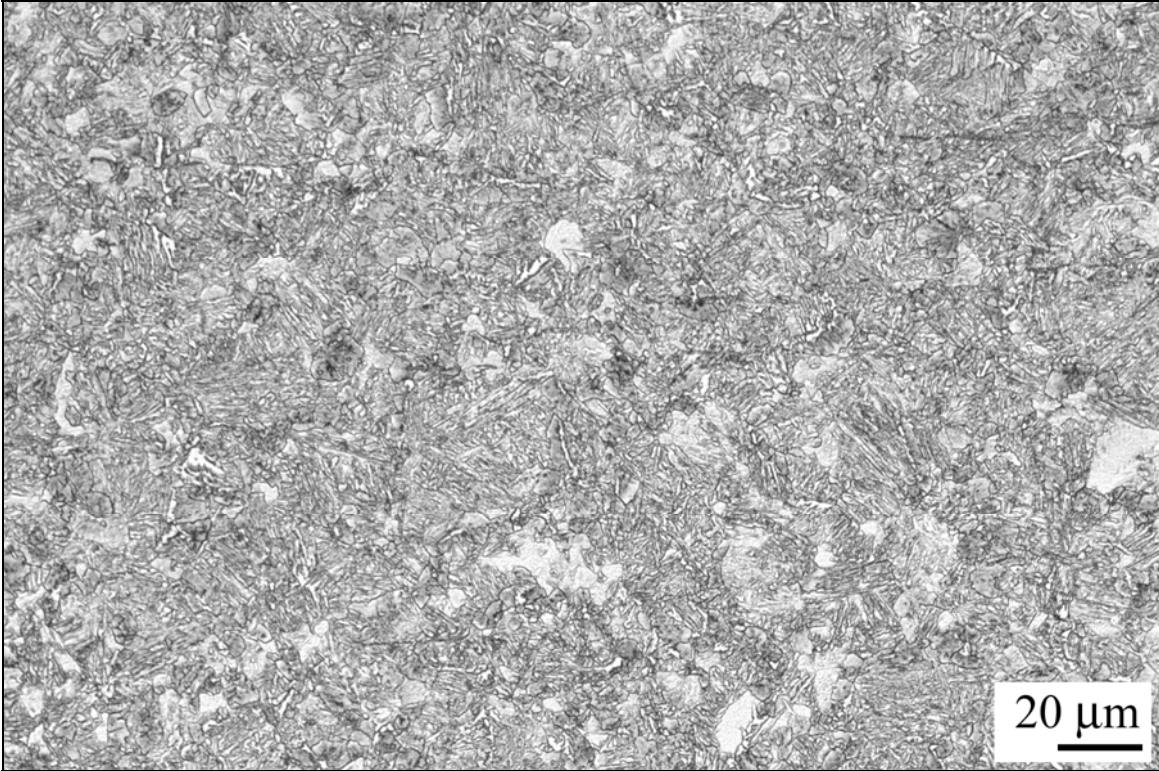
Source: NIST.

**Figure 5–17. Representative microstructure of spandrel splice plate. Sample was from panel N-101 (WTC 1, column 132, 101st floor). 2 percent nital and 4 percent picral etch.**



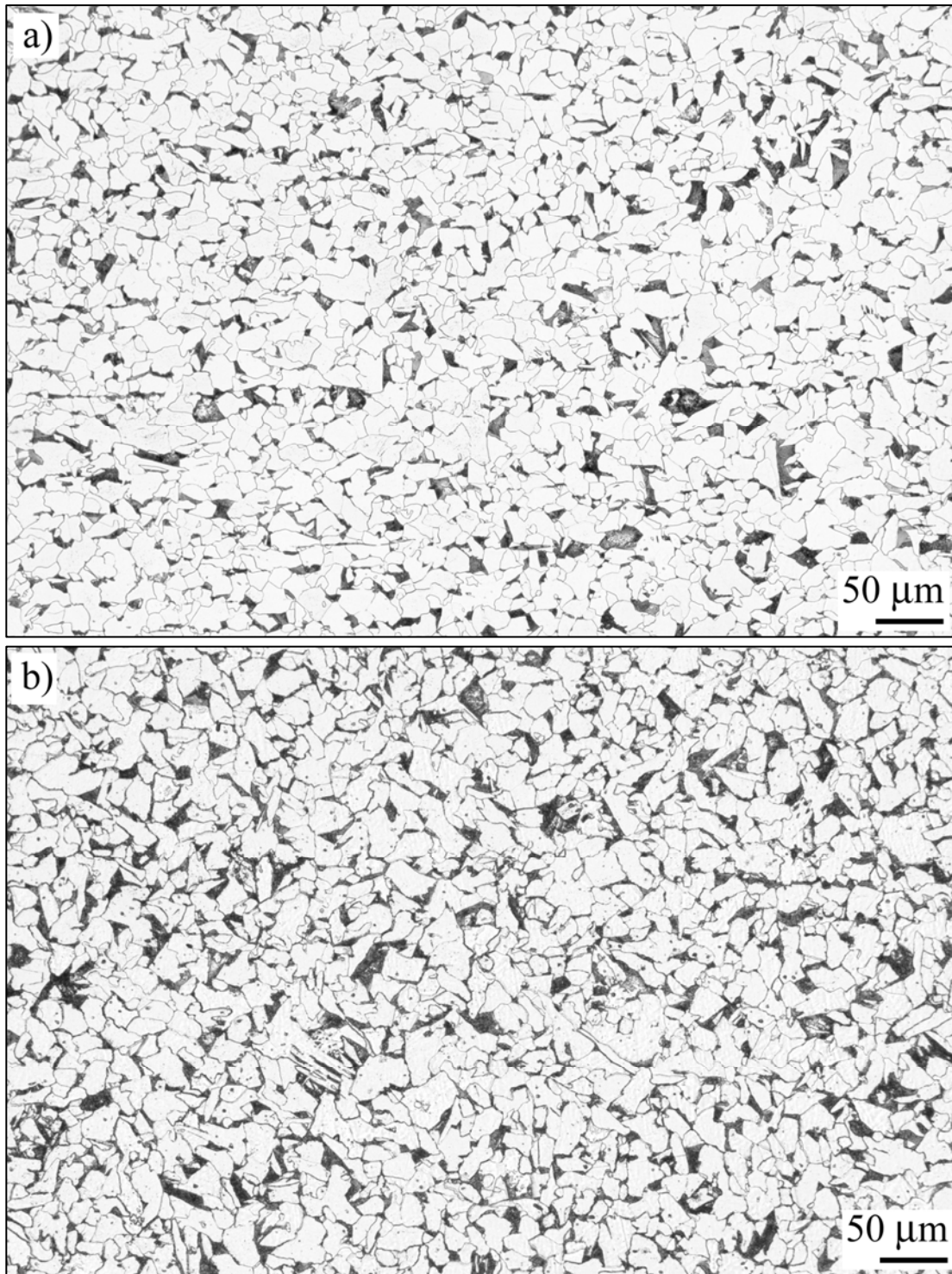
Source: NIST.

**Figure 5–18. Partially decarburized zone found near the surface of a perimeter floor truss seat. Sample shown taken from panel M-2 (WTC 1, column 131, 99th floor). 2 percent nital and 4 percent picral etch.**



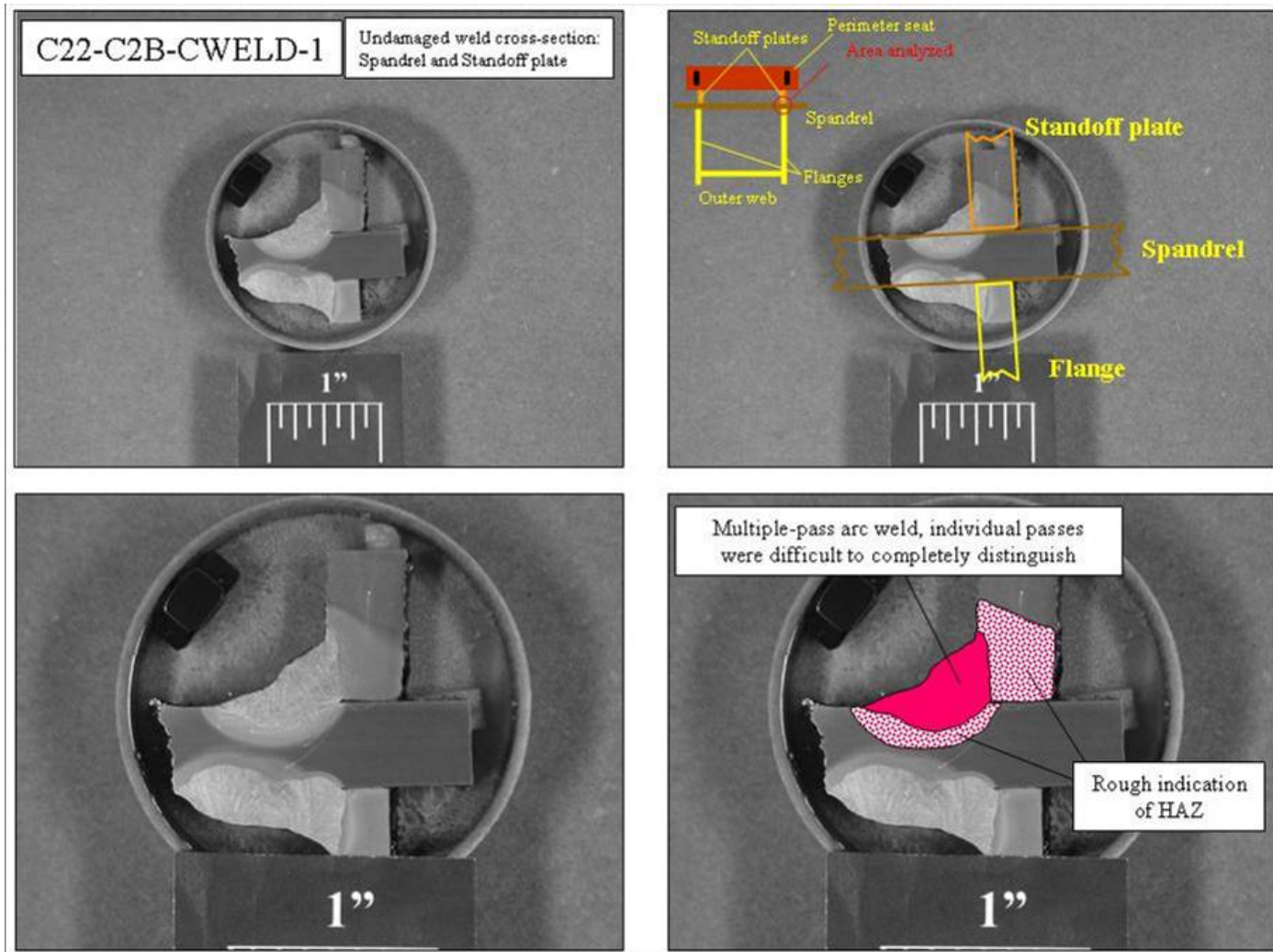
Source: NIST.

**Figure 5–19. Microstructure from an ASTM A 325 construction bolt. Sample shown was taken from a spandrel splice located at the 97th floor level next to column 131 of WTC 1 (panel M-2). 2 percent nital and 4 percent picral etch.**



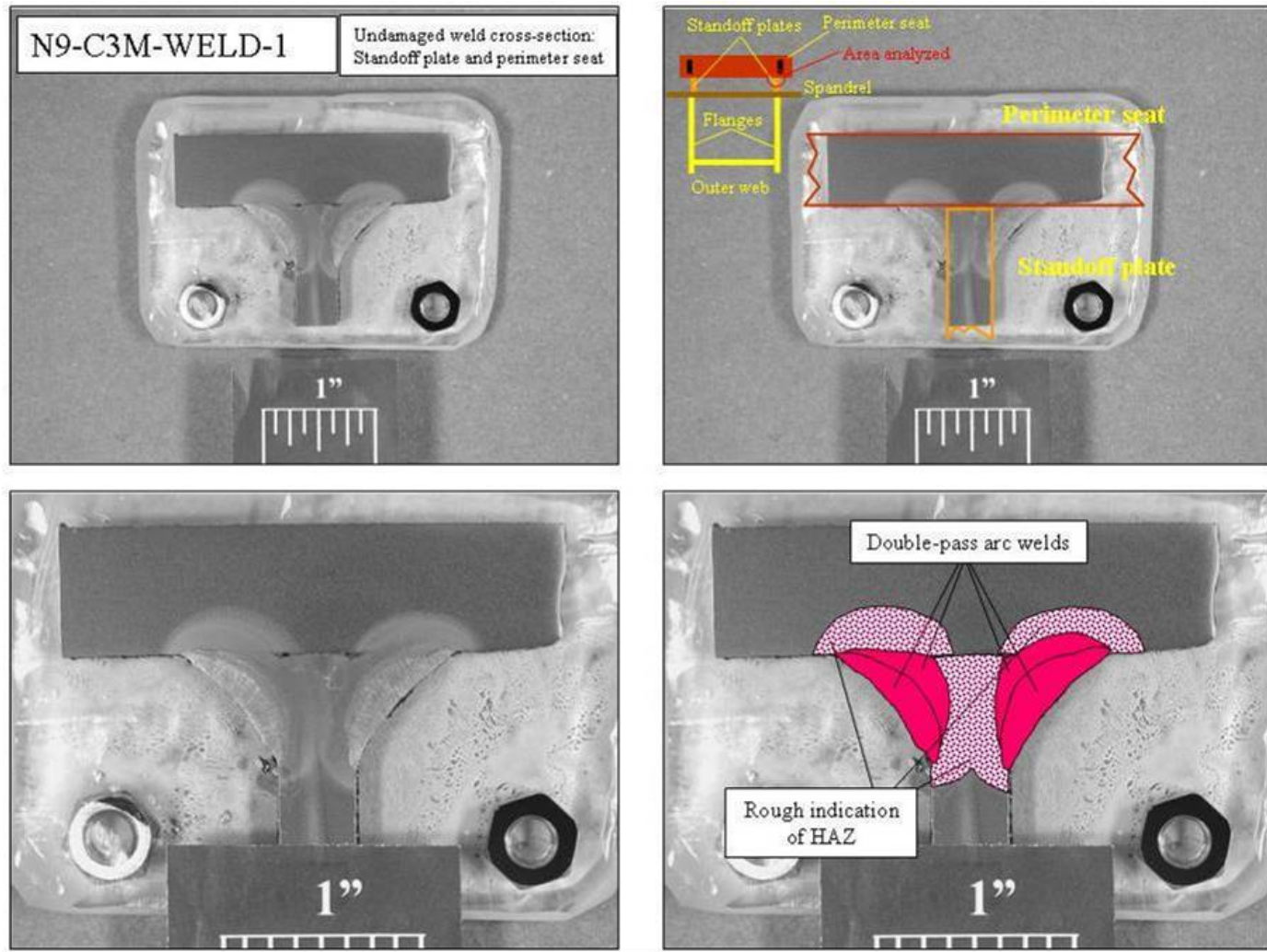
Source: NIST.

**Figure 5–20. Microstructures observed for standoff plates connecting floor truss seats to spandrel plates. Microstructures had relatively good distribution of the pearlite, however, the volume fraction and distribution within the structures was very different. a) sample with polygonal and irregular ferrite grains (panel M-2, WTC 1, column 129, 97th floor) and b) sample with both polygonal, irregular, and Widmanstätten morphologies (panel N-8, WTC 1, column 143, 98th floor). 2 percent nital and 4 percent picral etch.**



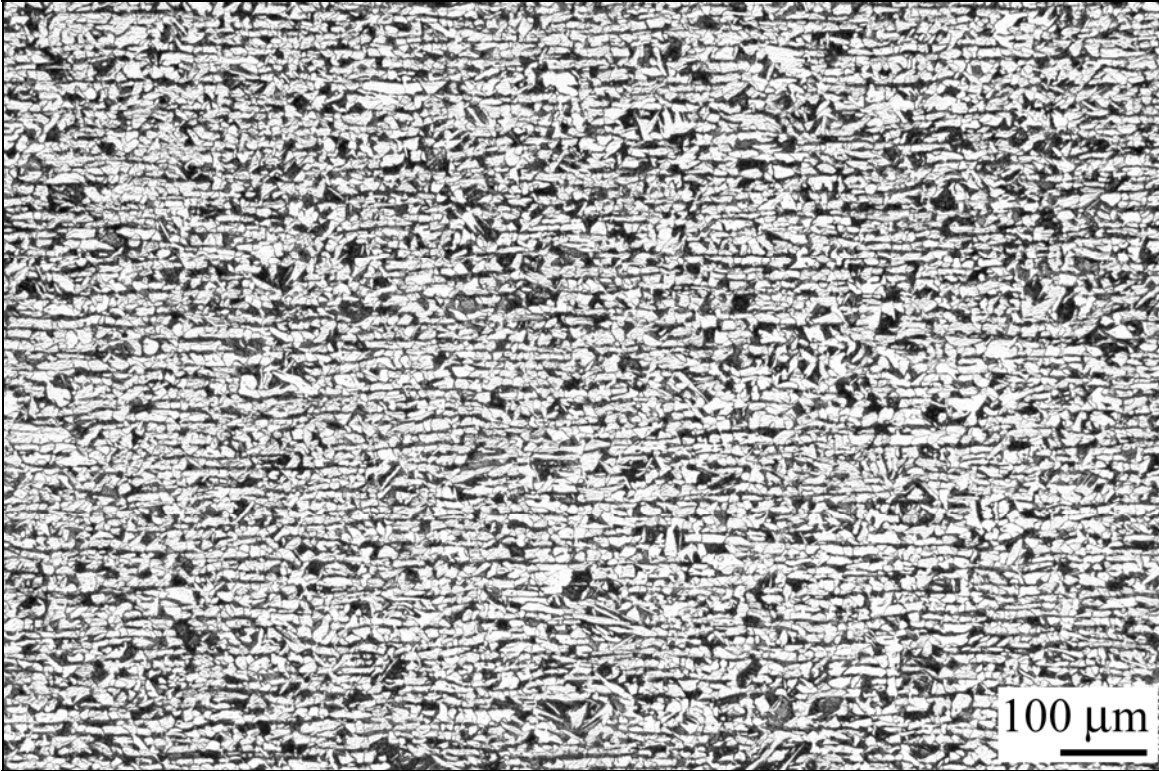
Source: NIST.

Figure 5–21. Etched cross-section of weld between spandrel plate (65 ksi) and standoff plate (42 ksi). Sample was from panel C-22 (WTC 1, column 157, 94th floor). 2 percent nital and 4 percent picral etch.



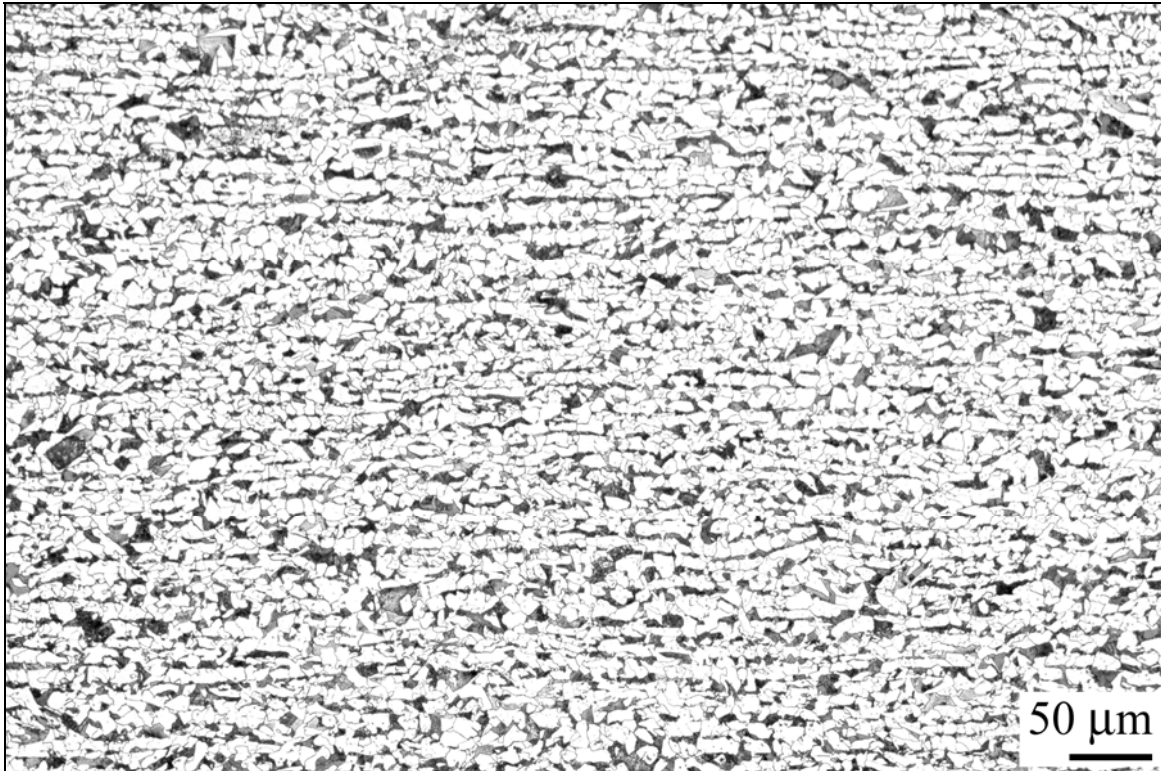
Source: NIST.

Figure 5-22. Etched cross-section of intact weld between a standoff plate and truss seat. Sample was from panel N-9 (WTC 1, column 153, 103rd floor). 2 percent nital and 4 percent picral etch.



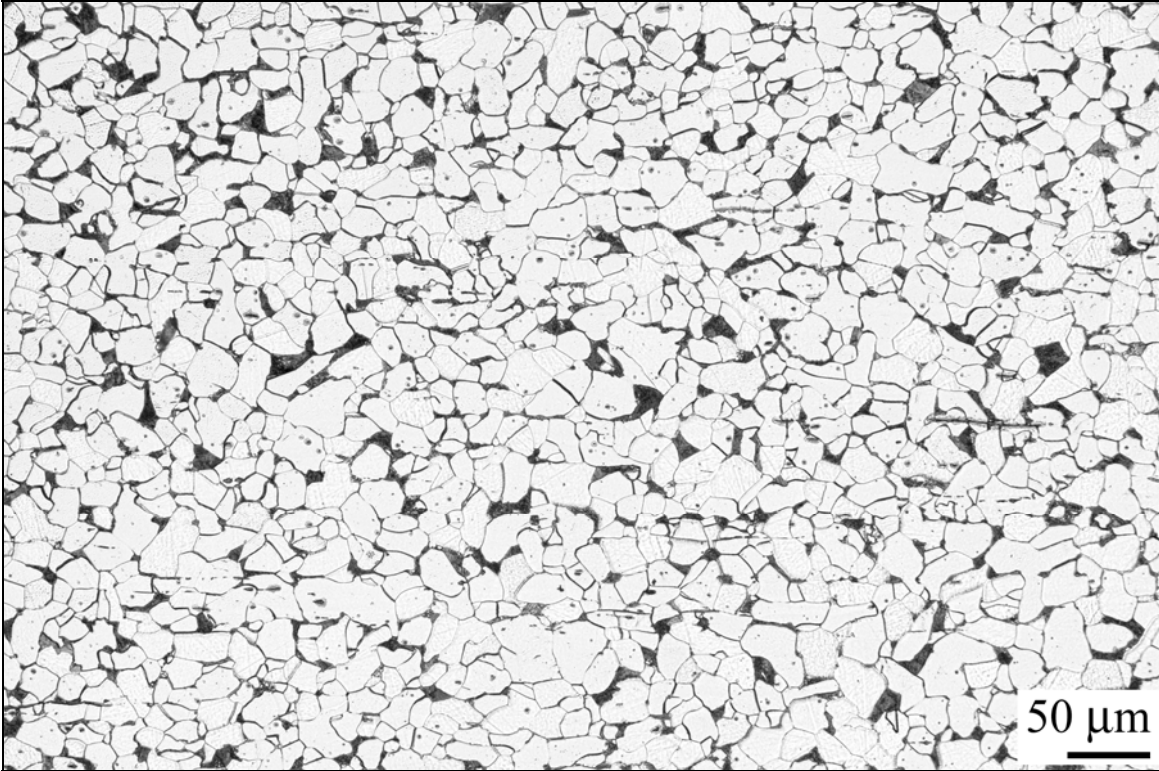
Source: NIST.

**Figure 5–23. Microstructure of a hot-rolled gusset plate welded to the top chord of the floor trusses. High volume fraction of pearlite and banding of the structure was noted. Sample shown was from panel N-8 (WTC 1, column 143, 98th floor). 2 percent nital and 4 percent picral etch.**



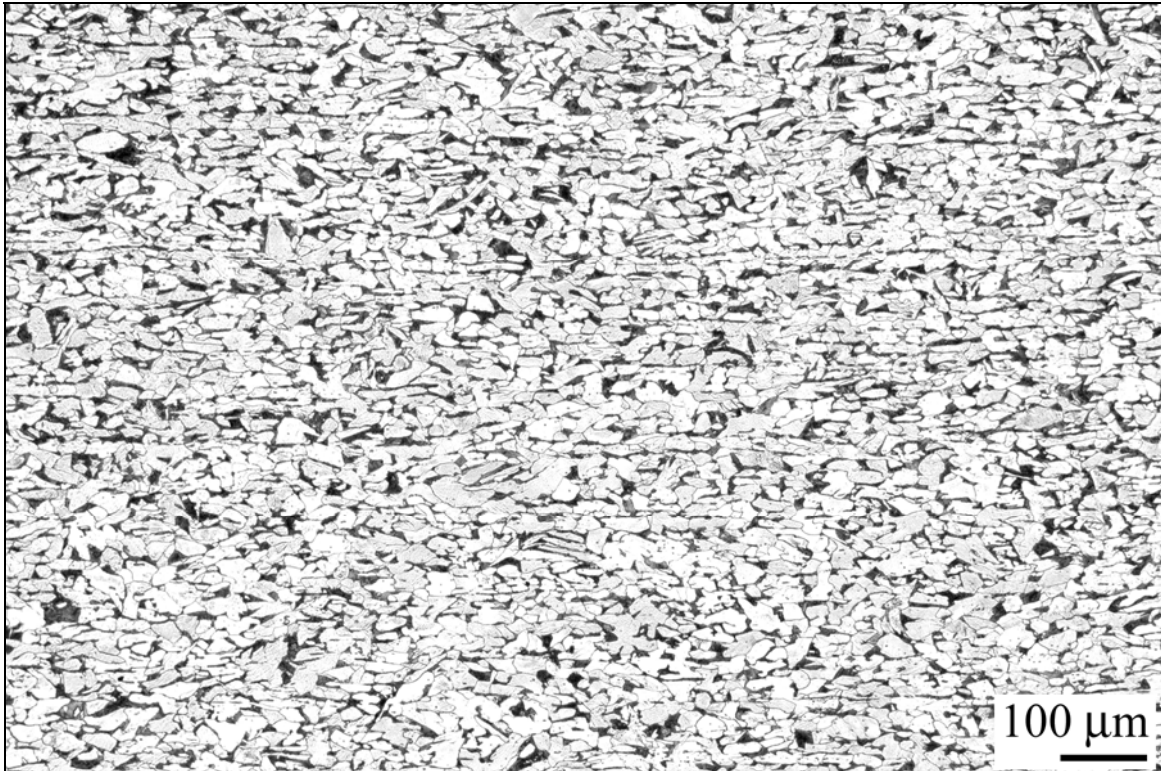
Source: NIST.

**Figure 5–24. Microstructure of a hot-rolled damper plate. Banding of the structure was noted. Sample shown from panel N-8 (WTC 1, column 143, 98th floor). 2 percent nital and 4 percent picral etch.**



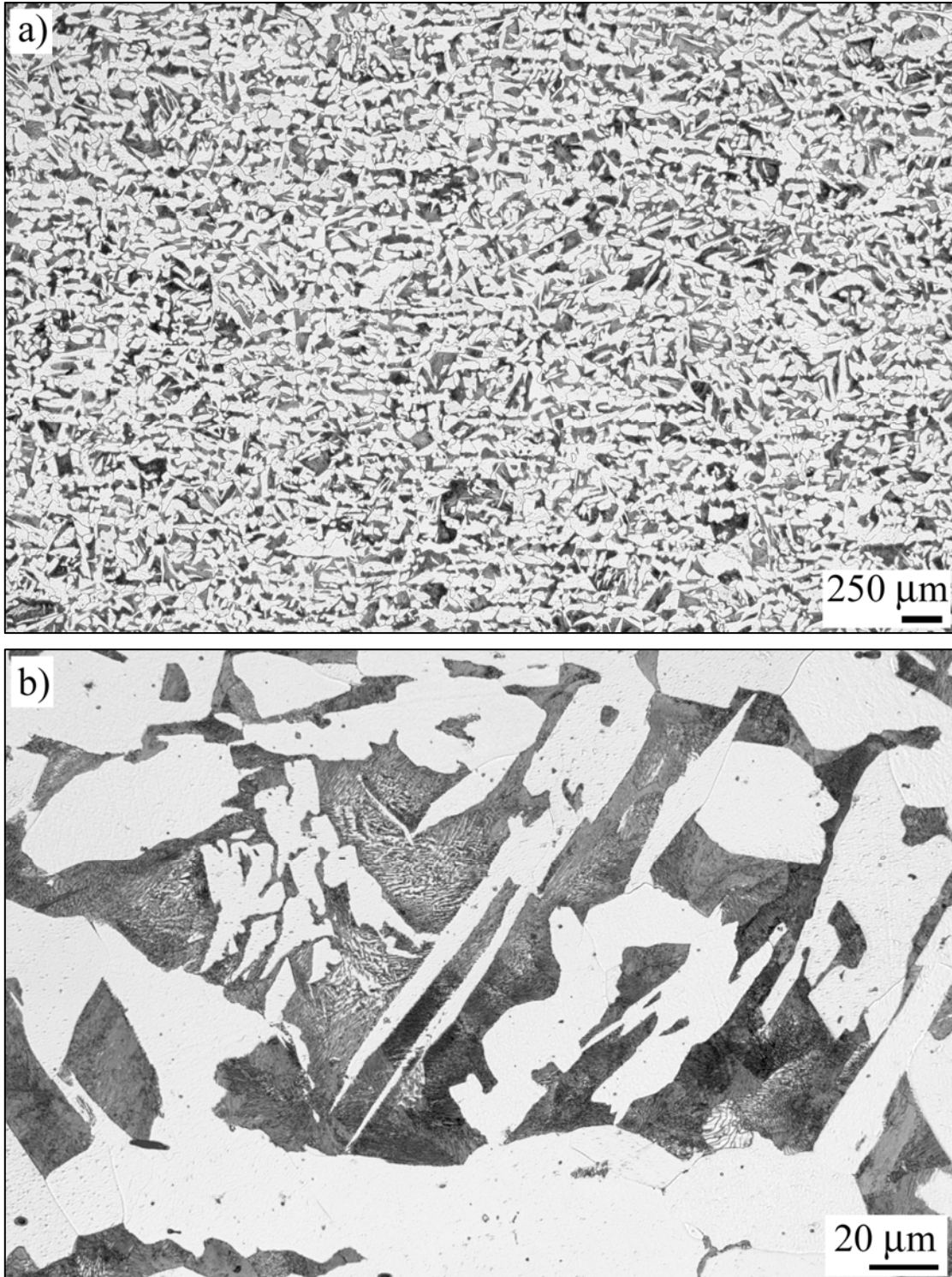
Source: NIST.

**Figure 5–25. Microstructure of a hot-rolled gusset plate used to attach the damper units and the diagonal bracing straps to the perimeter columns. Ferrite was primarily polygonal. Sample shown was from panel N-8 (WTC 1, column 142, 98th floor). 2 percent nital and 4 percent picral etch.**



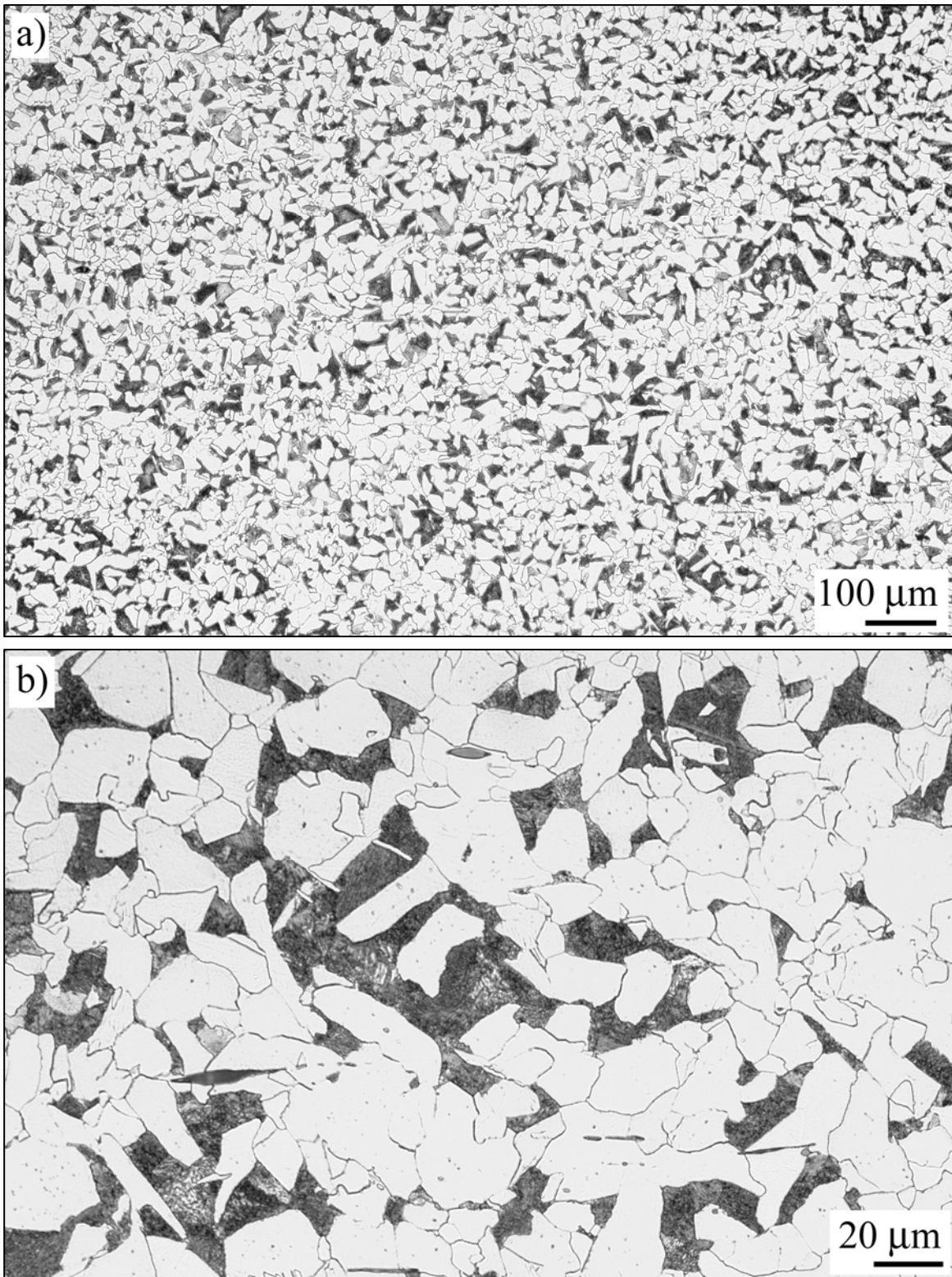
Source: NIST.

**Figure 5–26. Microstructure of a hot-rolled diagonal bracing strap. Ferrite was primarily polygonal and elongated in the RD. Sample shown was from panel N-8 (WTC 1, column 142, 98th floor). 2 percent nital and 4 percent picral etch.**



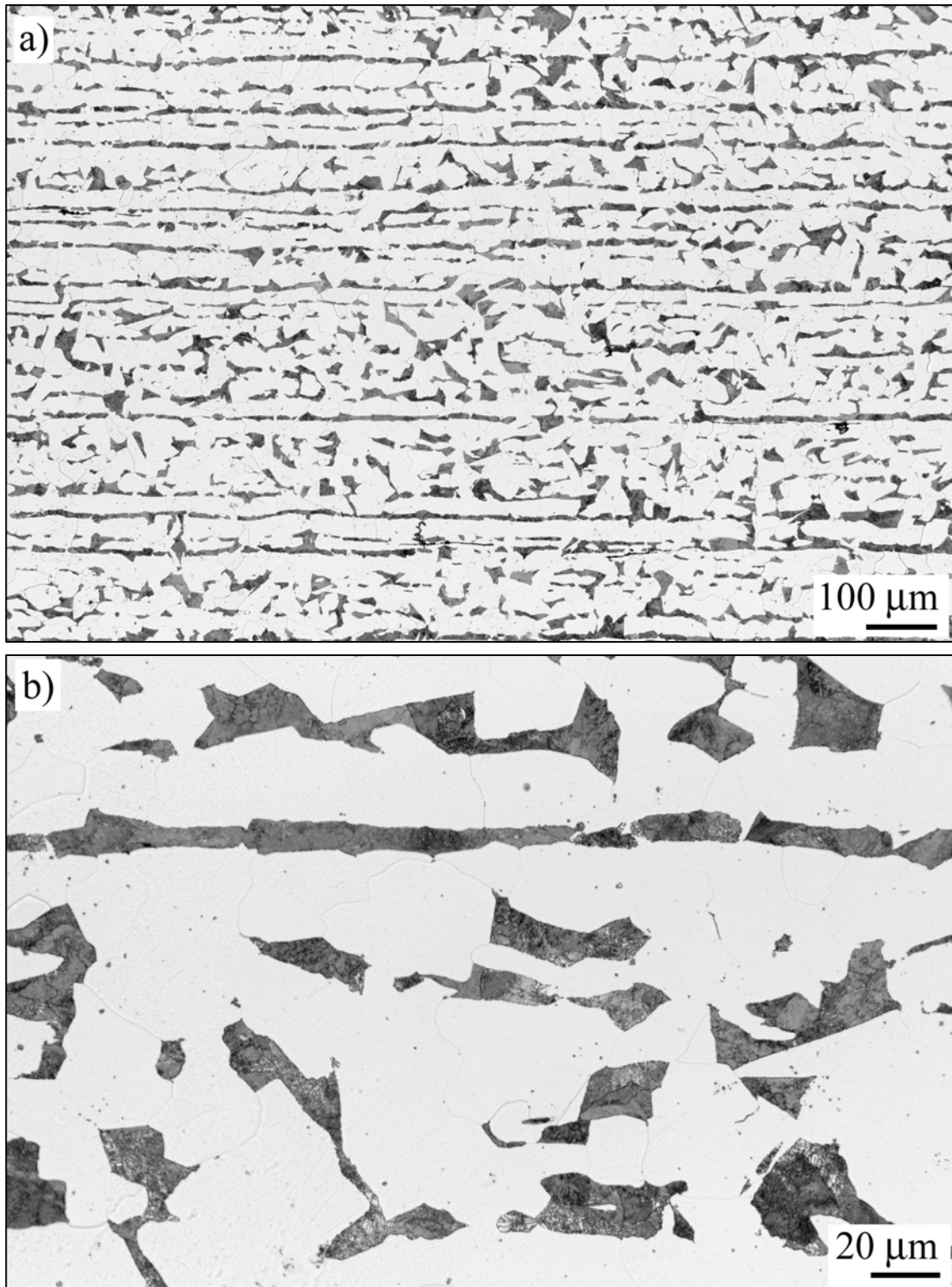
Source: NIST.

**Figure 5–27. Microstructure of a hot-rolled 36 ksi rolled wide flange. a) The majority of the ferrite is polygonal or blocky with some Widmanstätten and b) fine pearlite with some bainite possible where cementite precipitates are associated with ferrite. Sample is from C-80 (WTC 1, core column 603, 92nd floor). Both with 2 percent nital and 4 percent picral etch.**



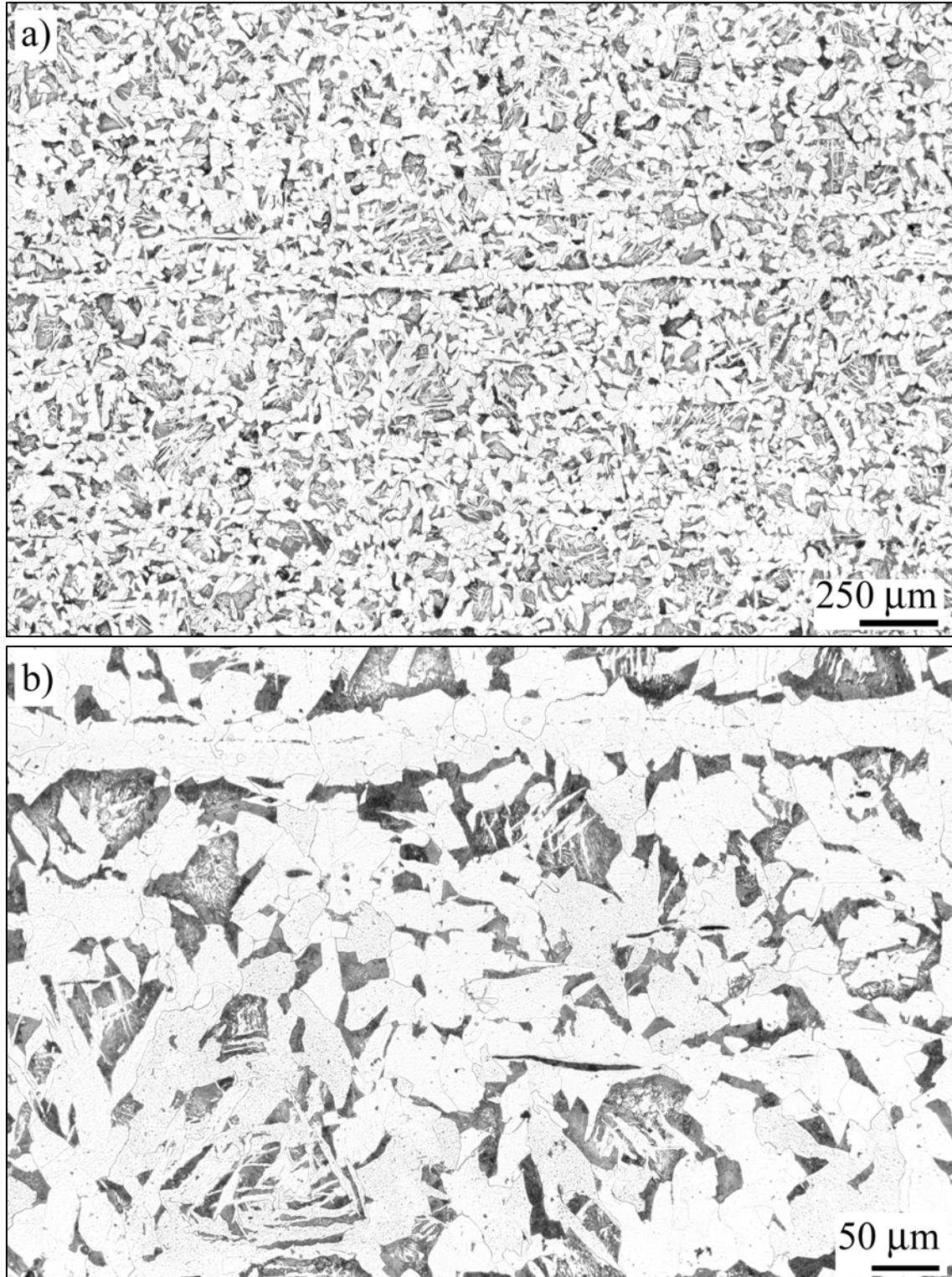
Source: NIST.

**Figure 5–28. Microstructure of a hot-rolled 42 ksi rolled wide flange. The majority of the ferrite is polygonal or blocky. Sample is from HH (WTC 1, core column 605, 98th floor). Both with 2 percent nital and 4 percent picral etch.**



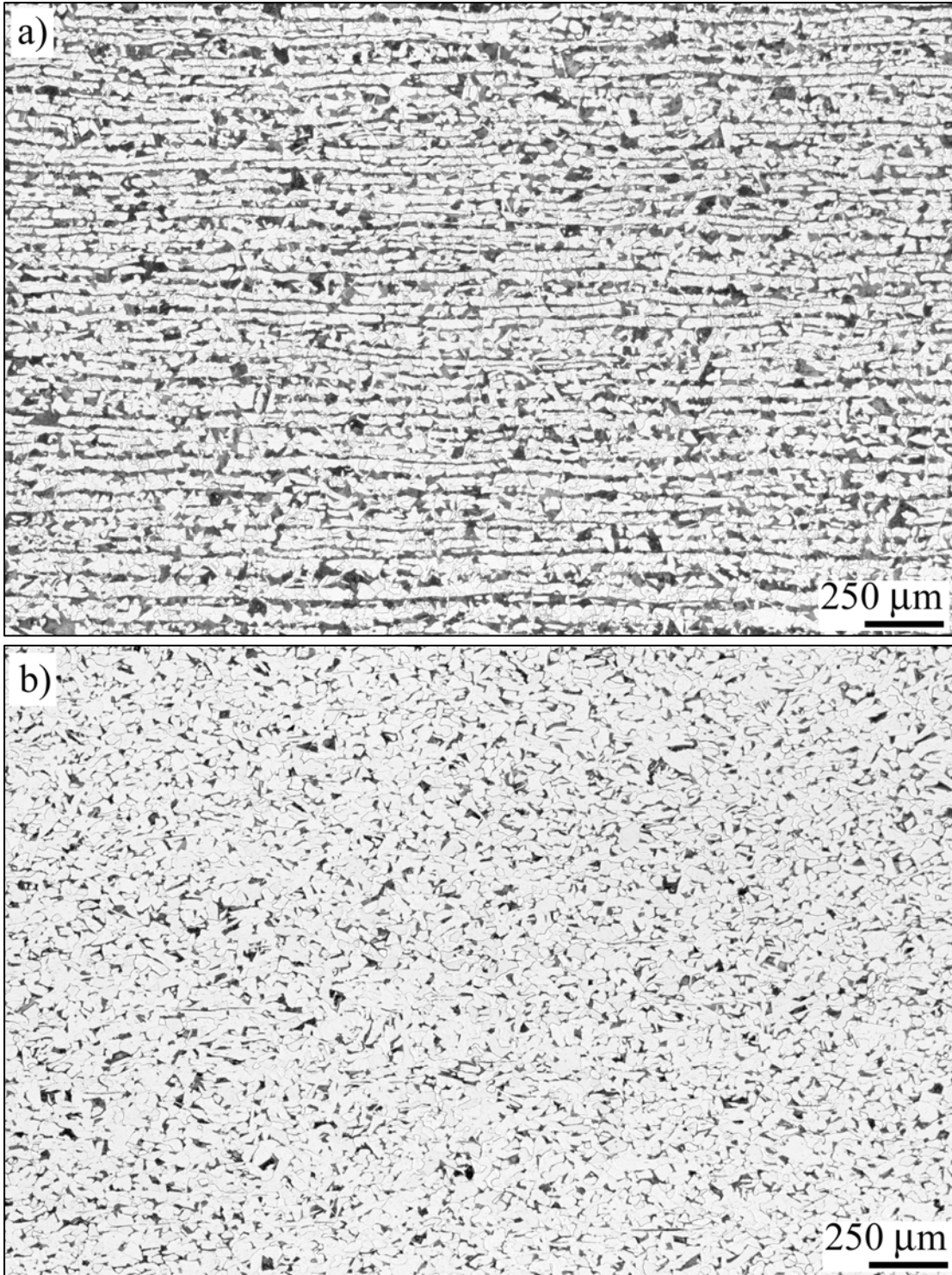
Source: NIST.

**Figure 5–29. Microstructure of a hot-rolled 36 ksi plate from a built-up box core column. The majority of the ferrite is polygonal. Sample is from B-6152-1 (WTC 1, core column 803, 15th floor). Both with 2 percent nital and 4 percent picral etch.**



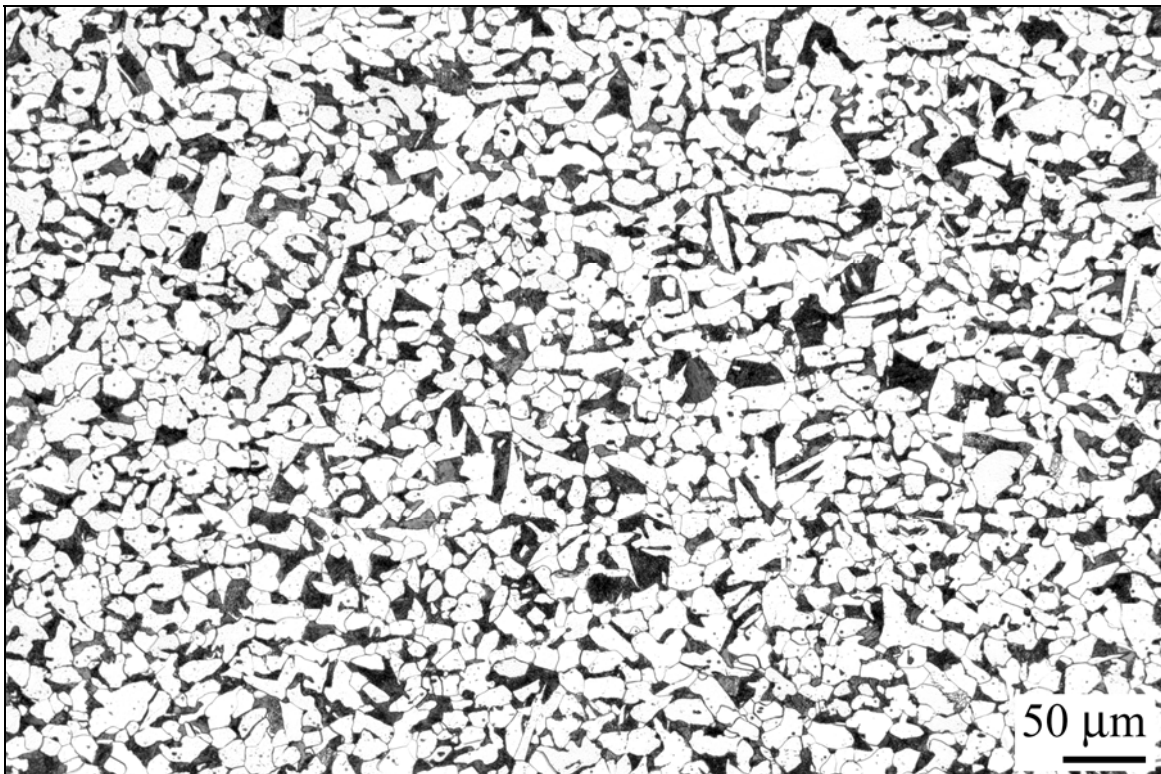
Source: NIST.

**Figure 5–30. Microstructure of a hot-rolled 42 ksi plate from a built-up box core column. a) The majority of the ferrite is polygonal with some Widmanstätten ferrite, moderate banding was observed, and b) Widmanstätten ferrite. Sample is from C-88b (WTC 2, core column 801, 80th floor). Both with 2 percent nital and 4 percent picral etch.**



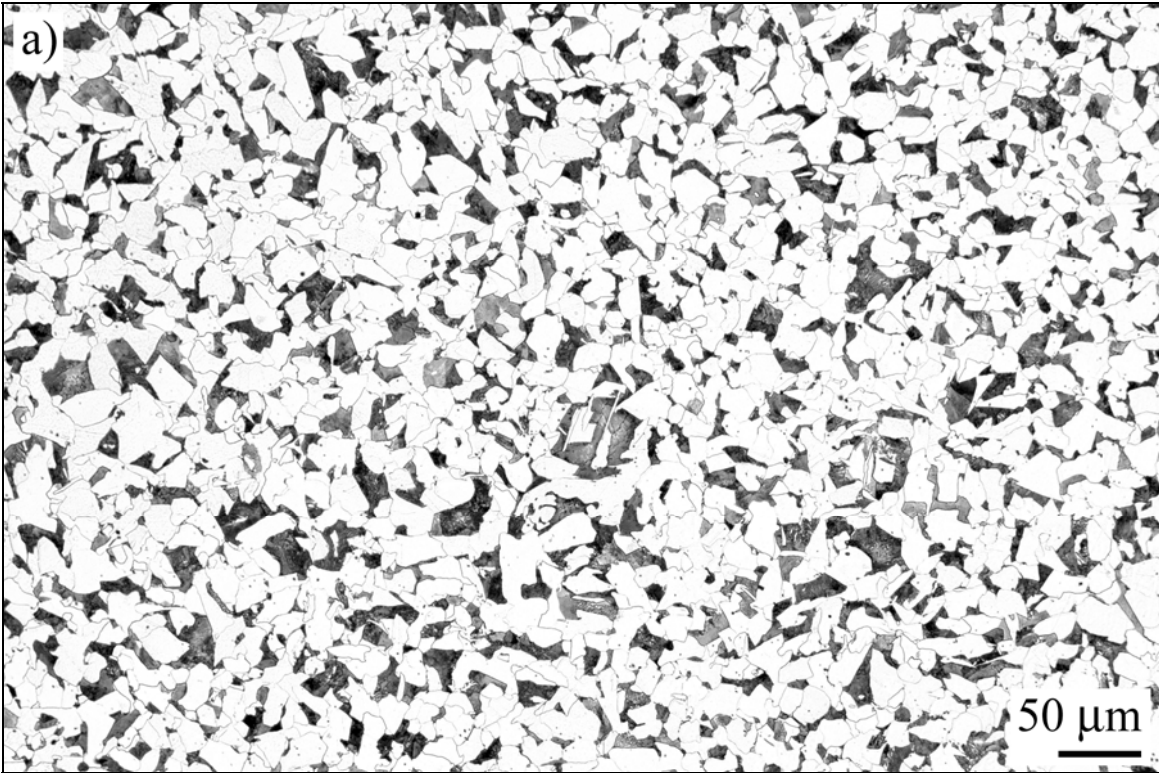
Source: NIST.

**Figure 5–31. Microstructures from channel material located in the core. Both samples were hot-rolled with different volume fraction and distribution of pearlite within the structures. a) Banded microstructure of sample C-107 and b) uniform distribution of sample M-24. Both with 2 percent nital and 4 percent picral etch.**



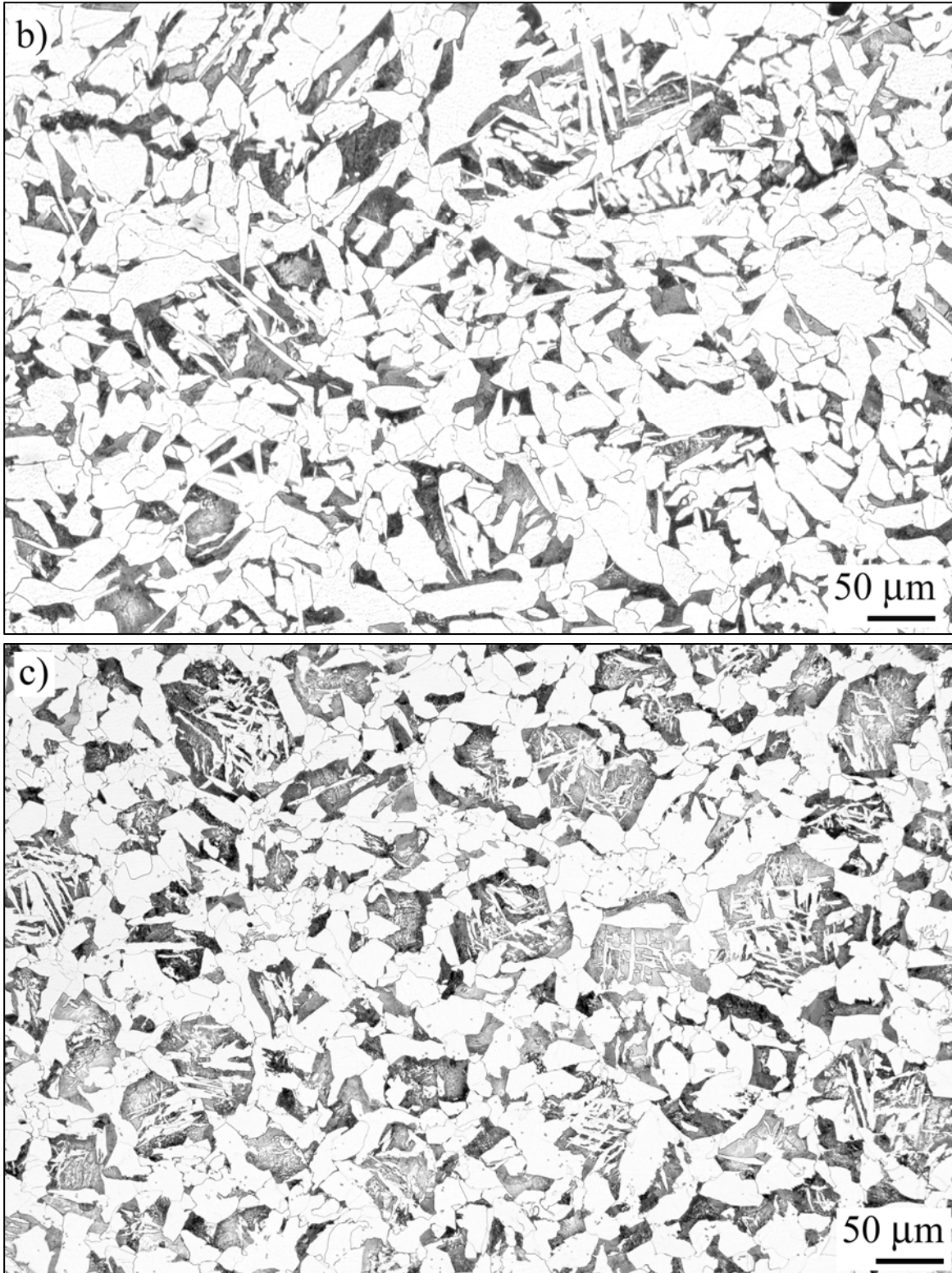
Source: NIST.

**Figure 5–32. Microstructure of a hot-rolled core floor truss seat. Majority of the ferrite is polygonal, but there are some irregular morphologies. Sample is from C-118. 2 percent nital and 4 percent picral etch.**



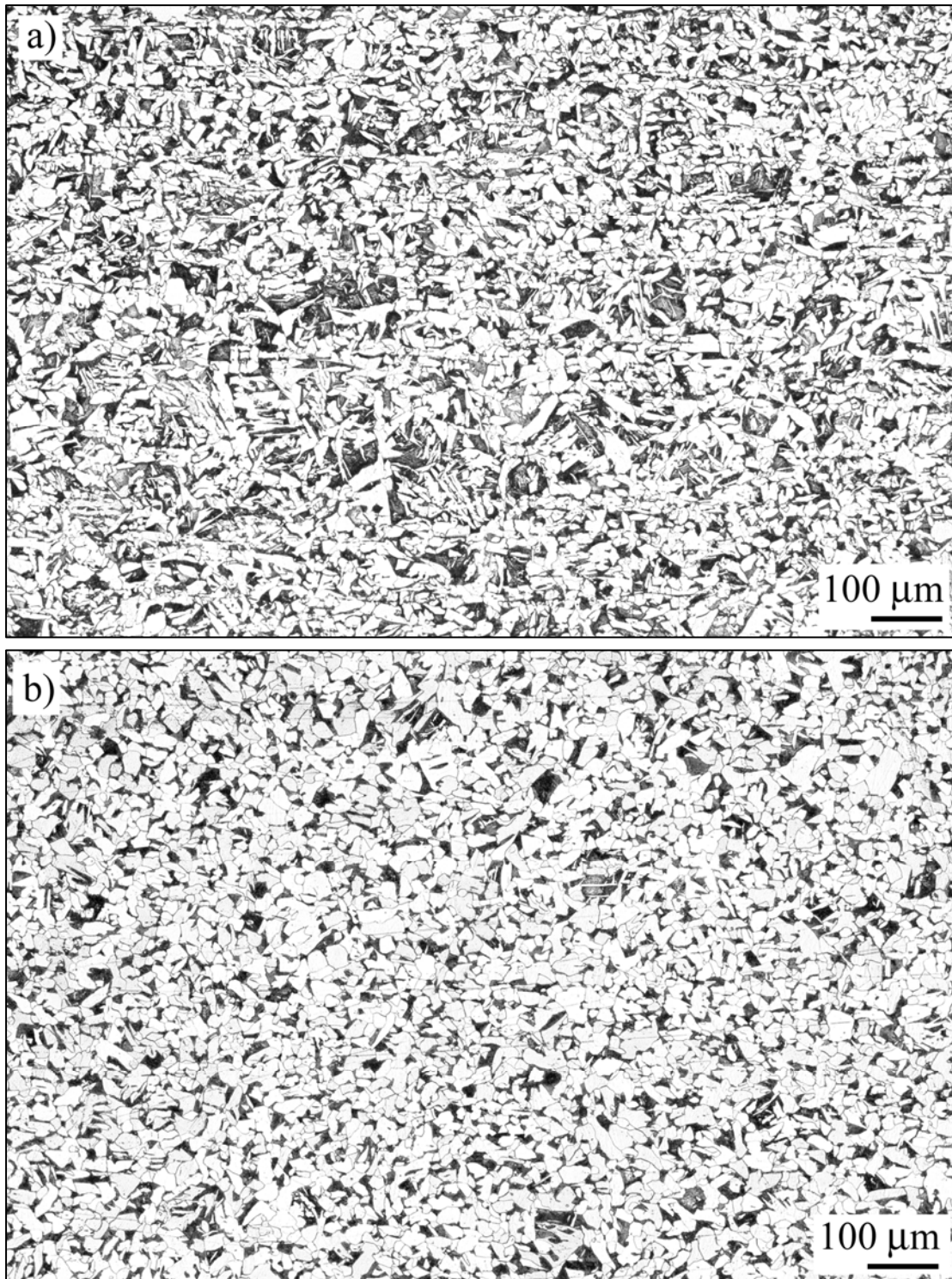
Source: NIST.

**Figure 5–33. Microstructure from floor truss rods. a) Uniform distribution of constituents of rod T1-SR-1. 2 percent nital and 4 percent picral etch.**



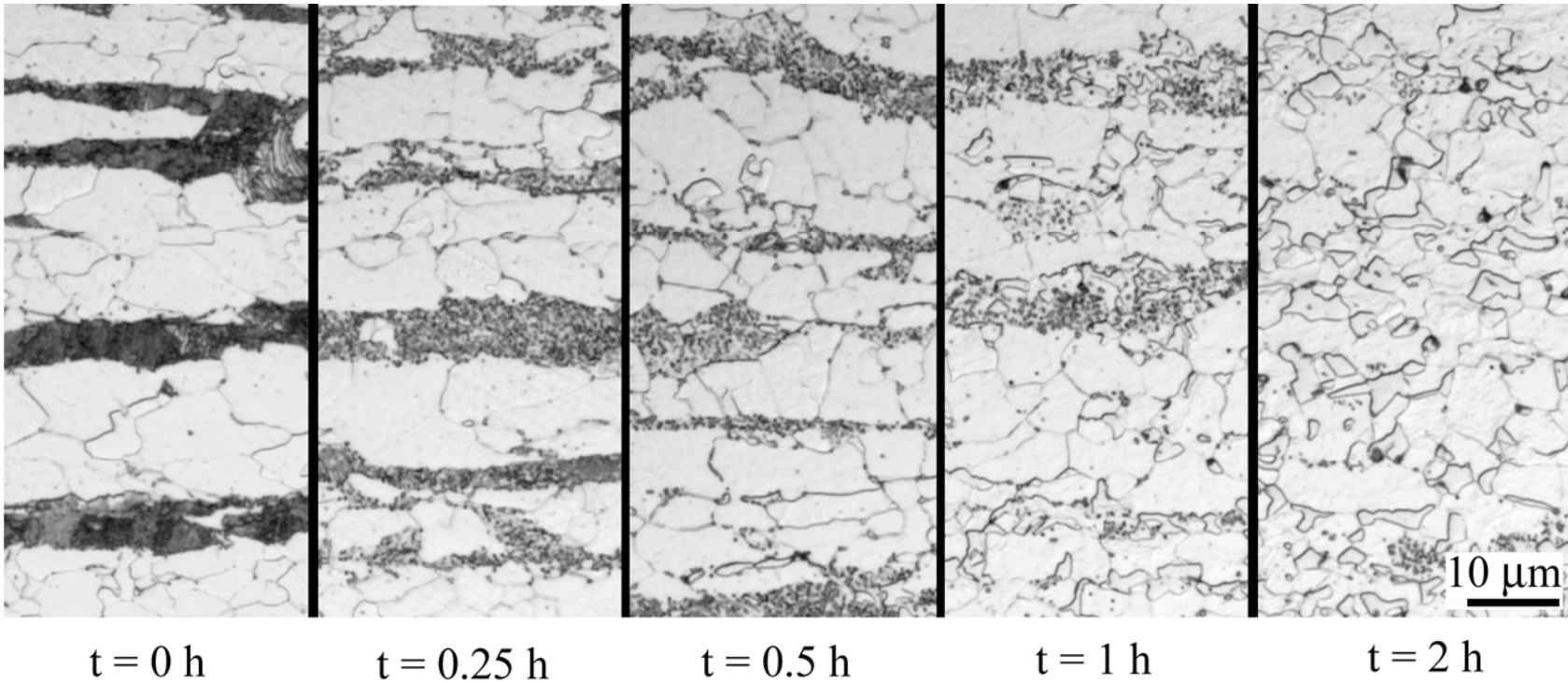
Source: NIST.

**Figure 5–33. Microstructure from floor truss rods. b) T1-LR-1 and c) M32-LR-1 showing different distributions of ferrite morphologies. Both with 2 percent nital and 4 percent picral etch (continued).**



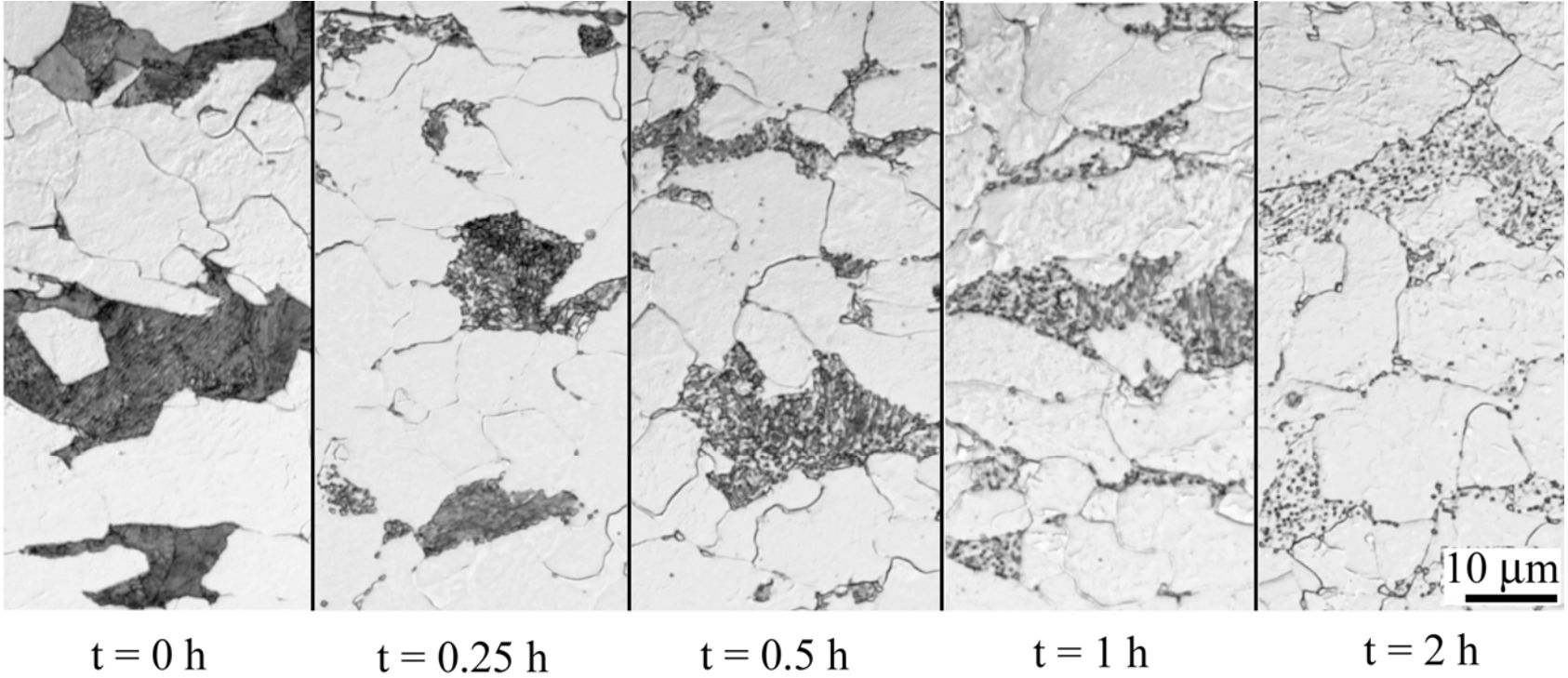
Source: NIST.

**Figure 5-34. Microstructures from floor truss angles. a) Angle samples with V additions had a higher volume fraction of the Widmanstätten morphology for the ferrite constituent (sample from C-137a) and b) samples lacking V contained primarily polygonal ferrite (sample from C-53a). Both with 2 percent nital and 4 percent picral etch.**



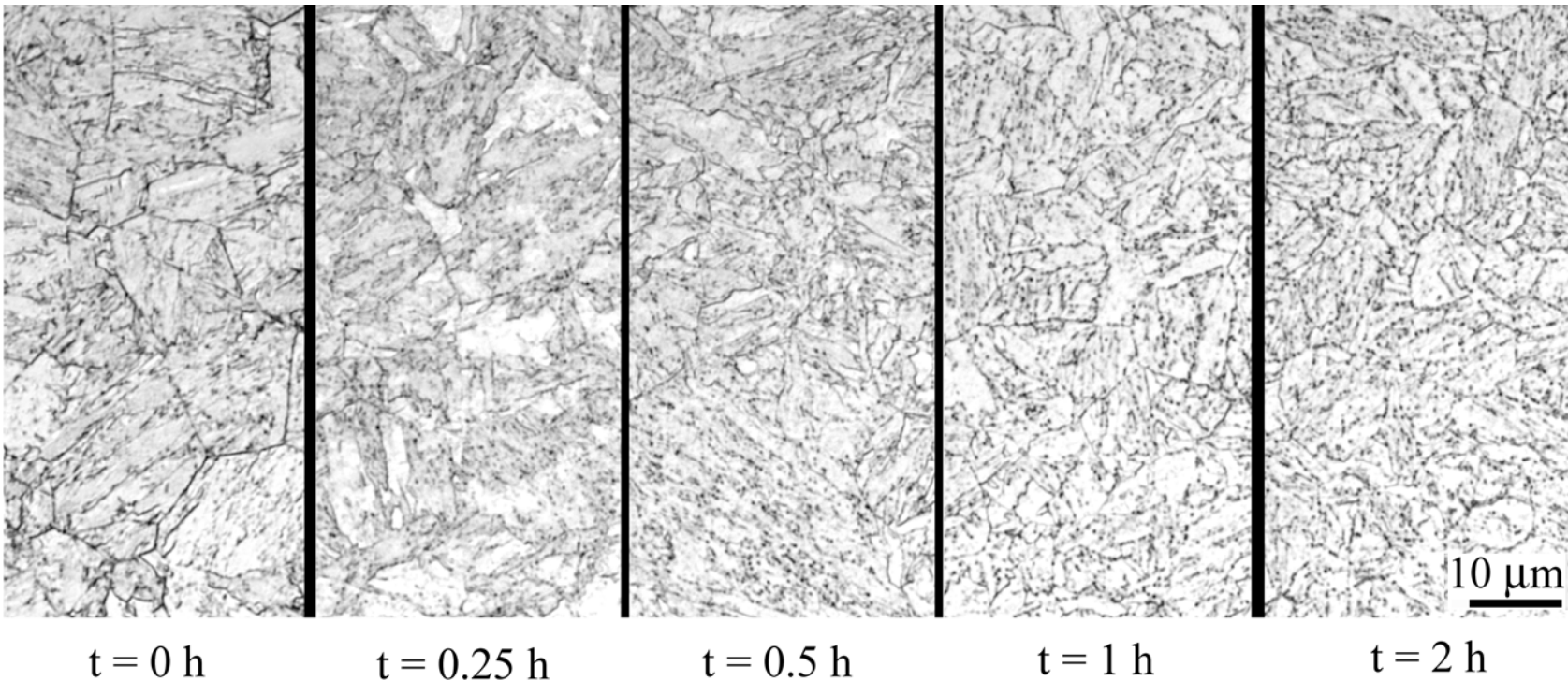
Source: NIST.

**Figure 5–35.** Change in microstructure of a 60 ksi flange plate that was heat treated in a laboratory furnace at 625 °C for various times. Pearlite was observed to spheroidize. Sample shown was from panel N-7 (WTC 1, column 126, 97th floor). 2 percent nital and 4 percent picral etch.



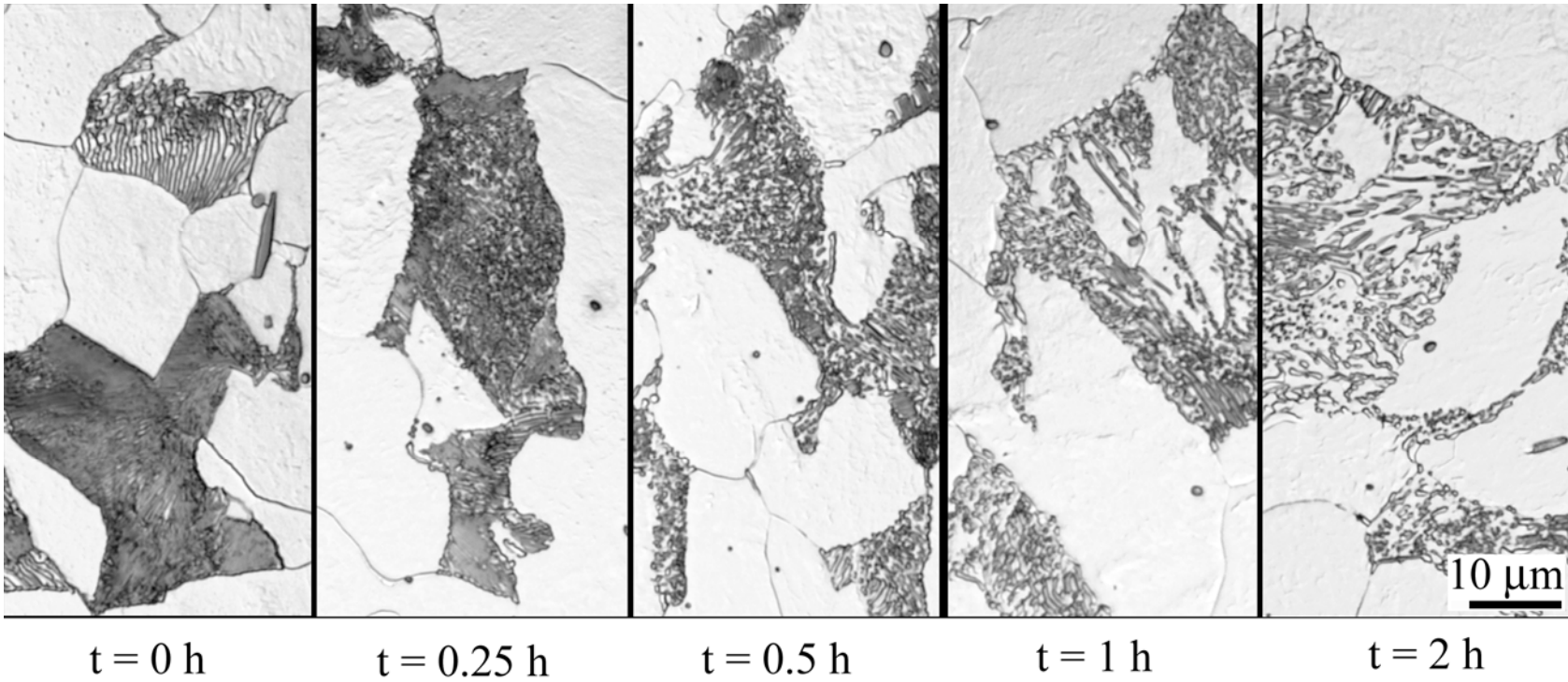
Source: NIST.

**Figure 5–36. Change in microstructure of a 42 ksi spandrel plate that was heat treated in a laboratory furnace at 625 °C for various times. Pearlite was observed to spheroidize. Sample shown was from panel N-9 (WTC 1, 102nd floor spandrel, near column 154). 2 percent nital and 4 percent picral etch.**



Source: NIST.

**Figure 5–37.** Change in microstructure of a 100 ksi flange plate that was heat treated in a laboratory furnace at 625 °C for various times ( $t$ ). Sharpness of lath boundaries was observed to decrease while the carbide precipitates became more discernable. Sample was from panel C-10 (WTC 1, column 451, 88th floor). 2 percent nital and 4 percent picral etch.



Source: NIST.

**Figure 5–38. Change in microstructure of a truss seat that was heat treated in a laboratory furnace at 625 °C for various times. Pearlite was observed to spheroidize. Sample shown was from panel C-18 (WTC 2, column 231, 95th floor). 2 percent nital and 4 percent picral etch.**

Table 5-1. ASTM grain size number and volume fraction pearlite for plates from the exterior panels.

Fy (ksi)	Flange				Inner web				Spandrel			
	Ferrite grain size		Pearlite %		Ferrite grain size		Pearlite %		Ferrite grain size		Pearlite %	
	Ave ASTM grain size #	Relative accuracy	Ave	St dev	Ave ASTM grain size #	Relative accuracy	Ave	St dev	Ave ASTM grain size #	Relative accuracy	Ave	St dev
36									12.1	1.1	24.5	1.3
42									12.5	0.8	18.3	1.1
45	10.4	0.6	27.2	2.5					13.4	1.0	17.5	1.3
46									12.3	1.0	26.0	1.4
50	11.6	0.6	27.4	2.9	13.2	0.6	29.0	3.2	14.2	0.7	23.9	1.7
55	12.3	0.5	27.1	2.1	12.1	0.7	29.8	3.6	14.5	0.6	28.3	1.4
60	12.3	0.5	25.4	1.9	13.0	0.8	26.4	3.2	14.4	0.7	26.7	1.5
65	12.2	0.5	27.4	3.0	13.7	0.7	37.4	2.8	12.8	0.7	26.5	2.0
70					13.8	0.6	42.7	2.6				
75					13.5	0.6	43.1	3.1				

**Table 5–2. ASTM grain size number, volume fraction pearlite, and hardness results for panel splice connectors and floor truss connectors.**

Element	Component	Fy (ksi)	Ave ASTM grain size #	Pearlite %	HRB	HVN
Perimeter panel truss connector	Truss seat	36	9.7	17.9	86.6	183
			0.8	0.9	2.1	15
	Standoff plates	42	11.9	17.3	78.6	161
			1.0	2.7	2.6	30
	Gusset plate welded to the top chord of floor truss	36	13.1	43.6	89.9	221
			0.8	2.6	6.1	24
	Bolt	120	n/a	n/a	26.7	340
					0.5	9
	Damper plate	36	13.3	30.9	87.9	187
			0.7	3.5	0.2	3
Gusset plate for attaching damper unit and diagonal bracing straps	36	10.3	13.4	81.3	169	
		0.8	0.7	6.7	26	
Diagonal bracing straps	36	10.5	19.9	86.7	190	
		0.7	2.6	3.4	28	
Perimeter panel splice	Butt plate	50	n/a	n/a	90.8	203
					0.3	13
	Splice plate	36	12.7	18.8	80.6	164
0.7			1.2	9.5	25	
Core column truss connector	Channel	36	9.8	24.5	80.7	178
			1.1	2.5	3.2	12
	Truss seat	36	10.3	28.8	85.3	212
			0.6	0.7	4.3	17

**Table 5–3. ASTM grain size number and volume fraction pearlite for core column material.**

Element	Component	Fy (ksi)	Thickness (in)	Ferrite grain size		Pearlite %	
				Ave ASTM grain size #	Relative accuracy	Ave	Stdev
Core Column	Box- flange	36	2.00	9.6	0.9	21.9	1.0
Core Column	Box- flange	42	1.55	11.0	1.1	28.9	3.0
Core Column	Wide- flange	36	1.38	11.1	1.1	36.6	2.7
Core Column	Wide- flange	36	1.50			28.2	1.9
Core Column	Wide- flange	36	1.55	10.0	1.2	31.1	2.3
Core Column	Wide- flange	42	0.88	9.6	0.8		

**Table 5–4. ASTM grain size number, volume fraction pearlite, and hardness results for floor truss material.**

Component	Sample ID	Diameter (in)	ASTM grain size #		Pearlite %		HRB		HVN	
			Ave	Relative accuracy	Ave	Stdev	Ave	Stdev	Ave	Stdev
Bottom angle/chord	C53-BA-3	NA					83.9	0.2		
	T1-BA	NA							189	3
Top angle/chord	T1-TA	NA	10	0.5	22.6	2.0	87.8	0.1	197	4
	C132-TA-3	NA					86.6	0.4		
	C137a-TA-3	NA	11.3	0.6	37.1	1.8	89.2	0.2	183	1
	C53-TA-2	NA					89.6	0.2	203	7
	C137f-TA-5	NA					86.5	0.4	172	3
	C53-TA-1	NA	11.7	1	24.4	2.2	88.3	0.8	209	3
Truss rod	C106-SR-1	0.68	10.2	1.1	25.6	3.8	83.5	0.8		
	T1-SR-1	0.76					89.5	1.0	160	4
	C53-MR-1	0.93	12.9	0.8	34.2	3.6	92.9	0.4	203	4
	T1-LR-1	1.00	12.5	0.9	29.2	2.3	86.5	0.4	163	7
	C53-LR-1	1.10					82.6	1.5	159	6
	M32-LR-1	1.13					95.6	0.7	189	5

## Chapter 6

# HARDNESS ANALYSIS RESULTS

---

Hardness is a mechanical property typically defined as a measure of the material's resistance to plastic deformation. These values correlate with the ultimate tensile strength obtained from uniaxial tensile testing. In the following section, both Rockwell hardness, with a sampling area of 1 mm<sup>2</sup> to 2 mm<sup>2</sup>, and microhardness, with a sampling area of 100 μm<sup>2</sup> to 200 μm<sup>2</sup>, were used in the study for all base plates/material of a component. Further, microhardness traces across weld cross-sections from perimeter panel columns were conducted to determine if a change in the microstructure of the heat affected zone occurred.

In addition to the “as-fabricated” plate hardness measurements, the furnace exposed samples described in Sec. 5.4 were tested. This testing was conducted to help detect changes in the mechanical properties as a result of microstructure alteration from the elevated temperature exposure.

### 6.1 PERIMETER PANEL MATERIAL

Tables 6–1 and 6–2 show Rockwell and Vickers data sets, respectively, for the perimeter column material. For Rockwell testing, most of the data for the high strength plates were reported in Rockwell C, as they were too hard for the B-scale. Similar results were observed for both sets of data; as the specified minimum yield strength increased, the hardness was also found to increase.

### 6.2 CORE COLUMN MATERIAL

Table 6–3 displays the individual hardness results for each of the 12 identified columns. In grouping them by their specified minimum yield strength, the 36 ksi and 42 ksi materials all had similar hardness values. However, the 36 ksi materials tested from the core columns had lower hardness values than were found for the 36 ksi plate materials from the perimeter columns.

### 6.3 FLOOR TRUSS MATERIAL

Table 5–4 displays the individual results from the floor truss material (rods and angles). As all the materials met chemistry specifications for ASTM International (ASTM) A 36 and ASTM A 242, deviations in the results were minimal. Two exceptions were observed for the 0.93 in. and 1.13 in. diameter rods that had Rockwell hardness values above 90 Rockwell Hardness B-Scale (HRB).

### 6.4 PANEL SPLICE CONNECTORS AND TRUSS CONNECTORS

Table 5–2 displays hardness results for connectors for both the panels and the floor trusses. As most of the materials were believed to have a minimum yield strength of 36 ksi, their average hardness values were very similar. Note that, with the exception of the bolt and the butt plate (both with only one sample measured), the standard deviations are all large. This may suggest that these components were supplied

by multiple suppliers or that the specification was very relaxed, as is the case for A 36. The only difference among this group was the A 325 bolt, which had a higher hardness due to the quenched-and-tempered microstructure.

## 6.5 HARDNESS TRAVERSES THROUGH WELDS ON PERIMETER COLUMNS

Knoop hardness traverses were conducted across welded joints found on perimeter columns. Joints between an inner web and flange were analyzed for base plates with specified minimum yield strengths of 55 ksi and 100 ksi. Figures 6–1 and 6–2 show the samples used for profiles through the joint for the 55 ksi and 100 ksi materials, respectively, with a line inserted schematically showing the approximate location of the hardness trace. Multiple indents at various locations along the weld were also dropped near the fusion line to yield more data points at various distances near this microstructural feature. To accomplish this task, samples were etched in order that the fusion line of the weld could be marked. Samples were re-polished before testing. Subsequent to Knoop indentation, the samples were again etched to reveal the weld structure and allow for exact determination of the indents from the fusion line.

On both samples, a spike in hardness was noted near the fusion line. In Sec. 5.1.1, it was observed that the welding of these steels produced areas near the weld in the un-melted base material that experienced diffusional transformations. As seen in the weld microstructures of Fig. 5–12c, a Widmanstätten morphology developed in the heat-affected zones (HAZs) near the fusion line for the hot-rolled steels (Fig. 5–12c) and the grain size was larger in this area compared to the as-fabricated plate. For the quenched-and-tempered steels, the formation of what appears to be martensite was observed (Fig. 5–13), thus increasing the hardness in this area.

## 6.6 HARDNESS OF FURNACE EXPOSED FLANGE PLATES

### 6.6.1 Hot-Rolled Flange and Spandrel Plates

The hardness data for exposed hot-rolled plates corresponds well with the observed microstructural changes at the higher temperatures. For the 60 ksi plate exposed at 625 °C, an initial decrease was observed with time for the first 30 min of exposure and then increased after that to a level greater than the “as-fabricated” hardness (Fig. 6–3). The initial hardness decrease was due to the spheroidization of the cementite lamellae found in the pearlite (Fig. 5–35). The strengthening mechanism for the increase in hardness with continued exposure was undetermined. Similar to the 60 ksi flange plate, the 42 ksi spandrel plate also had a decrease in hardness (Fig. 6–4). However, unlike the 60 ksi steels, there was no hardness increase with long exposure times.

For exposure at 500 °C, both materials experienced a slight decrease in hardness. No changes were observed in the microstructure at this temperature using light optical microscopy.

Samples exposed in the 200 °C to 400 °C range showed a slight increase in hardness. The mechanism for the increase in hardness was not determined.

### **6.6.2 Quenched-and-Tempered Flange Plate**

For the quenched-and-tempered plate, the hardness was observed to continually drop over the 2 h period at 625 °C (Table 6–4). This was most likely due to the diffusion of carbon out of the lattice to form carbides in the lath boundaries; these precipitates were observed to be more discernible after the 2 h period (Fig. 5–37).

### **6.6.3 Exterior Panel Floor Truss Seat**

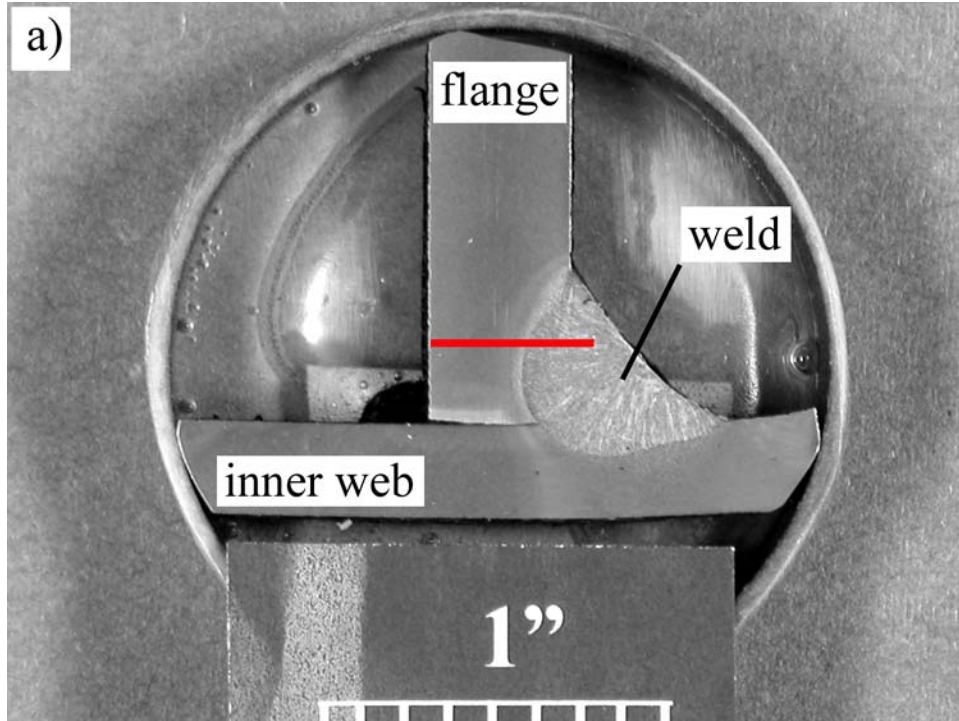
The truss seat exposed to 625 °C was observed to decrease in hardness with an increase in time (Table 6–4). Similar to the 42 ksi spandrel plate, no increase in hardness was observed after the 2 h exposure.

## **6.7 SUMMARY**

Hardness values were observed to increase with increasing specified minimum yield strength of the plate/component.

Microhardness traces across weld cross-sections from perimeter panel columns displayed an increase in hardness near the fusion line in the HAZ of the base plate. This was related to the alteration of microstructure due to the heat input from the welding process, and subsequent rapid removal, and is common when welding low carbon steels.

Hardness of furnace exposed samples varied for a given temperature, time, and microstructure.



Source: NIST.

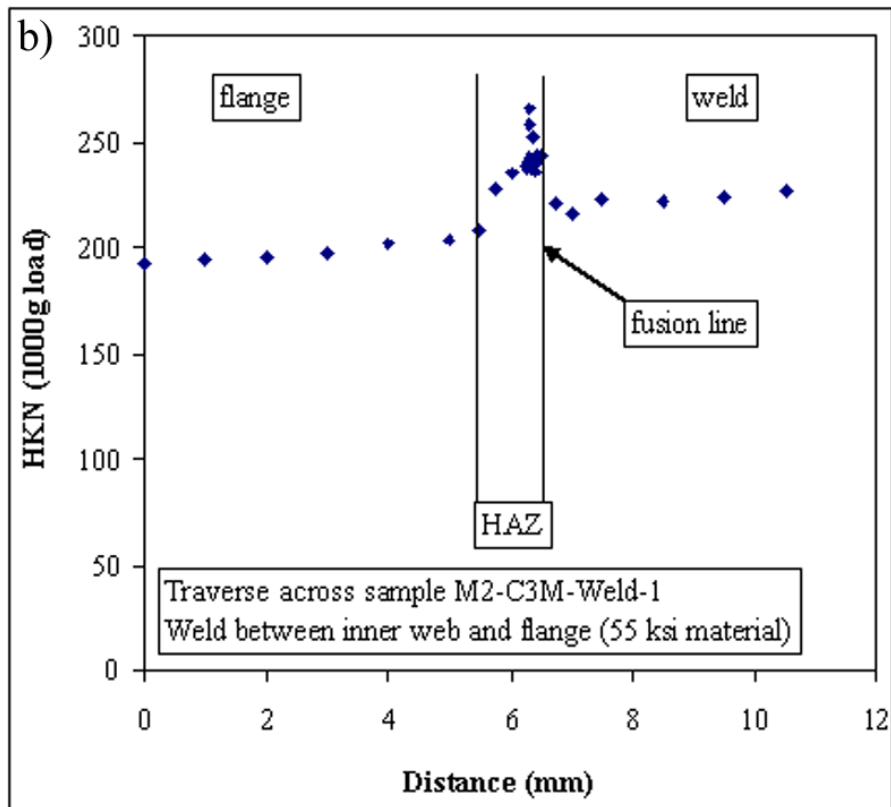
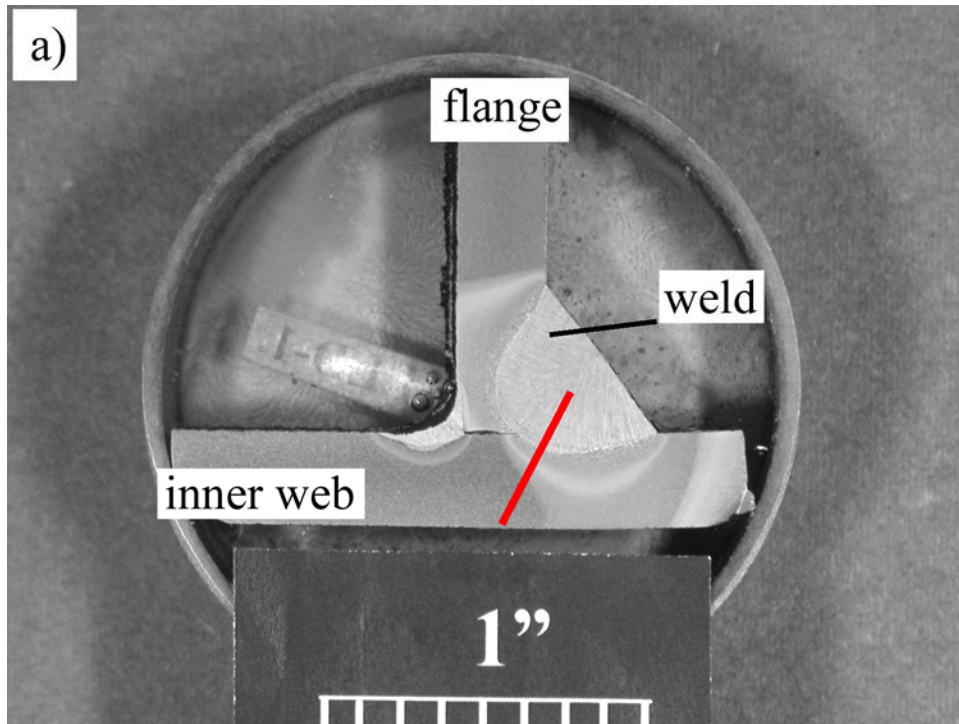


Figure 6–1. Knoop hardness traverses through welded joints. Joints shown were between an inner web and flange for hot-rolled plates. a) photomicrograph indicating trace through 55 ksi plates. 2 percent nital and 4 percent picral etch. b) Knoop hardness trace through 55 ksi material.



Source: NIST.

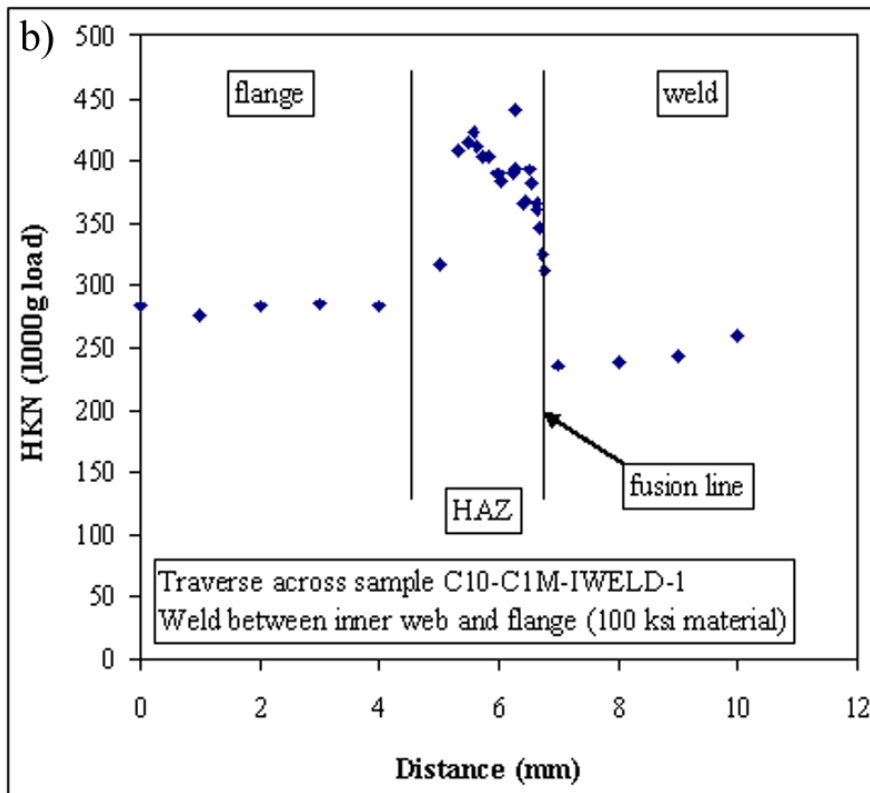


Figure 6–2. Knoop hardness traverses through welded joints. Joints shown were between an inner web and flange for quenched-and-tempered plates. a) photomicrograph indicating trace through 100 ksi plates. 2 percent nital and 4 percent picral etch. b) Knoop hardness trace through 100 ksi material.

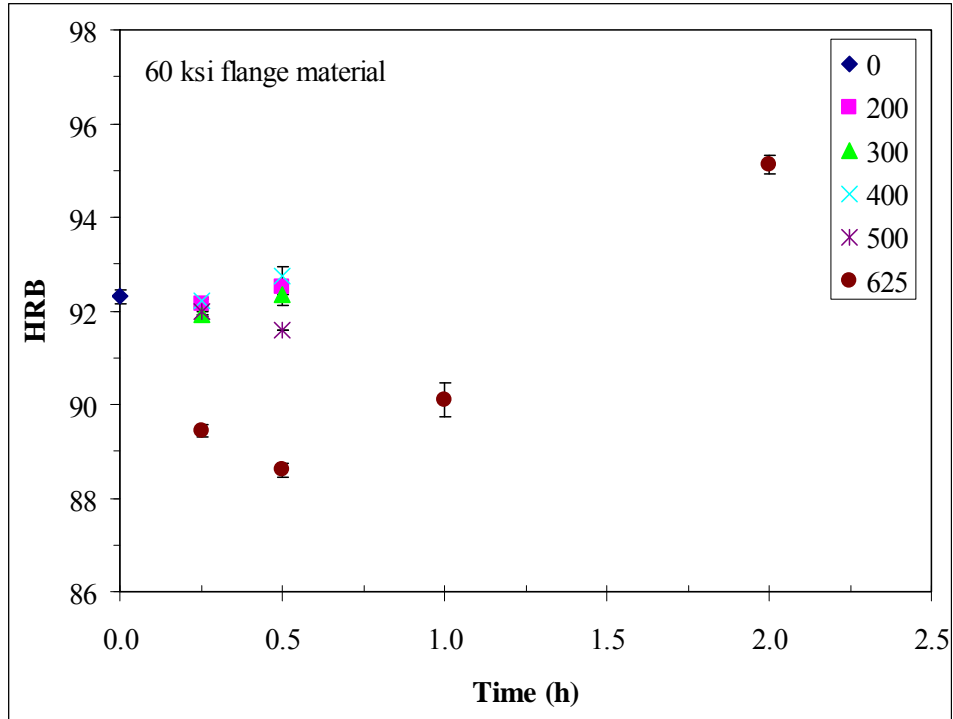


Figure 6–3. Hardness as a function of time and temperature for furnace exposure of 60 ksi flange plate.

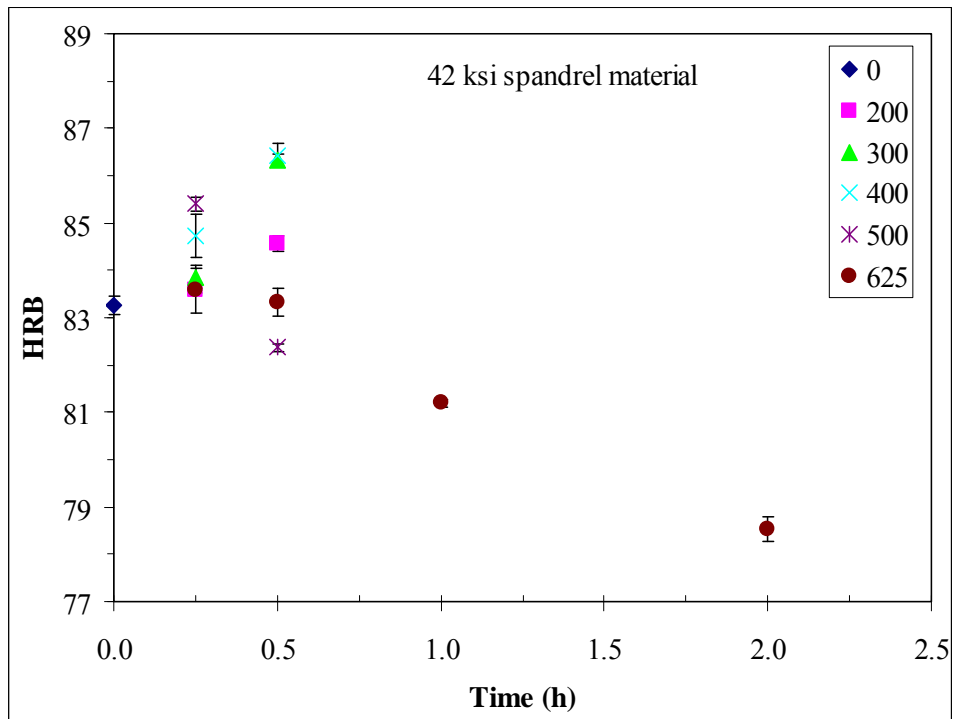


Figure 6–4. Hardness as a function of time and temperature for furnace exposure of 42 ksi spandrel plate.

**Table 6–1. Rockwell hardness data for exterior panel material.**

Fy (ksi)	Thickness (in)	Flanges	Outer web	Inner web	Spandrel	Fy (ksi)	Thickness (in)	Flanges	Outer web	Inner web	Spandrel			
36	0.375				84.7	65	0.25	96.1	94.9	94.0				
					5.8			1.1	2.6	2.2				
42	0.375				86.9			0.375					97.3	
					3.5								0.2	
45	0.375				86.8		0.5625					98.0		
	2.4				0.2									
46	0.375	81.7					0.625					96.6		
												0.8	0.3	
50	0.25		91.9	95.3			70	0.25	94.3	98.5	21.6 <sup>a</sup>			
			0.8	2.0					3.2	0.6	0.5			
	0.375			89.5	93.5			0.375						95.2
				0.8	1.4									97.4
	0.4375					0.4375							94.9	
													92.2	2.5
0.5		90.3			0.75						96.2			
											2.9		96.2	97.8
0.5625		91.0	85.3		0.25	75					3.0			
			0.0								3.0	0.7	0.3	
55	0.25	95.3	93.3	92.9		80	0.375					96.7		
			2.7	3.1								2.5	21.2 <sup>a</sup>	20.4 <sup>a</sup>
	0.3125	93.4					0.25						1.2	
													3.0	
	0.375	95.0					0.5625						20.7 <sup>a</sup>	
													2.6	
0.4375	96.1				0.625						98.5			
											1.0			0.8
0.5625	90.7				0.25	100					25.6 <sup>a</sup>			
											2.9			1.4
60	0.25	94.5	94.7	90.3		100	0.5625					23.4 <sup>a</sup>		
			0.8	1.8								3.7	102.0	
	0.3125	96.1					1.125						0.8	
													1.0	
	0.375												95.3	

a. Indicates that values are HRC.

**Note:** Unless indicated, all values are HRB.

**Table 6–2. Vickers hardness data for exterior panel material.**

Fy (ksi)	Thickness (in)	Flanges	Outer web	Inner web	Spandrel	Fy (ksi)	Thickness (in)	Flanges	Outer web	Inner web	Spandrel				
36	0.375				176	65	0.25	228	222	195					
					21			9	21	19					
42	0.375				183			0.375					238		
					16								4		
45	0.375				178		0.5625					252			
	15				7										
46	0.375	150					0.625					229			
												8	8		
50	0.25		204	227			70	0.25	226	243	254				
			4	16					30	13	7				
	0.375			187	215	0.375							226		
				4	21		4								
	0.4375					205	0.4375	232					8		
15															
0.5		199				75	0.25	236	231	241					
								18	12	8		10			
0.5625		205	168			80	0.375					246.5			
			6									257	242	277	
			11												
55	0.25	229	212	206		100	0.25	275	277	281					
			18	19				16	13	12		11			
	0.3125	216					216	0.5625	254					261	
						24								6	
	0.375	226				18	0.625	254						10	
19														18	
0.4375	226					1.125	272						6		
													17	7	
0.5625	200						275						7		
													18		
60	0.25	213	220	195											
		8	15	19											
	0.3125	226													
20															
0.375					220										
														6	

Table 6-3. Rockwell (HRB for all samples) and Vickers hardness data for core columns.

NIST ID	Column ID	Element	Component description	Fy (ksi)	Plate thickness (in)	HRB		HVN	
						average	st dev	average	st dev
B-6152-1	803A: 15-18	Type 380 box column	Flange	36	2	75.6	0.8	133.7	5.5
B-6152-2	504A: 33-36	Type 354 box column	Flange	36	2	73.5	0.8	150.8	5.8
C-90	701B: 12-15	Type 381 box column	Flange	36	3.15	69.7	0.0	141.2	3.6
C-88b	801B: 77-80	Type 378 box column	Flange	42	1.55	90.0	0.3	168.2	5.2
C-88b	801B: 77-80	Type 378 box column	Flange	42	1.55	88.6	0.3	187.7	13.5
C-88b	801B: 77-80	Type 378 box column	Web	42	1.55	83.9	0.3	174.5	10.2
C-88c	801b: 80-83	Type 378 box column	Flange	42	1.55	85.4	0.9	157.7	10.2
C-88a	801b: 80-83	Type 378 box column	Flange	42	1.55	88.8	0.6	204	12
C-80	603A: 92-95	14WF184	Flange	36	1.375	71.0	0.4		
C-65	904A: 83-96	12WF161	Flange	36	1.5	67.4	0.3		
C-155	904A: 83-86	12WF161	Flange	36	1.55	74.7	0.6	141.3	5.2
C-71	904A: 77-80	12WF190	Flange	36	1.75	82.1	0.1	167.2	8.3
C-30	1008B: 104-106	14WF287	Flange	36	1.75	66.8	0.2	137.0	4.0
HH	605A: 98-101	12WF92	Flange	42	0.875	86.3	0.7	205.0	13.9

**Table 6–4. Hardness values for various furnace exposed WTC steel.**

Panel	C-10		C-18	
Bldg	WTC 1		WTC 2	
Component	Q&T flange plate		Floor truss seat	
Column #	451		231	
Floor	88th		95th	
Fy	100 ksi		36 ksi	
Tempering time	<b>HRB ave</b>	<b>St Dev</b>	<b>HRB ave</b>	<b>St Dev</b>
<b>0 h</b>	25.9 <sup>a</sup>	0.0	71.2	0.9
<b>0.25 h</b>	98.6	0.2	69.6	0.2
<b>0.5 h</b>	96.5	0.2	67.7	0.3
<b>1 h</b>	94.0	0.1	67.5	0.4
<b>2 h</b>	92.1	0.3	67.2	0.4

a. Indicates value reported in HRC.

**Note:** Unless indicated, all values are HRB.

# Chapter 7

## THERMAL PROPERTIES OF WTC STRUCTURAL STEEL

---

### 7.1 INTRODUCTION

This chapter provides thermal property values as a function of temperature, which are needed for modeling the structural steel response to fire. These properties include:

- Specific heat ( $C_p$ ),
- Coefficient of thermal expansion ( $\alpha$ ), and
- Thermal conductivity ( $k$ ).

In general, properties are provided from room temperature up to 600 °C or 700 °C. On heating to approximately 727 °C, iron carbon alloys, such as structural steel, transform from a mixture of  $\alpha$ -phase (ferrite) and cementite ( $\text{Fe}_3\text{C}$ ) to a mixture of  $\alpha$  and  $\gamma$  (austenite). Most thermostructural properties are discontinuous at this transition, and the heat capacity becomes infinite. Furthermore the literature contains much less information on properties at temperatures higher than the phase transformation. Generally, though, the strength of steel above the phase transformation is reduced to 10 percent or less of the room-temperature value, so other properties become of minor importance.

Of the three thermal properties described here, only the thermal conductivity varies by more than a few percent among the different steels used in the building. The specific heat,  $C_p$ , and coefficient of thermal expansion,  $k$ , as a function of temperature can be represented by individual equations for all World Trade Center (WTC) steels. The thermal conductivity,  $k$ , depends strongly on chemical composition. In principle, it is possible to estimate the thermal conductivity from the steel chemistry. In the trusses, it is possible to estimate the thermal conductivity of all the components because a single mill supplied all the steel for the trusses. Similarly, for the perimeter columns enough is known about the chemistry of the steels to estimate the thermal conductivity of an individual plate in a given column. For the wide flange and welded core columns, the steel composition used in individual columns can not be uniquely identified. (Two mills supplied steel for the welded core columns. For the rolled, wide-flange core columns and beams, three or more mills supplied identical ASTM International (ASTM) grades of steel with different chemistries (NIST NCSTAR 1-3A). Those steel chemistries were relatively different, so it is impossible to assign a specific thermal conductivity to a given column or beam.

### 7.2 SPECIFIC HEAT

The specific heat at constant pressure is defined as

$$C_p = \left( \frac{dq}{dT} \right)_p \quad (7-1)$$

where  $q$  is the heat added per unit mass. To a first approximation, the molar specific heat of elements and mixtures at room temperature and above is a constant at approximately  $3R=24.94$  J/(mol K), which is the so-called law of Dulong and Petit. At the  $\alpha$ - $\gamma$  phase transformation (above about 720 °C in carbon steels) the heat capacity is effectively infinity, since all added energy goes into transforming the phase rather than raising the temperature.

Structural steels generally contain very low fractions of alloying elements. To a good approximation, then, it is possible to use the heat capacity as a function of temperature for pure iron without introducing an error of more than 3 percent. Figure 7–1 shows some experimental determinations of the heat capacity of various low-alloy steels and pure iron. In principle, it is possible to correct for the presence of alloying elements, but these corrections will be, at most, several percent.

### 7.2.1 Recommended Value

Of the many experimental determinations of the heat capacity of iron, the National Institute of Standards and Technology (NIST) has selected that of Wallace, Sidles, and Danielson (1960), listed in Touloukian and Buyco (1970), because it spans the temperature range of interest, is relatively recent, and has an uncertainty statement. To represent the data, a third-order polynomial was fitted to the data in the range  $0\text{ °C} < T < 650\text{ °C}$ :

$$C_p(T) = c_0 + c_1T + c_2T^2 + c_3T^3$$

where

$$\begin{aligned} c_0 &= 51.11 \pm 33.39 \\ c_1 &= 2.019 \pm 0.185 \\ c_2 &= (-3.0135 \pm 0.320) \times 10^{-3} \\ c_3 &= (1.829 \pm 0.175) \times 10^{-6} \end{aligned} \quad (7-2)$$

where  $C_p$  is expressed in J/(kg K) and  $T$  in kelvins.

### 7.2.2 Uncertainties

Wallace, Sidles, and Danielson (1960) reports an uncertainty of 2 percent in the measured value of  $C_p$ . The maximum deviation of  $C_p$  from other measured structural steels is at most several percent.

## 7.3 COEFFICIENT OF THERMAL EXPANSION

The coefficient of thermal expansion (CTE),  $\alpha$ , is used to predict the length of a member,  $L$ , as a function of temperature,  $T$ . There are two common definitions. The mean CTE,  $\alpha_M$ , is simply the two-point slope of the length of the specimen at two temperatures. As such, it ignores any changes in slope between the two fixed points.

$$\alpha_M = \frac{L_2 - L_1}{L_1(T_2 - T_1)} \quad (7-3)$$

The instantaneous CTE,  $\alpha$ , which permits integration along the temperature path to find the length of a member at any temperature is defined as

$$\alpha = \frac{1}{L} \left( \frac{\partial L}{\partial T} \right) \quad (7-4)$$

For pure iron, Touloukian et al. (1977) provides a recommended function for the fractional length change as a function of temperature, as well as tabulated values for the instantaneous coefficient of thermal expansion,  $\alpha$ . Although it is possible to derive an expression for  $\alpha$  from the function for  $L(T)$  using Eq. 7-4, the resulting expression is mathematically more complicated than necessary. It is more convenient to calculate the points of the expression for  $\alpha(T)$  and then fit a cubic polynomial to the data. The expression for  $\alpha(T)$  derived this way differs from the derived version by less than 1 part in 10,000.

$$\begin{aligned} \alpha(T) &= \alpha_0 + \alpha_1 T + \alpha_2 T^2 + \alpha_3 T^3 \\ \text{where} \\ \alpha_0 &= 7.3633 \times 10^{-6} \\ \alpha_1 &= 1.8723 \times 10^{-8} \\ \alpha_2 &= -9.8382 \times 10^{-12} \\ \alpha_3 &= 1.6718 \times 10^{-16} \end{aligned} \quad (7-5)$$

and  $T$  is measured in kelvins, for  $300 \text{ K} < T < 900 \text{ K}$ .

The American Institute of Steel Construction (AISC) Manual of Steel Construction (AISC 2001) recommends

$$\begin{aligned} \alpha_M &= b_1' + b_2' \left[ \frac{9}{5} (T - 273.15) + 32 \right] \\ \text{where} \\ b_1' &= (9/5) 6.1 \times 10^{-6} \\ b_2' &= (9/5) 1.9 \times 10^{-6} \end{aligned} \quad (7-6)$$

and  $T$  is expressed in kelvins, relative to a base temperature of 311 K (100 °F). It makes no distinction between grades of structural steel. The AISC Manual is not completely clear that this expression is for the mean coefficient of thermal expansion, rather than the instantaneous value. Converting to the instantaneous value of coefficient of thermal expansion yields

$$\begin{aligned} \alpha &= b_1 + b_2 T \\ \text{where} \\ b_1 &= 7.4954 \times 10^{-6} \\ b_2 &= 1.231 \times 10^{-8} \end{aligned} \quad (7-7)$$

when  $T$  is expressed in kelvins for  $311 \text{ K} < T < 922 \text{ K}$  ( $100 \text{ °F} < T < 1200 \text{ °F}$ ).

There are several difficulties in estimating the thermal expansion coefficient of structural steel from first principles. One serious problem is that the thermal expansion is discontinuous at the  $\alpha$ - $\gamma$  phase boundary

(910 °C in pure iron, and beginning as low as 723 °C in Fe-C alloys). Figure 7–2 illustrates the fraction length change  $\Delta L/L_0$  of iron as a function of temperature up to 1,650 °C, and shows the discontinuity at 910 °C at the  $\alpha$ - $\gamma$  phase boundary. Of course, because the phase transformation is not instantaneous, the details of the thermal expansion near the transformation will depend on the heating rate. Interpreting experimental thermal expansion curves is also complicated by the time-dependence of the phase transformation. Curves obtained on heating and cooling frequently differ because the transformation occurs at different rates, leading to a hysteresis. First principles calculation of the thermal expansion of multi-phase materials, such as the Fe-Fe<sub>3</sub>C in structural steel, is also difficult.

There is a great amount of literature on thermal expansion coefficient of steels; Touloukian et al. (1977) has tabulated many of the values. Figure 7–3 plots the instantaneous coefficient of thermal expansion ( $\alpha$  in Eq. 7–4) for several low alloy steels, as well as for pure iron and the AISC recommended value (Eq. 7–7). The difference between these curves is of the same magnitude as the difference between the different determinations for nominally pure iron. All of the data sets are truncated before they approach the  $\alpha$ - $\gamma$  phase boundary near 700 °C. The behavior of steels 6 and 7, which have anomalously low values of  $\alpha$  near room temperature, can not be explained. Note also the 2001 AISC recommended value severely over predicts all the other low-alloy steels for  $T > 550$  °C. The origin of the use of this equation for structural steels has not been found.

### 7.3.1 Recommended Value

Given the relative insensitivity to composition and microstructure, it is recommended that Eq. 7–4 be used, the value for pure iron, for all structural steels, in the temperature range 20 °C <  $T$  < 700 °C. If an expression for CTE for  $T > 700$  °C is necessary, it would be necessary to measure it on the steel in question.

Table 7–1 collects the values of the mean thermal expansion coefficient  $\alpha_M$  relative to both 273 K and 293 K calculated from Eq. 7–5.

### 7.3.2 Uncertainties

Touloukian et al. (1977) reports that the uncertainty in the expression for the change in length of iron with temperature (i.e., the integral of the CTE) is  $\pm 3$  percent for 300 K <  $T$  < 900 K  $\pm 5$  percent for 900 K <  $T$  < 1,185 K.

## 7.4 THERMAL CONDUCTIVITY AND DIFFUSIVITY

For one-dimensional heat flow, the thermal conductivity,  $k$ , relates the quantity of heat per unit time,  $Q$ , transported per unit area,  $A$ , to the temperature gradient  $\partial T / \partial x$  :

$$\frac{Q}{A} = k \left( \frac{\partial T}{\partial x} \right) \quad (7-8)$$

and has units of W/(m•K). For one-dimensional situations where the temperature depends on time, the thermal diffusivity,  $\alpha$ , is appropriate

$$\frac{\partial T}{\partial t} = \alpha \frac{d^2 T}{dx^2} \quad (7-9)$$

The thermal diffusivity,  $\alpha$ ,

$$\alpha = \frac{k}{\rho C_p} \quad (7-10)$$

is the ratio of the thermal conductivity,  $k$ , to the density,  $\rho$ , and specific heat  $C_p$ . It has units of a diffusion coefficient: m<sup>2</sup>/s.

Unlike the other thermal properties (CTE, specific heat), the microstructure of the steel affects the thermal conductivity. Identical chemistries processed differently will yield steels with different thermal conductivities. Because the various alloying elements and processing steps modify the microstructure, there is no generic relation between grade of steel and thermal conductivity. For instance, Fig. 7-4 plots the thermal conductivity as a function of temperature for twelve low-alloy steels. Even near room temperature, the data span 40 percent of the mean value.

In metals above room temperature, electronic conduction dominates the thermal conductivity. Conduction by lattice vibrations (phonons) is not usually significant. Because the thermal conduction in steel (and most metals) is primarily by electrons, the thermal ( $k$ ) and electrical ( $\sigma=1/\rho$ ) conductivity are related through the Wiedemann-Franz law:

$$L_0 = \frac{k}{\sigma T} \quad (7-11)$$

where  $L_0$  is called the Lorenz constant. In principle, then, one can predict the thermal conductivity from the electrical conductivity.

Data exist from a statistically planned experiment (Ludwigson 1971) to develop a relation between chemical composition (for extremely low alloy steels) and electrical conductivity at room temperature. To estimate the thermal conductivity of a given steel, NIST assumes that the effects of chemical composition are independent of temperature, and that the temperature dependence of the resistivity follows that of pure iron. For the former effect, NIST uses the electrical resistivity ( $\rho$ )-composition data of Ludwigson (1971) (at 26.75 °C):

$$\begin{aligned} \rho = & 0.01 \\ & (+10.1169 \\ & + 6.1995 [\text{Mn}] \\ & +14.3269 [\text{P}] \\ & +10.3715 [\text{S}] \\ & +11.7499 [\text{Si}] \\ & + 3.8815 [\text{Cu}] \\ & + 2.9775 [\text{Ni}] \\ & + 5.5696 [\text{Cr}]) \end{aligned} \quad (7-12)$$

where the resistivity,  $\rho$ , is measured in  $\mu\Omega\cdot\text{m}$  and the [ ] denotes % in percent. It was also assumed that the temperature dependence of the electrical conductivity is that of pure iron ( $\rho_{\text{Fe}}$ ), using the data reported by Schwerer (1986) Table 3 in the range  $300 \text{ K} < T < 1173 \text{ K}$ , but with the resistivity at 300 K equal to that of the constant term in Eq. 7-12:

$$\begin{aligned} \rho_{\text{Fe}}(T) = & 100 \\ & (+ (10.1169 - 9.7947) \\ & - 1.506 \\ & + 0.02276 T \\ & + 4.1966 \times 10^{-5} T^2 \\ & + 2.5879 \times 10^{-8} T^3 ) \end{aligned} \quad (7-13)$$

where  $\rho_{\text{Fe}}$  is measured in  $\mu\Omega\cdot\text{m}$  and  $T$  in K. The total resistivity of the steel alloy as a function of temperature and composition, evaluated from the combination of the two equations is

$$\begin{aligned} \rho \cdot (T) = & 0.01 \\ & (+ (10.1169 - 9.7947) \\ & + 6.1995 [\text{Mn}] \\ & + 14.3269 [\text{P}] \\ & - 10.3715 [\text{S}] \\ & + 11.7499 [\text{Si}] \\ & + 3.8815 [\text{Cu}] \\ & + 2.9775 [\text{Ni}] \\ & + 5.5696 [\text{Cr}] \\ & - 1.506 \\ & + 0.02276 T \\ & + 4.1966 \times 10^{-5} T^2 \\ & + 2.5879 \times 10^{-8} T^3), \end{aligned} \quad (7-14)$$

where  $\rho$ , is measured in  $\mu\Omega\cdot\text{m}$  and  $T$  in K. The constant term accounts for the additional resistivity due to alloying elements not enumerated.

Equation 7-11 relates the thermal and electrical conductivity through the Lorenz constant,  $L_0$ . Schwerer (1986) recommends a value of  $6.8 \times 10^{-3} \text{ cal } \mu\Omega / \text{K}^2 \text{ s}$  ( $= 2.84648 \times 10^{-2} \text{ J } \mu\Omega \cdot \text{m} / \text{K}^2 \text{ s}$ ). The final expression for thermal conductivity as a function of composition for temperatures  $0 \text{ }^\circ\text{C} < T < 700 \text{ }^\circ\text{C}$  is

$$\begin{aligned}
 k(T) = & 2.84648 \times 10^{-2} T / \\
 & [0.01 ( \\
 & +(10.1169 - 9.7947) \\
 & +6.1995 [\text{Mn}] \\
 & +14.3269 [\text{P}] \\
 & -10.3715 [\text{S}] \\
 & +11.7499 [\text{Si}] \\
 & +3.8815 [\text{Cu}] \\
 & +2.9775 [\text{Ni}] \\
 & +5.5696 [\text{Cr}] \\
 & -1.506 \\
 & +0.02276 T \\
 & +4.1966 \times 10^{-5} T^2 \\
 & +2.5879 \times 10^{-8} T^3 )]
 \end{aligned}
 \tag{7-15}$$

where  $k$  is measured in J/m s K,  $T$  in K, and [ ] denotes % in percent. The expression is not valid above 725 °C due to the phase change from  $\alpha + \text{Fe}_3\text{C}$  to  $\alpha + \gamma$  iron.

#### 7.4.1 Recommended Values

Thermal conductivities can be calculated from Eq. 7-14.

#### 7.4.2 Uncertainties

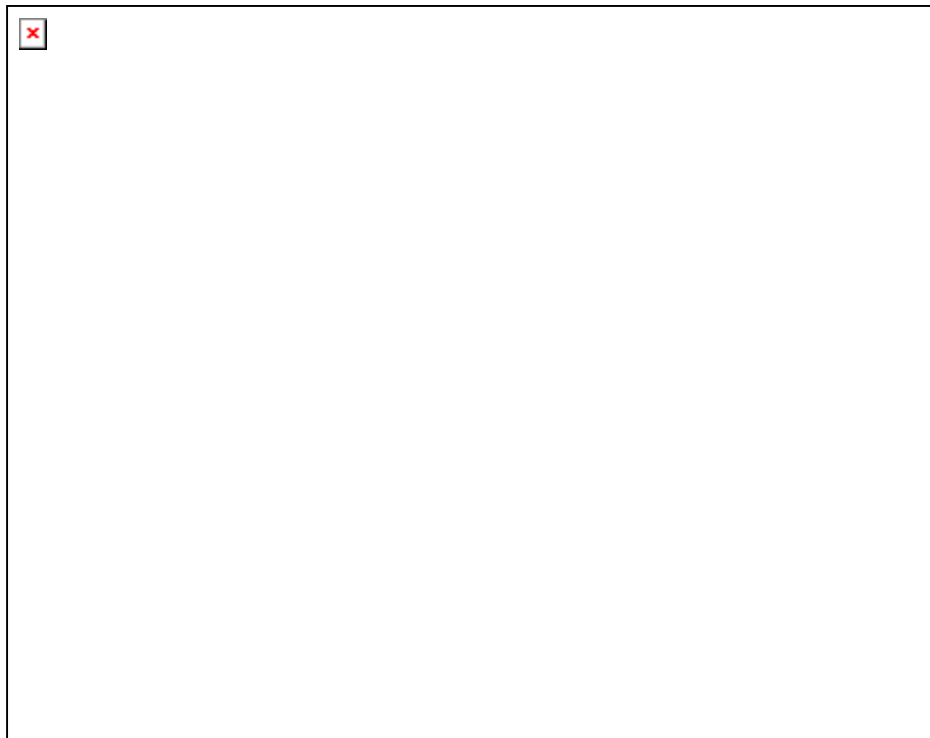
Figure 7-5 shows the fractional error ( $\frac{k_{calc} - k_{act}}{k_{act}}$ ) for several low alloy steels evaluated using Eq. 7-14. In all cases the thermal conductivity was reported as a function of temperature, and then also calculated using Eq. 7-14. In some cases the error can be greater than 20 percent, but it is usually less than 10 percent.

Figure 7-6 demonstrates that steels conforming to ASTM A 36 can have significant variation in thermal conductivity due to the wide range of allowable compositions. There is no single value for thermal conductivity of A 36. Because NIST cannot identify the mill that supplied the plate or wide flange shape in the core, it is not possible to state to better than 20 percent uncertainty the thermal conductivity of any core element.

### 7.5 NOTES ON DATA SOURCES

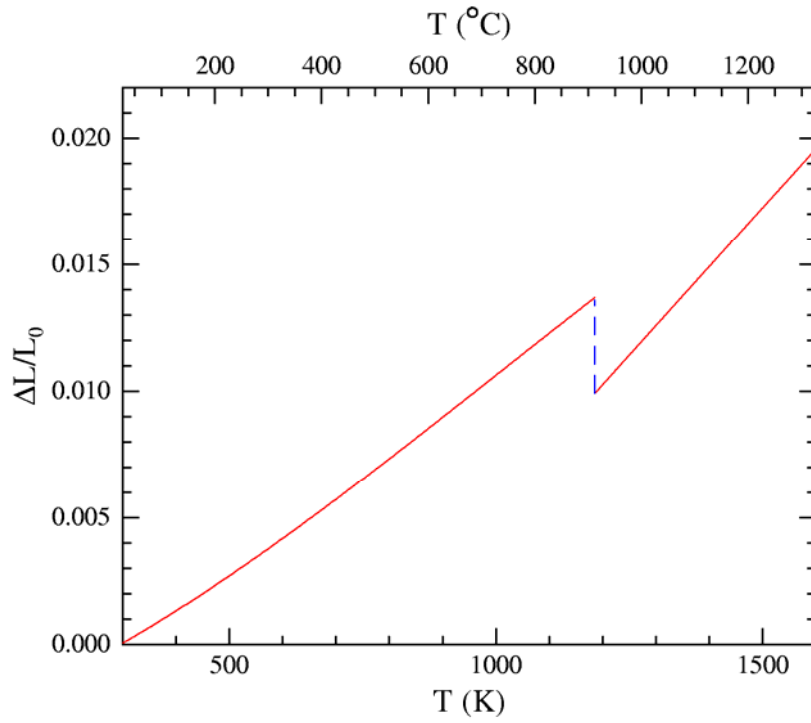
#### 7.5.1 Thermal Expansion Coefficient

Several American Society for Metals publications tabulate thermal expansion coefficients as a function of temperature for low-alloy steels. *High-Temperature Property Data: Ferrous Alloys* (Rothman 1988) repeats data already published in the 9th edition of the *Metals Handbook* (ASM 1978). It differentiates between different American Iron and Steel Institute 1000-grade steels, but has no sources for any of the information, so it is impossible to make any judgment on the reliability of this information.



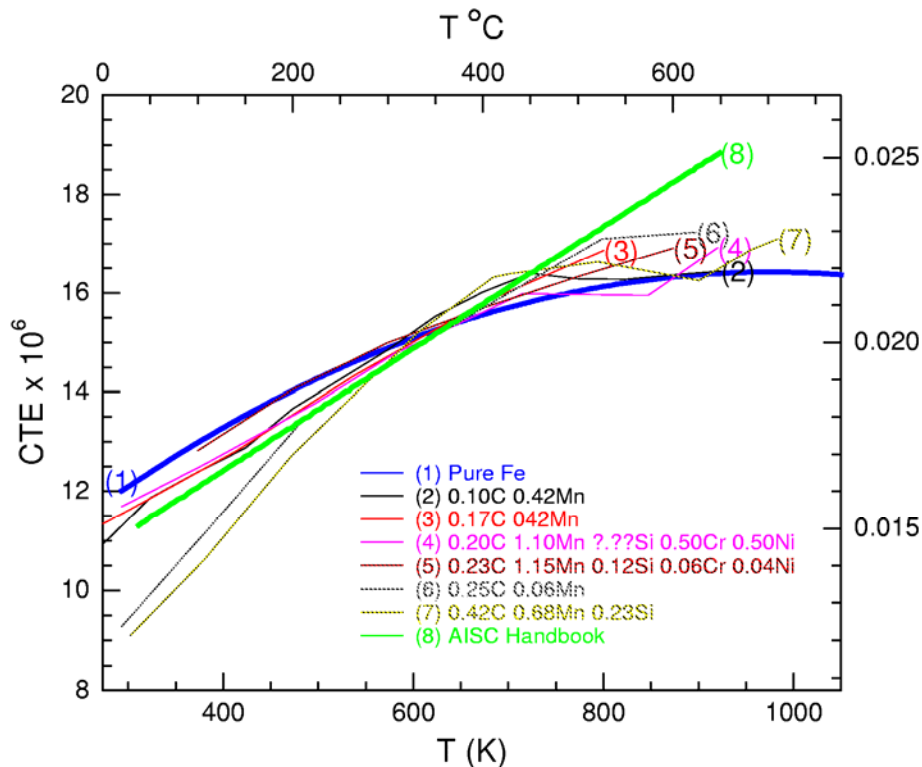
**Sources:** (1) (2) and (3) are Steels 4, 19, and 20 of the NPL report (1946), (4) Curve 1 of Specification Table 182 of Touloukian and Buyco (1970) (5) Curve 3 of Specification Table 182 of Touloukian and Buyco (1970), (6) from Wallace, Sidles, and Danielson (1960).

**Figure 7–1. Heat capacity as a function of temperature for several low-alloy steels and pure iron.**



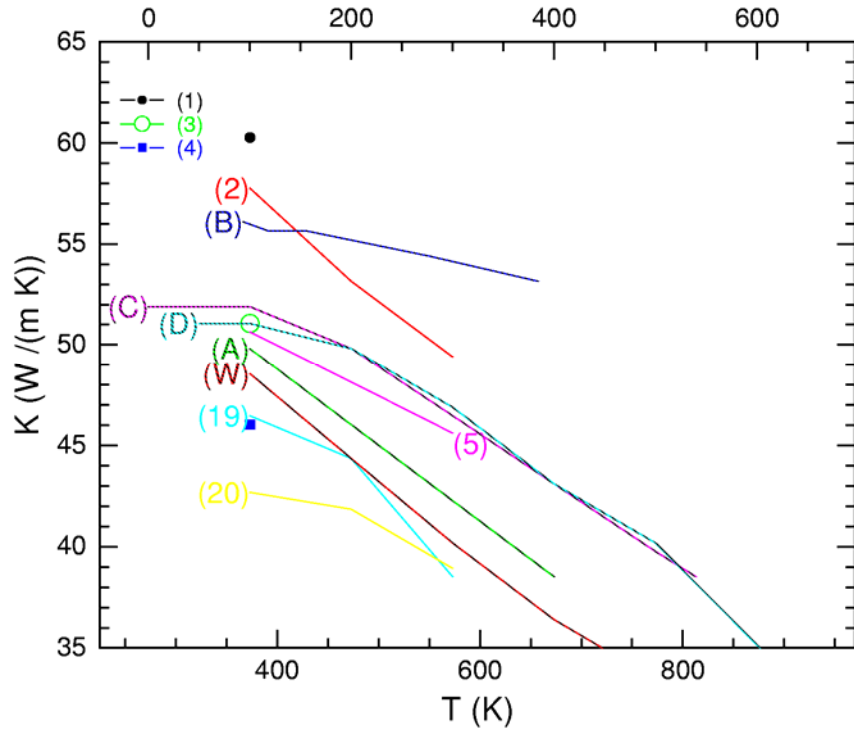
Source: Touloukian et al. 1977.

**Figure 7–2. Thermal expansion of pure iron showing the discontinuity in thermal expansion coefficient at the phase boundary.**



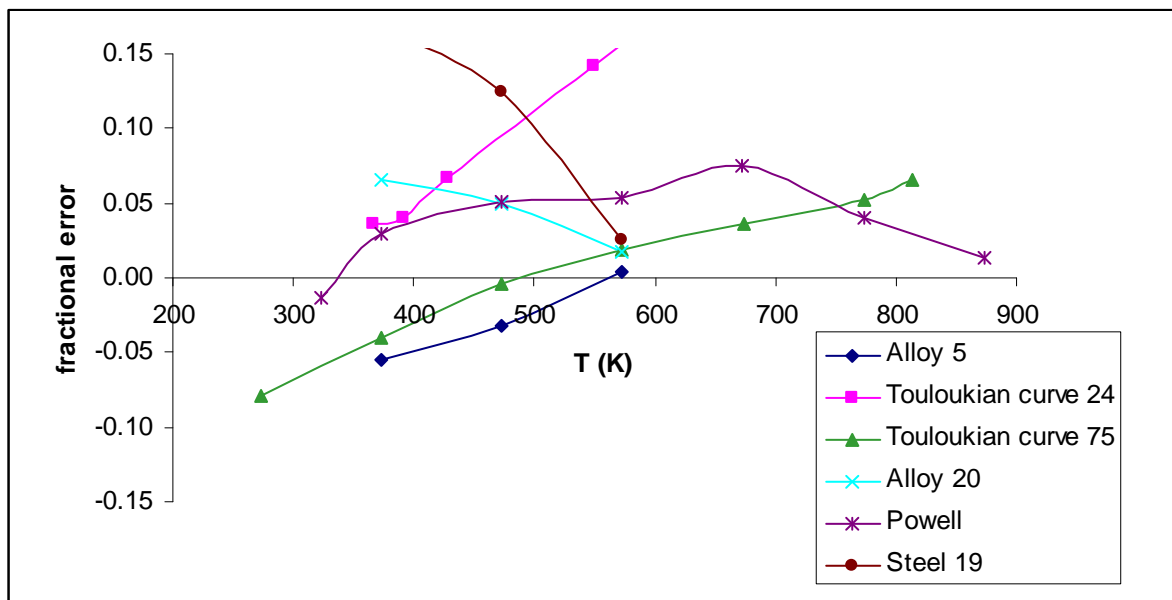
**Sources:** (1) Pure Fe (Touloukian et al. 1977), (2) Lucks, as reported in Touloukian et al. (1977), (3) Mochel, as reported in Touloukian et al. (1977), (4,6,7) Souder (1922) as reported in Touloukian et al. (1977), (5) NPL 1946, (8) AISC Manual of Steel Construction (AISC 2001).

**Figure 7-3. Instantaneous thermal expansion coefficient (Eq. 7-4) for several low-alloy steels.**



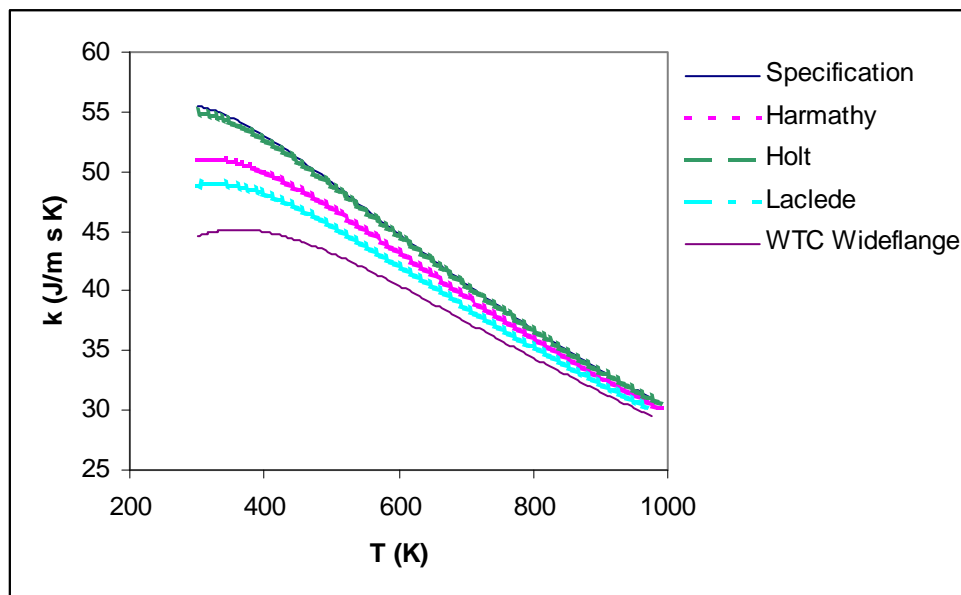
**Sources:** Curves 1-20 correspond to steels 1-20 in a report from the National Physical Laboratory (NPL 1946). Curves A-C correspond to curves 22, 24, and 79 of Specification Table 334 in Touloukian et al. (1970). Curve D appears in Specification Table 335 in Touloukian et al. (1970); the original data are from (Powell 1956). Curve W comes from a data sheet for WEL-TEN 80 (Yawata 1969).

**Figure 7-4. Thermal conductivity as a function of temperature for 12 low-alloy steels.**



**Sources:** Alloys 5, 19, and 20 correspond to steels 5, 19, and 20 in a report from the National Physical Laboratory (NPL 1946). Curves 24, and 79 come from of Specification Table 334 in Touloukian et al. (1970). Curve labeled Powell is from Powell (1956).

**Figure 7-5. Fractional error in estimating steel thermal conductivity from chemistry using Eq. 7-15.**



**Sources:** Harmathy 1970; Holt 1964.

**Figure 7-6. Thermal conductivity as a function of temperature, calculated from Eq. 7-15 for four grades of steel, all identified as conforming to ASTM A 36, Laclede and WTC wide-flange from column line 1008B, floors 104-106 (this report), and the allowable composition of A 36.**

**Table 7–1. Mean (Eq. 7–3) thermal expansion coefficient,  $a_M$ .**

<b>T</b>	<b><math>a_M</math></b>	<b><math>a_M</math></b>	<b>T</b>	<b><math>a_M</math></b>	<b><math>a_M</math></b>
°C	1/°C	1/°C	°C	1/°C	1/°C
	relative to 0 °C	relative to 20 °C		relative to 0 °C	relative to 20 °C
25	7.60E-06	7.79E-06	400	1.06E-05	1.08E-05
50	7.83E-06	8.01E-06	425	1.08E-05	1.09E-05
75	8.06E-06	8.24E-06	450	1.09E-05	1.11E-05
100	8.28E-06	8.45E-06	475	1.11E-05	1.13E-05
125	8.49E-06	8.67E-06	500	1.13E-05	1.14E-05
150	8.70E-06	8.88E-06	525	1.14E-05	1.16E-05
175	8.91E-06	9.09E-06	550	1.16E-05	1.17E-05
200	9.12E-06	9.29E-06	575	1.17E-05	1.19E-05
225	9.32E-06	9.49E-06	600	1.19E-05	1.20E-05
250	9.51E-06	9.68E-06	625	1.20E-05	1.21E-05
275	9.71E-06	9.87E-06	650	1.21E-05	1.23E-05
300	9.89E-06	1.01E-05	675	1.23E-05	1.24E-05
325	1.01E-05	1.02E-05	700	1.24E-05	1.25E-05
350	1.03E-05	1.04E-05	725	1.25E-05	1.26E-05
375	1.04E-05	1.06E-05	750	1.26E-05	1.28E-05

This page intentionally left blank.

## Chapter 8

# ANALYSIS OF ALUMINUM FAÇADE USED ON THE WTC TOWERS

A piece of the aluminum façade from the World Trade Center (WTC) towers was recovered and available for testing. These pieces fit around the outside face of the column and were one story in length. It was unknown which tower this piece was recovered from. Chemical analysis was conducted to determine the alloy type. This testing was done in accordance with ASTM International E227, and the results can be seen in Table 8-1. It appears that the chemistry would place it in the 3xxx-series alloys (Al-Mn alloy).

Differential thermal analysis of the aluminum was also conducted in a Ti gettered UHP Ar atmosphere. The heating rate was 10 K/min. The second melting scan for the sample is shown in Fig. 8-1, where a solidus temperature of 625 °C was observed. This was consistent with the non-heat treatable Al-Mn aluminum alloy AA 3003.

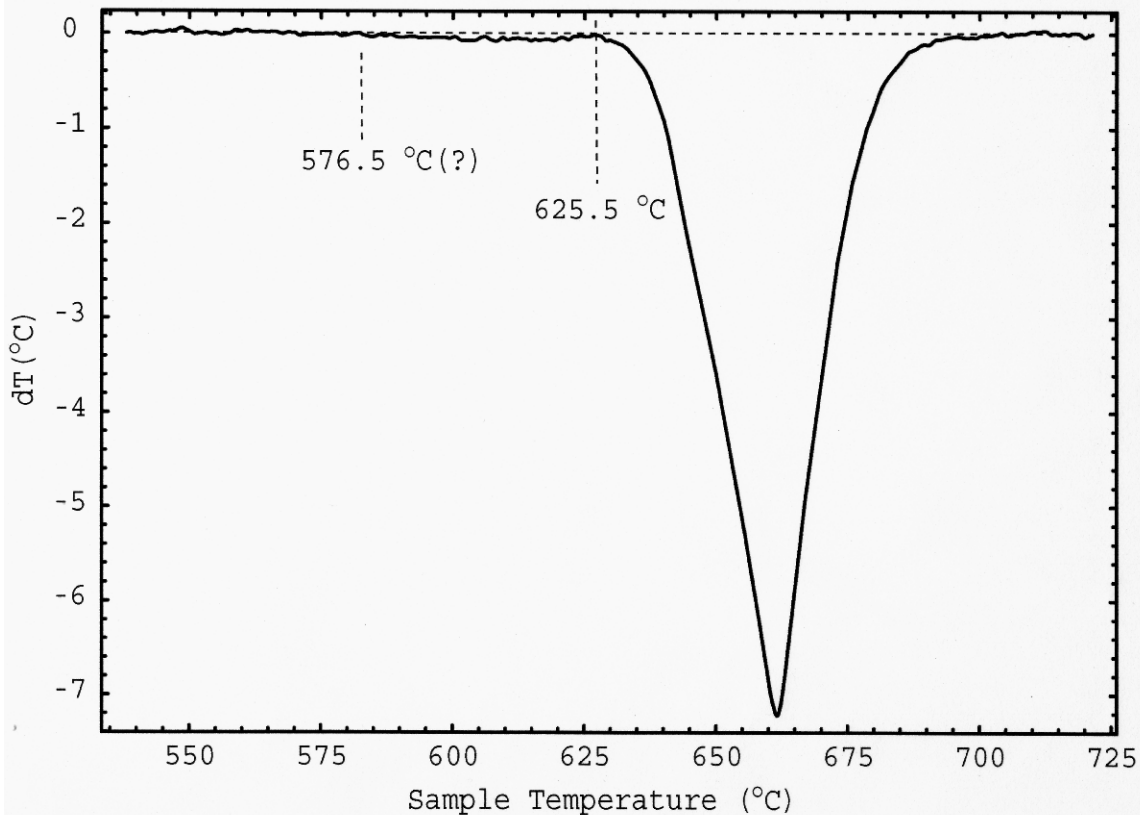


**Figure 8-1. Differential thermal analysis scan for aluminum façade used on the WTC towers. A solidus temperature of 625 °C was observed upon cooling.**

**Table 8–1. Chemistry results for the aluminum façade used on the WTC towers (in mass fraction  $\times 100$ ).**

Element	Aluminum façade
Si	0.19
Cu	0.13
Mg	<0.05
Fe	0.69
Ti	<0.05
Zn	<0.05
Mn	1.11
Pb	<0.05
Sn	<0.05
Ni	<0.05
Cr	<0.05
Others each	<0.05
Others total	<0.15
Al	97.88

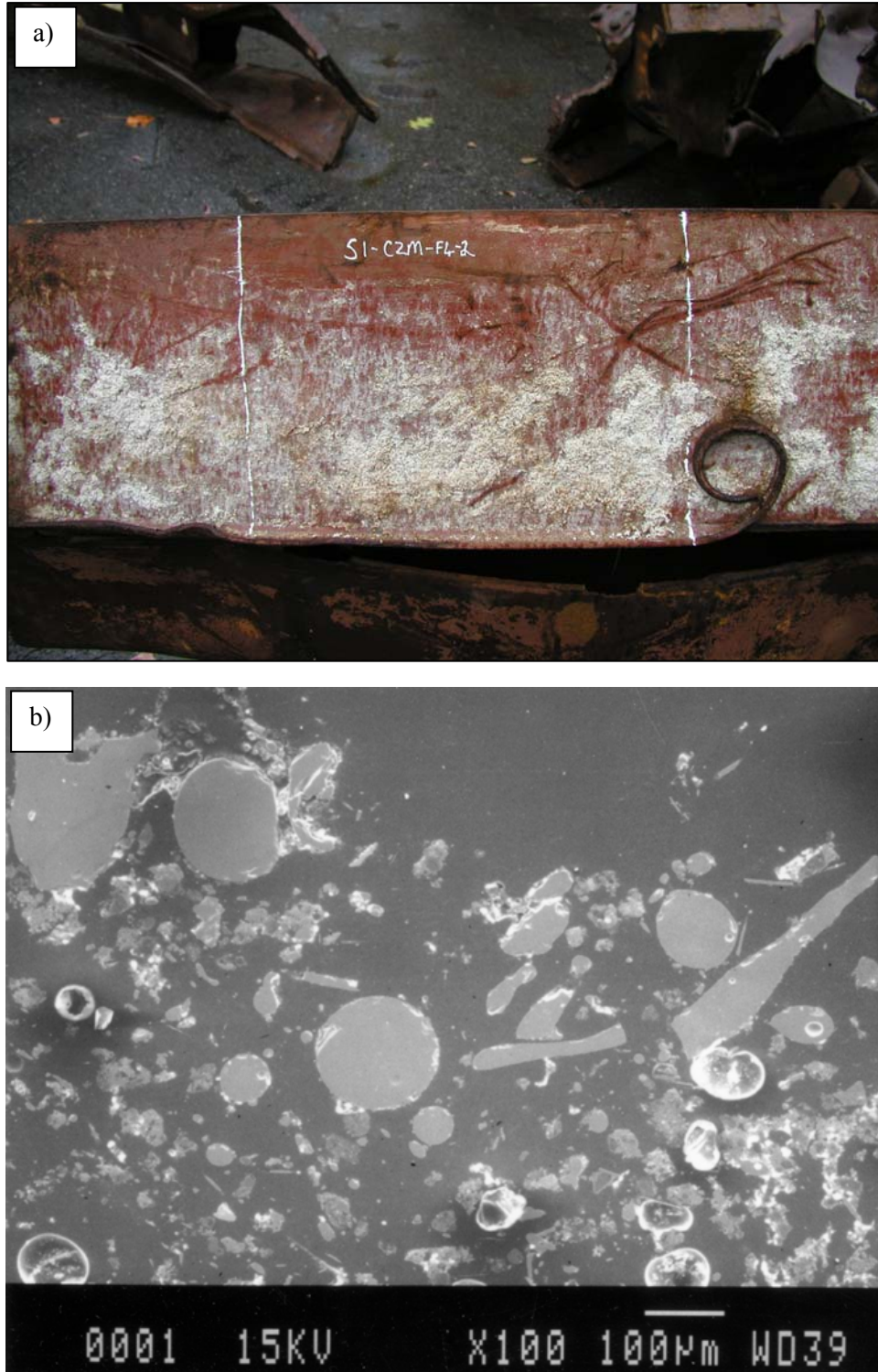
## Chapter 9

# ANALYSIS OF SPRAYED FIRE-RESISTIVE MATERIAL

---

A sample of sprayed fire-resistive material (SFRM) was scraped from a perimeter column of panel S-1 (A433: 79-82; west face of World Trade Center [WTC] 1). The exact location of removal was on column 433 in the vicinity of the 80th floor (Fig. 9–1a). The material was mounted in cold setting epoxy and polished using standard metallographic procedures. The sample was then examined using a scanning electron microscopy with x-ray energy dispersive spectroscopy (EDS). Figure 9–1b displays a secondary electron image of the material. Chemical analysis of 10 different areas was conducted with standardless EDS. The following conditions were used: accelerating voltage = 15 kV; probe current = 1 nA; working distance = 39 mm. Table 9–1 shows the average composition in weight percent.

Information was sought from the manufacturer concerning the chemical composition of the SFRM; this information was found to be proprietary. From the company's (Isolatek) web site, the SFRM was described as "a commercial density, compositely reinforced portland cement based SFRM. The formula for this product was listed as "slag wool and inorganic binders" with the "chemical family" of "silicates and calcium sulfites." Qualitatively, the results of this investigation were found to be consistent with the information presently on the manufacture's Web site.



Source: NIST.

**Figure 9–1. a) Location of sprayed fire-resistant material that was scraped from a perimeter column of panel S-1 (A433: 79-82). The exact location of removal was on column 433 in the vicinity of the 80th floor. b) secondary electron image of the sprayed fire-resistant material.**

**Table 9–1. Chemistry analysis of sprayed fire-resistive material (in mass fraction × 100).**

Element	Average	St Dev
Ca	45.4	0.4
Si	33.9	0.6
Al	9.9	0.1
Mg	9.0	0.2
Si	1.1	0.1
K	0.7	0.1

This page intentionally left blank.

## Chapter 10

# FINDINGS AND CONCLUSIONS

---

The physical properties assessment of the recovered World Trade Center (WTC) steel resulted in the following findings and conclusions:

- Two different microstructural types were observed for the recovered WTC steels: hot-rolled for low strength components and quenched-and-tempered for high strength components.
- In general, the steel used for the construction of the WTC towers was found to be of good quality. There did not appear to be atypical defects in the microstructure as a result of processing of the individual plates. Further, the weldments used to build-up the box columns and attach the floor truss connectors to the columns were sound with no visible flaws.
- For a given yield strength ( $F_y$ ), the flange, outer web, and spandrel steel in the perimeter panels were found to be nearly identical, with indistinguishable chemistries and similar microstructures and hardness values. The inner web was found to be distinguishable from the other plates for  $F_y$  less than 80 ksi, in terms of the physical properties evaluated. Inner webs with  $F_y$  equal to 80 ksi and 100 ksi were the same steel as used for the flanges. These results support the contemporaneous documents stating that the flange, outer web, and spandrel plates were produced by a single company (Yawata Iron and Steel Co.) and that the inner web plates were primarily supplied domestically.
- The recovered core columns were found to vary in composition for a given  $F_y$  and shape (built-up box, rolled wide-flange). This result is consistent with the contemporaneous documents stating that numerous suppliers produced the steel to be used for these structural components.
- Butt plates of the perimeter panel columns met chemistry specifications for several Yawata steels.
- Construction bolts were either A 325 or A 490 bolts. This was primarily determined by the stampings on the head. One bolt designated as A 325 was analyzed and met the chemistry specifications for A 325 Type 1.
- Chords and rods that composed the floor trusses, supplied by Laclede Steel Co., were either ASTM International (ASTM) A 36 or ASTM A 242.
- Other structural elements (floor truss connectors, core channels, spandrel splice plates, etc.) met composition specifications for ASTM A 36. Compositions varied significantly, which may indicate that numerous suppliers completed the steel orders for these components.
- Discernible changes to the microstructure of furnace exposed WTC steel were observed when exposed to a temperature of 625 °C for as little as 0.25 h. At or below 500 °C, no indication

of microstructural change was apparent using light optical microscopy. The hardness of these samples varied for a given temperature and material type, but correlated well with microstructural observations:

- Hot-rolled steels below 500 °C experienced a slight increase in hardness, which may be due to strain-age hardening effects;
- Hot-rolled steels at 500 °C and 625 °C experienced a decrease in hardness. Depending upon the prior thermomechanical history, an increase in hardness was observed if the extent of spheroidization was such that large carbide particles formed; and
- Quenched-and-tempered steels at 625 °C had a continual decrease in hardness up to the maximum exposure time of 2 h.

These results were used in the report “Damage and Failure Modes of Structural Steel Components” (NIST NCSTAR 1-3C) to assess the steel for fire-related damage.

- Microhardness traces across weld cross-sections from perimeter panel columns displayed an increase in hardness near the fusion line in the heat affected zone of the base plate. This was related to the alteration of microstructure due to the heat input from the welding process.
- Thermal property values as a function of temperature were derived from the literature and provided for modeling the structural steel response to fire. These properties include specific heat ( $C_p$ ), coefficient of thermal expansion ( $\alpha$ ), and thermal conductivity ( $k$ ).
- A piece of the aluminum façade used on the WTC towers was analyzed and found to be consistent with the non-heat-treatable aluminum-manganese alloy AA 3003.
- A sample of sprayed fire-resistive material scraped from a recovered perimeter column of WTC 1 was chemically analyzed. While the chemical composition of the material was proprietary, the results were consistent, on a qualitative basis, with the information presently found on the manufacturer’s web site.

## Chapter 11

# REFERENCES

---

- AISC. 2001. *Manual of Steel Construction Load and Resistance Factor Design*, Third Edition. American Institute of Steel Construction, 2-48.
- ASM. 1978. *Properties and Selection: Irons and Steels*. American Society for Metals, Metals Park, OH.
- ASM. 1983. "Arc welding of hardenable carbon and alloy steels." *Metals Handbook, Vol 6, 9th Edition*, American Society for Metals, Metals Park, OH.
- Bramfitt, B.L., and A.O. Benschoter. 2002. *Metallographer's Guide: Practices and Procedures for Irons and Steels*. American Society for Metals International, Metals Park, OH.
- Gladman, T. 1996. *Physical Metallurgy of Microalloyed Steels*. Institute of Materials.
- Harmathy, T.Z., and W.W. Stanzak. 1970. "Elevated-temperature tensile and creep properties of some structural and prestressing steels." *Fire Test Performance*. ASTM STP 464. American Society for Testing and Materials, 186-208.
- Holt, J.M. 1964. *Short-Time Elevated-Temperature Tensile Properties of USS Cor-Ten and USS Tri-ten High-Strength Low-Alloy Steels, USS Man-ten (A 440) High-strength Steel, and ASTM A 36 Steel. Report 57.19-901(1)*. Applied Research Laboratory, United States Steel. Monroeville, PA. Oct. 16.
- Irvine, K.J. 1967. "The development of high-strength structural steels." *Strong Tough Structural Steels, Proceeding of the Joint Conference Organized by the British Iron and Steel Research Association and the Iron and Steel Institute at the Royal Hotel in Scarborough*, The Iron and Steel Institute, 1-10.
- Isolatek. World Wide Web Home page, [http://www.isolatek.com/iso\\_msds/blazeshield-IIMSDS.pdf](http://www.isolatek.com/iso_msds/blazeshield-IIMSDS.pdf).
- Krauss, G. 1980. *Principles of Heat Treatment of Steel*, American Society for Metals, Metals Park, OH.
- Leslie, W.C. 1981. *The Physical Metallurgy of Steels*, McGraw-Hill Book Company.
- Ludwigson, D.C., and F.C. Schwerer. 1971. "The effect of composition on the resistivity of carbon steel sheet." *Metall. Trans.*, 2, 3500-3501.
- The National Physical Laboratory (NPL). 1946. "The physical properties of a series of steels.-Part II." *J. Iron Steel Inst.*, 154, 83P-121P.
- Powell, R.W., and R.P. Tye. 1956. "Thermal conductivity and electrical resistivity of a 0.4-0.5% manganese steel." *J. Iron Steel Inst.*, 184, 286-288.
- Rothman, M. F. 1988. *High-Temperature Property Data: Ferrous Alloys*. American Society for Metals International. Metals Park, OH.

- Samuels, L.E. 1980. *Optical Microscopy of Carbon Steels*, American Society for Metals, Metals Park, OH.
- Schwerer, F.C., and R.M. Fisher. 1986. "Steels: electrical resistivity and thermal conductivity." *Encyclopedia of Materials Science and Engineering*, vol. 6, R-S. M.B. Bever, ed. The MIT Press. Cambridge, MA, 4601.
- Souder, W., and P. Hidnert. 1922. "Thermal expansion of a few steels." *Sci. Pap. Bur. Stand.*, 17, 611-626.
- Touloukian, Y.S., and E.H. Buyco. 1970. *Specific Heat Metallic Elements and Alloys*. IFI/Plenum. New York, NY.
- Touloukian, Y. S., R.W. Powell, C.Y. Ho, and P.G. Klemens. 1970. *Thermal Conductivity Metallic Elements and Alloys*. IFI/Plenum. New York, NY.
- Touloukian, Y.S., R.K. Kirby, R.E. Taylor, and P.D. Desai. 1977. *Thermal Expansion Metallic Elements and Alloys*. IFI/Plenum. New York, NY.
- Wallace, D.C., P.H. Sidles, and G.C. Danielson. 1960. "Specific heat of high purity iron by a pulse heating method." *J. Appl. Phys.*, 31[1], 168-176.
- Well, R.G. 1975. "Metallographic techniques in the identification of sulfide inclusions in steel." *Sulfide Inclusions in Steel, Proceedings of an ASTM Symposium, Nov. 7-8, 1974*, Port Chester, NY, Ed. J. DeBarbadillo and E. Snape, American Society for Metals, Metals Park, OH, 123-134.
- Yawata Iron and Steel Co. 1969. WEL-TEN 80 material data sheet from Yawata Iron and Steel Co. Ltd., Japan, 142-164.